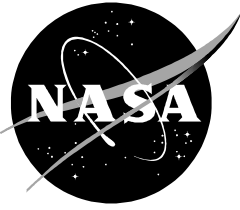


NASA/TP-98-201793



# **Photogrammetric Assessment of the Hubble Space Telescope Solar Arrays During the Second Servicing Mission**

## **Final Report**

C. A. Sapp  
M. W. Snyder  
J. L. Dragg  
M. T. Gaunce  
J. E. Decker

---

April 1998

## The NASA STI Program Office . . . in Profile

Since its founding, NASA has been dedicated to the advancement of aeronautics and space science. The NASA Scientific and Technical Information (STI) Program Office plays a key part in helping NASA maintain this important role.

The NASA STI Program Office is operated by Langley Research Center, the lead center for NASA's scientific and technical information. The NASA STI Program Office provides access to the NASA STI Database, the largest collection of aeronautical and space science STI in the world. The Program Office is also NASA's institutional mechanism for disseminating the results of its research and development activities. These results are published by NASA in the NASA STI Report Series, which includes the following report types:

- **TECHNICAL PUBLICATION.** Reports of completed research or a major significant phase of research that present the results of NASA programs and include extensive data or theoretical analysis. Includes compilations of significant scientific and technical data and information deemed to be of continuing reference value. NASA's counterpart of peer-reviewed formal professional papers but has less stringent limitations on manuscript length and extent of graphic presentations.
- **TECHNICAL MEMORANDUM.** Scientific and technical findings that are preliminary or of specialized interest, e.g., quick release reports, working papers, and bibliographies that contain minimal annotation. Does not contain extensive analysis.
- **CONTRACTOR REPORT.** Scientific and technical findings by NASA-sponsored contractors and grantees.

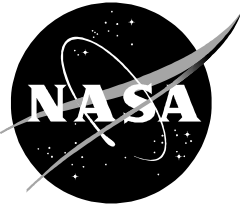
- **CONFERENCE PUBLICATION.** Collected papers from scientific and technical conferences, symposia, seminars, or other meetings sponsored or cosponsored by NASA.
- **SPECIAL PUBLICATION.** Scientific, technical, or historical information from NASA programs, projects, and mission, often concerned with subjects having substantial public interest.
- **TECHNICAL TRANSLATION.** English-language translations of foreign scientific and technical material pertinent to NASA's mission.

Specialized services that complement the STI Program Office's diverse offerings include creating custom thesauri, building customized databases, organizing and publishing research results . . . even providing videos.

For more information about the NASA STI Program Office, see the following:

- Access the NASA STI Program Home Page at <http://www.sti.nasa.gov>
- E-mail your question via the Internet to [help@sti.nasa.gov](mailto:help@sti.nasa.gov)
- Fax your question to the NASA Access Help Desk at (301) 621-0134
- Telephone the NASA Access Help Desk at (301) 621-0390
- Write to:  
NASA Access Help Desk  
NASA Center for Aerospace Information  
800 Elkridge Landing Road  
Linthicum Heights, MD 21090-2934

NASA/TP-98-201793



# **Photogrammetric Assessment of the Hubble Space Telescope Solar Arrays During the Second Servicing Mission**

## **Final Report**

*C. A. Sapp and J. L. Dragg  
Lockheed Martin Engineering Science & Services*

*M. W. Snyder  
Hernandez Engineering*

*M. T. Gaunce  
Johnson Space Center*

*J. E. Decker  
Goddard Space Flight Center*

National Aeronautics and  
Space Administration

**Lyndon B. Johnson Space Center**  
Houston, Texas

---

April 1998

## Acknowledgments

The authors would like to gratefully acknowledge the support and contributions of the following people: Mr. Dan Blackwood of the Goddard Space Flight Center; Mr. Dan Smith of CTA Corporation; the crew of STS-82; Mr. Donn Liddle, Dr. Premkumar Saganti, Mr. Kevin Crosby, and Ms. Teresa Morris of Lockheed Martin Corporation; Mr. Mark Holly, Mr. David Bretz, and Mr. Jose Pecina of Hernandez Engineering; Mr. Dave Williams of USA; and Mr. Jim Maida and Ms. Lorraine Hancock of the Graphics Research and Analysis Facility at the Johnson Space Center.

Available from:

NASA Center for AeroSpace Information  
800 Elkridge Landing Road  
Linthicum Heights, MD 21090-2934  
Price Code: A17

National Technical Information Service  
5285 Port Royal Road  
Springfield, VA 22161  
Price Code: A10

## Summary

During the first servicing mission (SM-1) of the Hubble Space Telescope (HST) in December 1993, the two solar arrays that power the telescope were replaced. Photographs taken of the new solar arrays during SM-1 showed geometric (or static) twists in the arrays. The estimated static twists ranged from 11 to 31 inches. Ground simulations by the Goddard Space Flight Center (GSFC) revealed that the static twist could grow due to on-orbit induced loads, and the structural integrity of the solar arrays could be compromised if the twist reached a certain level.

In April 1995, the GSFC HST Flight Systems and Servicing (FS&S) Project tasked the Image Science and Analysis Group (IS&AG) in the Johnson Space Center (JSC) Earth Science and Solar System Exploration Division to perform photogrammetric analyses of the motion and static twist of the HST solar arrays during SM-2. The requirements for static twist measurements were for three-dimensional (3D) positions of the eight solar array tips before the first extravehicular activity (EVA) and after four EVAs. The positional accuracy requirement was  $\pm 1.3$  inches. The solar array motion requirement was for the 2D out-of-plane amplitude and frequency of the tips of one solar array during a firing of the Shuttle vernier reaction control system (VRCS). SM-2 plans called for a partial reboost of HST using the Shuttle VRCS. The amplitude accuracy requirement was  $\pm 0.5$  inches. The results were required within 8 hours from downlink of all video data to allow the FS&S Project to make critical decisions regarding potential risks due to upcoming EVAs and the planned reboost of HST.

Post-mission analyses were also performed to determine the “best and final” positions of the array tips at the conclusion of SM-2 to support future HST operational planning, and to analyze the motions of the solar array tips from five separate array excitation events for use in structural dynamics analyses.

Accomplishing these static twist and solar array motion measurement objectives was a significant undertaking and is described in this report. The methodologies for performing the near-real-time analyses were adapted from technologies IS&AG has utilized for numerous Shuttle and Shuttle/*Mir* investigations. The method for determining the positions of the tips of the arrays required a two-camera phototheodolite approach using the four video cameras in the Shuttle payload bay (PLB). The orientation of each camera was determined independently from images containing features of known position on the HST. The position of the tip was then determined from the intersections of two vectors, one determined from each camera image, from the perspective center of the image to the conjugate image point of the tip. The method for measurement of solar array tip motion utilized a single video camera solution for each tip. The motion, in image space, was converted to object distance with a scale factor based on the distance of the object from the camera.

An extensive amount of pre-mission planning and development was performed to ensure that the required imagery data acquisition and analyses would be successful. This planning included performing viewing and lighting studies, simulations, testing, and flight crew and ground control personnel training; selecting cameras; developing HST reference control point data; and creating operating procedures, flight documentation, and training aids.

During SM-2, all required data were effectively acquired, all required near-real-time analyses were performed (except for the positions of two tips on one array on Flight Day 5), and all results (except the initial static twist result) were transmitted to the FS&S Project within the near-real-time requirement.

The static twist results for all four tip pairs were consistent for Flight Days 3, 4, 5, and 8. The results for Flight Days 6 and 7 were significantly different from the other four days, and were attributed to factors associated with the HST being placed in a different orientation on Flight Days 6 and 7. On the basis of these results, the FS&S Project concluded there were no significant structural changes in the arrays during the SM-2 mission.

Two motion analyses were performed during the mission on a VRCS-induced motion event and the motion from the airlock depressurization on Flight Day 8. The VRCS results for tips A and B included analyses of 180 video frames at a 3-Hz sampling rate. The results showed a peak-to-peak displacement of 0.6 inches for tip A and 0.7 inches for tip B. Both tips exhibited a dominant frequency of approximately 0.1 Hz as predicted for the first fundamental out-of-plane frequency. The airlock depressurization-induced motion involved the analysis of 161 video frames of the solar array tips G and H. The results indicated a total slew of approximately 22 inches, after which the array oscillated at a frequency of approximately 0.1 Hz. The initial peak-to-peak displacement was measured to be approximately 6 inches for tip G and 7 inches for tip H.

Post-mission analysis of static twist used a photogrammetric methodology commonly referred to as “bundle adjustment.” The bundle adjustment methodology simultaneously uses multiple images, control points, and common pass-points to determine camera position and orientation parameters, and subsequently to determine the position of all object points of interest simultaneously. It accomplishes these calculations through a weighted least-squares adjustment and the general law of propagation of errors to provide an overall best solution for all points. It has not been adapted for near-real-time analyses. The post-mission analysis of static twist was performed for the solar array tips on Flight Day 8. Different images were used than those used in the near-real-time analysis. The results for tips A/B, C/D, and G/H were consistent with the near-real-time results for Flight Days 3, 4, 5, and 8. Results were not obtained for tips E/F due to the limited number (8) of control points in the image.

Post-mission solar array motion analyses were performed for the VRCS-induced motion on Flight Day 3, the HST start- and end-of-rotation on Flight Day 5, the airlock depressurization on Flight Day 8, the HST start- and end-of-pivot on Flight Day 8, and the HST reboost on Flight Day 8. Several refinements of methods were developed to provide more precise determination of the peak-to-peak displacements and their accuracy. The peak-to-peak deflections for the VRCS-induced motion were  $0.65 \pm 0.05$  inches ( $1\sigma$ ) for tip A and  $0.73 \pm 0.08$  inches for tip B. The magnitudes of the peak-to-peak deflections for the airlock depressurization event were  $6.5 \pm 0.4$  inches for tip G and  $9.7 \pm 0.4$  inches for tip H. The next largest deflection for a solar array tip was 1.4 inches. All solar array motions exhibited a dominant frequency of 0.1 Hz.

In addition to the solar array motion and static twist analytical results, several recommendations are made for improvements to similar analyses on SM-3 and the International Space Station.

# Contents

---

Summary .....	iii
1. Introduction .....	1
2. Mission Support Requirements .....	3
3. Measurement Approach and Methodologies Used in the Real-Time Mission Support.....	5
3.1 Static Twist Methodology.....	6
3.1.1 Phototheodolite Technique .....	6
3.1.2 Phototheodolite Implementation for HST.....	8
3.1.2.1 Establishment of Image Reference Information.....	8
3.1.2.2 Coordinate System Conversions .....	9
3.1.2.3 Determination of Pointing Angles and Camera Focal Length .....	10
3.1.2.4 Phototheodolite Solution .....	10
3.1.3 Static Twist Position Error Estimation Technique .....	11
3.1.4 Validation Test Case .....	11
3.2 Solar Array Motion Analysis.....	12
3.2.1 Motion Analysis Methodology .....	13
3.2.2 Proof-of-Concept Analysis .....	14
4. Pre-Mission Planning and Analysis.....	15
4.1 Imagery Acquisition for Static Twist Analysis .....	15
4.1.1 Requirements for Imagery Acquisition for Static Twist Analysis.....	15
4.1.2 Imagery Acquisition Studies for Static Twist Analysis.....	17
4.1.2.1 Camera Selection.....	17
4.1.2.2 Viewing .....	17
4.1.2.3 Lighting .....	19
4.1.3 Imagery Acquisition Plan .....	19
4.1.4 Imagery Analysis Plan .....	20
4.2 Imagery Acquisition for Solar Array Motion Analysis .....	21
4.2.1 Imagery Acquisition Requirements .....	21
4.2.2 Imagery Acquisition Studies .....	22
4.2.2.1 Viewing Analysis .....	23
4.2.2.2 Lighting .....	24
4.2.3 Imagery Acquisition Plan .....	24
4.2.4 Imagery Analysis Plan .....	24
4.3 Mission Integration Activities .....	24
4.3.1 Flight Data File Inputs .....	25
4.3.2 Crew Training .....	25
4.3.3 Joint Integrated Simulation Support .....	26
5. Real-Time Mission Operations and Analyses .....	28
5.1 VDAS Laboratory Operations .....	29

## Contents (continued)

---

5.2	Static Twist Analysis .....	29
5.2.1	Data Acquisition and Analysis.....	29
5.2.2	Results for Solar Array Tip Coordinates .....	34
5.2.3	Calculation of Solar Array Twist.....	38
5.3	Solar Array Motion Analysis.....	40
5.3.1	VRCS-Induced Solar Array Motion on Flight Day 3 .....	40
5.3.2	Airlock Depressurization-Induced Solar Array Motion (Flight Day 8) .....	42
6.	Post-Mission Analyses .....	44
6.1	Static Twist Analysis .....	44
6.1.1	Analysis Approach.....	45
6.1.2	Implementation of Bundle Adjustment Solution .....	46
6.1.3	Results From Post-Mission Photogrammetric Analyses .....	49
6.1.4	Comparison of Post-Mission Results to Real-Time Results.....	51
6.1.5	Solar Array Twist Analysis.....	53
6.1.6	Summary of Static Twist Results.....	54
6.2	Array Motion Analysis .....	54
6.2.1	Analysis Approach.....	54
6.2.2	Motion Analysis Error Assessment Methodology.....	57
6.2.3	Solar Array Motion Analyses .....	57
6.2.4	Analysis of VRCS-Induced Solar Array Motion (Flight Day 3) .....	57
6.2.5	Analysis of Solar Array Motion During FSS Rotation (Flight Day 5).....	60
6.2.6	Airlock Depressurization-Induced Solar Array Motion (Flight Day 8) .....	64
6.2.7	Solar Array Motion During the FSS Pivot (Flight Day 8).....	65
6.2.8	Solar Array Motion During HST Reboost (Flight Day 8) .....	69
6.2.9	Summary of Array Motion Analyses.....	70
7.	Lessons Learned .....	71
7.1	Pre-Mission Planning.....	71
7.1.1	Resource Planning.....	71
7.1.2	Analysis Turnaround Time Estimation.....	72
7.1.3	Virtual Reality Crew Training .....	72
7.1.4	Reference Control Points .....	72
7.1.5	Lighting.....	73
7.2	Analysis .....	73
7.2.1	Analysis Techniques and Procedures.....	73
7.2.2	Error Estimation Capability .....	73
7.2.3	Analyst Point Selection Variation.....	74
7.3	Operations .....	74
7.3.1	Accuracy of Joint Integrated Simulations.....	74
7.3.2	Acquisition Procedure Review With INCO.....	74
7.3.3	Ku-Band Coverage Availability .....	74

## Contents (continued)

---

7.3.4	Training .....	74
7.4	Equipment .....	75
7.4.1	Camera Selection .....	75
7.4.2	Camera Calibration .....	75
8.	Conclusions and Recommendations.....	75
8.1	Conclusions From Static Twist Analyses .....	75
8.2	Conclusions From Solar Array Motion Analyses.....	76
8.3	Conclusions on Imagery Acquisition .....	77
8.4	Conclusions on Robustness of Methodologies .....	77
8.5	Recommendations.....	77
9.	References .....	78

### ***Appendixes***

Appendix A:	Validation Test Case Results
Appendix B:	Solar Array Motion Feasibility Study and Proof-of-Concept
Appendix C:	SM-1 Analysis
Appendix D:	Storyboards
Appendix E:	Lighting Study
Appendix F:	Daily Mission Reports
Appendix G:	Solar Array Motion Analysis Results

### ***Tables***

4-1	Required Camera Pairs to View Solar Array Tips for the Static Twist Analysis.....	18
5-1	Image Acquisition and Analysis Events .....	28
5-2	Camera Views Used for Each Array Tip on Each Flight Day .....	30
5-3	Real-Time Static Twist Results .....	35
5-4	Perpendicular Offset of Tips From Nominal Plane of Solar Arrays.....	38
5-5	Solar Array Twists and Standard Deviations.....	39
6-1	List of Cameras and Image Times Used in Post-Mission Static Twist Analyses.....	47
6-2	Number of Control Points Used in Single Image Resections .....	47
6-3	Post-Mission Computed Solar Array Tip Locations.....	50
6-4	Accuracies of Real-Time Coordinates Compared to Post-Mission Results .....	51
6-5	Perpendicular Offset of Tips From Conceptual Plane of Solar Arrays .....	53
6-6	Solar Array Tip Twist Values .....	53
6-7	Post-Mission Solar Array Motion Analysis Events .....	54
6-8	Summary of Post-Mission Solar Array Motion Results .....	71

## Contents (continued)

---

### *Figures*

1.1	The Hubble Space Telescope.....	1
1.2	HST solar array details.....	2
3.1	Shuttle camera locations in the payload bay.....	5
3.2	Illustration of HST in Shuttle payload bay, demonstrating solar array tips and Shuttle and HST coordinate systems .....	6
3.3	Elements of two-camera photogrammetric triangulation based on intersection of convergent rays in space .....	7
3.4	Diagram illustrating effect of solar array twist on the direction assumed for solar array motion.....	14
4.1	Multiplexed video showing simultaneous view of HST solar array tips A & B from cameras B and D	18
4.2	Representative CAD view used in image acquisition planning.....	23
5.1	Rotation view from cameras D and A.....	30
5.2	Reference points on rotation images.....	31
5.3	HST rotation calculation input sample .....	31
5.4	HST full FOV images from cameras B and D.....	32
5.5	HST views with identified reference points .....	32
5.6	Multiplexed images of HST solar array tips.....	33
5.7	Reference point data entry spreadsheet sample.....	33
5.8	Tip point data entry spreadsheet sample.....	34
5.9	Tip calculation and error analysis results sample.....	34
5.10	View of +V2 solar array tips A & B from camera B during the VRCS-induced solar array motion on Flight Day 3.....	41
5.11	Displacement of tips A and B during VRCS firing on Flight Day 3.....	42
5.12	View of -V2 solar array tips G & H from camera B during airlock depressurization-induced solar array motion.....	43
5.13	Displacement of tips G and H during airlock depressurization on Flight Day 8.....	44
6.1	Image of tips E and F taken from camera C, showing the linear configuration of control points .....	49
6.2	Point tracking method applied to tracking an HST solar array tip .....	55
6.3	Illustration of maximum peak-to-peak displacement of solar array tips.....	56
6.4	Solar array tip displacement during the VRCS-induced solar array motion (Flight Day 3).....	58
6.5	Frequency plot for tip A from VRCS-induced motion.....	59
6.6	Frequency plot for tip B from VRCS-induced motion .....	59
6.7	View of +V2 solar array tips A & B from camera B during start of rotation.....	60
6.8	View of -V2 solar array tips G and H from camera B at end of rotation .....	61
6.9	Solar array tip displacement during start of rotate event (Flight Day 5).....	62
6.10	Solar array tip displacement during end of rotate event (Flight Day 5).....	63
6.11	Solar array tip displacements during airlock depressurization (Flight Day 8).....	65
6.12	View of -V2 solar array tips E and F from the RMS elbow camera during beginning of pivot.....	66
6.13	View of -V2 solar array tips E and F from the RMS elbow camera during end of pivot.....	66
6.14	Solar array tip displacements during start of pivot event (Flight Day 8) .....	67
6.15	Solar array tip displacements during end of pivot event (Flight Day 8) .....	68
6.16	View of +V2 solar array tips A and B from camera B during reboost on Flight Day 8.....	69
6.17	Solar array tip displacements during reboost (Flight Day 8).....	70

# Acronyms

CAD	computer-aided design
CCTV	closed circuit television
CTVC	color television camera
deg	degrees (of angle)
EFL	effective focal length
EIRR	External Independent Readiness Review
EVA	extravehicular activity
FD	flight day
PDF	Flight Data File
FFT	fast Fourier transform
FOV	field-of-view
FS&S	flight systems and servicing
FSS	flight support structure
GRAF	Graphics Research and Analysis Facility
GSFC	Goddard Space Flight Center
HST	Hubble Space Telescope
INCO	instrumentation and communication officer
IS&AG	Image Science and Analysis Group
ISS	International Space Station
JIS	joint integrated simulation
JSC	Johnson Space Center
MLA	monochrome lens assembly
MLI	multilayer insulation
MMOD	micrometeoroid and orbital debris
OSVS	Orbiter space vision system
PLB	payload bay
PRCS	primary reaction control subsystem
RCS	reaction control subsystem
RMS	remote manipulator subsystem
SA	solar array
SAMA	solar array motion analysis
SM	servicing mission
STA	static twist analysis
STS	space transportation system
UMENS	unconventional mensuration system
UTC	Coordinated Universal Time
VDAS	video digital analysis system
VRCS	vernier reaction control system

# 1. INTRODUCTION

The Hubble Space Telescope (HST, Fig. 1.1) was launched on the Space Shuttle in April 1990. The HST is the first space-borne observatory designed to be serviced on orbit and is intended to be serviced by the Shuttle every 2-3 years. During the first servicing mission (SM-1) in December 1993, the two solar arrays that power the telescope were replaced. The new arrays, which were designed and built by British Aerospace, were a semi-rigid design, deployable from a central cassette, with structural rigidity provided by two interlocking metal bands called bistems. The arrays were designed to be able to be unfurled and furled multiple times to facilitate servicing and reboost of the HST. Figure 1.2 shows details of the HST solar array.

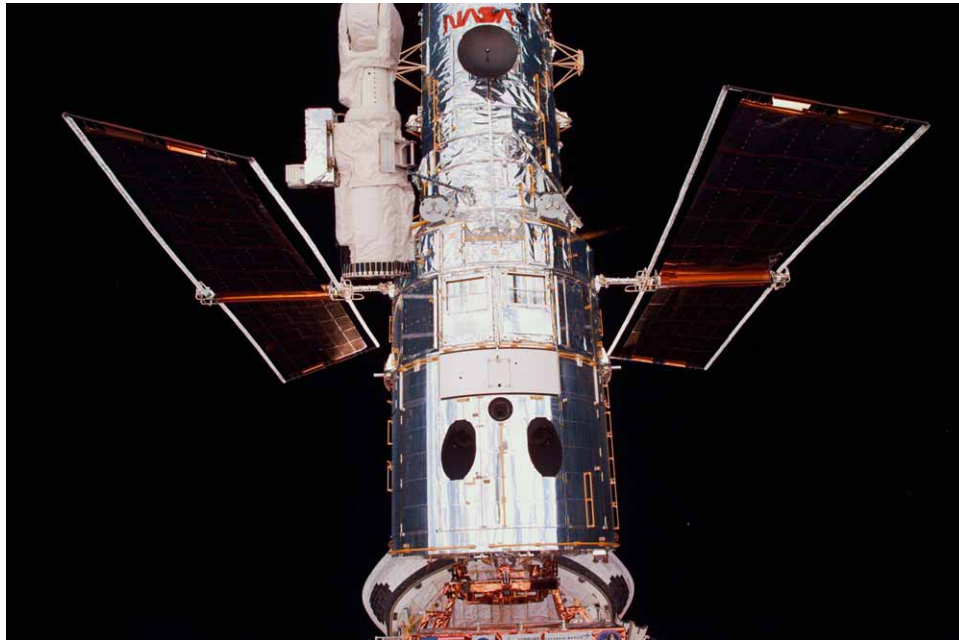


*Figure 1.1 The Hubble Space Telescope.*

During planning for the second servicing mission (SM-2), it was determined that the arrays should remain unfurled throughout the servicing and reboost by the Shuttle. This strategy was adopted to avoid the risks associated with retracting and redeploying the arrays. However, structural dynamic analyses indicated that the solar arrays might not be able to withstand the induced loads from the Shuttle primary reaction control system (PRCS) jet firings during reboost, and this could result in unacceptable stresses in the array bistems. These analyses also showed that the bistem stress could be directly related to the out-of-plane solar array tip displacement. As a result, a reboost test was proposed that would measure the dynamic displacement of the solar array tips in response to a prescribed set of PRCS jet firings during SM-2. Shuttle payload bay (PLB) video cameras would be pointed at the array tips and would record any induced motion due to the jet firings.

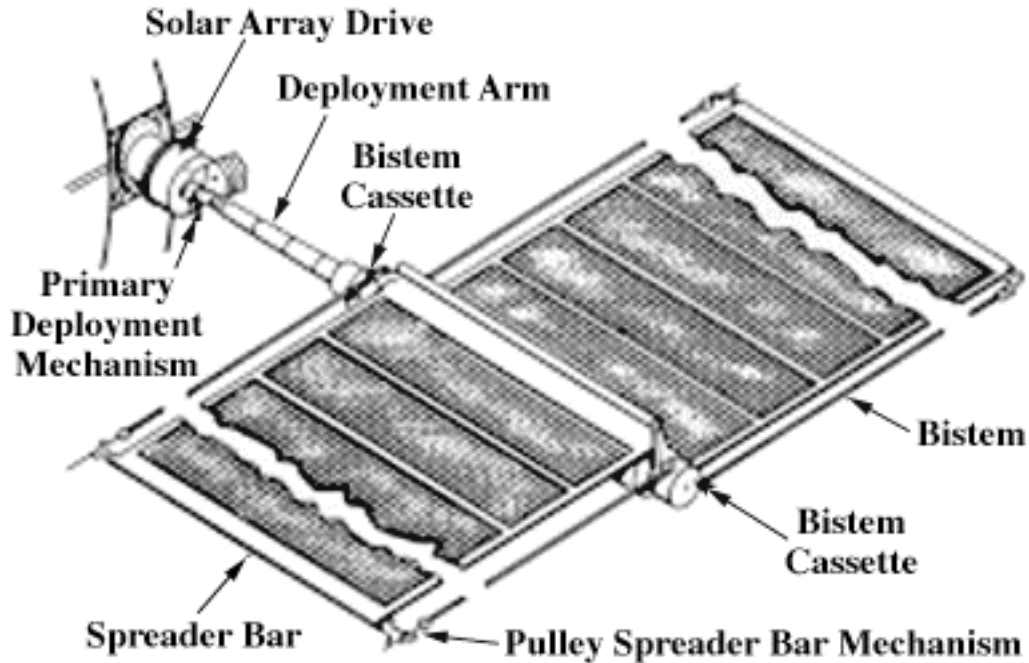


*Figure 1.2 HST solar array details.*

Photographs taken of the new arrays after their installation on SM-1 showed a geometric (or static) twist in the arrays. It was later discovered during ground tests, which simulated on-orbit load cycles on the bistems, that the static twist could grow due to induced loads, and that if the twist reached a certain level, the structural integrity of the bistems could be compromised. The result of this information was the Goddard Space Flight Center (GSFC) HST Flight Systems & Servicing (FS&S) Project's decision that a planned PRCS reboost should not be performed. It was later determined that a partial reboost of the HST could be performed using the vernier reaction control system (VRCS) jets. The significantly lower thrust of the VRCS jets would allow acceptable loading of the arrays.

In April 1995, the HST FS&S Project tasked the JSC Image Science & Analysis Group (IS&AG) was tasked to analyze the solar array motion and static twist of the arrays using imagery obtained during the servicing mission, and to report this information during the course of the mission. To accomplish this, a significant amount of on-orbit video imagery was acquired of the arrays, and was analyzed both during and after the mission. The primary analyses of this imagery included measurements of solar array motion due to a nominal VRCS firing, VRCS reboost, and HST repositioning (both pivot and rotate), and geometric twist measurements of each of the eight array tips before and after each extravehicular activity (EVA) day. Additional analyses, including array motion measurement during the airlock depressurization, were made as required.

This report documents the photogrammetric assessment of the HST solar arrays the JSC Image Science & Analysis Group conducted during SM-2. This report is divided into the following sections:

- Section 2 describes the mission support requirements for the solar array analyses.

- Section 3 describes the analysis methodology and implementation used to perform the static twist and solar array motion analyses during the mission.
- Section 4 describes the pre-mission planning and studies conducted to define imagery acquisition procedures.
- Section 5 documents real-time analysis support provided during the mission, and the results of both solar array motion and static twist measurements performed during the mission.
- Section 6 describes analysis methods and results of the post-mission analysis of data.
- Section 7 provides a summary of lessons learned on solar array imagery analysis from SM-2.
- Section 8 provides a summary, conclusions, and recommendations.

In addition, as a part of the postflight analysis of HST, IS&AG performed two damage assessments to determine the extent of damage to the multilayer insulation (MLI) surrounding the upper surfaces of the telescope, and to identify and measure impacts by micrometeoroids and orbital debris (MMOD). Both of these assessments used a combination of video, 35- and 70-mm positive films, and electronic still camera imagery taken over the course of the mission. These damage assessments are documented in the following reports:

JSC-27943, Hubble Space Telescope SM-2 Multilayer Insulation Damage (MLI) Damage Photobook. [Ref. 1]

[Shuttle Transportation System] STS-82 SM-2, Hubble Space Telescope MMOD Imagery Survey. [Ref. 2]

## **2. MISSION SUPPORT REQUIREMENTS**

Requirements for the scope of imagery acquisition and analysis evolved during the development of the servicing mission. Originally, when the PRCS jets were to provide a partial reboost of the HST, the focus of the imagery analysis requirements was to verify the dynamic response of the arrays to a series of jet test firings, and to provide that information to the HST FS&S mission management in real time so that the total loading on the arrays due to the reboost could be assessed. This image analysis requirement is a rather straightforward detection, tracking, and measurement of the array tip displacement as a function of time. Later, as it was learned the static geometry of the arrays could change as a function of the array loading, and that sufficiently high loading could cause the loss of structural integrity of the arrays, the focus of imagery analysis shifted to the precise measurement of the three-dimensional (3D) static position of each array tip. This is a more difficult measurement to make, as overlapping camera views are required for the 3D position triangulation. Factors such as the viewing angle of the camera relative to the array tip, and the need for multiple calibrated control points for the image pointing and scaling measurements, have a strong effect on the achievable accuracy of this type of measurement. Moreover, compared to typical close-range photogrammetric measurements, the limited spatial resolution and lack of camera calibration data of the Space Shuttle video system limits the ability to make extremely accurate measurements.

The final requirements that emerged were to measure both the dynamic solar array motion and static (or geometric) twist of the arrays at various times during the servicing. This required that a significant amount of imagery of the arrays be acquired each flight day, which then had to be quickly downlinked for analysis. These requirements were integrated into the complete set of photographic and video requirements for the servicing mission, the scope of which is too detailed to be presented in this report. In fact, due to the requirements for a whole range of imagery of the telescope, which would be used for subsequent servicing planning and for exterior damage assessment, the total amount of survey, analytical, and documentary photography and video taken of the Hubble during SM-2 is unprecedented in the Space Shuttle program, or in all of human space flight.

The imagery analysis requirements for the solar array measurements to be conducted during the servicing mission were as follows:

#### **Solar array static twist measurement**

- Description: 3D position of the solar array tips in HST coordinates.
- Amount: 5 analyses, 1 before first servicing EVA, 4 after each EVA, 8 tips per analysis.
- Turnaround Time: 8 hours from downlink of all video data. Results from video acquired at the beginning of the crew sleep period were to be reported before the beginning of the following crew day's EVA.
- Accuracy:  $\pm 1.3$  inches.
- Other: Measurement of HST rotation around the Orbiter +Z axis in the flight support structure (FSS) required. Rotation used to confirm precise 3D position of array tips. No required accuracy.

Based on imagery obtained of the HST solar arrays upon release during SM-1, the estimated array twist ranged from 11 to 31 inches. Little or no growth in the twist was expected between SM-1 to SM-2.

#### **Solar array motion measurement**

- Description: 2D out-of-plane amplitude and frequency of one solar array tip during a VRCS firing. The tip displacement was measured about a mean or undisturbed position.
- Amount: 1 analysis of two tips, 30 seconds of video data.
- Turnaround Time: 8 hours from downlink of the video data.
- Accuracy:  $\pm 0.5$  inches.
- Other: No estimate of damping required. No required sampling frequency.

Based on pre-mission analysis, the expected solar array motion for planned activities during the servicing would range from 0.5 to 4.0 inches peak-to-peak, with a first out-of-plane frequency of 0.1 Hz.

The imagery analysis requirements listed here provided the basis for the real-time analysis methodology described in Section 3. The image analysis requirements and the analysis methodology were the basis of a flow-down to imagery acquisition and operations requirements described in Section 4.

In addition to the near-real-time support to be provided during the servicing mission, the FS&S Project requested IS&AG support a number of pre-mission planning activities, including:

- Concept and technique validation analyses for both the solar array motion and static twist measurements.
- Development of imagery acquisition procedures.
- The implementation of those procedures in the Flight Data File (FDF).
- Crew training.
- Support to several SM-2 joint integrated simulations (JISs).

The JISs' purpose was to practice the analysis procedures, as well as the communications and management protocols, during a simulated mission flight day. Finally, the FS&S Project would require some additional postflight processing of the imagery data to better characterize the response of the arrays during the servicing mission. The scope of the postflight work was determined after a preliminary assessment of the overall success of the servicing mission and a review of the total available imagery obtained during the six days of the HST servicing mission. This additional postflight analysis included measurement of solar array motion during VRCS reboost, HST pivot and rotation, and airlock depressurization.

### 3. MEASUREMENT APPROACH AND METHODOLOGIES USED IN THE REAL-TIME MISSION SUPPORT

Although both static twist measurements and solar array motion measurements were performed using video imagery, the two measurement approaches are distinctly different. Both measurements were configured around a common, available imagery source: the four video cameras in the PLB of the Shuttle and the video camera located on the elbow of the Shuttle remote manipulator subsystem (RMS) as shown in Figure 3.1. This section describes the methodologies used to apply image measurements to the determination of the static twist and motion of the HST solar arrays. Section 6 describes additional methods used in post-mission analyses of the data.

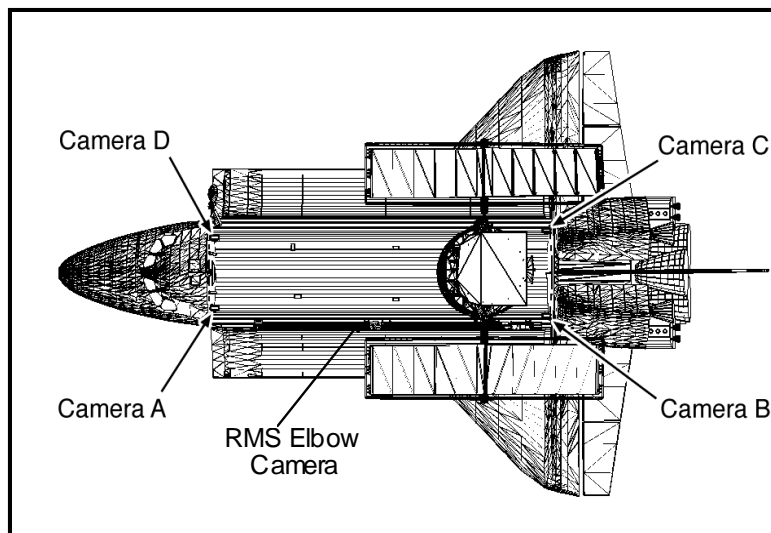


*Figure 3.1 Shuttle camera locations in the payload bay.*

### 3.1 Static Twist Methodology

The objective of the static twist analysis was, for specified times, to determine the positions of tips of the solar arrays in the Hubble coordinate system. (Figure 3.2 is an illustration of the HST in the Shuttle PLB, the tips of the solar arrays, and the HST and Shuttle coordinate systems.) The Shuttle PLB cameras provided imagery for determining the 3D position of each array tip, using a two-camera phototheodolite technique. This section describes the phototheodolite method, the implementation of the phototheodolite technique to the array tip location task, the method for estimation of the accuracy of the phototheodolite solutions, and the validation test of the methodology.

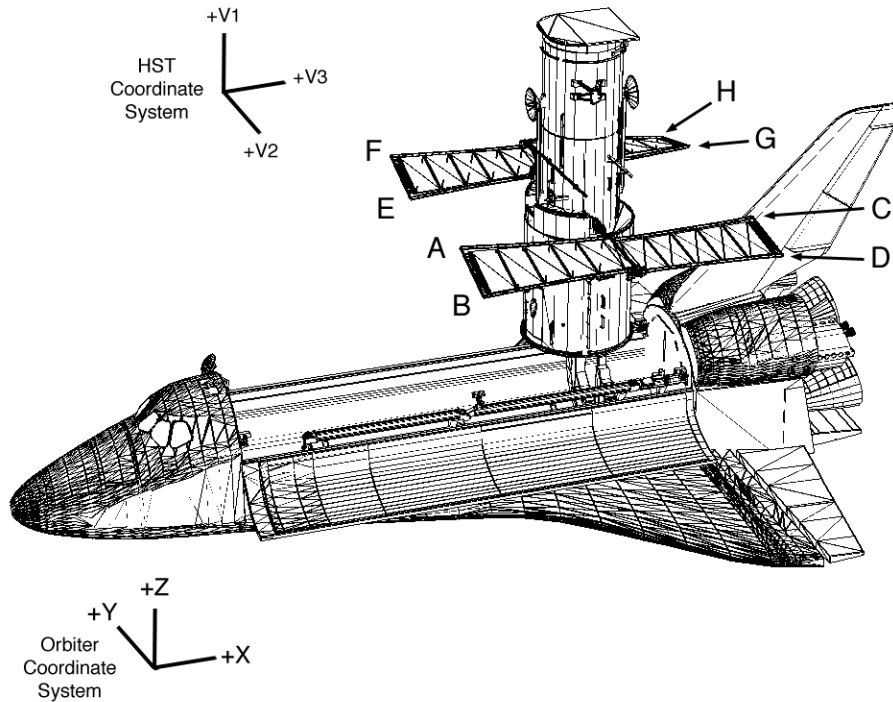


*Figure 3.2 Illustration of HST in Shuttle payload bay, demonstrating solar array tips and Shuttle and HST coordinate systems.*

#### 3.1.1 Phototheodolite Technique

The two-camera phototheodolite technique is a standard 3D triangulation method of photogrammetry and surveying based on the intersection of convergent rays in space. To accomplish the accurate determination of this intersection, a complete reconstruction is required of the relationship between the images and the object coordinate system. The relationship is illustrated in Figure 3.3. In this figure, the vector rays  $A_1$  and  $A_2$  to the object point  $P$  are determined by the positions and directional orientations of the cameras, the coordinates of the conjugate points ( $p_i$ ) in the two images, and the cameras' principal distances (effective focal lengths,  $f_i$ ). (Note that the camera location is defined as the perspective center of the image.) The conjugate points are measured with respect to the principal point of intersection of the optical axis with the image plane. The camera principal distance ( $f_i$ ) and the principal point location ( $x_o, y_o$ ) in the image plane are referred to as the interior orientation elements of the camera. These parameters allow the geometric reconstruction of all bundles of rays internal to the camera from the image

points of the rays. (Note that conventional terminology for the principal distance is  $c$ , for camera constant. However, we are using cameras with zoom lenses, in which case the principal distance is specific to each camera setting.)

The external orientation parameters are those which allow geometric reconstruction of the bundle of rays from the camera lens to object space. The parameters of exterior orientation are the location  $(X_c, Y_c, Z_c)$  of the camera in the object coordinate system and three angles, two of which define the direction of the optical axis in the object coordinate system, and one which defines the rotation of the image plane about the optical axis. These angular elements may be expressed in terms of the direction cosines that the image coordinate system  $x_i, y_i, f_i$  makes with respect to the object coordinate system  $X, Y, Z$ . These direction cosines are usually expressed in terms of rotational angles such as pitch, roll, yaw, pan, tilt, swing, etc., which rotate the object coordinate axes to align with the image coordinate axes.

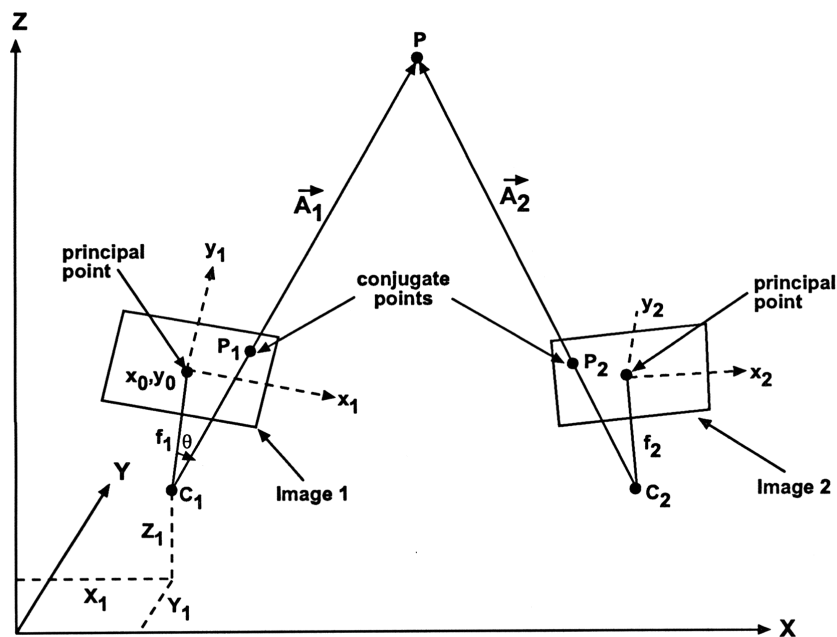


**Figure 3.3** *Elements of two-camera photogrammetric triangulation based on intersection of convergent rays in space.*

Once the interior and exterior orientations of the two cameras are determined, the intersections of the two vector rays to the object point can be determined from the image measurements. These are, of course, not trivial measurements or calculations, especially for non-metric cameras such as the Shuttle video cameras. All of the parameters, including determinations of the effective focal length (EFL) of the zoom lens and lens distortions, contribute to the vectors' failure to intersect. A common solution to the issue of the two vectors' failure to intersect at a point is to calculate the shortest distance miss of the two vectors and take the midpoint as the position of the object point of interest. Solutions that take advantage of having multiple images of the object of interest employ methods of photogrammetry called "bundle adjustments" to determine the point of intersection. The method of bundle adjustments was used in the post-mission analyses and is described in Section 6.1.

The a priori determination of the positions of identifiable points in object space (i.e., on Hubble or Shuttle) is critical to the determination of the interior and exterior orientation of the cameras. The use of known points to calculate these parameters is referred to as camera resection and calibration. These known points are referred to as control points or reference points.

### **3.1.2 Phototheodolite Implementation for HST**

With conventional phototheodolites (a combination of a metric camera and a theodolite used in terrestrial triangulation), the elements of interior orientation are precalibrated and are enforced in the triangulations. The positions of the cameras are surveyed in, and the exterior elements of camera orientation are obtained from, instrument dials and levels. These values provide the nine orientation elements required to establish the vectors to an object in space based on the measured values of the conjugate points in the image. However, in very precise surveys using phototheodolites, the exterior orientation parameters are often determined from the imagery taken with the phototheodolite.

To apply the phototheodolite approach using the Shuttle video cameras, alternate approaches to the conventional phototheodolites had to be employed. The alternate approaches and rationale were:

- The Shuttle video cameras have zoom lenses that did not provide for pre-calibration of the interior orientation parameters, especially the EFL, for all possible zoom settings of the cameras. This parameter would have to be determined from the imagery.
- The design positions of the PLB cameras in Shuttle coordinates are known and provide a close approximation to the true positions. Therefore, the positions of the camera are tightly constrained.
- The camera orientation also has to be determined from imagery. The Shuttle cameras have the ability to transmit pan and tilt information, however this information is relative to an arbitrary position and the accuracy of the readout is variable. Furthermore, the pan-tilt units are friction driven and are designed to slip when resistance is encountered, resulting in read-out error in the relative pan/tilt.

The use of imagery to determine the elements of camera orientation is a common photogrammetric practice. If the object of interest (e.g., solar array tips) is also in the field-of-view (FOV) of the camera, then all elements and positions can be simultaneously determined. The following sections describe the methods used to determine the required orientation parameters.

#### ***3.1.2.1 Establishment of Image Reference Information***

To determine the camera orientation parameters from imagery, it was necessary to establish a database of reference (control) points on the Hubble itself. Furthermore, to meet the turnaround time requirements for the static twist analysis, it was necessary to streamline the entire analysis process as much as possible. One method used in streamlining the analysis process was to pre-select a set of reference points that would be used. Due to uncertainties in image content, it was not possible to select the exact reference points that would be visible for a given analysis. Instead, a superset of reference points was selected which was considered to most likely provide distinguishable points within the video imagery.

A set of annotated diagrams of the HST was used to identify the points to be designated as reference points. Initially, the FS&S Project requested the coordinates for 257 points on the HST outer surface, but because a labor-intensive effort was required to determine the information from engineering diagrams, the total quantity of points was reduced. The FS&S Project subsequently provided IS&AG the coordinates for 132 HST reference points. In addition, IS&AG derived an additional 25 reference points.

The coordinates for each reference point were received in one of two separate HST coordinate systems. There are two primary HST coordinate systems: a Cartesian coordinate system (V1, V2, V3) and a cylindrical coordinate system (alpha, station, radial distance). Most of the reference coordinates the FS&S Project provided were in the Cartesian coordinate system, with the remaining positions specified in the cylindrical coordinate system. To maintain consistency in the coordinate system used in the photolith analyses, all reference points were converted into the HST cylindrical coordinate system and put into a database. Each point in the reference point database was assigned a unique ID number, and a set of diagrams of the HST was annotated with the ID numbers and locations. The database was implemented in a spreadsheet. In this way, the analyst need only indicate the ID number of a reference point, and the spreadsheet would extract the required 3D coordinates from the reference database.

### ***3.1.2.2 Coordinate System Conversions***

Given a set of HST reference points distributed over the image, it is possible to determine the camera coordinates and orientation in HST coordinates. However, to retain the camera positions in Shuttle coordinates, reference points were converted to Shuttle coordinates. In addition, the HST position relative to the Shuttle was variable because the HST was mounted to a FSS, which can rotate and pivot the HST. This meant that the HST coordinate system would rotate and pivot relative to the Shuttle coordinate system at different times during the servicing mission. The Shuttle flight crew manually controlled the rotation and pivot of the FSS, and there was no instrumentation available that accurately measured the rotation and pivot angles. The pivot angle of the FSS was planned to be such that the HST would almost always be vertical during static twist data acquisition, and had a hard stop position at vertical. Therefore, the assumption was made that the pivot angle was exactly vertical. However, the rotation angle had no hard stop positions, and was to change on a regular basis throughout the mission. Therefore, a procedure was developed to estimate the HST rotation from a single image containing the full width of the HST body, and thus convert the HST reference point coordinates to the Shuttle coordinate system. This estimate required as inputs the camera positions, one or more reference points with coordinates in the HST coordinate system, and image coordinates of the visible sides of the HST body.

The procedure for determining the rotation of the HST, and the conversion of reference point coordinates to the Shuttle coordinate system, was as follows:

1. An image of the HST aft shroud was taken from one of the two forward PLB cameras.
2. The analyst would extract the image coordinates of several reference points and the visible edge positions of the HST within the image.
3. This information and the reference point ID numbers were entered into a spreadsheet for the specific rotation position to be calculated.
4. The 3D coordinates of the selected reference points in the HST cylindrical coordinate system were retrieved from the database.

5. The FSS rotation value was calculated and used to transform the positions of all reference points in the database from HST to Shuttle coordinates.

### ***3.1.2.3 Determination of Pointing Angles and Camera Focal Length***

The solutions for the EFL and the pointing angles for a single camera were performed simultaneously. The algorithm for estimating these values used an iterative, least-squares minimization approach, where the residuals to be minimized were the included angles between pairs of unit vectors for each reference point. The angles were calculated as the arc cosines of the dot product of the two unit vectors. Therefore, the minimization will seek to determine the solution for which the included angles are closest to zero, at which the vector pairs will be parallel. This principle of collinearity (a vector from the perspective center to the image point is collinear with a vector from the perspective center to the object point) is the fundamental basis of photogrammetry. Note that factors such as lens distortions cause the path of a light ray to deviate from a perfect straight line, and introduce errors in the solution.

For each reference point, one vector was defined as the vector between the known camera position and the estimated reference point position. The second vector for each reference point would be defined by the currently estimated central line of sight (direction of optical axis) with the added angular offset of the reference point. This angular offset is the angle,  $\theta$ , in Figure 3-3. This angular offset is determined as the angle whose tangent is equal to the distance of the reference point image from the image principal point, divided by the current EFL estimate. The initial value for the camera pointing angle was set as the average of the pointing angles corresponding to all the reference points, and the initial value of the EFL was set at half the minimum and maximum possible values for the camera. The iterative, least-squares minimization was initiated and then converged on the solution, which resulted in the minimum sum of the angles between all the unit vector pairs. The vector to the solar array tips would then be calculated as the sum of the pointing angle and the angular offset calculated from the image coordinates. The process was then repeated for the second camera.

The procedural implementation of the above analysis required the image analyst to extract the image coordinates and ID numbers of multiple reference points, as well as the image coordinates of the solar array tips, within each of two images viewing the solar array tip to be measured. This information would be entered into the user input section of a spreadsheet, and the spreadsheet implementation would extract the newly converted Orbiter body coordinates of each of the reference points from the database, and perform the iterative solution of the camera pointing angles and EFL.

### ***3.1.2.4 Phototheodolite Solution***

With the positions of the two cameras, the EFLs and pointing angles of the cameras, and the pointing vectors to the solar array tips, the required information for performing the phototheodolite solution was determined. The information was input to the phototheodolite algorithm implemented in a spreadsheet, and the estimated solar array tip positions (as well as the magnitude of the vector miss) were calculated. The solar array tip positions were then converted into the HST coordinate system using the FSS rotation value described above.

### **3.1.3 Static Twist Position Error Estimation Technique**

To estimate what analysis accuracies could be expected during SM-2, a Monte Carlo error estimation routine was developed. A Monte Carlo error analysis is a common method for estimating errors in complex analyses. In the Monte Carlo analysis, randomly distributed errors are input to the variables in the static twist position analysis, and the resulting position calculated. This process is repeated a statistically significant number of times, and the variance is calculated from the output values. The standard deviation of the output values can then be considered the standard deviation of the expected results. In the static twist analysis, three times the standard deviation has been used to provide a conservative error bound on the results.

The Monte Carlo error estimation tool was used throughout the planning phase of the project for defining the image acquisition and analysis procedures. It was also incorporated into the integrated analysis application to enable an error analysis for each static twist analysis performed during the mission. Although the relative errors accurately depicted the solution stability required for planning, its applicability to the real imagery was limited because image quality parameters (e.g., camera lens distortion) were not incorporated into the model.

### **3.1.4 Validation Test Case**

At the request of the HST External Independent Readiness Review (EIRR) Board, a validation test case was performed before STS-82 to demonstrate the robustness of the phototheodolite analysis technique. Three different types of test cases were considered: (1) ground tests involving mock-ups of HST targets, (2) a preplanned test on an upcoming mission (STS-80) before SM-2, and (3) existing on-orbit video from previous Shuttle missions. Within each of these approaches, a number of possible test cases were considered, each with its own advantages and disadvantages. The most common disadvantage of the possible options was the uncertainty in the true positions of the objects to be measured, i.e., lack of reliable control data.

The most promising option was to utilize existing video from STS-76. This video was taken in support of an OSVS (Orbiter space vision system) test. The image content was of the Orbiter docking system, which had multiple, high-contrast, circular, optical targets on it. The advantages of this test case were that (a) these targets had a high precision ground truth accuracy (0.03 inches), and (b) the video quality was representative of what could be expected on SM-2. The disadvantages were that (a) the case was not representative of the viewing geometry (e.g., object distance, viewing angles, etc.) expected for SM-2, and (b) the errors associated with the HST rotation were not present.

The specific test case analyzed video for three sets of views from Shuttle PLB cameras A and D. Each view had six OSVS targets within the FOV. Each target represented a separate test case. Each view also had 5 or 6 reference points (e.g., handrail edges) from which camera pointing angles could be determined. The phototheodolite methodology was used to determine the 3D coordinates of each of the OSVS targets from each image set. A Monte Carlo error analysis was performed in the same fashion as for the SM-2 case, but with the appropriate changes to match the SM-2 viewing geometry.

Eighteen 3D analyses were performed (six targets per video segment, three separate video segments with varying degrees of image quality). After performing the phototheodolite analysis, the calculated positions of the OSVS targets were compared to the surveyed target positions, and the differences between the two figures were considered the true errors. The results provided errors between the surveyed and calculated positions ranging from 0.13 to 1.10 inches, with a mean of 0.67 inches. In general, the error model agreed with the calculated error, although the error model under-predicted the estimated error in off-nominal conditions. The conclusion, based on comparing the true error to the predicted error, was that the error model correctly accounted for geometric variations, but did not account well for poor image quality.

An error model estimate, with the same input errors used in the validation test case, was made for the SM-2 geometric configuration, simulating positions of solar array tips A and B derived from Shuttle cameras B and D. The initial  $3\sigma$  error was  $\pm 2.8$  inches compared to a requirement of  $\pm 1.0$  inch. We expected the error would be reduced through improvements in the acquisition and analysis procedures, and follow-up modifications did reduce the  $3\sigma$  error to  $\pm 1.3$  inches.

The results from the validation test case were provided to the FS&S Project and presented to the NASA EIRR Board on October 10, 1996. The EIRR Board concurred with the demonstration results. See Appendix A for additional details on the validation test case.

### **3.2 Solar Array Motion Analysis**

Solar array motion analysis consisted of two major activities. First, there was the requirement to measure the motion of one pair of array tips before the first EVA day. Solar array motion would be induced as a result of a VRCS attitude control thruster firing. As a way of monitoring the loads on the arrays, the out-of-plane solar array tip displacement as a function of time would be measured. Should unacceptable array motion occur, certain planned EVA activities and VRCS reboost might be delayed or canceled. Additional solar array motion analyses would also be performed during the mission if requested.

The second activity was to collect imagery for potential post-mission analysis of solar array motion occurring during HST reboosts, rotations and pivots, solar array slews, and EVA operations, such as FSS berthing and positioning system support post installation.

For each of the solar array motion analyses, video from a single PLB camera would be used. The primary reason for a single camera analysis was that the PLB cameras were scheduled to support crew activities for HST servicing and only one camera was made available at the time of required acquisitions. A secondary reason was that the 8-hour turnaround time for analysis did not accommodate a multiple camera analysis approach. The primary limitation of the single camera analysis is that the direction of motion must be assumed.

### 3.2.1 Motion Analysis Methodology

The motion analysis approach consisted of two activities, tracking and scaling. Tracking an object can either be performed manually or in an automated fashion. Manual tracking is labor-intensive and is, at best, accurate to only 1 pixel. The process consists of an analyst displaying image frames on a monitor one at a time and positioning a cursor over the point being tracked. Automated tracking can be performed using a number of different algorithms, but basically the activity consists of an analyst defining the start and stop times of the sequence to be tracked, and selecting the point to be tracked in the first frame of the sequence. The tracking program then uses an algorithm to discriminate the tracked point from the surrounding area, and performs this algorithm on each frame in the sequence.

IS&AG developed a technique to permit the automated tracking of multiple straight lines within an image sequence. This technique made use of a Canny-type gradient edge detector and a least-squares linear fit of a line to the edge pixels of a linear feature. The output from this algorithm was the line slope and Y-intercept for each frame. By making use of the information in all of the pixels on the edge being tracked, accuracies on the order of 0.1 pixel were achieved. The solar array bismes and the spreader bar were tracked by this application, and the solar array tips were defined as the intersection of these lines. The displacement (motion) of the tips from image frame to image frame is approximately accurate to 0.1 pixel times the scale conversion factor.

The outputs from the tracking algorithm are the image coordinates of the tracked point as a function of time. Usually, this information is scaled from image space into object space coordinates. If two simultaneous views from two different positions are available, then a 3D triangulation can be performed. In this case, the scaling information is derived from the camera separation and the angular measures. Scaling the motion observed from a single viewpoint is a function of the camera's angular FOV, distance to the object, and the direction of motion with respect to the camera line of sight. If only a single view is available, then either the direction of motion must be known (or assumed) or only the component of motion (projected motion) that is perpendicular to the camera line of sight can be measured.

The distance from the camera to the array tip was defined by using the results from the most current static twist analysis after compensating for any changes in the solar array slew positions and FSS rotations. The same approach used in the static twist analysis was used to determine the angular FOV. Two assumptions were made when performing this scaling operation. One assumption was that the solar array twist, or bistem degradation, had not changed significantly since the most current SM-2 static twist analysis. A second assumption was that any motion observed in the solar array was out-of-plane motion, i.e., perpendicular to the solar array plane.

The twist in the solar arrays created a problem in defining a common plane to which the motion of both tips could be assumed perpendicular. The twist caused separate planes for each tip to be defined. (See Figure 3.4.) Each plane was defined by three points: the solar array tip, and the inner and outer edges of the bistem cassette for that array. The inner and outer bistem cassette edge coordinates were determined by using the fixed HST coordinates of those two points, and transforming them into the Shuttle coordinate system using the current FSS rotation value. However, because of the twist, the radii of the two tips are not aligned and hence the direction of motion of each tip is different.

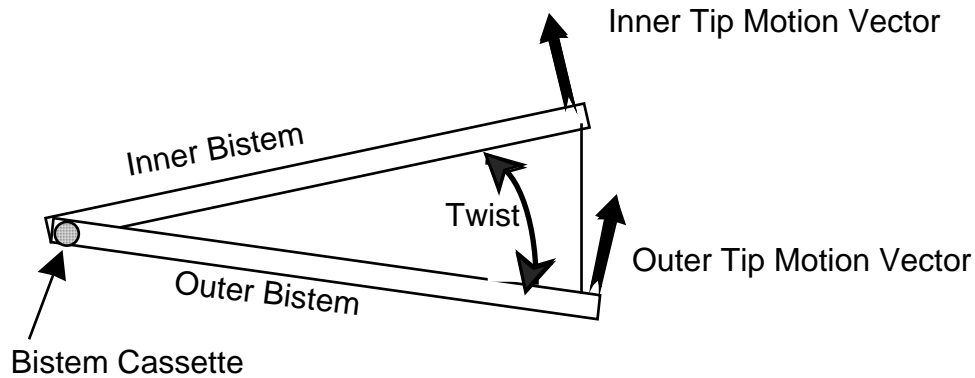


*Figure 3.4 Diagram illustrating the effect of solar array twist on the direction assumed for solar array motion.*

### 3.2.2 Proof-of-Concept Analysis

A proof-of-concept analysis was also performed using video from SM-1 on STS-61. The goal of the analysis was to assess the achievable accuracy of the solar array motion analysis technique and identify any technical or procedural issues that might be required to improve the accuracy or speed for the SM-2 analysis. After screening approximately 14 hours of video from SM-1 looking for solar array motion, we selected a 48-second segment of video and performed the motion analysis. Appendix B contains the report on this proof-of-concept analysis. The results from this proof-of-concept test yielded a maximum deflection of approximately 1 inch for both tips analyzed. The dominant frequencies were 0.1 Hz. Another, barely distinguishable peak occurred at approximately 0.3 Hz. The results of this analysis were provided to the FS&S Project, who reported that the amplitude and frequency of displacement matched their model predictions. Note that the scaling portion of the analysis was necessarily different than that planned for SM-2, due to the fact that no static twist analyses were performed during SM-1. Appendix C contains the SM-1 report.

An error assessment of the SM-1 and projected SM-2 results provided error values ranging from 0.14 to 0.40 inches in displacement depending on whether full-screen or half-screen images were used. This study showed that the accuracy of the solar array motion analysis results would be well within the required accuracy of  $\pm 0.5$  inches. Appendix B contains the results of this study. This initial estimate involved a simple stacking of errors in a worst-case scenario, but failed to account for uncertainties in the static tip position and uncertainties in the position of objects within the PLB due to thermal expansion. An improved approach to estimating the error was derived after the Hubble mission and is described in Section 6.2.2.

## 4. PRE-MISSION PLANNING AND ANALYSIS

To ensure a successful implementation and execution of the SM-2 static twist and solar array motion analyses, an extensive amount of pre-mission planning was required. The pre-mission planning included the development and implementation of methodology described in Section 3 as well as imagery acquisition studies and planning, development of the image analysis plans and procedures, and mission operations integration activities, including mission simulations. These additional pre-mission planning activities are described in the following sections.

Imagery acquisition planning was required to ensure that acceptable imagery was acquired for accurate photogrammetric measurements. Important factors for imagery acquisition planning included:

- Selection of the cameras.
- Determination of the camera views and orientations.
- Analysis of the lighting conditions.
- Identification of the appropriate imagery acquisition times.
- The integration of these procedures into the Shuttle mission and flight operations plans.

In addition, IS&AG internal procedures for acquiring the imagery data, processing and analyzing the data, and delivering the results to the FS&S Project were developed as part of the pre-mission procedures development.

These planning activities are interrelated, with extensive feedback between the activities. In the following sections, the imagery acquisition planning, the image analysis plans, and the mission integration activities and results are described.

### 4.1 Imagery Acquisition for Static Twist Analysis

The planning activities for acquiring adequate imagery to meet the static twist and solar array motion measurement requirements presented in Section 2.0 are described in the following sections. Although the activities are similar, the requirements for imagery acquisition for analyses of static twist are different from the requirements for motion analysis. Therefore, the image acquisition planning for the two analysis types are presented separately.

#### 4.1.1 Requirements for Imagery Acquisition for Static Twist Analysis

In this section, the imagery acquisition requirements for static twist analysis are defined and the rationale described. These requirements were the basis of acquisition planning.

1. Unobstructed, simultaneous views for each HST solar array tip from two separate cameras were required.

*Rationale:* Two unobstructed camera views of the same solar array tip were required for the photogrammetric triangulation solution. Simultaneous views were required to avoid the possibility that Shuttle thruster firings (for attitude control) might result in displacements of the HST solar array tips

if the two views were taken at different times. Crew safety concerns and erratic Ku-band downlink prohibited Shuttle operations in free-drift mode, for which there would be no thruster firings.

2. Sufficient imagery of the solar arrays was required to measure the array at-rest position. The at-rest position is the position from which the solar array tip positions are measured.

*Rationale:* The simultaneous views eliminated the requirement for the Shuttle to be in free-drift mode, but did not ensure that the positions of the array tips were the same as their at-rest position. The at-rest position of the array was defined as the mean array position averaged over a number of oscillatory cycles. The HST solar arrays have an approximately 0.1 Hz first natural out-of-plane frequency caused primarily by Shuttle attitude control thruster firings. It was determined, based on the solar array frequency, that at least 20 seconds of video should be acquired to ensure that the at-rest tip position could be determined. This was selected based on the need to sample a sufficient number of video frames to accurately determine the at-rest tip position.

3. To determine the camera pointing and image scale, a sufficient number of known reference points on the HST and Shuttle were required to be in the camera FOV.

*Rationale:* The camera pointing information is an essential input to the phototheodolite program. As described earlier, the pointing information helps determine the vector from the camera to the HST solar array tip, which is then used in the 3D triangulation to determine the position of the array tip. Having a sufficient number of reference points in the FOV of the camera to accurately determine the camera pointing information was probably the most critical aspect of imagery acquisition planning.

4. Lighting conditions were required such that imagery of sufficient quality for analysis would be acquired.

*Rationale:* Sufficient lighting was required so that the array tip and a sufficient number of control points were clearly visible in the imagery. Without adequate lighting, the solar array tip positions could not be determined.

5. The relative viewing angles between the two cameras and the HST solar array tips should be as close to 90 deg as possible.

*Rationale:* This requirement influenced the selection of camera combinations for viewing each HST solar array tip. The accuracy of the phototheodolite solution is especially dependent on the relative viewing angles between the two cameras imaging a solar array tip.

6. Imagery must be acquired and downlinked for analysis at least 8 hours before each EVA day.

*Rationale:* IS&AG determined that the static twist analysis for all eight HST solar array tips would require 8 hours to complete and the results were required before the beginning of each EVA day. HST mission planners would use the results from the static twist analysis to assess whether the solar arrays could withstand the loads that may be induced by EVA activities and VRCS reboot.

## **4.1.2 Imagery Acquisition Studies for Static Twist Analysis**

To respond to the imagery acquisition requirements, technical studies were performed to select the cameras, evaluate the camera views, and evaluate the expected lighting conditions. These studies provided the information needed to produce an imagery acquisition plan for meeting the acquisition requirements during the mission.

### **4.1.2.1 Camera Selection**

The Shuttle PLB video cameras were the primary resources for imaging the HST solar arrays. Two types of video cameras were manifested for STS-82: the color television camera (CTVC) and the monochrome lens assembly camera (MLA). The CTVC is a solid-state charge-coupled device array camera system, while the MLA has a silicon-intensified target tube camera system. The CTVC has a zoom lens with a FOV range from approximately 10.5 deg to 76.5 deg. The MLA camera has a zoom lens with a FOV range from approximately 6.5 deg to 38.5 deg. The MLA cameras usually produce lower-quality imagery than the CTVCs.

IS&AG recommended that the higher-quality CTVCs be used in the four PLB camera positions. However, two MLA cameras, which have greater sensitivity to low light levels, were required for HST rendezvous operations. IS&AG examined the impact of using the MLA cameras and concluded that the measurement accuracy requirements could still be met using the MLA cameras. The specific placement of the two MLA and two CTVC cameras was based on planned static twist and solar array motion analysis procedures. The highest-priority solar array tips for both static twist and solar array motion analyses were tips A and B because SM-1 results showed they had the greatest twist in the most critical structural direction. Error model simulations were performed and cameras D and B provided the highest predicted accuracy for these tips. Therefore, based on IS&AG recommendations, CTVC cameras were placed in positions D (starboard forward) and B (port aft), while MLA cameras were placed in positions A (port forward) and C (starboard aft). A CTVC was also mounted on the elbow of the RMS.

### **4.1.2.2 Viewing**

The viewing analysis was used to determine which pairs of cameras, and the camera settings, were required for acquiring the video for making the 3D tip position measurements. The Shuttle PLB camera views were simulated from JSC Graphics Research and Analysis Facility (GRAF) computer-aided design (CAD) drawings.

As described in Section 3, two camera views of the same tip are required for the phototheodolite analysis. The following criteria were used to determine the suitability of using a camera for analysis: visibility of the HST solar array tip, resolution of the solar array in the image, availability of a sufficient number of control points in the camera FOV, and the angular separation between the two cameras. The key parameters needed for determining camera views are the camera's angular FOV and orientation or pointing angles (pan and tilt). The angular FOV determines how large an area is visible and therefore the number of control points available in the scene. The FOV also influences the image resolution, which affects the accuracy of selecting the position of the solar array within an image. The camera pointing angles determine the approximate angle of intersection that the two camera vectors make with each other, which affects the accuracy in determining the point of closest intersection. The FOV size required for each camera is based on obtaining the zoom setting that would maximize spatial resolution while

ensuring that a sufficient number of reference points would be visible on the HST for the determination of the camera orientation and FOV.

The camera pairs selected to provide views for each solar array tip were determined based on the pair that resulted in the lowest error (as determined from a Monte Carlo error estimation) for the static twist analysis for that tip. Table 4-1 lists the nominal camera pairs used to view each tip. Figure 4.1 shows a representative simultaneous view of solar array tips A and B from cameras B and D. The views from the two cameras are multiplexed onto the frame, which is performed by combining the center half of the two cameras' FOVs into a single frame.

**Table 4-1 Required Camera Pairs to View Solar Array Tips for the Static Twist Analysis**

<b>HST Solar Array Tips [SA Spreader Bar Location]</b>	<b>PLB Camera Combination: HST -V3 forward</b>	<b>PLB Camera Combination: HST +V3 forward</b>
A&B [+V2,-V3]	B&D	C&D
C&D [+V2,+V3]	A&B	A&C
G&H [-V2,+V3]	C&D	B&D
E&F [-V2,-V3]	A&C	A&B

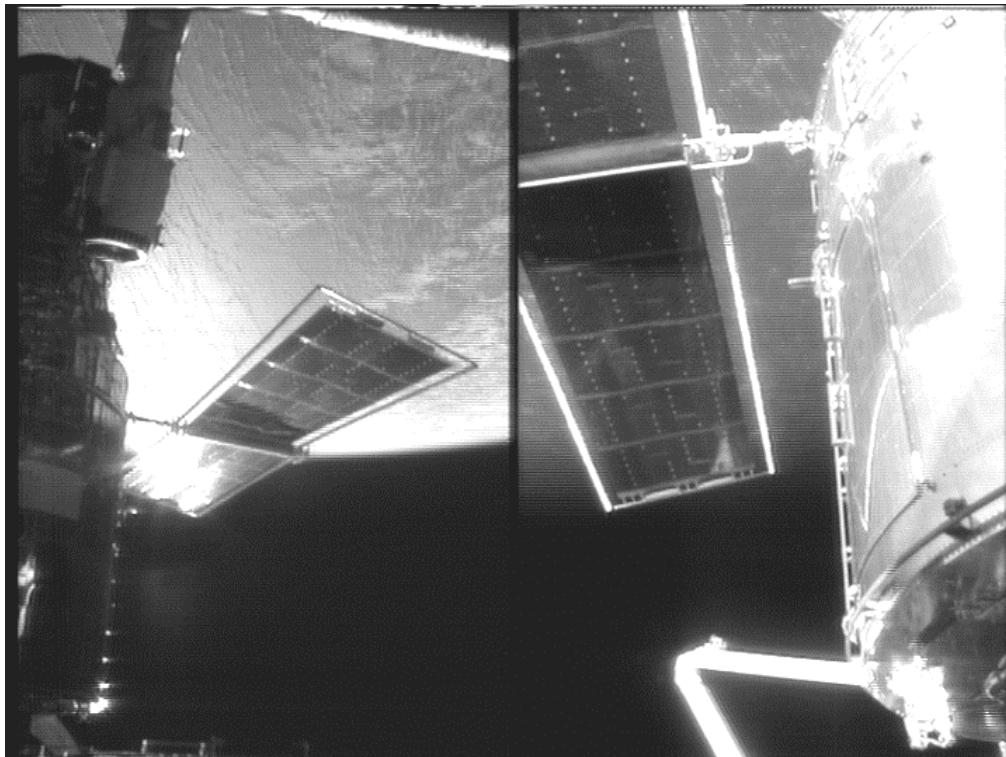


**Figure 4.1 Multiplexed video showing simultaneous view of HST solar array tips A & B from cameras B and D.**  
(left view is from camera D, right view is from camera B)

Both the FOV and the pointing angles for each camera view are used to define the initial camera setups to be used for acquiring imagery of solar array position. Each pair of camera views and settings required to image a specific array tip for static twist analysis was incorporated into a collection of views and procedures called a storyboard. Appendix D contains the storyboards for all tip analyses. In addition to the primary views, a pair of backup camera views was chosen for each tip. The backup views were to be used in case a primary camera was not available or was obstructed.

#### **4.1.2.3 Lighting**

An analysis of the expected lighting conditions during the static twist analyses, selected solar array motion analyses, and selected HST surveys was conducted with the assistance of the JSC GRAF. The lighting analysis was used for imagery data acquisition planning and as an aide to real-time imagery acquisition.

The lighting conditions were simulated for an STS-82 launch date of February 13, 1997. (The actual launch occurred two days earlier on February 11, 1997.) An Orbiter attitude of -ZLV-XVV was used with an altitude of 313 nautical miles and an orbital inclination of 28.5 deg. The range of solar beta angles (inclination angle plus declination angle) was 9.87 to 17.23 deg.

Static twist analyses occurred during crew sleep periods 3, 4, 5, 6, and 7. A daylight pass during crew sleep period number 5 was chosen as representative of the lighting conditions for all required static twist analyses based on the range of solar beta angles for each crew sleep period. The lighting analysis was performed for the actual static twist analysis data acquisition views for each array tip plus the rotation view.

Results indicated that for each camera view, there would be periods of acceptable and unacceptable lighting. Unacceptable lighting would be conditions in which the sun would shine directly into the camera, or unacceptable specular reflection off the HST would reflect into the camera. In general, the lighting was poor (i.e., excessive reflection or direct sun shining into cameras) at sunrise and near sunset with periods of 20 to 50 minutes of good lighting in between. Since the lighting conditions were to vary, it was suggested that the camera aperture control be set on manual and adjusted by the instrumentation and communication officer (INCO), who controlled the PLB cameras from Mission Control.

See Appendix E for a detailed description of the lighting analysis that was performed for SM-2 solar array imagery acquisition.

#### **4.1.3 Imagery Acquisition Plan**

After selecting the cameras and performing the necessary viewing and lighting analyses, we developed a plan for the acquisition of imagery. The following procedures were implemented for meeting the imagery acquisition requirements:

### **Procedures for imagery data acquisition and control of the cameras**

- All analysis data would be acquired from the Shuttle's CTVC and MLA PLB cameras.
- Video from the Shuttle PLB cameras would be obtained during the crew sleep periods.
- The INCO console in Mission Control would control the cameras.
- An IS&AG representative would assist the INCO console in the imagery acquisition.
- The procedures as described above and in the imagery acquisition storyboards would be used to collect the data.

### **Procedures for setting up the views and acquiring imagery**

- Simultaneous, full FOV images would be captured with the solar array in the center of the image. (The full FOV images were required to capture a sufficient number of reference points for determining camera pointing and EFL.)
- The video from the camera pairs would be multiplexed. (Multiplexed views ensure that the array tips are imaged simultaneously, but this is accomplished at the expense of reducing the FOV.)
- Multiplexed video of each tip would be acquired for at least 30 seconds to get sufficient imagery to determine the at-rest tip positions. (Getting 30 seconds would provide a safe margin for obtaining 20 seconds of usable video.)
- Additional imagery, centered on the bottom end of the aft shroud of the HST, would be gathered each sleep period for determining the precise rotational orientation of the HST.

#### **4.1.4 Imagery Analysis Plan**

A number of operational procedures were developed for processing and analyzing the video data, as well as distributing the analysis results. These procedures included data capture procedures in IS&AG's video digital analysis system (VDAS) laboratory, detailed procedures for analyzing the video data, and procedures for delivering the results to the FS&S Project.

VDAS laboratory procedures included the general setup of the communications, video, and computer systems for data capture, analysis, and transfer. Communications systems procedures included the setup of the digital voice intercommunication system and establishment of protocols for communicating with Mission Control and the HST Mechanical Systems console in the Space Telescope Operations Control Complex. Video configuration involved establishing the routing of the video and audio signals from the JSC video control room to the VDAS laboratory and then to the appropriate videotape recorders. The Orbiter downlink of camera views selected at the INCO console, based on the imagery acquisition plan, were directly recorded in the VDAS and used in the real-time analyses.

Detailed analysis procedures involved establishing standardized methods for using the image analysis software and the logistics of coordinating the work of multiple analysts. Determining the 3D positions of all eight array tips within the required 8-hour timeframe required extensive planning and coordination. The following steps summarize the operational procedures developed to perform the analysis:

1. The downlink videos of the camera views selected at the INCO console are digitally recorded in the VDAS laboratory. The views included the multiplexed and non-multiplexed views of each tip. The multiplexed views are recorded for approximately 30 seconds.

2. The digital video frames are analyzed on a computer workstation where the tip positions and control points are selected using an image analysis package. Control points are selected from the non-multiplexed views to provide camera pointing and EFL information, while the tip positions are acquired from the multiplexed views. Note that a slight correction factor is applied to the tip coordinates in the multiplexed views. The multiplexed view correction is required because the two views do not always equally occupy exactly one-half of the image. Instead, one camera view usually occupies slightly more of the multiplexed view than the other. The multiplexing correction factor for each camera only needs to be calculated once and is obtained before the HST rendezvous and grapple.
3. The tip and control point positions are entered into the phototheodolite program for the determination of the 3D tip positions. Each tip location is measured four times, with 5 seconds of video separating each measurement, i.e., the video stills chosen from the 30 seconds of video are spaced 5 seconds apart. An average of these four measurements is then calculated. Two analysts measure each tip-pair twice (for a total of four measures per tip-pair-per flight day) to help mitigate any systematic errors (e.g., analyst selection bias) and/or random errors.
4. The tip positions (in HST coordinates) resulting from the static twist analysis are then electronically mailed to GSFC HST engineers.

## **4.2 Imagery Acquisition for Solar Array Motion Analysis**

The planning activities for acquiring adequate imagery to meet the solar array motion analysis measurement requirements presented in Sections 2.0 and 3.2 are described in the following sections.

### **4.2.1 Imagery Acquisition Requirements**

The imagery acquisition requirements for the solar array motion analysis differed from those for the static twist analysis in that only a single camera was required for each array motion measurement and no reference points were required in the FOV. Although only a single camera view was required for each solar array motion analysis measurement, multiple camera views, in combination, were required to characterize certain solar array motion analysis events. For example, the measurement of the motion of a particular tip during the rotation of the HST would require one camera view for measuring motion during the beginning of the rotation, and another camera to measure motion at the conclusion of the rotation. In this section, the imagery acquisition requirements for solar array motion analysis are defined, and the rationale is described. These requirements were the basis of acquisition planning. The solar array motion analysis acquisition requirements were as follows:

1. Camera views were required to be set up for the planned VRCS-induced solar array motion measurement on Flight Day 3.

*Rationale:* On Flight Day 3, sufficient imagery of an array tip would be acquired to ensure that at least one VRCS attitude thruster firing event occurs. The VRCS thruster firing would excite the array, and the resulting motion of the array would then be measured.

2. Imagery for the planned solar array motion measurement of Flight Day 3 was to be acquired and downlinked for analysis at least 8 hours before the EVA.

*Rationale:* IS&AG determined that the solar array motion analysis on Flight Day 3 would require at least 8 hours to complete and the results were required before the beginning of the first EVA day.

3. Camera views would be acquired as necessary to measure solar array tip motion for the following events: reboosts, EVA activities, array slews, and HST repositioning events such as pivots and rotations.

*Rationale:* Imagery was required of the solar array motion events to provide for additional analyses to be defined post-mission.

4. For each solar array motion analysis, an unobstructed view of the entire end of the solar array (to include both tips) was required from at least one camera. Motion must be measured for both tips of the array separately.

*Rationale:* To determine the torsion or twisting of the arrays, measurements of the motion of both the inboard and outboard tips were required.

5. The angle between the camera line of sight and the solar array motion vector should be as close to 90 deg as possible (i.e., the array motion should be parallel to the image plane).

*Rationale:* Array motion can best be measured when the motion is parallel to the image plane. Accurate measurement of motion could not be obtained if the motion were perpendicular to the image plane.

6. The lighting conditions were required to be such that imagery of sufficient quality for analysis could be acquired.

*Rationale:* This requirement meant that the lighting must be sufficient for the array tip to be clearly visible in the imagery. For line tracking analysis techniques, there should be sufficient image contrast and no drastic lighting changes, such as shadows, moving across the edges of the array.

7. The camera was required to be set to the narrowest FOV that included both tips and would also include the full extent of the expected array motion.

*Rationale:* The narrower the FOV, the higher the image resolution—and the accuracy—of the motion tracking. Since the array motion was expected to have peak-to-peak displacements of less than 1 inch, high resolution was required to achieve accurate results.

#### **4.2.2 Imagery Acquisition Studies**

Technical studies were performed to select the appropriate cameras, evaluate alternate camera views, and evaluate the expected lighting conditions. These studies provided the information needed to produce an imagery acquisition plan for meeting the acquisition requirements. No additional camera selection analysis was performed for the solar array motion analysis, since the solar array motion analysis would use the same Shuttle PLB CTVC and MLA cameras as used for the static twist analysis. However, the

camera views required for the solar array motion analysis were quite different than those required for the static twist analysis, and were defined by a separate viewing analysis.

#### 4.2.2.1 Viewing Analysis

The viewing analysis identified the cameras and camera settings to use for the measurement of solar array motion. The camera views were simulated from JSC GRAF CAD drawings. Figure 4.2 shows a representative simulated view.

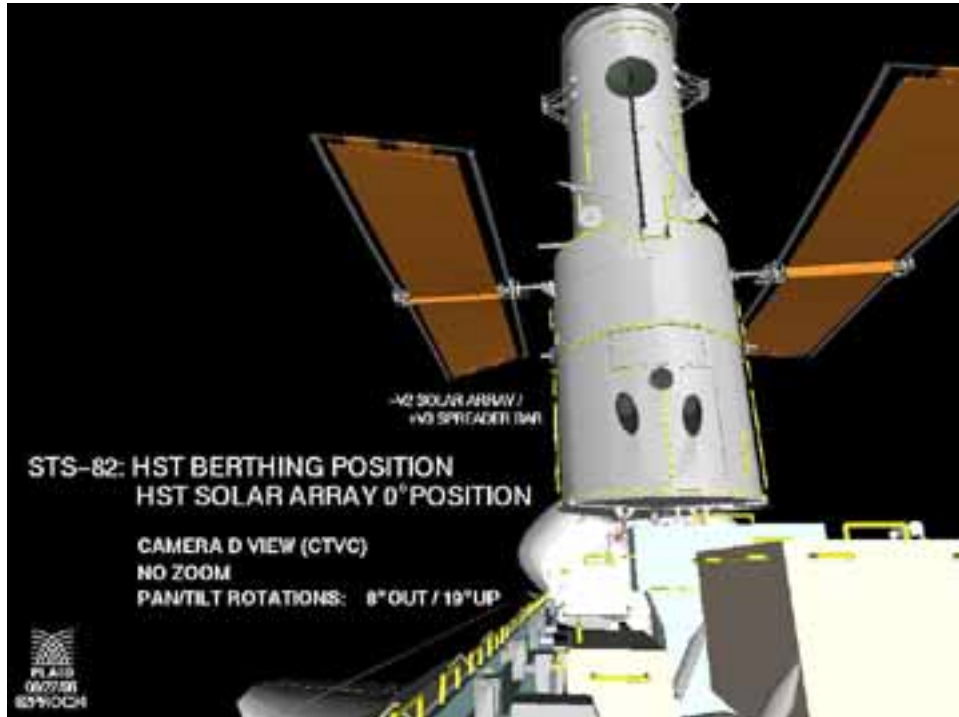


*Figure 4.2 Representative CAD view used in image acquisition planning.*

Views were chosen to image arrays such that out-of-plane array motion was nearly perpendicular to the camera line of sight. To achieve this, the camera chosen for viewing solar array motion was generally opposite the tips being imaged. For example, camera B was used to measure the tips oriented towards the port forward part of the Shuttle PLB.

Based on FS&S Project priorities, the analysis of solar array motion on Flight Day 3 was to be conducted for solar array tips A and B. Based on a comparison of measurement accuracies using different cameras, camera B was chosen as the best camera to image the tips A and B with the HST in the -V3 orientation. In addition, options were established for the possible contingency that the primary view of tips A and B from camera B might be unavailable. The views required for the VRCS solar array motion analysis were placed in the storyboards and included in the Photo/TV Checklist. Appendix D contains these views.

A set of views was also generated for acquiring imagery for the potential post-mission solar array motion analyses. The crew was to capture these views during HST repositioning events, solar array slews, reboots, and EVAs. See the storyboards in Appendix D and the Photo/TV Checklist for a detailed description of the views.

#### **4.2.2.2 Lighting**

See Section 4.1.2.3 and Appendix E for details of the lighting analysis.

#### **4.2.3 Imagery Acquisition Plan**

This section presents the procedures for the planned VRCS solar array motion analysis on Flight Day 3. The detailed procedures for the imagery acquisition by the crew of solar array motion during HST reboost, EVAs, solar array slews, and HST repositioning was included in the Photo/TV Checklist, and guidelines for the imagery acquisition are presented in the storyboards in Appendix D.

The data acquisition plan for the VRCS solar array motion analysis on Flight Day 3 was to capture a video sequence lasting several minutes of array tips A and B from camera B. The solar array spreader bar was to be centered vertically in the camera FOV to take approximately 75% of the horizontal FOV.

An assumption was made that, during the time for which video would be captured, at least one VRCS jet firing to control the Shuttle attitude would occur. Motion analysis would then focus on a 30-second video sequence, beginning 10 seconds before a VRCS jet firing and continuing for 20 seconds after the firing. FS&S Project engineers at GSFC, monitoring the Shuttle's VRCS jet firing telemetry, would inform IS&AG when VRCS jet firings occurred within the period of video data collection.

The camera setup and views would be controlled at the INCO console and a representative from the IS&AG would assist in the imagery acquisition. The solar array motion analysis data would be acquired immediately following the static twist analysis imagery acquisition during crew sleep on Flight Day 3.

#### **4.2.4 Imagery Analysis Plan**

The procedures for data capture in the VDAS were the same as for the static twist analysis, however, detailed procedures for analyzing the data and data analysis logistics were very different. The following steps summarize the procedure to analyze the solar array motion:

1. Record downlink video, showing a view of the entire spreader bar during an array excitation event, onto digital composite tape in VDAS.
2. Transfer the video data to a VAX mini-computer, and use line-tracking software to follow the motion of the tips of the arrays.
3. Transfer the results of the line tracking to a computer workstation and then calculate the array motion (tip displacement vs. time) using a spreadsheet-based motion analysis program.

Appendix F contains a detailed description of the operational procedures for the solar array motion analysis.

### **4.3 Mission Integration Activities**

Integration of the results of the imagery acquisition and analysis plans and requirements into the overall operations for the STS-82 HST servicing mission required an extensive effort. The critical activities included support and inputs into the flight data requirements, training the flight and ground crews in the

procedures for acquisition of data, and participation in simulations under the direction of Mission Operations. An important aspect of the mission integration effort was to communicate the HST static twist and solar array motion imagery acquisition to the operations community. In addition, IS&AG coordinated the inputs of the HST survey imagery acquisition requirements to the flight operations team.

#### **4.3.1 Flight Data File Inputs**

The Mission Operations FDF documented the operational procedures for the flight static twist and solar array motion imagery acquisition. The two primary FDFs for which IS&AG provided input, and which included the HST image acquisition requirements, were the Flight Plan timeline [Ref. 3] and the Photo/TV Checklist [Ref. 4].

##### **Flight Plan Timeline**

IS&AG coordinated with the flight activity timeline planning personnel to integrate the required times for imagery acquisition into the Flight Plan, and worked to ensure image acquisition occurred during daylight periods. It was also important to understand changes to the Flight Plan that could affect scheduled image acquisition. These Flight Plan changes were discussed with HST FS&S Project mission managers and IS&AG offered suggestions and approaches to accommodate these changes.

##### **Photo/TV Checklist**

The Photo/TV Checklist contains the detailed procedures for the crew to acquire on-orbit imagery. The checklist contains detailed instructions to the crew and ground controllers for setting up the camera equipment, positioning the cameras to the required views, and recording or downlinking the data. IS&AG provided the views and camera positioning settings (pan and tilt angles) for the Photo/TV Checklist. Photo/TV Checklist procedures were updated continuously as required by changes in HST operations plans.

For the static twist, the acquisition procedures were in the ground-control section of the Photo/TV Checklist, since it was not planned for the crew to acquire the imagery. However, in the event of a contingency in which ground control could not acquire the imagery, the procedures would have also been available for the crew to acquire the imagery. For the solar array motion, the Photo/TV Checklist contained the detailed storyboard information for the crew to follow to acquire the required imagery.

#### **4.3.2 Crew Training**

Three training sessions were held to familiarize the STS-82 crew with the imagery acquisition procedures. The first two sessions focused on those crew members responsible for the image acquisitions. The third session reviewed the final procedures and Photo/TV Checklist with the entire crew. The solar array motion analysis procedures included the image acquisition procedures for coverage of the berthing and positioning system installation, HST pivot and rotation sequences, nominal VRCS thruster firings, selected EVAs, and reboosts. The crew was trained in static twist analysis data acquisition as a backup contingency.

All data acquisition procedures were verified by IS&AG analysts, photo/TV trainers in Mission Operations, and the STS-82 crew in the JSC Virtual Reality Laboratory. The Virtual Reality Laboratory was able to accurately simulate views from the Shuttle PLB cameras. In the virtual reality simulations, the

crew followed the procedures outlined in the Photo/TV Checklist for setting up the camera views for each type of image acquisition event.

### **4.3.3 Joint Integrated Simulation Support**

To establish the readiness of all elements of a flight mission, Mission Operations conducts Joint Integrated Simulations (JISs). IS&AG supported three JISs that exercised the full complement of IS&AG support (i.e., static twist analyses, solar array motion analyses, and HST surveys). IS&AG also supported another JIS with on-call support only. The JISs were critical in testing and refining the data acquisition and data analysis procedures that would be used during the mission. Solar array motion and static twist analyses were performed using simulated CAD and video data. The simulation of data and logistical communications between Mission Operations and the HST FS&S Project was also demonstrated.

#### **Joint integrated simulation #1**

JIS #1 simulated the first two HST servicing EVAs on Flight Days 4 and 5. IS&AG's role in this JIS was to support the static twist analysis and VRCS-induced solar array motion analysis during the crew sleep period before EVA Day 2.

The HST SM-1 video from STS-61 was used for the static twist analysis during the JIS. However, one of the camera views was from the RMS elbow camera, which did not have a known 3D location. Since the location of the camera was required for the phototheodolite solution, this view provided inaccurate results. The tip positions were completed within 8 hours, but there were difficulties with electronic communication with GSFC. The communications problems were apparently the result of JSC network security problems and were remedied before the next JIS.

One of the simulated problems involved a real-time requirement to remove one of the PLB cameras for use as an EVA camera. IS&AG concluded that the loss of camera C would have the least impact to solar array analysis activities, and developed work-around procedures for static twist and solar array motion analysis data acquisition without camera C.

#### **Joint integrated simulation #5**

JIS #5 covered the fourth EVA and the HST release. IS&AG's role in this JIS was to support the static twist analysis during the crew sleep period before EVA Day 4 (Flight Day 7).

IS&AG performed the static twist analysis based on GSFC video from HST CAD graphics. Solar array tip positions were measured for tips A, B, E, and F. However, due to a lack of control points in camera B and C views, positions for tips C, D, G, and H could not be measured. As a result, requirements and methods were identified for obtaining control points for the camera B and C views. The turnaround time for the analysis was within 8 hours.

IS&AG also conducted a solar array motion analysis based on a CAD graphic video simulating solar array motion during the VRCS excitation event. IS&AG successfully determined the amplitude and frequencies of the simulated tip deflections within 8 hours.

## **Joint integrated simulation #2**

JIS #2 covered HST rendezvous and grapple and the first EVA day. IS&AG's role in this JIS was to support the static twist analysis and VRCS-induced solar array motion analysis during the crew sleep period before EVA Day 1 on Flight Day 3.

IS&AG conducted the static twist analysis based on GSFC video from HST CAD graphics. These graphics were of higher quality than those used for JIS #5. From the video, HST solar array tip positions for tips A, B, C, and D were determined, although the uncertainty was large due to an insufficient number of control points. Additional reference points were needed in the views of the aft solar array tips from cameras B and C. (Additional control points would be available in time for the mission.) The turnaround time for the analysis was within 8 hours.

Positions for solar array tips E, F, G, and H could not be determined due to missing camera views for the E and F tips and lack of control points needed to determine the G and H tip positions from camera C. In fact, the view of the starboard aft tips (G/H in -V3 orientation) from camera C could not be used because there were no control points in the FOV. The image acquisition procedures were changed to use camera D and (B or A) instead of camera D and C for viewing the G/H tips.

IS&AG conducted a solar array motion analysis based on a CAD graphic video produced by GSFC simulating solar array motion during the VRCS excitation event. IS&AG successfully determined the amplitude and frequencies of the tip deflections within 8 hours.

The two-week period between JIS #2 and the Shuttle launch and capture of HST were used to resolve the outstanding issues, make the procedures more efficient, and perform additional training and rehearsals.

## **Principal benefits**

The JISs were highly beneficial to the successful accomplishment of the real-time analyses. The principal benefits were:

- Control points were not adequately available for the analyses. This led to additional control points being defined and changes in planned camera selections for analysis of selected tips.
- It was demonstrated that the required analyses could be performed within the required 8-hour time frame.
- Logistics and communications issues were identified and resolved.
- A problem was identified with the phototheodolite program at high tilt angles. This problem was corrected before the mission.
- A potential problem with the RMS obscuring views of the solar array tips was discovered. Alternate views and backup procedures were developed to compensate for the problem.

## 5. REAL-TIME MISSION OPERATIONS AND ANALYSES

This section describes the real-time and near-real-time support during the STS-82 mission. This support included the VDAS lab operations, static twist and solar array motion data acquisition, and analyses conducted during the HST servicing mission from February 11 to 19, 1997.

The STS-82 launch of Discovery (OV-103) occurred on Tuesday, February 11, 1997 at 3:55:17 a.m. eastern standard time (042:08:55:17 Coordinated Universal Time [UTC]). The HST grapple occurred on Flight Day 3 at approximately 044:08:30 UTC, and the HST release occurred on Flight Day 9 at approximately 050:06:41 UTC. The STS-82 mission ended with the landing of Discovery at Kennedy Space Center on February 21, 1997. During the mission, IS&AG supported all planned and unplanned static twist and solar array motion analysis activities, as well as HST survey activities.

Table 5-1 presents the key image acquisition and analysis events that occurred during the mission. It includes events for which real-time analysis was conducted as well as events that were recorded for post-mission analysis. HST surveys were performed during the crew sleep periods starting with Flight Day 3 and ending with Flight Day 8. In addition, a survey of the +V2 side of the HST was conducted on Flight Day 4.

*Table 5-1 Image Acquisition and Analysis Events*

<b>Flight Day</b>	<b>Image Analysis Event</b>	<b>Approximate Time UTC (day, hour, and minute)</b>	<b>Approximate Mission Elapsed Time (MET) (day, hour, and minute)</b>	<b>Orientation (Side facing forward)</b>
3	Survey	044:22:00	02:13:00	-V3
	STA (baseline)	044:22:56	02:14:00	-V3
	SAMA (VRCS)	044:22:56	02:14:00	-V3
4	Survey	045:10:30	03:01:30	+V2
	Survey	045:22:00	03:13:00	-V3
	STA (update #1)	045:22:56	03:14:00	-V3
5	<i>SAMA (Rotate)</i>	046:11:02	04:02:06	-V3 to +V3
	Survey	046:22:00	04:13:00	-V3
	STA (update #2)	046:22:56	04:14:00	-V3
6	Survey	047:22:00	05:13:00	+V3
	STA (update #3)	047:22:56	05:14:00	+V3
7	Survey	048:22:00	06:13:00	+V3
	STA (update #4)	048:22:56	06:14:00	+V3
8	<i>SAMA (Airlock Depressurization)</i>	049:03:12	06:18:16	+V3
	<i>SAMA (Pivot)</i>	049:08:35	06:23:39	-V3
	<i>SAMA (Reboost)</i>	049:10:29	07:01:33	-V3
	Survey	049:22:00	07:13:00	-V3
	STA (update #5)	049:22:56	07:14:00	-V3

\*Events in italics were analyzed post-mission.

\*STA: static twist analysis, SAMA: solar array motion analysis

## 5.1 VDAS Laboratory Operations

The VDAS laboratory was staffed continuously from Flight Day 3 until the release of the HST on Flight Day 9. Personnel worked on a three-shifts-per-day schedule, with at least two analysts per shift. The primary data analysis shift coincided with the crew sleep period, when the static twist analysis, and the analysis of the VRCS-induced solar array motion, was performed. During this shift, an IS&AG representative assisted the JSC Mission Control INCO in the acquisition of the video imagery. Analysts in VDAS coordinated with the IS&AG analyst at the INCO console to obtain the best views, with the best lighting, for analysis. As views were obtained, the VDAS staff recorded the imagery onto digital recorders and began the analysis procedures. At the conclusion of the analysis, the results were sent electronically to HST FS&S Project engineers at GSFC.

The other shifts monitored the mission status and the video downlink. Solar array motion imagery was recorded and provided to the data analysis shift. An activity log was maintained and daily reports were prepared that summarized the results from each day's static twist and solar array motion analyses. At the conclusion of each shift, briefings were conducted to inform the following shift of significant events and upcoming tasks. All raw data and results were saved onto multiple computer disks as backups. See Appendix F, Daily Mission Reports, for additional details of IS&AG's real-time support.

## 5.2 Static Twist Analysis

Six static twist analyses were performed during the mission. Static twist analyses were performed before each of the five EVAs, starting with Flight Day 3, and concluded with a final analysis prior to Shuttle release of the HST. All static twist data acquisition and analysis occurred during the crew sleep periods. The following sections present a description of the data acquisition and analysis activities, as well as the static twist results from the STS-82 mission.

### 5.2.1 Data Acquisition and Analysis

In general, the video acquisition occurred as planned. Data acquisition for all eight tips required approximately three complete daylight orbital passes (approximately 2.5 hours) each day. INCO personnel were instructed to pan and tilt the cameras to each predefined view of the solar array tips and to cycle through different camera exposure settings until adequate image contrast was obtained. However, imagery transmission to JSC was slowed due to intermittent loss of the Ku-band downlink. Due to Shuttle attitude and other orbital dynamics issues, the line of sight to the Tracking and Data Relay Satellite was frequently interrupted, thereby slowing the acquisition of video data at JSC.

The following deviations occurred from the planned acquisitions and analysis procedures:

1. Camera pairs used to acquire static twist imagery of certain array tips were modified to respond to variable and harsh lighting conditions. Poor lighting conditions caused array tips and control points to be difficult to distinguish from the background. The modifications from the original imagery acquisition were:
  - Cameras D and C were used to image the starboard forward solar array tips (tips E & F in -V3 forward orientation). Originally, cameras A and C were to be used.
  - Cameras D and B were used to image the starboard aft tips (tips G & H in -V3 forward orientation). Originally, cameras C and D were to be used.

2. Some cameras were obstructed from viewing specific solar array tips. The obstructions were caused by the aft bulkhead of the Shuttle and by the EVA manipulator foot restraint on the RMS. When these obstructions were in the imagery the precise location of the array tip within the image was estimated by extrapolating the bistem and the spreader bars in the image, and calculating their point of intersection. Estimating the tip position was not considered to have a serious effect on the analysis results, since multiple analysts were consistent to within 1 to 2 pixels in determining the tip intersection. The following array tips were obstructed during the mission:

- Tip A from camera D on Flight Day 4
- Tip A from camera D on Flight Day 5
- Tip H from camera B on Flight Day 5
- Tip B from camera B on Flight Day 6

Table 5-2 shows the camera views used for the static twist analysis on each flight day.

*Table 5-2 Camera Views Used for Each Array Tip on Each Flight Day*

<b>Flight Day</b>	<b>HST Orientation</b>	<b>Tip A&amp;B</b>	<b>Tip C&amp;D</b>	<b>Tip E&amp;F</b>	<b>Tip G&amp;H</b>
3	-V3 forward	D and B	A and B	D and C	D and B
4	-V3 forward	D and B	A and B	D and C	D and B
5	-V3 forward	D and B	A and B	D and C	D and B
6	+V3 forward	D and B	D and C	A and B	D and B
7	+V3 forward	D and B	D and C	A and B	D and B
8	-V3 forward	D and B	A and B	D and C	D and B

The procedure used to analyze the 3D tip positions, for one array tip (G & H), is described in the following 17 steps, with examples:

1. Acquire HST rotation view and required static twist analysis views. (See Figure 5.1.)

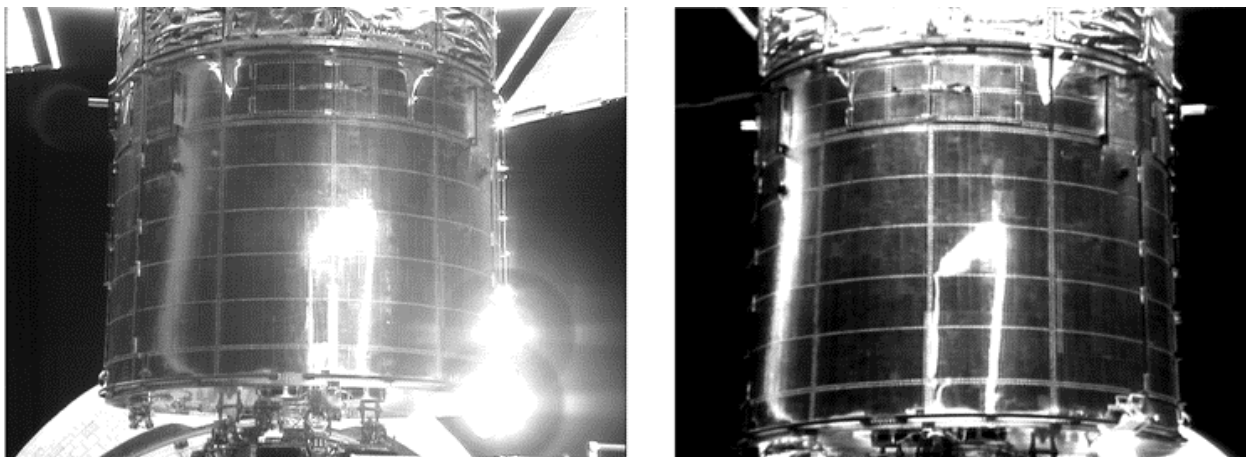


*Figure 5.1 Rotation view from cameras D (left) and A (right).*

- Digitize, label, and correct aspect ratio of rotation image.
- Select reference points from rotation image. (Note: Rotation calculations were performed only once per day.) (See Figure 5.2.)

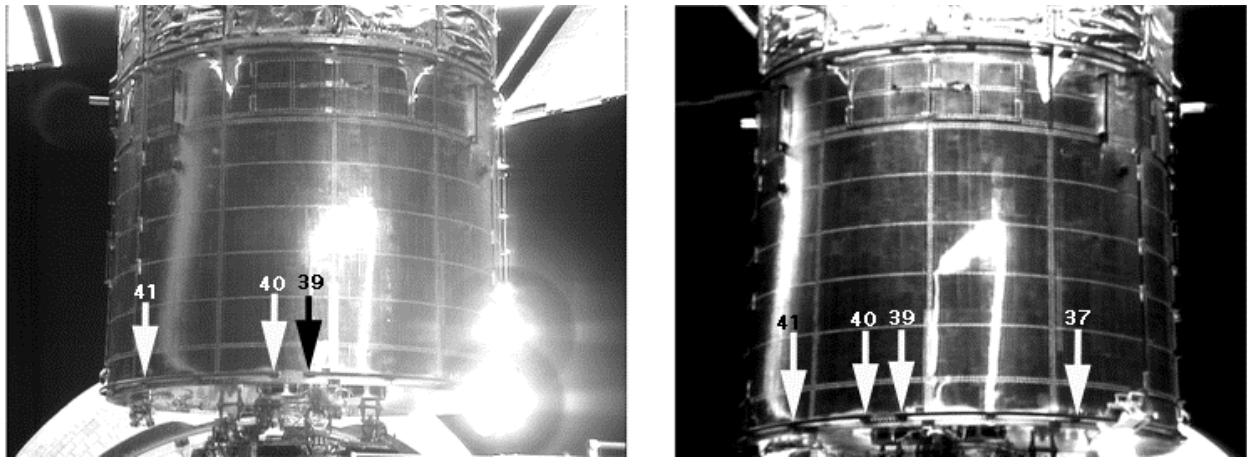


Figure 5.2 Reference points on rotation images.

- Enter reference point ID numbers onto the data collection sheet and insert the reference image coordinates into the rotation calculation spreadsheet. (See Figure 5.3.)

Identify Rotation Camera 1 here -->					<b>D</b> Must be one of: (A, D)			Identify Rotation Camera 2 here -->					<b>A</b> Must be one of: (A, D)					
Identify image x coordinates for Bottom of HST								OPTIONAL Identify image x coordinates for Bottom of HST										
Left side -->	201	Right side -->		512				Left side >	146	Right side -->		514						
	201			512					146			514						
<b>D</b>					589	71.5	446	camera 1	<b>A</b>				589	-71.5	446	camera 2		
Identify rotation references for Camera 1 below								Identify rotation references for Camera 2 below										
image coord.s				orbiter coordinates				image coord.s				orbiter coordinates						
Reference p ID	x	y	xerr	yerr	X	Y	Z	Description of reference point	REF NO	Referenc pt ID	x	y	xerr	yerr	X	Y	Z	Description of reference point
41	325	150	325	150	1095.9753	65.0502	499.999	HR1D	1	39	250	171	250	171	1071.005	30.8213	499.999	HR1A
40	376	157	376	157	1076.6013	42.353617	499.999	HR1D	2	37	327	189	327	189	1069.917	-27.903	499.999	HR1A

Figure 5.3 HST rotation calculation input sample.

- Select imagery to be used for phototheodolite calculation from acquired video. This should include a full FOV image from each camera, as well as four multiplexed views, each separated by 5 seconds. (See Figure 5.4.)
- Digitize, label, and correct aspect ratios of images.

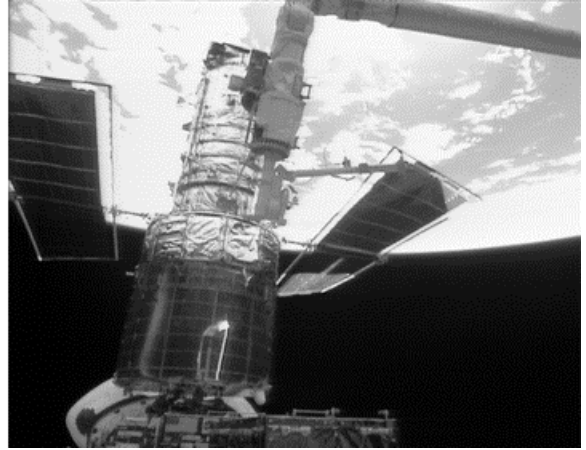
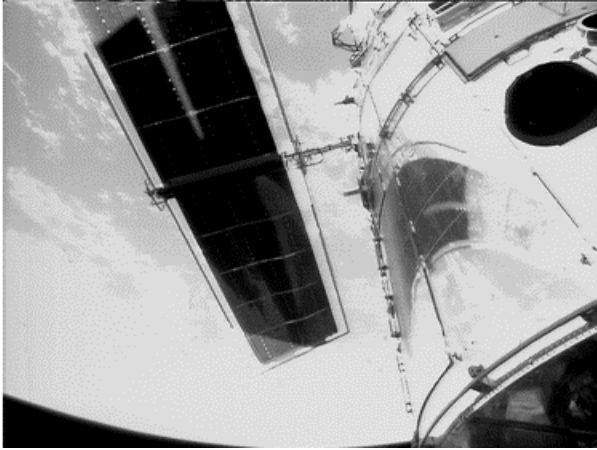


*Figure 5.4 HST full FOV images from cameras B (left) and D (right).*

7. Select reference point image coordinates from full FOV images. (See Figure 5.5.)

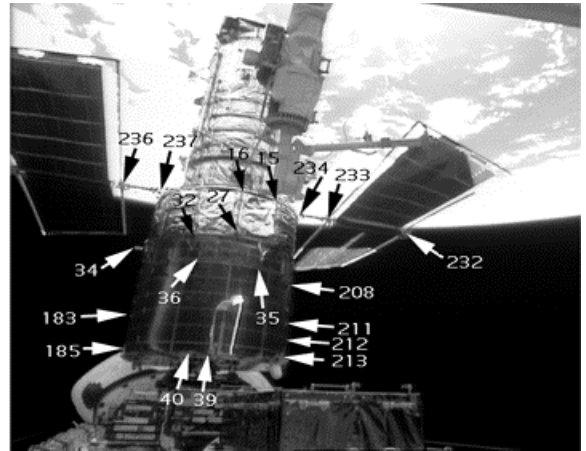
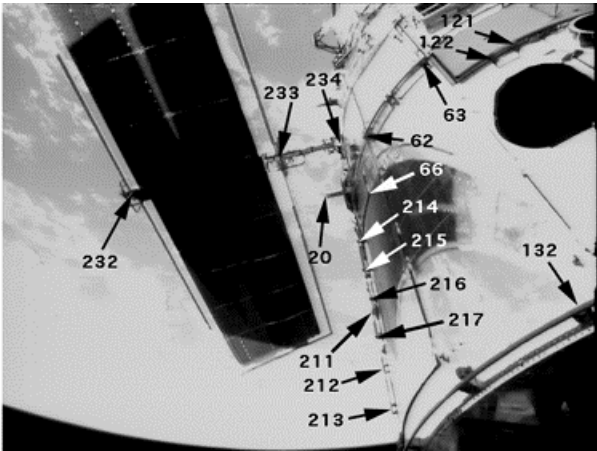


*Figure 5.5 HST views with identified reference points.*

8. Enter reference point ID numbers on data entry sheet.
9. Select solar array tip image coordinates from multiplexed views. (See Figure 5.6.)
10. Enter reference point image coordinates into user input spreadsheet.

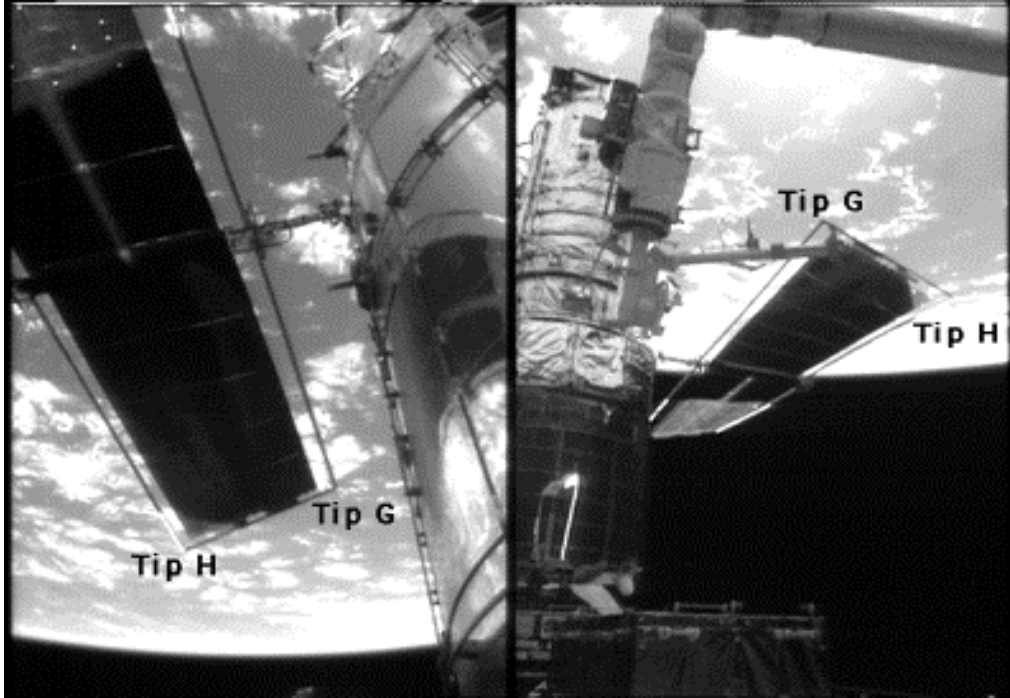


Figure 5.6 Multiplexed images of HST solar array tips.

11. Enter reference point ID numbers from data entry sheet into user input spreadsheet. (See Figure 5.7.)

Reference Points for Twist Image Points of Interests																										
Outputs																										
Camera 1	median																	Camera 2	median							
	azim.	166.17																	azim.	25.71						
	elev.	50.33																	elev.	25.90						
	Focal Length	485.34																	Focal Length	469.20						
	HFOV	73.13																	FOV	74.99						
Inputs																										
Camera 1 -	<b>B</b>																	Camera 2 --	<b>D</b>							
	image coord.s				orbiter coordinates														image coord.s				orbiter coordinates			
Reference ID	x	y	xerr	yerr	X	Y	Z	Description reference point	REF. NO	Reference point	x	y	xerr	yerr	X	Y	Z	Description reference point								
132	694	183	694	183	1218.3509	-47.7761	499.999	HR1B	1	40	184	108	184	108	1067.7145	20.603646	499.999	HR1D								
212	481	80	481	80	1135.8513	-83.32756	529.904	HR7	2	39	199	107	199	107	1065.529	7.9729159	499.999	HR1A								
211	473	124	473	124	1135.8513	-83.32756	547.744	HR7	3	34	126	228	126	228	1162.5023	97.847392	636.594	TRUNNION								
217-s1	459	161	459	161	1160.2573	-86.69067	546.959	HR8-standoff	4	213	275	107	275	107	1135.8513	-83.32756	512.289	HR7								
215-s1	445	236	445	236	1160.2573	-86.69067	582.629	HR9-standoff	5	212	276	123	276	123	1135.8513	-83.32756	529.904	HR7								
214-s1	439	267	439	267	1161.7686	-86.48449	600.459	HR9-standoff	6	211	277	138	277	138	1135.8513	-83.32756	547.744	HR7								
20	404	320	404	320	1163.897	-97.64763	636.594	TRUNNION	7	35	250	207	250	207	1071.2953	-32.44261	603.789	FGS#2								
233	350	361	350	361	1150.1203	-128.9967	716.594	S/A (-V2, cell side)	8	36	188	216	188	216	1070.8403	31.327736	603.789	FGS#2								
66	452	319	452	319	1181.6426	-77.90474	603.789	FGS#1	9	32	184	240	184	240	1074.8133	39.128273	631.719	HR2A								
62	450	386	450	386	1194.2957	-70.92797	631.719	HR2D	10	27	227	247	227	247	1049.8425	-0.708869	636.594	KEEL								
63	513	468	513	468	1220.7508	-44.10078	631.719	HR2D	11	15	265	280	265	280	1076.2448	-41.97538	694.644	BAY8								
122	594	466	594	466	1228.798	-28.03278	598.844	HR14	12	16	232	290	232	290	1065.0757	-1.45609	694.644	BAY8								
121	618	479	618	479	1230.8756	-21.23112	598.844	HR14	13	233	316	260	316	260	1150.1203	-128.9967	716.594	S/A (-V2, cell side)								
					--	--	--	--	14	236	113	299	113	299	1148.2797	128.99672	716.594	S/A (+V2, cell side)								

Figure 5.7 Reference point data entry spreadsheet sample.

12. Insert solar array tip image coordinates into user input spreadsheet. (See Figure 5.8.)

Twist Points (S/A Tips)							
INPUT							
Twist Point (Tip 1)				Twist Point (Tip 2)			
Camera 1 left	<i>D</i>	Camera 2 right	<i>B</i>	Camera 1 left	<i>D</i>	Camera 2 right	<i>B</i>
Muxed image coord.s		Muxed image coord.s		Muxed image coord.s		Muxed image coord.s	
x	y	x	y	x	y	x	y
226.5	373.5	522	159	322	313	410	121
Mux factor		Mux factor		Mux factor		Mux factor	
179.5	2.5	-179	4	179.5	2.5	-179	4
Unmuxed image coord.s		Unmuxed image coord.s		Unmuxed image coord.s		Unmuxed image coord.s	
406	376	343	163	501.5	315.5	231	125

Figure 5.8 Tip point data entry spreadsheet sample.

13. Initiate camera pointing and focal length iterative solution.
14. Examine residuals from solution. If outliers exist, remove (or re-measure) and repeat iterative solution.
15. Initiate Monte Carlo error analysis.
16. Enter results into daily compilation file. (See Figure 5.9.)

	HST Coordinates (in.)				Orbiter Coordinates (in.)						Rotation (deg.)		Analysis Date & Time
	<i>V1</i>	<i>V2</i>	<i>V3</i>	<i>Err</i>	<i>Xo</i>		<i>Yo</i>		<i>Zo</i>		Mean	+/-	
	Mean	Mean	Mean	+/-	Mean	+/-	Mean	+/-	Mean	+/-	Mean	+/-	
Tip1	363.34	-134.05	230.06	4.26	917.29	2.82	-130.83	1.94	759.94	2.54	-180.80	0.35	11/11/97 12:54
Tip2	323.70	-239.52	232.55	4.43	913.33	3.03	-236.25	2.47	720.30	2.09	-180.80	0.35	11/11/97 12:54

Figure 5.9 Tip calculation and error analysis results sample.

17. E-mail the tip positions (in HST coordinates) to HST FS&S Project.

### 5.2.2 Results for Solar Array Tip Coordinates

For each static twist analysis, the tip position (in HST coordinates), the uncertainty in each tip measurement, the number of analyses per tip, the camera pair used per tip, and the camera pointing information (pan and tilt angles) were reported. Table 5-3 presents a compilation of the measured solar array tip positions on each flight day.

**Table 5-3 Real-Time Static Twist Results**

<b>Flight Day 3</b> <b>SM2 Hubble Solar Array Tips Coordinates</b> (all units are in inches)						
<b>S/A Tip</b>	<b>No. of Analyses</b>	<b>Average V1</b>	<b>Average V2</b>	<b>Average V3</b>	<b>Mission Average Std. Dev. (1 <math>\sigma</math>)</b>	<b>Corrected Avg. Std. Dev. of the Mean (1 <math>\sigma</math>)</b>
A	4	342.2	134.0	-228.6	0.6	1.8
B	4	316.4	246.9	-230.4	0.7	2.0
C	3	318.1	125.0	243.1	0.9	2.5
D	3	299.1	233.2	239.8	0.8	2.6
E	1	297.9	-130.5	-239.9	0.9	2.1
F	1	328.4	-241.3	-237.0	1.2	2.4
G	4	337.7	-129.0	230.3	0.9	1.7
H	4	303.9	-231.3	232.1	0.8	1.9

<b>Flight Day 4</b> <b>SM2 Hubble Solar Array Tips Coordinates</b> (all units are in inches)						
<b>S/A Tip</b>	<b>No. of Analyses</b>	<b>Average V1</b>	<b>Average V2</b>	<b>Average V3</b>	<b>Mission Average Std. Dev. (1 <math>\sigma</math>)</b>	<b>Corrected Avg. Std. Dev. of the Mean (1 <math>\sigma</math>)</b>
A	8	335.7	136.3	-230.8	0.6	1.7
B	8	311.6	248.9	-228.0	0.7	1.9
C	6	327.0	125.2	242.5	0.6	1.7
D	6	306.0	231.8	235.9	0.6	1.7
E	2	303.1	-128.5	-236.5	0.9	1.6
F	2	330.6	-233.5	-237.0	1.0	1.7
G	4	338.6	-128.9	225.7	0.7	1.4
H	4	304.1	-231.6	225.2	0.8	1.5

<b>Flight Day 5</b> <b>SM2 Hubble Solar Array Tips Coordinates</b> (all units are in inches)						
<b>S/A Tip</b>	<b>No. of Analyses</b>	<b>Average V1</b>	<b>Average V2</b>	<b>Average V3</b>	<b>Mission Average Std. Dev. (1 <math>\sigma</math>)</b>	<b>Corrected Avg. Std. Dev. of the Mean (1 <math>\sigma</math>)</b>
A	6	337.1	131.9	-236.2	0.5	1.8
B	6	313.6	244.2	-237.2	0.6	1.9
C		N/A	N/A	N/A		
D		N/A	N/A	N/A		
E	4	281.3	-134.4	-225.4	0.6	1.6
F	4	309.9	-238.5	-226.6	0.6	1.7
G	3	361.6	-125.5	224.6	0.8	2.3
H	3	327.5	-228.6	229.2	1.2	2.8

**Table 5-3 Real-Time Static Twist Results (continued)**

<b>Flight Day 6</b> <b>SM2 Hubble Solar Array Tips Coordinates</b> (all units are in inches)						
S/A Tip	No. of Analyses	Average V1	Average V2	Average V3	Mission Average Std. Dev. (1 $\sigma$ )	Corrected Avg. Std. Dev. of the Mean (1 $\sigma$ )
A	4	326.7	127.3	-230.9	0.7	1.5
B	4	309.2	237.1	-232.0	0.8	2.0
C	4	331.3	130.8	235.7	0.5	1.7
D	4	310.1	239.6	235.7	0.5	1.7
E	3	286.6	-133.1	-232.3	0.8	1.7
F	3	309.7	-236.3	-224.8	0.8	1.7
G	3	358.3	-133.0	234.5	0.8	1.9
H	3	319.4	-239.1	235.3	0.8	2.0

<b>Flight Day 7</b> <b>SM2 Hubble Solar Array Tips Coordinates</b> (all units are in inches)						
S/A Tip	No. of Analyses	Average V1	Average V2	Average V3	Mission Average Std. Dev. (1 $\sigma$ )	Corrected Avg. Std. Dev. of the Mean (1 $\sigma$ )
A	3	335.9	126.9	-229.4	1.0	1.8
B	3	317.6	236.8	-231.0	1.1	2.2
C	4	324.4	130.9	233.2	0.8	1.8
D	4	302.6	240.6	231.7	0.8	1.9
E	4	304.5	-132.7	-235.5	0.8	1.7
F	4	327.2	-236.7	-227.4	0.8	1.8
G	3	343.8	-132.7	235.4	0.8	1.8
H	3	304.7	-238.6	234.0	0.8	2.0

<b>Flight Day 8</b> <b>SM2 Hubble Solar Array Tips Coordinates</b> (all units are in inches)						
S/A Tip	No. of Analyses	Average V1	Average V2	Average V3	Mission Average Std. Dev. (1 $\sigma$ )	Corrected Avg. Std. Dev. of the Mean (1 $\sigma$ )
A	4	309.1	130.8	-235.6	0.6	1.7
B	4	286.0	241.2	-234.1	0.6	1.9
C	4	347.6	128.5	237.6	0.8	1.8
D	4	327.3	236.0	233.2	0.8	1.8
E	4	279.7	-132.5	-230.4	0.7	1.7
F	4	310.4	-238.9	-232.1	0.8	1.9
G	4	363.8	-127.9	229.1	0.8	1.8
H	4	329.4	-232.6	233.2	0.9	2.1

A high camera tilt angle (>90 deg) during image acquisition caused difficulties in the analysis of the C & D tips on Flight Day 5. Four separate analyses were performed, none of which converged on a solution with acceptable errors. HST FS&S Project engineers were notified of the problem, and agreed to accept analysis of three of the four tips. The image acquisition procedure was subsequently modified so that the camera tilt angle would be as low as possible for subsequent static twist analyses.

### **Estimates of the uncertainties in the tip locations**

Table 5-3 lists the average tip coordinates (V1, V2, V3), which are the averages of multiple analysts' results. The uncertainty value provided during the mission, listed in the column "Mission Average Std. Dev.", was determined as the weighted average of the root mean square uncertainty estimates computed for each tip coordinate. It was calculated by first computing the root mean square (spherical) uncertainty estimate for each separate tip based upon one standard deviation value in each coordinate (V1, V2, V3) axis. Next, the average root mean square uncertainty was computed over the "n" number of multiple calculations for the specific tip during the flight day. Finally, the average root mean square value was divided by the square root of the number of tip calculations (n) used to compute the average, as shown in the following equation:

$$Mission\_Std.Dev = \frac{1}{\sqrt{n}} \left( \frac{\sum_{n=1}^n \sqrt{(1\sigma V1_n)^2 + (1\sigma V2_n)^2 + (1\sigma V3_n)^2}}{n} \right)$$

Post-mission analyses revealed two problems with the Monte Carlo implementation. First, a software coding error was discovered in the Monte Carlo simulation resulting in a general underestimation of the computed tip errors. Second, dividing the average root mean square tip uncertainties by the square root of the number of calculations was not statistically correct. After correcting these errors in the Monte Carlo routine, all HST tip errors were recalculated, based on a subset of the original analyst results. The corrected error estimates were then used to compute the statistical sample standard deviation of the mean in each axis ( $\sigma_{MEANV1}$ ,  $\sigma_{MEANV2}$ ,  $\sigma_{MEANV3}$ ) for the multiple calculations of the tip on the specific flight day. The root mean square (spherical) uncertainty estimate was then computed from the three axial standard deviations of the mean (see equation below) and is presented in the last column of Table 5.3.

$$Corrected\_Std.Dev. = \sqrt{(1\sigma_{MEAN}V1)^2 + (1\sigma_{MEAN}V2)^2 + (1\sigma_{MEAN}V3)^2}$$

Despite the correction of the software and algorithmic errors, statistical comparisons of the results obtained from multiple-day calculations revealed the variability in the coordinates exceeded the 3-sigma ( $3\sigma$ ) level the Monte Carlo simulations predicted. This indicated that the Monte Carlo error simulation did not adequately model the true coordinate uncertainties. A standard method of uncertainty calculation, based on the general law of error propagation, was employed in the post-mission photogrammetry analyses, discussed in Section 6.

### 5.2.3 Calculation of Solar Array Twist

The previous section described the results for the calculation of the coordinate positions of the tips of the solar arrays. Based on these position results, the offsets of the computed tip positions from the nominal solar array position of the tips were calculated. The geometric twists in the solar arrays are calculated from the offsets. The twist is determined by the amount that the two tips at an end of an array are offset (one tip below and one tip above) the nominal plane of the array. The nominal (non-twisted) plane is defined by the array mast and a longitudinal line midway between the two bistems.

Offset is calculated as the distance between the computed tip position and the nominal plane of the “non-twisted” array. The distance is measured in a direction perpendicular to the nominal plane. This technique accurately computes the offset of the measured tip from the nominal plane of the array regardless of slew angle and independent of the solar array length. Table 5.4 gives the perpendicular offsets of the measured tips from the nominal plane of the array.

*Table 5-4 Perpendicular Offset of Tips From Nominal Plane of Solar Arrays*

Flight Day	HST Orientation	Slew Angle (deg)	Computed Tip Location Relative to Nominal Solar Array Plane	Perpendicular Distance From Computed Tip to Nominal Solar Array Plane (all units are in inches)							
				Tip A	Tip B	Tip C	Tip D	Tip E	Tip F	Tip G	Tip H
3	-V3	-1.3	Above	14.4		6.2			10.7	15.4	
	Forward	-0.07	Below		11.4		12.9	19.8			18.4
4	-V3	0.1	Above	13.5		9.2			7.8	21.1	
	Forward	-1.3	Below		10.6		11.8	19.7			13.4
5	-V3	-0.4	Above	12.8		N/A			10.3	21.3	
	Forward	4.5	Below		10.7		N/A	18.3			13.1
6	+V3	1	Above	8.1		9.8			6.0	21.3	
	Forward	3.5	Below		9.4		11.4	16.6			17.6
7	+V3	-1.14	Above	8.7		11.6			7.2	23.9	
	Forward	-0.66	Below		9.6		10.2	15.6			15.2
8	-V3	4.85	Above	6.5		10.0			12.4	21.9	
	Forward	4.8	Below		16.7		9.9	18.3			12.8

Analysis of the results in Table 5-4 reveals the following observations about the geometry of the solar arrays:

1. Each tip pair is twisted such that one tip is above and the other is below the nominal plane of the array. None of the tip pairs deflected in a common direction from the nominal array plane.
2. Each of the solar array tip pairs has a different amount of inboard and outboard offsets.

3. Tips pairs A-B, C-D and G-H are similarly twisted, such that the inboard tip is above the nominal solar array plane, while the outboard tip is below the nominal solar array plane. Tip pair E-F is just the opposite; the outboard tip is above the nominal solar array plane, while the inboard tip is below the nominal solar array plane.

Solar array twist was calculated as the sum of the perpendicular offsets of a tip pair from its respective solar array, as computed in Table 5-4. Table 5-5 gives the computed solar array twists and the standard deviation values.

**Table 5-5 Solar Array Twists and Standard Deviations**  
(inches)

Flight Day	HST Orientation	Tip A/B		Tip C/D		Tip E/F		Tip G/H	
		Twist	Std. Dev.						
3	-V3 Forward	25.8	2.7	19.1	3.6	30.5	3.2	33.8	2.5
4	-V3 Forward	24.1	2.5	21.0	2.4	27.5	2.3	34.5	2.1
5	-V3 Forward	23.5	2.6	N/A	N/A	28.6	2.3	34.4	3.6
6	+V3 Forward	17.5	2.5	21.2	2.4	22.6	2.4	38.9	2.8
7	+V3 Forward	18.3	2.8	21.8	2.6	22.8	2.5	39.1	2.7
8	-V3 Forward	23.1	2.5	19.9	2.5	30.7	2.5	34.6	2.8
During Mission - Average		22.1		20.6		27.1		35.9	
During Mission - Std. Dev. of Mean			1.1		1.2		1.0		1.1

Comparisons and analyses of the solar array twists reveal the following:

1. Tip G-H has the highest level of twist.
2. A significant difference could not be detected between the calculated twists on Flight Days 3, 4, 5, and 8.
3. The twist of tips A-B, E-F, and G-H on Flight Days 6 and 7 are considerably different from the values for the remaining days. Only tips C-D are consistent with the other days. Our conclusion is that the real-time results for the tip twists on Flight Days 6 and 7 may have a bias, and that the probable cause could be attributed to the following:
  - Changes in HST Orientation: Before the Flight Day 6 measurement, the HST was tilted, rotated to a +V3 forward orientation, and tilted back to vertical. Before the measurements on Flight Day 8, the process was reversed to orient the HST to a -V3 forward orientation, as existed on Flight Days 3, 4, and 5. The phototheodolite calculations were based upon the assumption that the HST V1-axis was perfectly aligned with the Z-axis of the Orbiter's coordinate system. If this condition had not been maintained on Flight Days 6 and 7, a bias would have been introduced into the calculations.

- **Different Control Points and Cameras:** Different control points were used to resect different camera pairs during the Flight Days 6 and 7 tip calculations. Differences in the number of control points used, and their relative 3D distribution, may have increased or decreased the quality of the camera solution.

Additional static twist calculations were completed post-mission. Section 6.1 describes the post-mission analysis approach, results, and comparisons to real-time results.

### **5.3 Solar Array Motion Analysis**

Two solar array motion analyses were performed in real time during the mission. The first was the planned solar array motion analysis on Flight Day 3, and the second was the unexpected solar array slew that occurred on Flight Day 8. The results of these analyses are described in the following sections. Analyses of other array motion events acquired during the mission were performed after the release of the HST. Section 6.2 describes these postflight analyses.

#### **5.3.1 VRCS-Induced Solar Array Motion on Flight Day 3**

A 30-minute sequence of solar array video was captured starting at approximately 044:020:11 UTC. During this time, HST FS&S Project engineers monitoring the VRCS jet firing telemetry noted a thruster firing occurring at 044:20:28:39.48 UTC and requested that the solar array tip motion for a one-minute sequence, starting at 044:20:28:34.67, be analyzed. This differed from the pre-mission plan, which was to analyze only 30 seconds of video starting 10 seconds before the thruster firing. The video sequence that was analyzed began approximately 5 seconds before the VRCS jet firing, and lasted approximately 1 minute.

The 1-minute sequence of video that was used for analysis extended from 044:20:28:39.48 to 044:20:29:39.48 UTC. The video data was of very good quality although lighting was variable. Camera positioning was as expected. The analysis required approximately six hours to complete. See Figure 5.10 for a representative image showing the camera view.

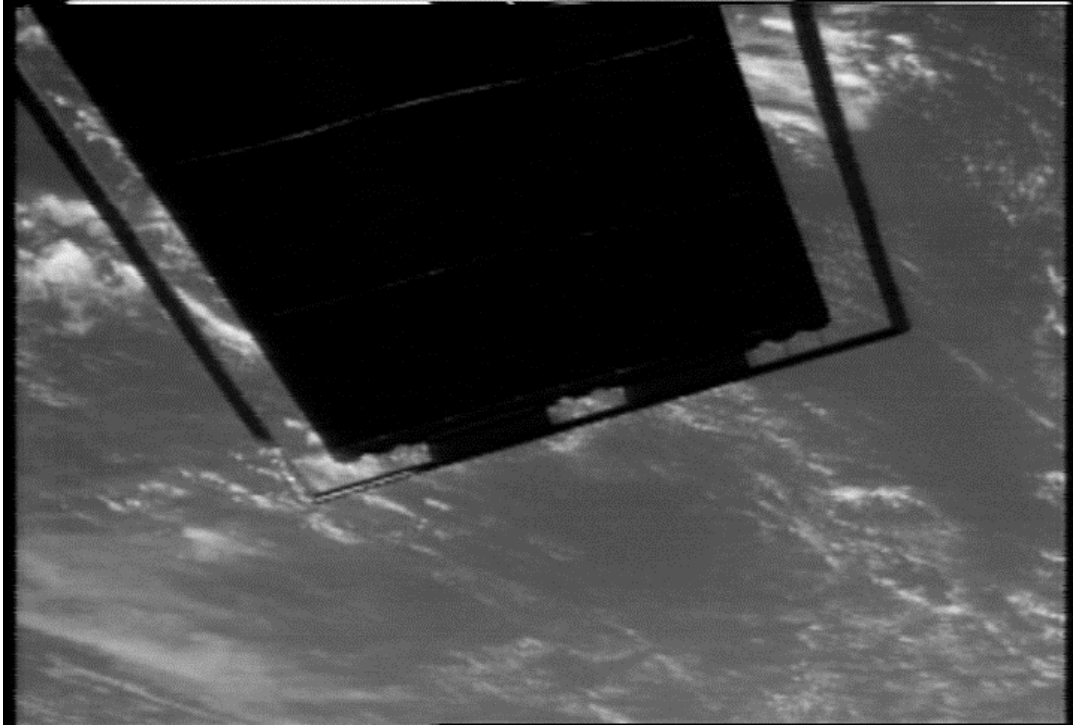


*Figure 5.10 View of +V2 solar array tips A & B from camera B during the VRCS-induced solar array motion on Flight Day 3.*

Based on the solar array motion analysis procedures defined pre-mission, the video frames were sampled at a rate of 3 frames per second (3 Hz), for a total of 180 frames analyzed. The results showed a maximum peak-to-peak displacement of approximately 0.7 inches for tip B and 0.6 inches for tip A, with a frequency of approximately 0.1 Hz for both tips (see Figure 5.11). The displacements and the frequency were as expected, based on HST FS&S Project structural dynamics models. The motion continued for approximately 3 minutes after the analysis interval and no apparent damping was noted.

The plot of tip displacement vs. time depicted in Figure 5.11 shows an apparent discrepancy in tracking the tips, since the displacement for tip A crosses that of tip B. Post-mission, it was determined that this effect was caused by a shift in the line-tracking intersection point for both tips during the tracking process. The line intersection that defines the tip position migrated from one edge of the spreader bar to the other causing an apparent translational motion. This problem was caused by variable lighting conditions that changed the appearance of the spreader bar edges and caused the fitted line to move from one side of the spreader bar to the other. To correct for this problem and to analyze the motion over a longer period, the solar array motion was re-analyzed after the mission using improved motion analysis methods. See Section 6.2.4 for the results of the post-mission analyses.

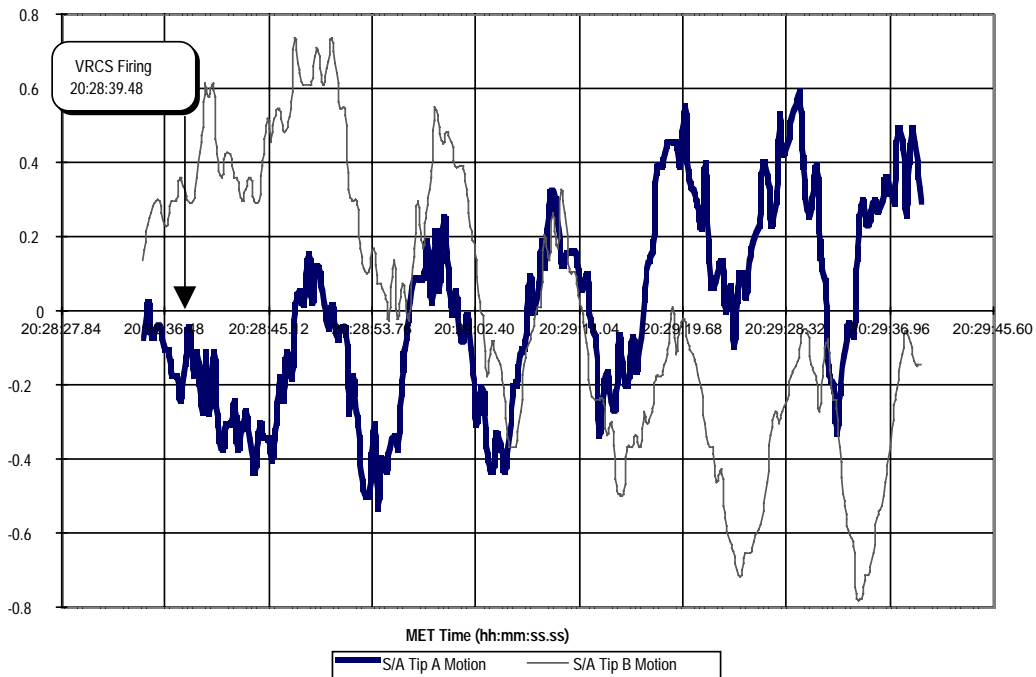


*Figure 5.11 Displacement of tips A and B during VRCS firing on Flight Day 3.*

### 5.3.2 Airlock Depressurization-Induced Solar Array Motion (Flight Day 8)

An unexpected solar array slew of approximately 5 deg on the -V2 solar array was observed at approximately 049:03:12:44.052 UTC (Flight Day 8). The array slew occurred during the airlock depressurization before EVA #5. A force of air from the airlock impinged on the solar array, causing it to slew upward. The slew and resulting solar array motion was captured on downlinked video. The event lasted for approximately 3 minutes. The HST FS&S Project subsequently requested a solar array motion assessment to determine the displacement of the solar array tips. (A similar event occurred on Flight Day 4, in which the array slewed approximately 40 deg upward when the air was released from the airlock. This event was not captured on video.)

A video sequence of approximately 1 minute (UTC 049:03:12:32 to 049:03:13:32), taken from camera B of the -V2 forward solar array tips G & H, was analyzed. Figure 5.12 is a representative view of the solar array during the airlock depressurization event. Because of the low contrast of the spreader bar in the image, the automated edge detection and line-tracking analysis procedure was not used. Therefore, all data points were extracted manually. To minimize point selection bias, the data points were independently selected by two analysts, whose results were in very good agreement ( $\pm 1$  pixel). The motion analysis was completed in approximately 5 hours. The analysis sample rate was 3 frames per second, for a total of 161 frames analyzed.

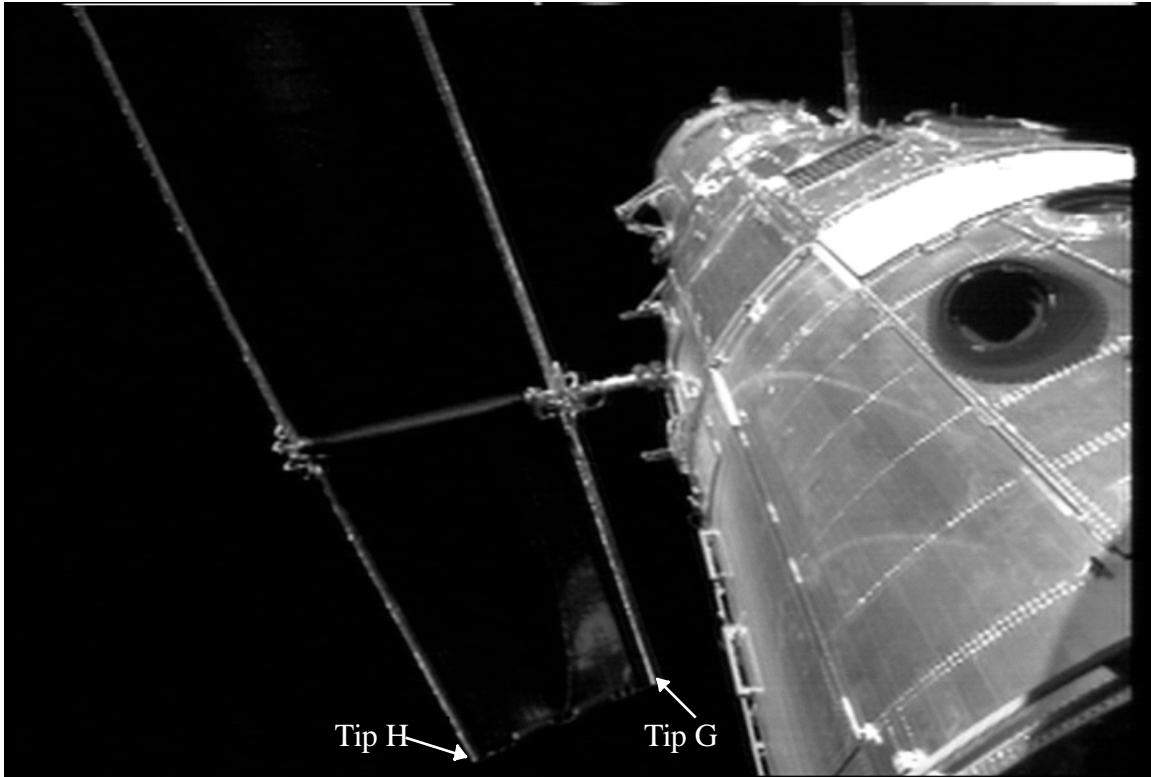


*Figure 5.12 View of -V2 solar array tips G & H from camera B during airlock depressurization-induced solar array motion.*

The results indicated a total slew at the tip of approximately 22 inches. After the initial slew, the array was seen to oscillate at a frequency of approximately 0.1 Hz as shown in Figure 5.13. The initial peak-to-peak displacement was measured to be approximately 7 inches for tip H and 6 inches for tip G, with the last measured displacement for both tips being approximately 5 inches. The plot of the tip displacement using the manual method was not as smooth as the automated method since it only had 1-pixel, rather than sub-pixel, resolution.

The airlock depressurization-induced solar array motion was re-analyzed after the mission using improved motion analysis methods. See Section 6.2.6 for the results of the post-mission airlock depressurization analysis.

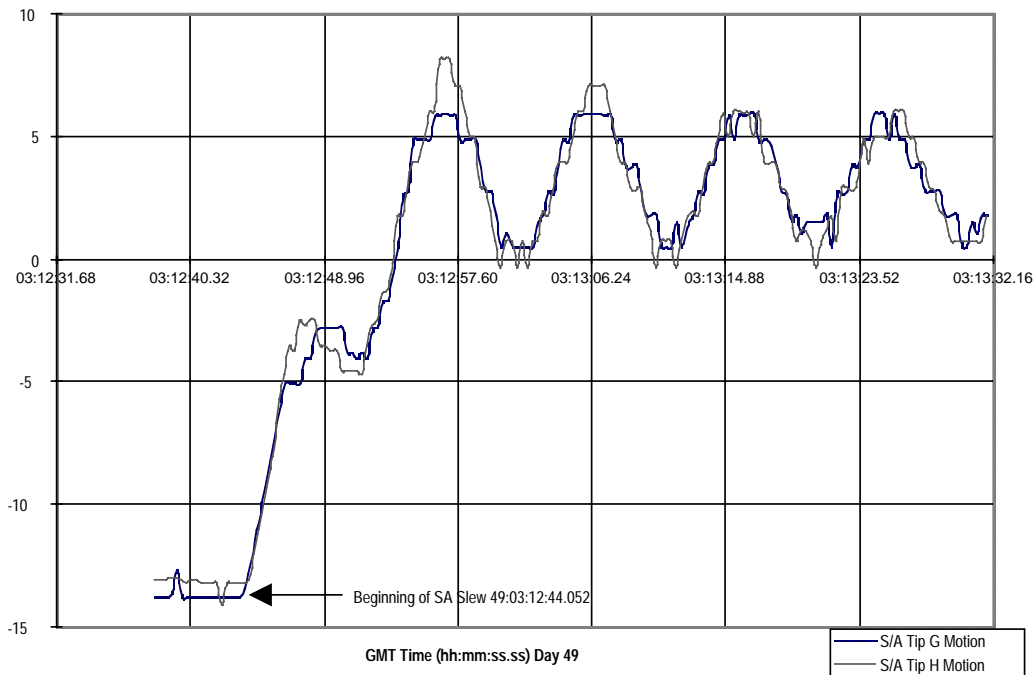


**Figure 5.13** Displacement of tips G and H during airlock depressurization on Flight Day 8.

## 6. POST-MISSION ANALYSES

Upon completion of the real-time analyses, IS&AG was directed to initiate post-mission analyses as follows:

- Determine the “best and final” static twist positions for the eight solar array tips before releasing the HST from the Shuttle.
- Perform additional solar array motion measurements for use in HST solar array structural dynamics analyses.
- Establish the accuracy of the results.
- Evaluate the static twist and solar array motion measurements and methodologies for potential impact to future applications.
- Document the results and findings.

This section of the report describes the post-mission analyses, results, and evaluations.

### 6.1 Static Twist Analysis

The primary purpose of the post-mission static twist analyses was to analyze the static twist imagery (without the real-time turnaround constraints) and validate the final coordinate locations and accuracies for the eight solar array tips. This analysis documents the final relative geometric configuration of the arrays on Flight Day 8 before HST release. Conceptually, the relative configuration of the arrays should remain unchanged after SM-2 and until SM-3.

### 6.1.1 Analysis Approach

The phototheodolite approach of camera resection and photo-triangulation, used during SM-2, is a restricted case of photogrammetry which utilized basic principles of photogrammetry in a two-camera solution of the location of the HST solar array tips. Post-mission calculations of HST solar array tip locations were accomplished using the analytical photogrammetric methodology of bundle adjustments. The method of bundle adjustments can be applied to multiple images. It provides for simultaneous solutions of the interior and exterior orientations of the cameras and the solutions for the positions of the object points. Moreover, the rigorous mathematical approach of bundle adjustments employs both the principles of least-squares adjustments and the general law of propagation of errors in converging to the solutions, with error estimates (standard deviations) as an integral part of the solution. The following paragraphs provide a summary description of the photogrammetric methodology applied in bundle adjustments. Reference 3 provides a more complete description.

#### Principle of Collinearity

The bundle adjustment approach is based on the fundamental principle of collinearity. Referring back to Figure 3.3, the collinearity relationship between a control point  $(X_i, Y_i, Z_i)$  and its conjugate image point  $(x_i, y_i, -f_i)$  can be expressed by:

$$\begin{bmatrix} x_i - x_o \\ y_i - y_o \\ -f_i \end{bmatrix} = \text{Scale\_Factor} * \text{Rotation\_Matrix} * \begin{bmatrix} X_i - X_c \\ Y_i - Y_c \\ Z_i - Z_c \end{bmatrix},$$

which simplifies to the classic collinearity equations:

$$x_i = x_o - f_i * \frac{[m_{11} * (X_i - X_c) + m_{12} * (Y_i - Y_c) + m_{13} * (Z_i - Z_c)]}{[m_{31} * (X_i - X_c) + m_{32} * (Y_i - Y_c) + m_{33} * (Z_i - Z_c)]}$$

and

$$y_i = y_o - f_i * \frac{[m_{21} * (X_i - X_c) + m_{22} * (Y_i - Y_c) + m_{23} * (Z_i - Z_c)]}{[m_{31} * (X_i - X_c) + m_{32} * (Y_i - Y_c) + m_{33} * (Z_i - Z_c)]}$$

where the  $m_{ij}$  are the elements of the standard 3 X 3 rotation matrix which are a function of the axial rotation angles  $\omega$ ,  $\Phi$ ,  $\kappa$ .

Standard close-range photogrammetry tasks (such as the HST solar array tip measurement) require the following input data:

$X_i, Y_i, Z_i$       Object coordinates of control points on the object being measured.

$x_i, y_i$       Image coordinates of each control point in the image, obtained by physically measuring the location of each control point in the image.

This leaves nine parameters in the collinearity equations that are unknown for an image:

$f_i$	Principal distance.
$x_o, y_o$	Principal point location relative to the x-y origin used as the basis for the image coordinate measurements.
$X_c, Y_c, Z_c$	Location of the perspective center of the image relative to the object coordinate system.
$\omega, \Phi, \kappa$	The three angular rotations applied to the object coordinate system, which aligns it with the image coordinate system.

The nine unknown parameters are computed by constructing and solving a set of simultaneous collinearity equations for five or more sets of control/image point coordinates. This technique, called a single image resection, fixes the location and orientation of the camera, at the instant of exposure, relative to the object's coordinate system. Furthermore, if an adequate number of 3D control points are distributed over the image, lens distortions can be estimated. This was done in the post-mission SM-2 analyses.

The bundle adjustment approach, rather than computing the unknown point's coordinates by simple vector intersection, employs a simultaneous solution of the collinearity equations. Four collinearity equations are constructed using the known camera location/orientation data from two cameras. Any three of the equations can be solved for the coordinates of the unknown point. If the point was viewed by additional cameras, additional equations can be constructed and the over-determined solution is obtained using least-squares adjustments.

### **Simultaneous multi-camera and unknown point solutions**

In practice, the locations and orientations of multiple cameras and the coordinates of all unknown points are simultaneously computed using an iterative, weighted least-squares adjustment methodology. This simultaneous solution interrelates each camera to every other camera based on commonly seen control, and unknown points, thereby building a level of strength and consistency into the final solution. The use of this overall simultaneous least-squares solution is commonly referred to as a bundle adjustment.

### **Error propagation**

The least-squares adjustment algorithm automatically generates the uncertainty estimate for each computed parameter based on the general law of propagation of errors. In the case of a photogrammetric application, the bundle adjustment computes the  $1\sigma$  standard deviations for the nine camera parameters of each image, as well as for the X, Y, Z locations of all computed points.

### **6.1.2 Implementation of Bundle Adjustment Solution**

The post-mission photogrammetric calculations performed by IS&AG utilized a photogrammetry package, Unconventional MENSuration System (UMENS), developed in 1996 by CALGIS Inc. [Ref. 6.], under contract to the Central Intelligence Agency. This Windows-based package allows in-program image coordinate measurement via manual digitization. Control point data and measured image coordinates are then available for processing by several different photogrammetric algorithms including single image resection and bundle adjustment. Mathematical algorithms implemented in this software have been independently verified.

**Image acquisition**

IS&AG personal recorded imagery from the Flight Day 8 static twist analysis tests in real time on D-2 digital videotapes. New images, different from those used for the real-time analyses, were extracted from the video and used for the post-mission analysis.

Multiplexed views were not used during post-mission calculations. The initial purpose of these views was to remove positional errors due to possible timing differences and the natural in-plane oscillation of the solar arrays. However, no motion was detected which exceeded the standard uncertainty level (0.75 pixels) for manually digitized image coordinates.

Table 6-1 lists the video images (correlated to PLB camera and Greenwich mean time [GMT] of the image) used in the post-mission static twist analyses.

***Table 6-1 List of Cameras and Image Times Used in Post-Mission Static Twist Analyses***

Photo #	Camera	Solar Array Tips Viewed	Time (GMT - Day:Hour:Minute:Second:Frame)
1	B	Tip A & B	49:17:44:29:00
2	D	Tip A, B, & G	49:17:48:22:20
3	B	Tip G & H	49:17:50:30:00
4	D	Tip D, E, F, G & H	49:17:52:20:00
5	C	Tip E & F	49:17:57:13:00
6	A	Tip C, D & H	49:17:59:32:00
7	B	Tip C & D	49:18:02:44:20

Post-mission calculations of HST solar array tip locations were conducted in the following manner:

1. Image digitization and resection approximations were conducted independently for each image:
  - a. The radiometrically enhanced image is loaded into the UMENS software.
  - b. The image coordinates were measured for each control point visible in the image.
  - c. The image coordinates were measured for all solar array tips visible in the image.
  - d. A single image resection was performed to compute the nine unknown elements of the camera location and orientation (to be used as approximations in the bundle adjustment). Statistical outliers were identified and removed, re-digitized, or statistically de-weighted, as appropriate. Table 6-2 lists the number of control points used in the single image resections.

***Table 6-2 Number of Control Points Used in Single Image Resections***

Photo #	Camera	Number of Control Points used in Single Photo Resection	Solar Array Tips Measured in Photo
1	B	11	A & B
2	D	23	A, B, & G
3	B	15	G & H
4	D	27	D, E, F, G & H
5	C	8	E & F
6	A	16	C, D & H
7	B	12	C & D

2. The collinearity equations were used to compute approximate solar array tip locations/coordinates (to be used as approximations in the bundle adjustment) based upon the approximate camera location/orientations computed in step1-d.
3. A simultaneous adjustment of the approximated camera parameters and solar array tip locations was performed to compute their best statistical values and propagated standard deviations.

Inputs to the final bundle adjustment were restricted to the following elements:

1. Image coordinates of control points and solar array tips as measured on each image.
2. The  $1\sigma$  uncertainty estimate of measured image coordinates. A value of 0.75 pixels was used, based on the results of a statistical test conducted within IS&AG to quantify the uncertainty of manually digitized image coordinates.
3. The object coordinates of HST control points were used.
4. The  $1\sigma$  uncertainty estimate of HST control points. A value of 0.5 inches was used, based on estimates provided by GSFC.
5. A geometric constraint to hold the distance between computed tip coordinate pairs A-B, C-D, E-F and G-H to the nominal length of the solar array spreader bar at 113.50 inches. Although the design uncertainty of the composite spreader bar is nominally 0.01 inches, lack of image clarity and resolution made it impossible to hold the solution to this level of accuracy. A  $1\sigma$  value of 0.25 inches was used, based on the available image-to-object resolution.

One significant problem was encountered in the bundle adjustment calculations. The image (taken from Shuttle camera C) could not be integrated into the final solution, which prohibited production of coordinates for array tips E and F. Image #5, shown in Figure 6.1, consisted of a monochrome image taken from an MLA camera. These cameras have a much narrower FOV than the CTVC cameras, and in this particular case, the FOV was so restricted that it included only eight HST control points as shown in Figure 6.1. Of the eight points, seven were arranged in a linear geometric configuration, and the eighth (control point #20) was approximately linear with the other seven. Because they were linear, an indeterminate solution was produced for the camera rotation parameters.

Note that the control point numbers with the attached post-script “-s” designate control points that were originally located at the handrail attach points, but were extended 3.003 inches radically outward from the HST “V1” axis to produce a control point on the top surface of the handrail.

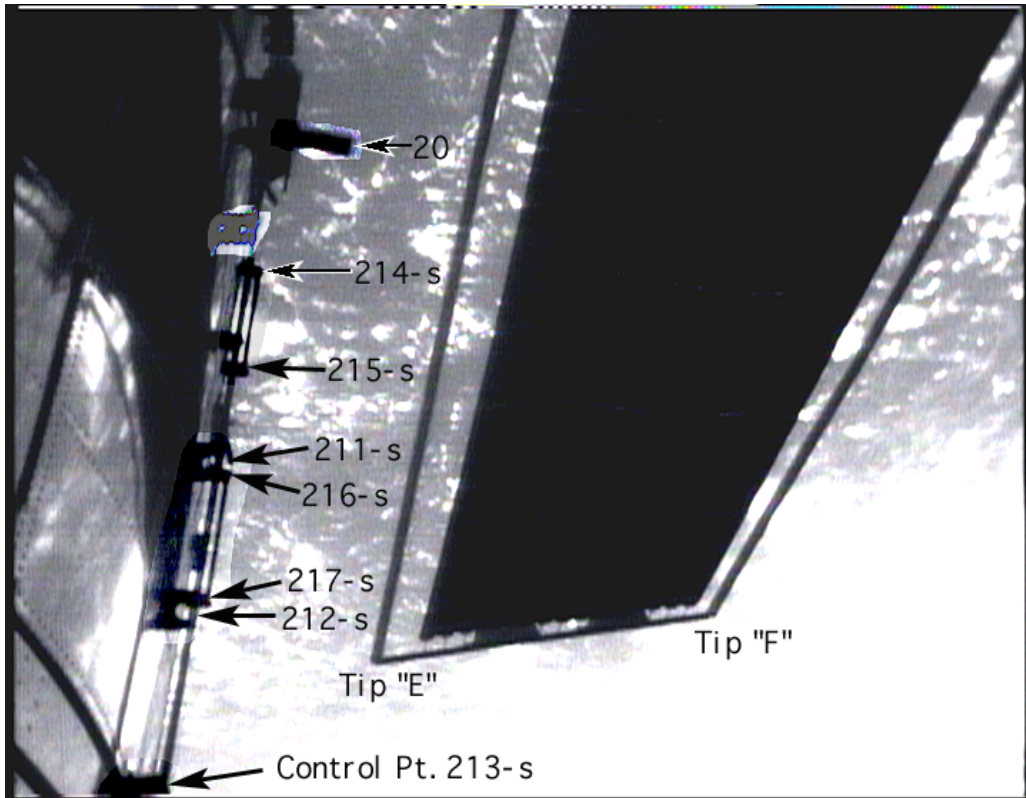


*Figure 6.1 Image of tips E and F taken from camera C, showing the linear configuration of control points.*

### **6.1.3 Results From Post-Mission Photogrammetric Analyses**

Table 6-3 presents the final HST coordinates for the solar array tips computed by photogrammetric bundle adjustment and their respective  $1\sigma$  error estimates.

The final bundle adjustment incorporates the following advantages over a solution based upon a single photo resection and point intersection technique.

1. All camera parameters and computed tip locations are bound into a single uniform solution.
2. The computed coordinates for tips D, G, and H are based on a three-camera solution, thereby increasing the degrees of freedom in the least-squares calculation.
3. Standard deviations for computed parameters were produced as a normal output of the bundle adjustment in accordance with the general law of propagation of errors.

**Table 6-3 Post-Mission Computed Solar Array Tip Locations**

Tip	Coordinates and Standard Errors (all values in inches)						
	V1	1 $\sigma$	V2	1 $\sigma$	V3	1 $\sigma$	Total 1 $\sigma$
<b>A</b>	310.54	1.98	131.21	1.83	-237.26	2.53	3.70
<b>B</b>	288.52	1.95	242.72	1.88	-238.38	2.93	3.99
<b>C</b>	348.78	2.37	132.83	1.48	238.06	2.39	3.68
<b>D</b>	330.82	1.85	244.53	1.59	234.89	2.61	3.58
<b>E</b>							
<b>F</b>							
<b>G</b>	362.52	2.19	-131.41	1.60	231.81	3.29	4.26
<b>H</b>	328.39	1.92	-239.52	1.60	235.28	3.58	4.36

The error estimates in each axis were larger than originally desired for the project. The following factors degraded the accuracy estimates of HST results:

1. The resolution and clarity (sharpness) of the CTVC and MLA cameras limit the results. In the case of images from cameras A and D, one image pixel represents one object inch. It is not unreasonable to expect a 1- to 2-pixel error in measuring the image coordinates for the “true” location of any control point. This image error would result in a 1- to 2-inch error in the control point location when projected to the surface of the HST. Propagating this error into the resected camera locations and then into the tip locations contribute to the higher-than-desired coordinate error estimates. Higher resolution imagery is mandatory to produce the desired accuracies.
2. Camera imperfections, such as radial and tangential lens distortions, cause the path of a ray of light to deviate from a straight line from the object point to the image point. Until recently, the image distortions in the Shuttle cameras have not been characterized. Camera calibration is currently under way, the results of which are only now being made available to IS&AG. Without having this data a priori, estimates of the distortion parameters were calculated during the photogrammetric bundle adjustment using an enhanced version of the collinearity equations expanded to model lens distortion. In what is termed a “self-calibration” bundle adjustment, accurately calculated focal length and distortion parameters are only assured if control is well distributed about the image. In the HST photos, control point availability was somewhat less than well distributed, and limited the accuracies in the computed focal length and lens distortion parameters. Camera characterization is required to produce the desired accuracies.
3. To achieve optimal accuracy in a close-range photogrammetric application, the object being measured should be centered in a work area, the corners of which are defined by the camera locations. The HST was placed well aft in the cargo bay. A more centrally located HST in the cargo bay would produce more desirable accuracy estimates.

### 6.1.4 Comparison of Post-Mission Results to Real-Time Results

Table 6-4 shows the total difference in the tip coordinates computed on Flight Day 8 by the phototheodolite technique in real time, compared with the values computed post-mission using the bundle adjustment technique. The “Deltas” in Table 6-4 are the number of sigma intervals between the real-time and post-mission derived coordinates (using the sigma values calculated in the bundle adjustment solution).

*Table 6-4 Accuracies of Real-Time Coordinates Compared to Post-Mission Results*

Tip	Delta-V1 (Inches)	Delta-V2 (Inches)	Delta-V3 (Inches)	Total Difference
A	1.44	0.41	-1.66	2.23
B	2.52	1.52	-4.28	5.19
C	1.18	4.33	0.46	4.51
D	3.52	8.53	1.69	9.38
E				
F				
G	-1.28	-3.51	2.71	4.61
H	-1.01	-6.92	2.08	7.30

**Index:**

	Difference within 1σ of real-time results
	Difference within 2σ of real-time results
	Difference within 3σ of real-time results
	Difference greater than 3σ of real-time results

Inspection of the results in Table 6-4 shows differences ranging from 0.41 inches to 8.53 inches. These differences are primarily due to the inaccuracy sources discussed in the previous section (poor image resolution, lack of camera characterization, and less than optimal geometry) and how these errors are handled in the phototheodolite and bundle adjustment solutions. These include:

1. Different final solution types. The phototheodolite solution was completed independently for each pair of tips A-B, C-D, E-F, and G-H. The post-mission calculations employed a single simultaneous solution for the six photos and six calculated tips. Slight differences in computed point coordinates will always occur when six cameras are interrelated, as compared to a solution with only two cameras. Coordinates that differ by 2σ, or less, from the during-mission results must, statistically, be expected.

2. Differences in the final solution implementations. Four coordinates differ by more than  $2\sigma$ , when compared to real-time results. Although these values may be statistically possible, they are much less likely. Differences in the implementation of the solutions account for these larger coordinate differences, as explained below:

a. In the phototheodolite solution, the camera location (perspective center of image) was fixed as the camera mounting coordinates from Orbiter engineering design drawings. Although the engineering plans provided coordinates for the geometric center of the camera, they are not the precise coordinates of the perspective center of the image. Additionally, since the cameras are equipped with a variable focus lens, the perspective center of any image shifts as the focal length changes. Although it is believed that the perspective center of any image (created over the full range of focal length settings) is within 2 to 3 inches (in any axis) from the engineering design coordinates, the precise location is not known.

In the bundle adjustment solution, the location of the perspective center ( $X_c, Y_c, Z_c$ ) is calculated for each image, allowing it to come to rest at the point which best fits the image. The results of the bundle adjustment show that the computed location of the perspective center varied anywhere from 0.1 inches to 3 inches from the engineering design coordinates of the camera center. Allowing the perspective center of the image to vary from engineering design coordinates accounts for the larger differences between the real-time and post-mission values.

b. There are advantages in multi-camera solutions. In the phototheodolite solution, only two camera views were used to compute the coordinates of each tip. Since the bundle adjustment was based on a simultaneous solution for the six images, coordinates of tips D, G, and H were each computed using three cameras. Variations in the number of cameras used in the point coordinate solution, in the presence of varying amounts of random error, makes it statistically impossible to produce the exact same results.

c. The error estimation techniques are different. A Monte Carlo technique was used to compute the error estimates in the real-time computations. The least-squares bundle adjustment computed standard deviations based on the general law of propagation of errors. Differences in these methods account for the difference in coordinate accuracy estimates.

d. Different images and control points were used. The post-mission analysis was completed using a new set of images digitized from the during-mission videotape. Each image was selected to optimize object view, contrast, lighting, control point availability, and number of array tips visible. The post-mission analysis images were then radiometrically enhanced to better clarify the image location of each control point. Radiometric enhancement was not performed during the real-time mission analyses.

e. Different numbers and types of control points were used. Different individual control points and the total quantity of control points used in the solution varied between the real-time and post-mission analyses. Variations in the geometric distribution and clarity of points used in the real-time and post-mission analyses caused some variability in results.

### 6.1.5 Solar Array Twist Analysis

The distance of the computed tip coordinates from the conceptual plane of the solar array was calculated using the same mathematical technique discussed in Section 5.2.3. Table 6.5 shows post-mission results and a comparison to the average during-mission results. Post-mission results are generally comparable to the during-mission results.

**Table 6-5 Perpendicular Offset of Tips From Conceptual Plane of Solar Arrays**  
(inches)

Flight Day	HST orientation	Slew Angle (deg)	Computed Tip Location Relative to Nominal Solar Array Plane	Perpendicular Distance From Computed Tip to Nominal Solar Array Plane								
				Tip a	Tip B	Tip C	Tip D	Tip E	Tip F	Tip G	Tip H	
8	-V3 Forward	4.85	Above	8.0		11.1				N/A	20.4	
Post-Mission		4.8	Below		13.8		6.5	N/A				13.9
Average			Above	10.7		9.4			9.1	20.8		
During Mission			Below		11.4		11.2	12.8				15.1

Solar array twist was calculated as the sum of the perpendicular offsets of a tip pair from its respective solar array, as computed in the above table. Table 6.6 shows the post-mission computed twist values and the average during-mission values. Again, post-mission results are generally comparable to the during-mission results.

**Table 6-6 Solar Array Tip Twist Values**  
(inches)

Flight Day	HST Orientation	Tip A/B		Tip C/D		Tip E/F		Tip G/H	
		Twist	Std. Dev.						
8 Post-Mission	-V3 Forward	21.8	2.8	17.6	3.0	N/A	N/A	34.3	2.9
Average During Mission		22.1		20.6		27.1		35.9	
Pre-Mission (SM-1) Estimate		25 ± 2		11 ± 2		26 ± 2		31 ± 2	

### 6.1.6 Summary of Static Twist Results

During-mission results are generally comparable to the post-mission results based upon the post-mission uncertainty estimates. It is believed that the during-mission Monte Carlo simulations underestimated the uncertainty in the computed tip coordinates. The post-mission uncertainty estimates were based upon a standardized error propagation technique that better reflects the uncertainty in the results. Coordinate uncertainties would have been substantially decreased with increased image resolution, a priori camera calibration parameters, and statistical averaging of multiple calculations.

## 6.2 Array Motion Analysis

Following the STS-82 mission, IS&AG performed additional analyses of solar array motion from the excitation events. The solar array excitation events selected for analysis were in response to specific requests from GSFC FS&S engineers and were based on data availability and quality. For each solar array excitation event, the dominant frequency and the peak-to-peak solar array tip displacement as a function of time were measured.

IS&AG performed post-mission solar array analyses for the HST rotation on Flight Day 5, the airlock depressurization on Flight Day 8, the HST pivot on Flight Day 8, and the HST reboost on Flight Day 8. In addition, the VRCS solar array motion analysis on Flight Day 3 was re-analyzed using improved motion tracking methods described below. Table 6-7 provides a listing of the solar array motion events that were analyzed. The following sections describe the analysis approach, each of the motion analyses that were performed, and the results from each analysis.

*Table 6-7 Post-Mission Solar Array Motion Analysis Events*

<b>Event</b>	<b>Flight Day</b>	<b>Time (UTC)</b>	<b>Solar Array Tips</b>	<b>Camera</b>
VRCS Firing	FD 3	044:20:28	A,B	B
Rotate	FD 5	046:11:02	A,B and G,H	B
Airlock Depress	FD 8	049:03:12	G,H	B
Pivot	FD 8	049:08:35	E,F	RMS elbow
Reboost	FD 8	049:10:29	A,B	B

### 6.2.1 Analysis Approach

The post-mission approach for solar array motion analysis also used a three-hertz sampling of video frames used in the real-time data analysis, with the displacements of the array tips normalized about a mean or rest position. The analyses also used an automated point-tracking capability at the sub-pixel level in addition to the line-tracking methodology. The line-tracking methodology is described in Section 3. The point-tracking methodology is described in the following paragraphs.

### **Point-tracking methodology**

Point tracking follows the movement of a pattern surrounding a point of interest in a sequence of images and automatically tracks the point from one frame to the next. The point-tracking software allows the user to select a point to be tracked (i.e., HST solar array tip), and a rectangular region of interest containing that point. The image pattern in the rectangular region is searched for, in subsequent frames, by comparing similarly sized image regions to the pattern. The comparison to areas on subsequent frames to the initial pattern uses a normalized cross-correlation function. The pixel for which the highest correlation is computed is defined as the point of interest. This X and Y position data of the pixels in image coordinates, as well as a measure of the correlation between each of the frames, are saved to a data file. In this way, the motion of the solar array tip is tracked from frame to frame.

The point-tracking method was generally more robust at tracking than the line-tracking method. The point-tracking software works well in low-contrast situations and can be used when a suitable edge cannot be determined for the line tracking software. However, a loss of tracking can occur if the scene lighting or background significantly changes. The point-tracking method was used exclusively for all post-mission solar array analyses except for the start of rotation, for which both point- and line-tracking methods were used. A lighting condition was encountered during the rotation motion analyses in which one tip could not be tracked using the point-tracking method, but could be tracked using the line-tracking method.

Figure 6.2 illustrates the point-tracking method as it was applied to the HST solar array motion-tracking task. The search pattern surrounding the array tip is shown in (a). The window in the next video frame to search for the pattern is shown in (b). The pattern passing over the window is shown in (c). Correlation values are computed for each pixel that the pattern passes over and (d) shows the pattern matching over the target. The correlation should be the highest at this pixel position (i.e., at the center of the white box). The coordinates of this position are saved and the same steps are repeated for the next frame.

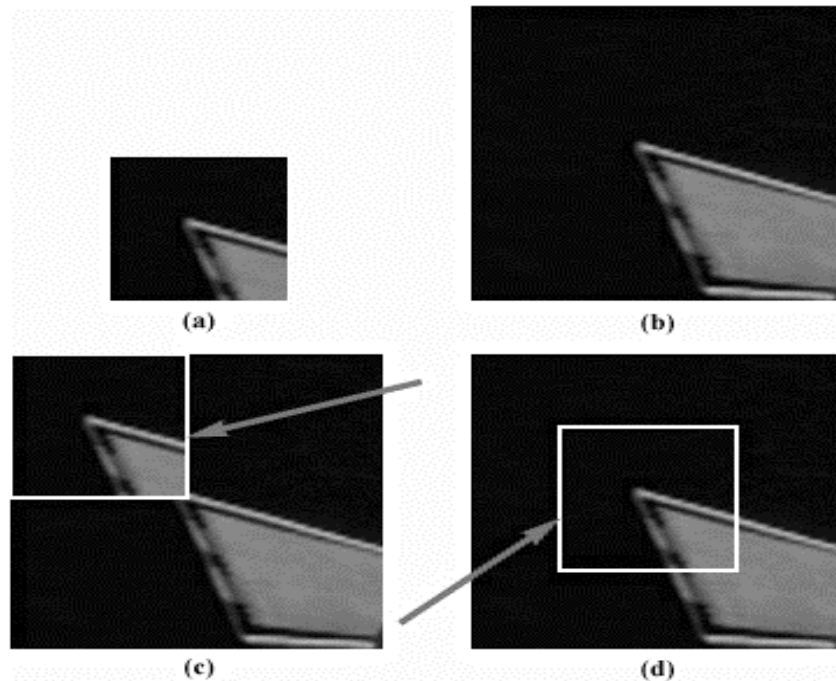


***Figure 6.2 Point tracking method applied to tracking an HST solar array tip.***

### **Determination of maximum peak-to-peak displacement**

During the mission, the peak-to-peak displacements were provided as visual examinations of the raw motion data. To be more accurate and consistent, the post-mission determination of the maximum peak-to-peak displacement of solar array tips was performed in the following steps and is illustrated in Figure 6.3:

1. The “raw” displacement data, at the 3-Hz sampling rate, was smoothed using a 5-point moving average filter. This smoothing reduced the random, high-frequency, sub-pixel noise that was a by-product of the motion tracking. The 5-point filter was based on selecting the smallest range that smoothes the noise and still exhibits the peaks in the data.
2. The half-cycle (adjacent maximum positive and negative displacements relative to a mean or “rest” position) that represents the maximum peak-to-peak displacement was selected by inspection of the plot of displacement as a function of time. This selection was, in almost all cases, the first peak-to-peak half-cycle after the excitation event.
3. The peak-to-peak displacements were obtained from the smoothed displacement data. The peak-to-peak displacement was calculated by finding the values for the peak maximum and peak minimums for the selected peak-to-peak displacement. The difference in the peak maximum and peak minimum values was then used as the peak-to-peak displacement.

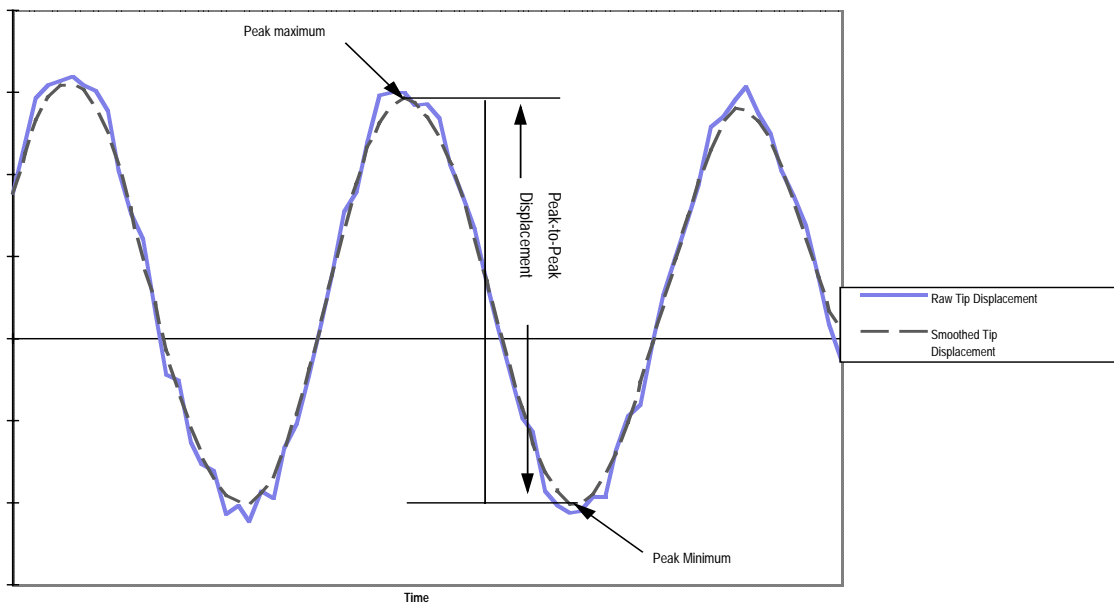


***Figure 6.3 Illustration of maximum peak-to-peak displacement of solar array tips.***

## **Determination of the dominant frequency of tip displacement**

The frequency of the tip displacements was determined by calculating the fast Fourier transform (FFT) for each of the tip displacement data sets. The dominant frequency was then obtained as the maximum value from the magnitude of the FFT.

### **6.2.2 Motion Analysis Error Assessment Methodology**

The solar array motion error analysis method involved the determination of the error or uncertainty about the maximum peak-to-peak tip displacements for each of the solar array motion displacement plots. The initial accuracy requirement for the measurement of the solar array motion was  $\pm 0.5$  inches in zero-to-peak deflection. Treating the  $\pm 0.5$  inches as a  $3\sigma$  value, this translates to  $\pm 0.71$  inches ( $3\sigma$ ) in peak-to-peak deflection. Note that this accuracy requirement only specified for the analysis of the planned VRCS-induced solar array motion on Flight Day 3.

The accuracy assessment method is composed of two components. First, the random error in the raw pixel peak-to-peak tip displacement is determined, and then the error caused by scaling the pixel values to real world coordinates (inches) is applied. A 5-point moving average smoothing method is used to estimate the random noise in the tip displacement data, and a Monte Carlo simulation is used to determine the effect of scaling errors. This procedure is run for 300 iterations and the standard deviations of the peak-to-peak displacement are determined. The standard deviation is then used as the overall error in the peak-to-peak displacement measurement.

### **6.2.3 Solar Array Motion Analyses**

The results from each of the solar array motion analyses are described in the following sections. Section 6.2.9 presents a summary of the results from each of the analyses.

### **6.2.4 Analysis of VRCS-Induced Solar Array Motion (Flight Day 3)**

The post-mission analysis of the VRCS-induced solar array motion on Flight Day 3 was more extensive than the analysis performed during the mission. A video sequence lasting 3 minutes was analyzed using the automated point-tracking software to track the solar array tip positions from frame to frame. The post-mission analysis began 45 seconds before the VRCS thruster firing, and continued for over 2 minutes after the firing.

Figure 6-4 presents a plot of the array displacement as a function of time. This plot represents a smoothing of the original data using a five-point moving average filter, and Appendix G presents the original unsmoothed tip displacement plot. Filtering of the data was necessary to remove high-frequency noise in the motion tracking. This noise was caused by subtle lighting variations in the scene. Note that, unlike the analysis performed during the mission, the solar array tips did not lose tracking and the inboard (A) and outboard (B) tips tracked together.

### Solar Array Tip Deflection during VRCS Firing (FD 3)

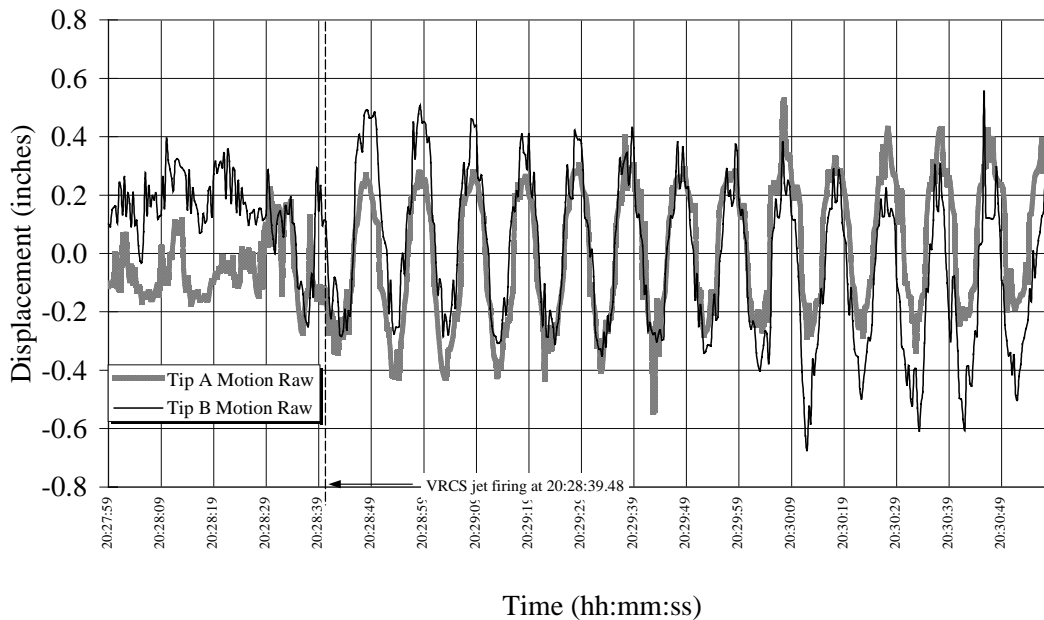


**Figure 6.4** Solar array tip displacement during the VRCS-induced solar array motion (Flight Day 3).

The response of the solar array tip displacements to the VRCS jet firing is more evident in the post-mission plot. There is clearly a larger tip displacement after the firing. Before the firing, there was a “background” peak-to-peak displacement of approximately 0.2 inches when there was no major excitation event. After the VRCS jet firing, the peak-to-peak displacement increases to a maximum of  $0.65 \pm 0.05$  inches for tip A at 20:28:47.7 UTC and  $0.73 \pm 0.08$  inches for tip B at 20:28:48.03 UTC. The accuracy for measuring tip B is lower than for tip A due to more noise in the point tracking for tip B. A shadow moved over the spreader bar from tip B toward A causing a change in lighting for tip B. The shadow did not reach tip A. Another large peak-to-peak displacement was observed later in the sequence at 20:30:09. At this time, the peak-to-peak displacement for tip A was 0.65 inches and tip B was 0.84 inches. The cause of this increased displacement is not known, but was probably the result of another thruster firing.

Note that the oscillations in the displacements for the two tips did not correlate well before the VRCS jet firing, but after the firing the two tip oscillations were in nearly perfect correlation. Also, the displacements for tip B starts out with a higher positive amplitude and tip A starts out with a lower negative amplitude. (The peak-to-peak displacements are about the same.) This effect is reversed later in the sequence with tip A having a higher positive amplitude and tip B having a lower negative amplitude. A twisting in the array could cause this effect.

The dominant frequencies are revealed in the plots of the log magnitude of the frequency response as a function of frequency for each tip. Figures 6.5 and 6.6 show plots for tips A and B. The dominant frequency of the array tip displacements is shown (large magnitudes) to be 0.1 Hz for both tips, which was the same frequency measured during the mission.

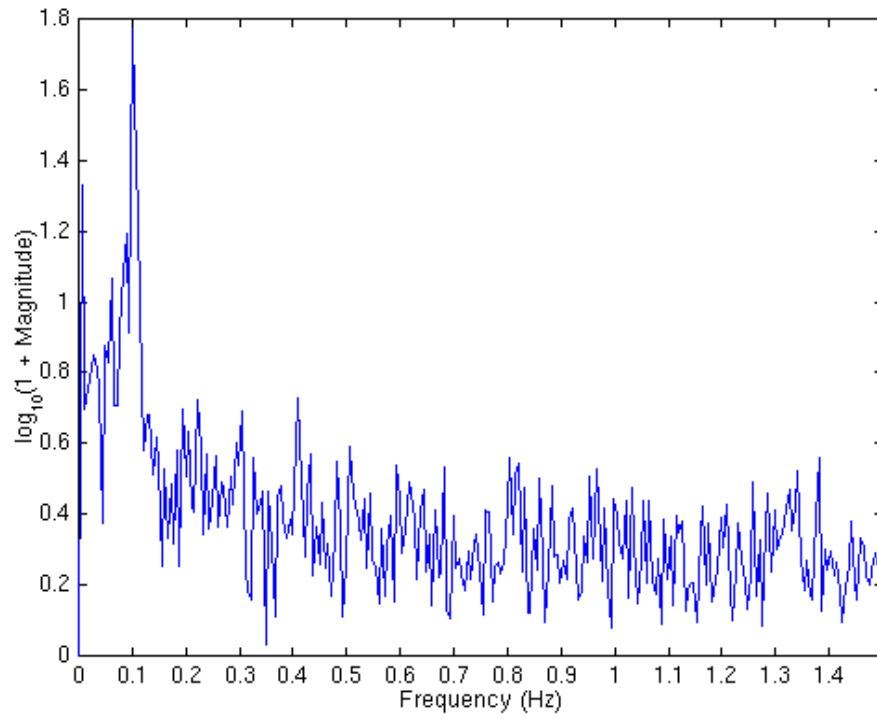


**Figure 6.5** Frequency plot for tip A from VRCS-induced motion.

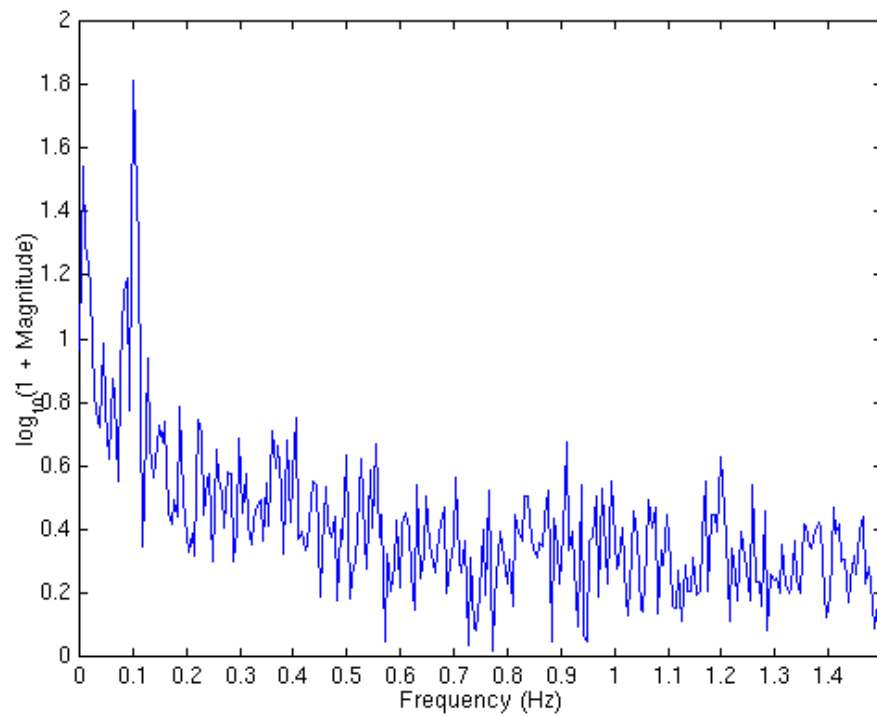


**Figure 6.6** Frequency plot for tip B from VRCS-induced motion.

### 6.2.5 Analysis of Solar Array Motion During FSS Rotation (Flight Day 5)

The rotate event (HST repositioning) on Flight Day 5 occurred just after a pivot of 15 deg. At the start of the rotation, camera B was viewing tips A and B on the +V2 solar array. At the end of rotation, camera B was viewing tips G and H on the -V2 array. Therefore, the camera remained fixed and the array tips moved through the camera FOV.

Figures 6.7 and 6.8 are representative images showing the views at the beginning and end of the rotate event. These views differed from the views planned before the mission. Before the mission, the plan was to acquire views of tips G and H at the start of rotation with camera C and acquire the same tips at the end of rotation with camera B. In this pre-mission scenario, the tips were to remain constant and the camera was to change. However, neither of the planned videos was obtained for the start and end of rotation. Therefore, only rotation views from camera B were used as described above. The FS&S Project concurred with this approach.

The solar array motion analysis for the HST rotation event on Flight Day 5 required a motion analysis to determine the time for the start and end of rotation. First, the array motion was analyzed from just before the start of rotation until several minutes after rotation began, such that a sudden change in the plot of array displacement vs. time would indicate the exact time that rotation began. Second, the array motion was analyzed from just before the end of rotation until several minutes after the end of the rotation event, so that a sudden change in the array displacement plot would indicate the exact time that rotation ended.

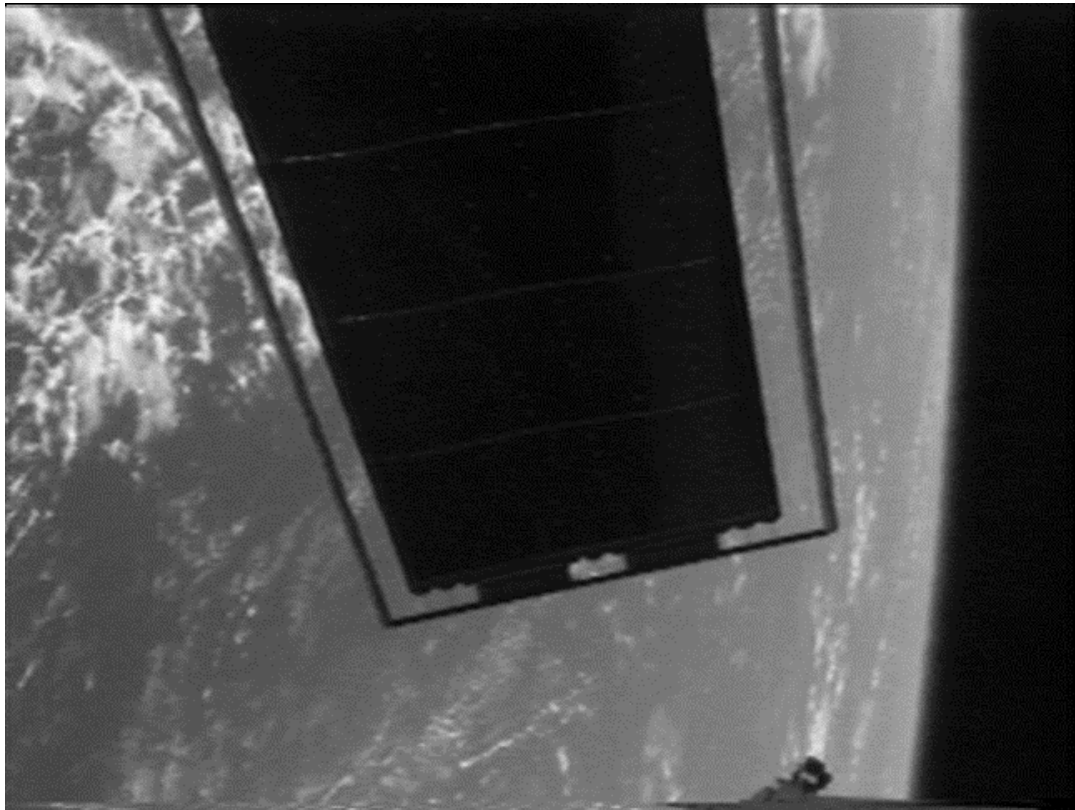


*Figure 6.7 View of +V2 solar array tips A & B from camera B during start of rotation.*

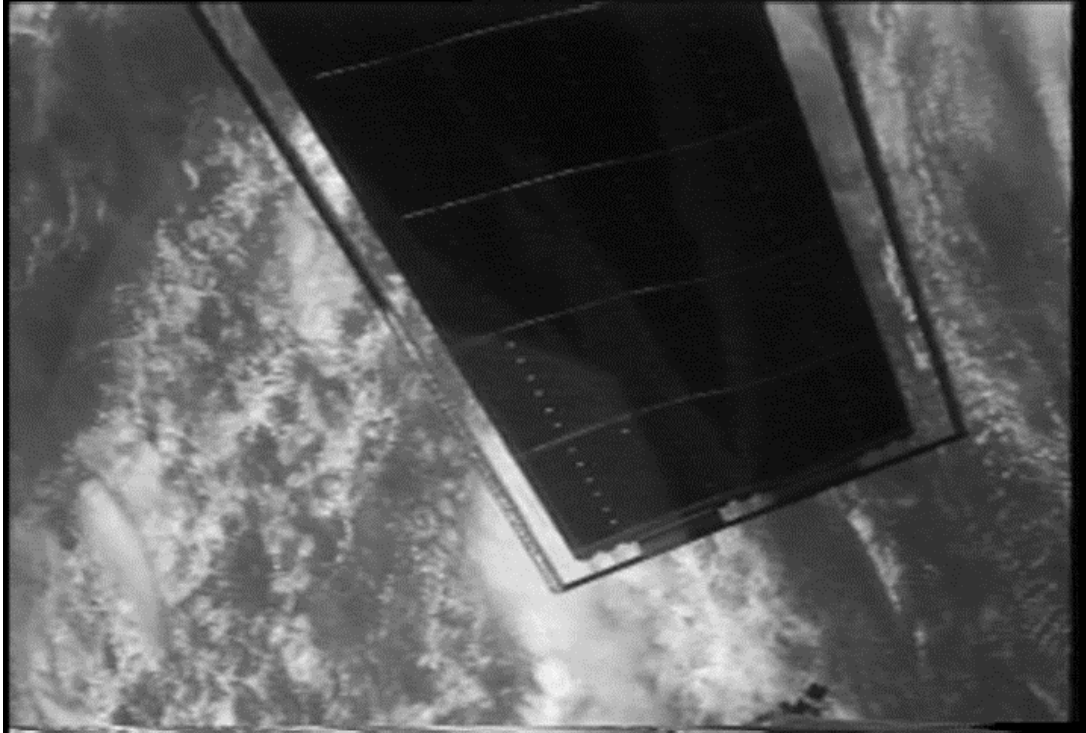


*Figure 6.8 View of -V2 solar array tips G and H from camera B at end of rotation.*

Rotation causes a translational tip displacement in addition to an oscillatory displacement. The translational displacement must be subtracted from the measured tip displacement to determine the out-of-plane tip displacement. The translational motion was modeled by fitting a least-squares, second-order, polynomial curve to the raw motion. The raw tip displacements were then subtracted from the fitted curve to remove the translational motion and obtain the oscillatory motion. The oscillatory motion is assumed to be caused by out-of-plane solar array tip displacement.

In general, the solar array motion measurements for the rotation event had more noise and tracking problems than the other solar array motion events. This was caused by poor lighting and background contrast that created difficulty in maintaining accurate tracking of the tip position. For the point-tracking method, this caused the search pattern to no longer match the pattern surrounding the solar array tips before the background changed. A request had been made to keep the darkness of space in the background during the imagery acquisition, but this was not possible due to Shuttle propellant constraints. In addition, the tilt of HST was such that there was a poor angle between the camera line of sight and the solar array motion vector. The tilt of the HST caused more of the out-of-plane array motion to be along the camera line of sight and this caused the noise in the data to be amplified.

Despite the noisy tracking of the array tips, the overall error in measuring the maximum peak-to-peak tip displacements during the rotation events was not as large as the error for the displacements caused by the airlock depressurization or the pivot events. This is because the scale conversion from image pixels to displacement (in inches) was much smaller for the rotation event. This was the result of the camera being zoomed in to a tighter FOV for the rotation images than for the airlock depressurization or pivot events.

## **Beginning of rotation**

An approximately 2-minute video sequence showing the beginning of HST rotation on Flight Day 8 was analyzed. Camera B was used to image tips A (inboard) and B (outboard) during the start of rotation. The video sequence that was analyzed began at 11:02:02.85 UTC, which was just before the beginning of rotation, and ended at 11:04:09.51 UTC. Tip A was tracked using the line-tracking method because the point-tracking method could not remain fixed on the tip due to the background pattern change from the blackness of space to the blue/white of the Earth. The background for tip B did not change, and tip B was tracked with the point-tracking method. Tip A had a maximum peak-to-peak displacement of  $0.62 \pm 0.07$  inches at 11:03:02.18 UTC, and tip B had a maximum peak-to-peak displacement of  $0.64 \pm 0.07$  inches at 11:03:01.51 UTC. Both tips had a dominant frequency of approximately 0.1 Hz. Figure 6.9 shows the plot of the oscillatory displacement of the solar array tips as a function of time. The plot in Figure 6.9 represents a smoothing of the original data using a five-point moving average filter. Filtering of the data was necessary to remove high frequency noise in the motion tracking. Appendix G contains the raw, unsmoothed, displacement plot and the translational motion and frequency plots.

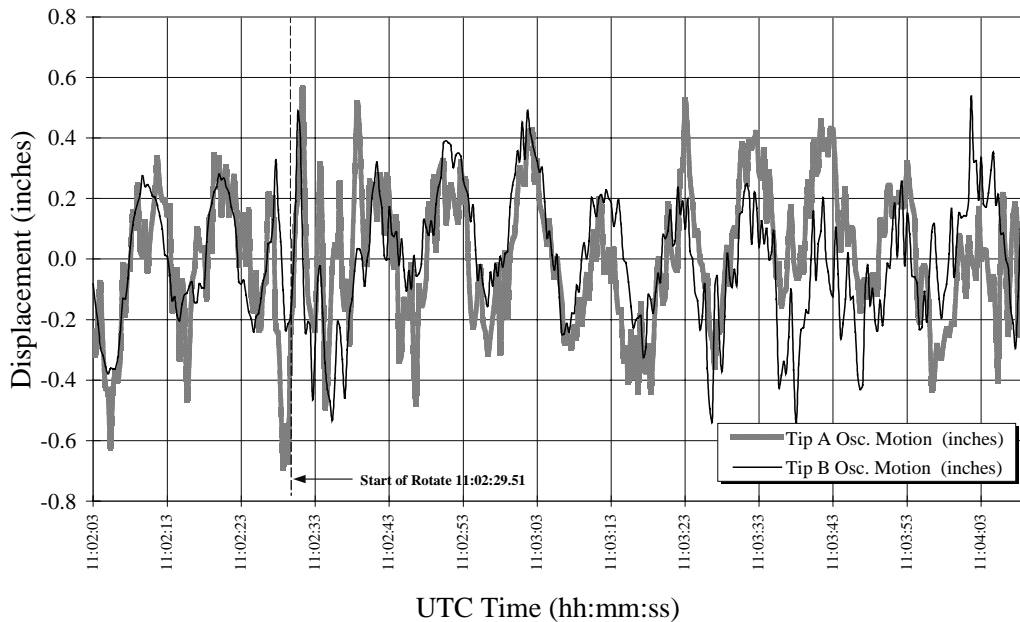


***Figure 6.9 Solar array tip displacement during start of rotate event (Flight Day 5).***

Note that there was considerable noise in the displacement of tip A at the beginning of rotation. This noise was caused by a bowing of the bistems at the time that rotation began. This bowing distorted the bistem edge that was being tracked by the line-tracking method and accounts for the noise in the tip displacement.

### End of rotation

An approximately 2.5-minute video sequence showing the end of HST rotation on Flight Day 8 was analyzed. Camera B was used to image tips G (inboard) and H (outboard) during the end of rotation. The video sequence began at 11:14:00 UTC, which was just before the end of rotation, and ended at 11:16:35 UTC. Tip G had a maximum peak-to-peak displacement of  $1.05 \pm 0.14$  inches at time 11:15:29.01 UTC with a dominant frequency of 0.1 Hz. Tip H had a maximum peak-to-peak displacement of  $0.97 \pm 0.11$  inches at time 11:15:38.35 UTC with a dominant frequency of 0.1 Hz. Both tips were tracked using the point-tracking method. Figure 6.10 shows the plot of the displacement of the solar array tips as a function of time. Filtering of the data was necessary to remove high-frequency noise in the motion tracking. Appendix G contains the raw displacement plot and the translational motion and frequency plots.

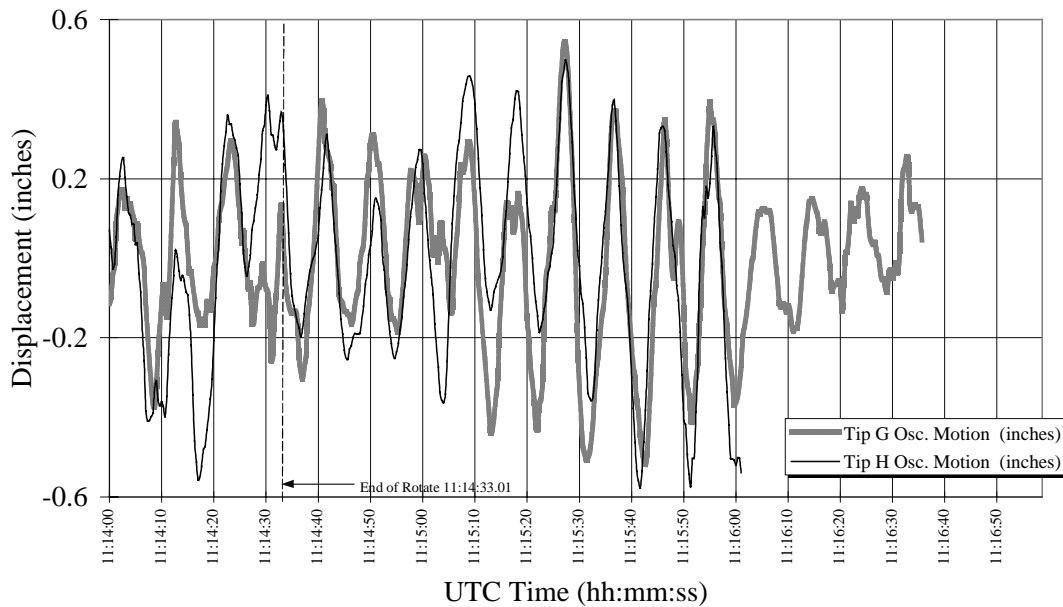


**Figure 6.10** Solar array tip displacement during end of rotate event (Flight Day 5).

Noise in the point-tracking during rotation was caused largely by a changing background. Since part of the pattern about the array tips consisted of the background, the constantly changing patterns contributed to tracking error. Note that tip H was only tracked until 11:16:00 or approximately 35 seconds less than tip G. This was due to a loss in tracking for tip H at this time due to excessive background pattern changes.

## 6.2.6 Airlock Depressurization-Induced Solar Array Motion (Flight Day 8)

The airlock depressurization event on Flight Day 8 was analyzed post-mission to observe the damping of the tip-to-tip displacement. The data were also reanalyzed to obtain better accuracy using sub-pixel motion analysis techniques. (The analysis during the mission used manual point selection.) See Figure 5.12 for a representative image showing the view for the HST during the airlock depressurization event.

The post-mission analysis included the entire 3 minutes of array motion, and used the point-tracking method. The video sequence began at 03:11:58.57 UTC and ended at 03:15:22.43 UTC. During the mission, the time of the solar array slew was obtained from telemetry and there was no independent verification of that time based on imagery. During the post-mission analysis, the time of the solar array slew, as determined from video imagery, was 049:03:12:41.43 UTC or 2.6 seconds earlier than reported during the mission. (Timing using imagery is based on Interrange Instrumentation Group [IRIG] time placed in the audio channel of the video.) The cause of this discrepancy has not yet been resolved.

The post-mission analysis of the tip displacement accounted for the change in the scaling from image to object space caused by the slew of the array. (This was not accounted for in the analysis done during the mission.) Also, in computing the out-of-plane oscillatory motion, the slew of the array was subtracted out.

Figure 6.11 gives the plots of the displacement of the solar array tips and Appendix G contains plots of the displacement before the slew of the array was subtracted out. The plot in Figure 6.11 represents a smoothing of the original data using the five-point moving average filter. For the airlock-depressurization solar array displacement plot, the data had very little noise and smoothing was minimal. The plots of the raw tip displacements and frequency analyses are also in Appendix G. The maximum peak-to-peak displacement was  $9.66 \pm 0.41$  inches at time 03:12:53.77 UTC for tip H and  $6.53 \pm 0.37$  inches at time 03:12:53.43 UTC for tip G. The dominant frequency was approximately 0.1 Hz. Note that the background or base array motion was very evident before the airlock depressurization-induced slew. The peak-to-peak displacement of this background motion was approximately 0.2 inches and the frequency was 0.1 Hz. A clear damping of the tip displacement was observed for both tips. The displacement for tip G was measured for a shorter timeframe (170 seconds) than tip H (210 seconds), because a shadow passed over tip G, changing the background, and causing a loss of tracking. When the shadow passed over tip G, the change in lighting altered the pattern of pixel intensities surrounding the tip so much that the search pattern could no longer recognize the tip.

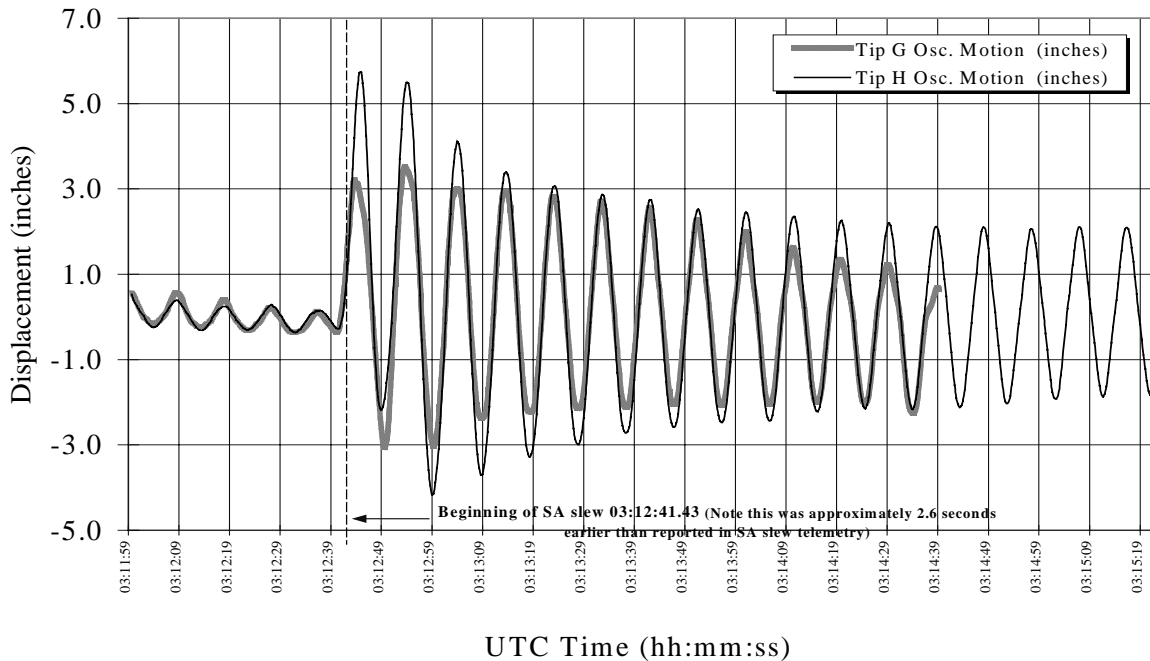


**Figure 6.11** Solar array tip displacements during airlock depressurization (Flight Day 8).

### 6.2.7 Solar Array Motion During the FSS Pivot (Flight Day 8)

The pivot event on Flight Day 8 took place just after a rotation of the HST from the +V3 to the -V3 orientation. The pivot moved the HST from a tilt of 75 deg to a vertical orientation of 90 deg. The RMS elbow camera view of the pivot event was chosen for analysis due to the difficulty in obtaining an acceptable view from a PLB camera. The solar array motion accuracy was projected to be somewhat reduced by using the RMS elbow camera due to the fact that the RMS elbow camera position was not known. The HST FS&S Project was informed about the reduced accuracy, and they concluded the RMS elbow camera would still be acceptable. See Figures 6.12 and 6.13 for representative images showing the views from the beginning and end of pivot.

Like the analysis of solar array motion during the rotation on Flight Day 5, the analysis of the array motion during the HST pivot event on Flight Day 8 was a two-step process. First, the array motion was analyzed from just before the beginning of pivot until several minutes after pivot. The video was analyzed just before the pivot so that a sudden change in the plot of array displacement vs. time would indicate the exact time that pivot began. Second, the array motion was analyzed from just before the end of pivot until several minutes after the end of the pivot event. For the conclusion of the pivot, the video was analyzed just before the end of pivot so that the sudden change in the array displacement plot would indicate the exact time that pivot ended.

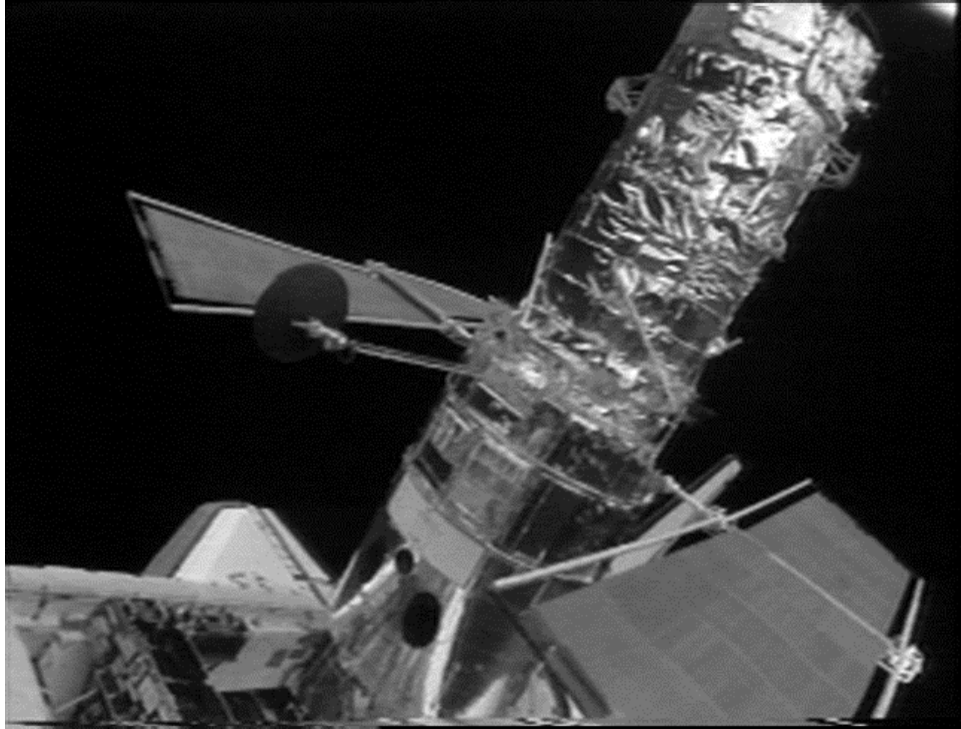


*Figure 6.12 View of -V2 solar array tips E and F from the RMS elbow camera during beginning of pivot.*

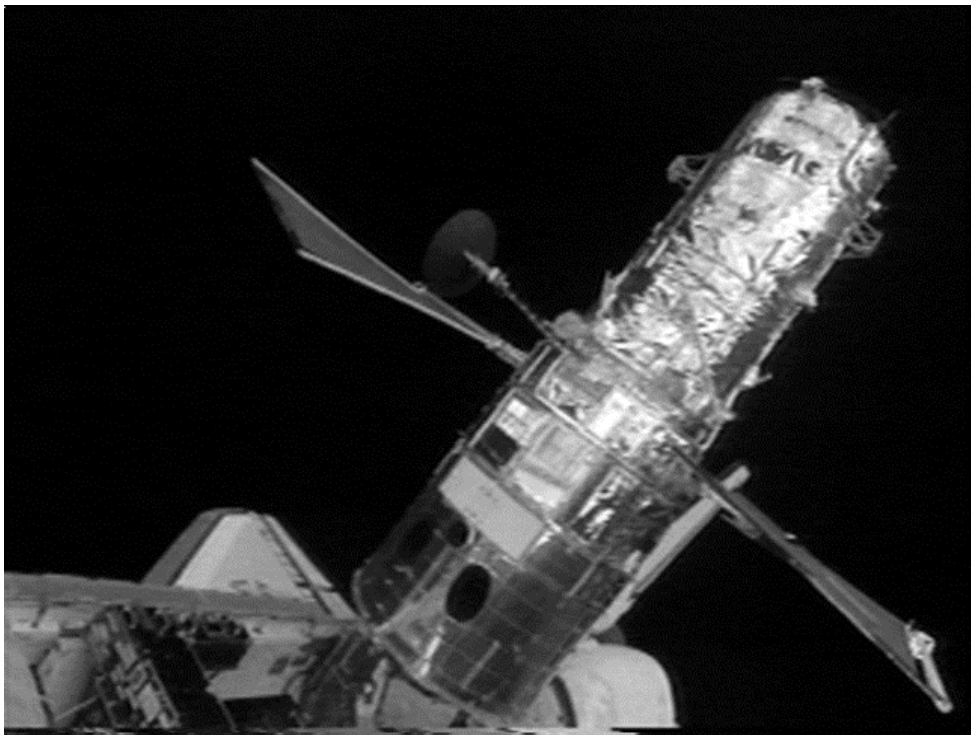


*Figure 6.13 View of -V2 solar array tips E and F from the RMS elbow camera during end of pivot.*

As with the solar array analysis during the rotation event, translational motion was subtracted from the raw solar array tip positions, leaving only the oscillatory out-of-plane motion. The out-of-plane solar array motion was computed as the deviation from a least-square second-order polynomial fitted to the translational motion of the array tip during the pivot operation.

**Beginning of pivot**

A 3-minute video sequence showing the beginning of HST pivot on Flight Day 8 was analyzed. The video sequence that was analyzed began at 08:35:00.8 UTC, which was just before the beginning of the pivot, and ended at 08:38:00.8 UTC. The RMS elbow camera was used to image tips E (inboard) and F (outboard) during the start of pivot. Because the elbow camera position was not fixed, the position had to be estimated. The elbow camera position was estimated using RMS joint position angles and the dimensions of the RMS arm. Knowing the RMS pointing (derived from the joint angles) and the length of the arm, the approximate position of the RMS elbow camera was determined.

Figure 6.14 gives the plots of the displacements of the solar array tips as a function of time, and Appendix G contains plots showing the displacements before the translational correction. The plots in Figure 6.14 represent a smoothing of the original data using the five-point moving average filter. The raw displacement plots and the frequency plots are also in Appendix G. The maximum peak-to-peak displacement for tip E was  $1.43 \pm 0.14$  inches at 08:35:50.46 UTC while the maximum peak-to-peak displacement for tip F was  $1.36 \pm 0.21$  inches at 08:35:50.13 UTC. The dominant frequency for both tips was 0.1 Hz. Again note that the background motion had a peak-to-peak displacement of approximately 0.2 inches with a 0.1 Hz frequency.

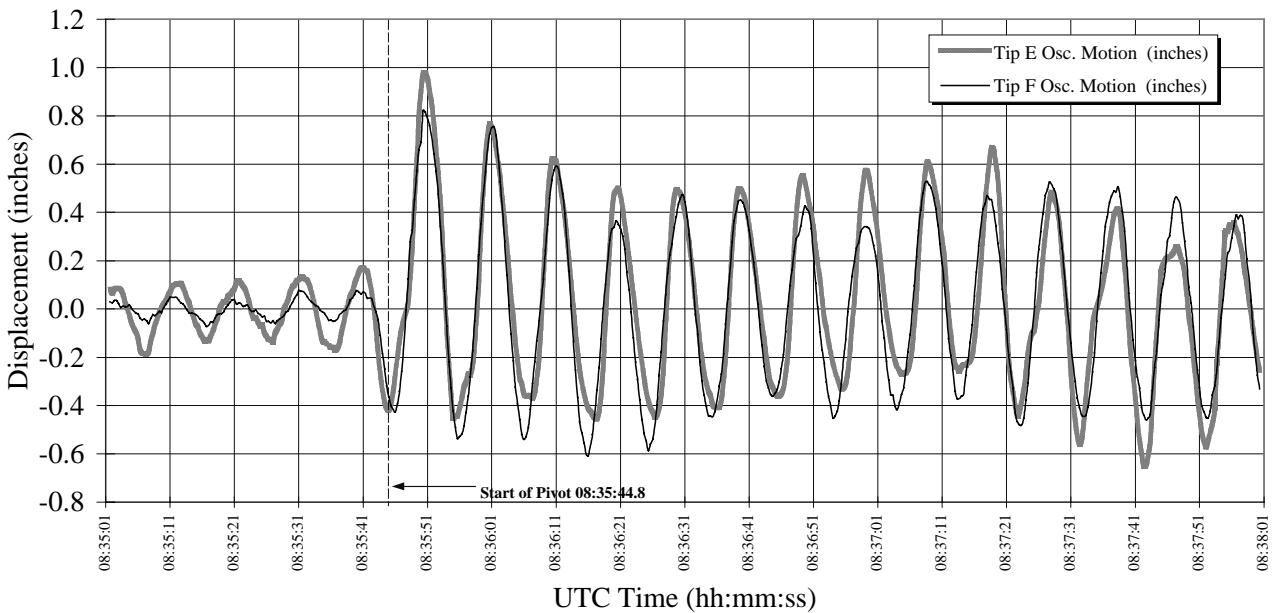


***Figure 6.14 Solar array tip displacements during start of pivot event (Flight Day 8).***

The maximum peak-to-peak tip displacement of 1.43 inches occurred at 08:35:51 (just after the start of pivot) after which the displacements damped to a low of approximately 0.9 inch at 08:36:41. After the low at 08:36:41, the displacements increased again, reaching another high of over 1.2 inches at 08:37:21, before damping to 0.8 inches at the end of the measured sequence. This oscillation of the peak-to-peak displacement implies that a lower frequency mode of approximately 0.01 Hz may be involved in the tip displacement during the pivot operation.

The video data quality for the start of pivot was excellent. The lighting was stable with no shadows moving over the array tips, and tracking was excellent.

### **End of pivot**

A 3-minute video sequence showing the end of HST pivot on Flight Day 8 was analyzed. The video sequence began at 08:38:33.0 UTC, which was just before the end of the pivot and ended at 08:41:33.0 UTC. As with the start of pivot, the RMS elbow camera was used to image tips E (inboard) and F (outboard) during the end of the pivot. Figure 6.15 gives the plots of the displacements of the solar array tips, and Appendix G contains plots showing the displacements before the translational correction. Figure 6.15 represents a smoothing of the original data using a five-point moving average filter. The raw displacement plots and the frequency plots are also included in Appendix G. The maximum peak-to-peak displacement for tip E was  $1.37 \pm 0.13$  inches at 08:39:32 UTC and the maximum peak-to-peak displacement for tip F was  $1.07 \pm 0.29$  inches at 08:39:32.00 UTC. Both maximum displacements occurred just as the pivot operation ended. The dominant frequency for both tips was 0.1 Hz. The accuracy for measuring the tip displacement for tip F was less than for tip E. This can be clearly seen in the raw displacement plots, with tip F being noisier. The cause for the poorer tracking for tip F was not readily apparent in viewing the imagery. No significant lighting or background changes were observed.

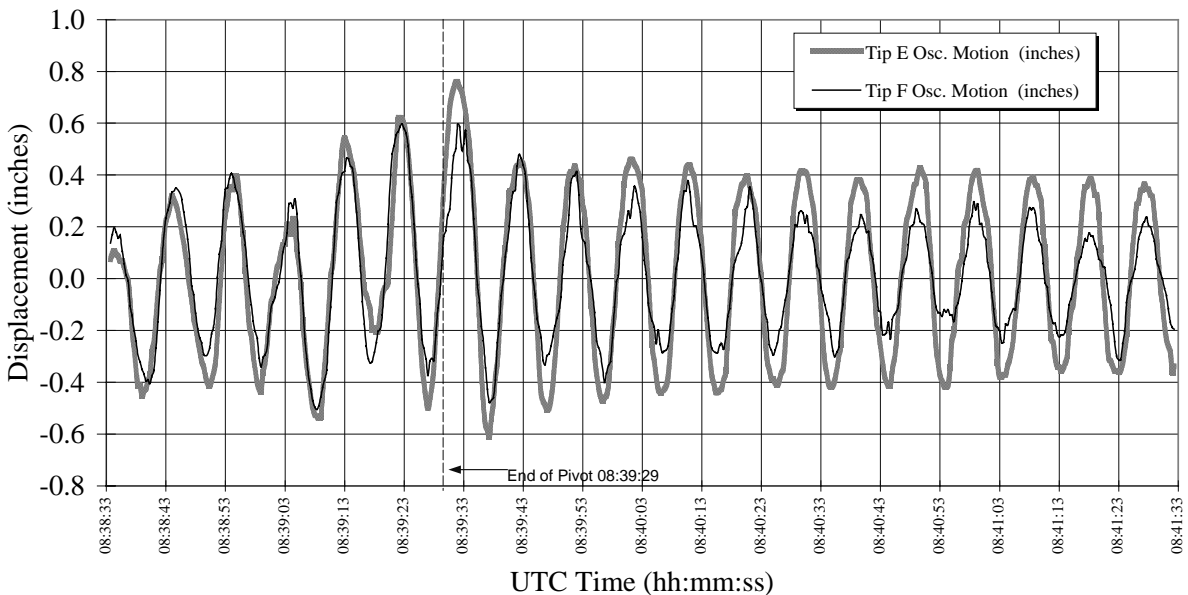


**Figure 6.15** Solar array tip displacements during end of pivot event (Flight Day 8).

Note that the maximum peak-to-peak displacement occurred when the pivot maneuver ended. Also note that the displacement for the two tips were about the same before the end of pivot but, after pivot ended, the peak-to-peak displacement for the inboard tip E was noticeably higher than for tip outboard F.

The tip displacements for the end-of-pivot data were noisier than those for the beginning of pivot. The lighting appeared to be stable with no noticeable shadows moving through the view. The cause for the increased noise in the data was not determined.

### **6.2.8 Solar Array Motion During HST Reboost (Flight Day 8)**

The reboost event on Flight Day 8 was the last in a series of four successful VRCS firings to boost the HST into higher orbits. Figure 6.16 is a representative image showing the view during reboost.

A 3-minute video sequence showing the HST during reboost on Flight Day 8 was analyzed. This was the fourth and last reboost of the mission occurring at UTC 049:10:26 and lasting for 20 minutes. Camera B was used to image tips A (inboard) and B (outboard) during the reboost. Tip A had maximum peak-to-peak displacement of approximately  $1.0 \pm 0.05$  inches at 10:30:06.04 UTC, while tip B had a maximum peak-to-peak tip displacement of  $1.09 \pm 0.06$  inches at 10:30:06.04 UTC. Both tips had a dominant frequency of approximately 0.1 Hz. Figure 6.17 gives the plots of the displacements of the solar array tips and Appendix G contains the raw displacement plots and the frequency plots. Figure 6.17 represents a smoothing of the original data using the five-point moving average filter. The video quality was excellent with steady lighting, no background changes, and no shadows moving through the view. The tracking was very accurate with little noise observed.

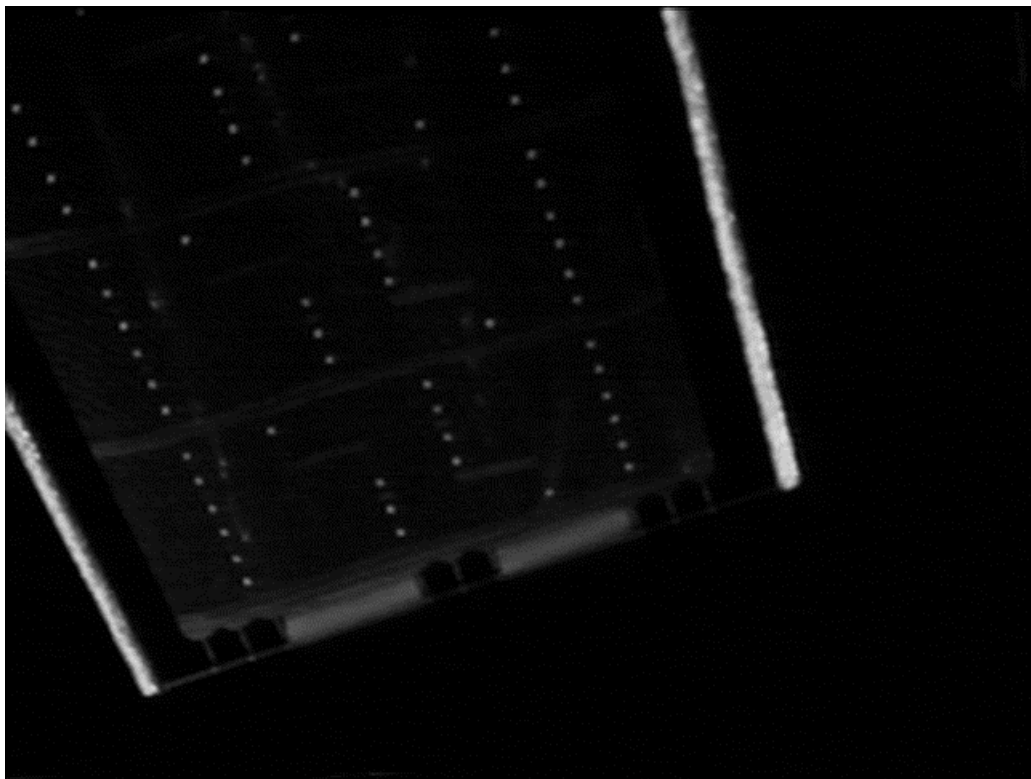


*Figure 6.16 View of +V2 solar array tips A and B from camera B during reboost on Flight Day 8.*

Telemetry for the VRCS firings was not obtained, however there appears to have been a jet firing at approximately 10:29:14 since, before this time, the peak-to-peak displacement was consistent with the 0.2-inch background displacement, and after that time, the deflection increased to nearly 1 inch. Another firing appeared to occur at approximately 10:30:04 when another displacement spike occurs. Note that at the beginning of the sequence, tip B starts out with a positive offset in its displacement from tip A, and at the end of the sequence, the tip A displacement has a higher offset than tip B. This was also noted on the Flight Day 3 VRCS analysis and may be the result of a twisting of the array. (Note that the same effect was observed for the same tips during the VRCS-induced motion. See Figure 6.4.) The plot of the reboost tip displacements appeared similar, although less noisy, than those for the VRCS analysis. This is to be expected since both displacement plots are based on VRCS firings.

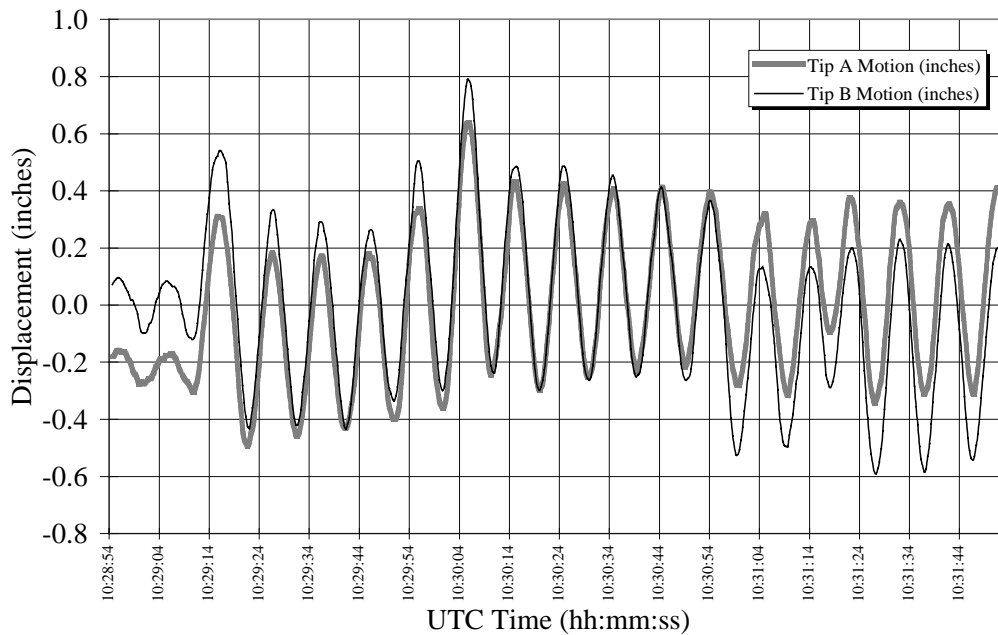


**Figure 6.17** Solar array tip displacements during reboost (Flight Day 8).

### 6.2.9 Summary of Array Motion Analyses

Table 6-8 gives the results from the analysis of the solar array motion events. All solar array motion had a 0.1-Hz frequency as expected. The peak-to-peak displacements ranged from 0.6 inches, for the VRCS- and pivot-induced motion, to 9.7 inches during the airlock depressurization event. The response of the arrays to known excitation events was well-defined for the airlock depressurization, the VRCS firing, the start of pivot, and the reboost. The estimated error was primarily a function of image scale, which ranged from 0.30 inches per pixel for the reboost to 1.3 inches per pixel during the airlock depressurization.

**Table 6-8 Summary of Post-Mission Solar Array Motion Results**

Solar Array Excitation Event	Solar Array Tip	Time of Peak-to-Peak Tip Measurement	Peak-to-Peak Displacement (inches)	Error in inches ( $1\sigma$ )	Dominant Frequency (Hz)
VRCS firing on Flight Day 3	A	20:28:47.7	0.65	0.05	0.1
VRCS firing on Flight Day 3	B	20:28:48.03	0.73*	0.08	0.1
Start Rotate Flight Day 5	A	11:03:02.18	0.62	0.07	0.1
Start Rotate Flight Day 5	B	11:03:01.51	0.64	0.07	0.1
End Rotate Flight Day 5	G	11:15:29.01	1.05	0.14	0.1
End Rotate Flight Day 5	H	11:15:38.35	0.97	0.11	0.1
Airlock Depressurization Flight Day 8	G	03:12:53.43	6.53	0.37	0.1
Airlock Depressurization Flight Day 8	H	03:12:53.77	9.66	0.41	0.1
Start Pivot Flight Day 8	E	08:35:50.46	1.43	0.14	0.1
Start Pivot Flight Day 8	F	08:35:50.13	1.36	0.21	0.1
End Pivot Flight Day 8	E	08:39:32.00	1.37	0.13	0.1
End Pivot Flight Day 8	F	08:39:32.00	1.07	0.29	0.1
Reboost Flight Day 8	A	10:30:06.04	1.00	0.05	0.1
Reboost Flight Day 8	B	10:30:06.04	1.09	0.06	0.1

\* A higher peak-to-peak displacement of 0.85 inches was noted at 20:30:09, but was not confirmed to be the result of a known thruster firing. The displacement presented in the table is known to have occurred immediately following a known VRCS thruster firing.

## 7. LESSONS LEARNED

The following section summarizes the lessons learned from the HST solar array photogrammetric analyses performed during the second servicing mission. These lessons learned are applicable not only for imagery analyses that may be performed during the third servicing mission of the HST, but also to analyses planned during the assembly and operation of the International Space Station (ISS).

### 7.1 Pre-Mission Planning

#### 7.1.1 Resource Planning

The overall resources to perform the required analysis tasks were inadequate. This was caused both by the underestimation of resources JSC would require to perform the analyses, and JSC's and GSFC's mutual desire to keep the scope of the solar array analysis as small as possible so that other important objectives of the servicing mission would not be significantly impacted. In addition, there were significant revisions to the analysis requirements as the planning for the servicing mission progressed, which required a rework or re-scope of pre-mission planning tasks. Further, there was no contingency or reserve funding. The lack of funding led to manpower staffing problems, which primarily meant a large amount of work was on the shoulders of a very small number of people. Future analyses of this type

require a reserve budget to accommodate scope changes and overruns of manpower estimates to complete reworked tasks.

### **7.1.2 Analysis Turnaround Time Estimation**

The estimate of analysis turnaround time was overly optimistic, especially in not accounting for the “little things” that ended up taking a lot of time:

- (a) Imagery pre-processing, including video digitizing and reformatting
- (b) Computer speed, which affected the time to analyze each frame and to run the error model
- (c) Results integration, i.e., bringing the results from different analysts or image sets together to produce the final product

The time these items required was not simulated in the JISs, and was not fully appreciated, as the “real” data were not being analyzed. This meant additional, unplanned manpower was required during the mission to complete the analyses.

### **7.1.3 Virtual Reality Crew Training**

Crew procedures for acquiring photographic and video imagery make extensive use of computer-generated graphics to illustrate representative views and specific camera setups. These graphics are printed and incorporated into the FDF Photo/TV Checklist. Normally, the crew training is a review of the checklist procedures. However, the setups can be simulated in a crew-based virtual reality training laboratory that closely replicates the steps the crew will take during actual in-flight imagery acquisition. These capabilities should be more frequently used to better train the crew by simulating and verifying the acquisition procedures so that acquisition problems can be identified and resolved before the flight.

### **7.1.4 Reference Control Points**

The number and distribution of reference control points on the body of the HST was a critical factor in controlling the error in the photogrammetric solution of the array tip position. Although the selection and determination of these control points on the telescope body was labor-intensive, the control points were used in each of the eight camera views used to analyze the eight array tips. In general, a minimum of six, well-distributed control points are required to analyze each camera view. In addition, at least one backup control point is required in case lighting or geometry variations, reflections, shadows, etc., appear in the acquired imagery. Some of the reference points selected a priori, which were believed to be easily identifiable on the HST, were, in fact, quite difficult to discern in the resultant imagery. For analysis of solar array tip positions of the HST berthed in the Space Shuttle, the minimum number of required control points is in the range of 100-150. GSFC provided position data for 132 points.

As each tip position analysis is being performed, the photogrammetric solution should be concurrently performed on the reference points, and a comparison of the variance of the residuals should be made as a check of the solution for each analysis case. For SM-2, this was not performed during the mission, but was checked postflight. If time permits (which it did not during SM-2), a sensitivity analysis can be performed to reduce the photogrammetric solution error by randomly deselecting individual control points and recalculating the solution error residuals multiple times.

Finally, future photogrammetric analyses for either HST or the ISS require additional reference points located in the Shuttle PLB to supplement reference points on the target body. They are used as verification of the camera location and to account for potential Orbiter body on-orbit dimensional distortions.

### **7.1.5 Lighting**

To acquire and measure solar array motion, it was planned to obtain the required imagery when the solar array was sunlit, with the darkness of space serving as the background. Due to Orbiter attitude operational requirements, it was not always feasible to obtain imagery under the required lighting conditions. Since the automated point- and line-tracking algorithms used for the solar array motion analysis were not operationally robust for tracking dark or silhouetted arrays with the rotating Earth as the background, there were several cases where the tracking of the motion was lost. This made the analysis process significantly more difficult. For cases where attitude requirements or other operational constraints preclude optimal lighting for imagery acquisition, additional pre-processing of the imagery will likely be required to enhance the contrast of the tracked object in relation to the background (in this case, the contrast of the array tip compared to the Earth).

## **7.2 Analysis**

### **7.2.1 Analysis Techniques and Procedures**

Many of the analysis techniques and procedures IS&AG used were developed to analyze a specific type of imagery in a quick-response mode during mission operations or flight contingency investigations. The established techniques are often valid for a narrow range of analysis problems and may not be suitable for other problems with different geometries, etc. It is recommended that a general review be conducted of all analysis assumptions (e.g., scale across FOV, pointing, coordinate space conversions, etc.) and procedures (e.g., ability of the motion tracking algorithm to self-correct for off-nominal conditions, use of lens distortion and calibration data, etc.). This review of the existing set of analysis techniques will serve to focus additional technique development tasks and to assess potential impacts to future analysis.

### **7.2.2 Error Estimation Capability**

Before STS-82, IS&AG did not have a well-defined error estimation capability, since many of the analyses performed by the group were quick, one-time, in-flight analyses which characterized Shuttle or payload anomalies. Some error estimates had been made on previous analyses, but these were rudimentary and not systematic. The measurement of the errors was extremely important for the HST solar array static twist analyses since, as the static twist measurement error increased, the overall analysis margin for total allowable array twist was reduced.

Although the Monte Carlo error analysis capability developed for SM-2 (see Section 3) was a useful tool, it did not account for all measurement errors. In fact, it only accounted for errors associated with the camera setup, viewing geometry, and vehicle/hardware distortions. It did not account for errors associated with variable lighting and focus, motion blur, camera lens distortions, etc. The error estimation capabilities for future imagery analyses should be upgraded to account for these image quality or distortion effects. This is being incorporated into current capability upgrades, along with the ability to better define and track propagated errors.

### **7.2.3 Analyst Point Selection Variation**

The point-of-interest selection variation between the analysts of the array tip static twist imagery—which was evaluated over five flight days—was low, consistent, and accurately modeled as an input to the overall measurement error estimate. The analyst-to-analyst variation was less than 1 pixel, which minimized its contribution to the overall measurement uncertainty.

## **7.3 Operations**

### **7.3.1 Accuracy of Joint Integrated Simulations**

The JISs did not accurately represent the actual mission support and analysis turnaround, in that tasks were omitted (see 7.1.2 above) which took extensive amounts of time in the actual mission. No specific recommendation is made here, except to say that each and every mission support step should be replicated in the JIS, to make sure the actual support gets carried off as planned.

### **7.3.2 Acquisition Procedure Review With INCO**

On-orbit video acquisition procedures were reviewed with the INCO personnel before the mission. The INCO was responsible for the ground-control of the PLB cameras and the prediction and downlink of available on-orbit imagery based on Ku-band signal downlink. Having the INCO understand the purpose and nature of the acquisition requirements greatly improved communications between Mission Control and the VDAS laboratory, and improved the quality of the on-orbit imagery obtained.

### **7.3.3 Ku-Band Coverage Availability**

The prediction of concurrent Ku-band coverage and proper scene lighting for real-time video downlink was problematic, especially when the Orbiter was in free-drift attitude control, and impacted both the array static twist imagery quality and acquisition time. During some daylight passes, there were often only a few minutes of available Ku-band. Thus, acquiring 10 minutes of array data took as long as 3 hours.

### **7.3.4 Training**

IS&AG staff training before the JISs was well-organized and thorough. However, before the mission, the training program for the backup personnel was discontinued due to workload and resource limitations. Consequently, there was not a full backup capability during the mission. This meant that the primary mission support personnel worked two shifts rather than one.

## **7.4 Equipment**

### **7.4.1 Camera Selection**

Although two MLA cameras were selected as a part of the PLB video complement for operational considerations, the MLA was not well-suited for the photogrammetric measurements of the HST solar array. This was due both to the narrower FOV of the MLA vs. the CTVC, and the lower signal-to-noise ratio of the MLA vs. the CTVC.

### **7.4.2 Camera Calibration**

There are lens distortions in the Orbiter CCTV cameras, and these distortions affect the utility of using the cameras for photogrammetric measurements. For future analyses of this type, the technical characteristics of the CCTV video cameras should be measured and documented. This includes calibration of the camera principal point and the distortion of the lens for multiple zoom settings.

## **8. CONCLUSIONS AND RECOMMENDATIONS**

IS&AG has conducted numerous imagery analyses in support of spaceflight missions. However, the scope, precision, and turnaround requirements for the photogrammetric characterization of the HST solar arrays presented a formidable challenge. In fact, this is likely the first time such precise motion and position analysis has been conducted on orbit using non-metric, uncalibrated cameras. The principal results of this work are summarized as follows:

### **8.1 Conclusions From Static Twist Analyses**

- No statistically (or structurally) significant difference was detectable in the solar array twist between the first (Flight Day 3) and the last (Flight Day 8) day of SM-2.
- Within the ability to estimate the errors in the static twist measurements, there were no appreciable changes in static twist during SM-2. The results for Flight Days 6 and 7 are discounted, for the reasons stated in Section 5.2.3.
- The post-mission analysis results for static twist of the solar array tips on Flight Day 8 were generally comparable to the real-time results.
- Although solar array tips G and H had the largest overall twist, tips A and B had the largest twist in the most structurally critical direction, as was reported from SM-1 results.
- The required static twist analyses (5 analyses, 8 tips each) were completed within the required turnaround time of 8 hours from downlink of video data, with one exception. A solution was not obtained for tips C and D on Flight Day 5. This was due to the camera tilt being greater than 90 deg, which had not been accounted for in the implementation of the phototheodolite technique.
- Post-mission analyses were performed to provide the “best and final” positions of the static twist solar array tip positions on Flight Day 8. These were performed with the most robust photogrammetric technique available. However, solutions were not obtained for tips E and F because the control points were linear in object space, and a solution for the HST rotation could not be determined.

- Based on post-mission analyses, neither the real-time analyses nor the post-mission analyses provided results that satisfied the stated  $\pm 1.3$ -inch accuracy requirement for the static twist positions of the solar array tips. Moreover, the analyses and results make it clear that significant improvements in the Orbiter onboard camera capabilities would be required to meet the accuracy levels stated in the requirements. Some improvements can be made by incorporating camera calibrations and improved control points, etc., in the future, but these measures alone will not suffice to meet future analytical requirements for this level of accuracy.
- The HST FS&S Project was advised before the mission that the uncertainties in the static twist measurements would be larger than the requirement. Nevertheless, the HST FS&S Project wanted the best results that could be obtained, and the results were considered sufficient for the FS&S Project to make critical real-time decisions regarding the safety of the HST solar arrays.

## 8.2 Conclusions From Solar Array Motion Analyses

- The required analysis of the out-of-plane amplitudes and frequencies, for two tips of one HST solar array, was performed for the required VRCS-induced motion on Flight Day 3. In addition, IS&AG was able to respond to an in-flight requirement to measure the unexpected HST solar array slew that resulted from the EVA airlock depressurization on Flight Day 8. Both of these solar array motion analyses were performed within the required 8-hour turnaround time.
- Post-mission analyses were also performed to measure the solar array motion for all required events:
  - VRCS-induced motion on Flight Day 3
  - HST start- and end-of-rotation on Flight Day 5
  - Airlock depressurization on Flight Day 8
  - HST start- and end-of-pivot on Flight Day 8
  - HST reboost on Flight Day 8
- Post-mission analyses were performed to determine the peak-to-peak solar array displacements. Error estimates were also determined for the measured peak-to-peak displacements. The maximum peak-to-peak displacement for the VRCS event was determined to an accuracy of  $\pm 0.15$  inches ( $3\sigma$ ) for tip A and  $\pm 0.24$  inches ( $3\sigma$ ) for tip B, which is significantly more precise than the required accuracy of 0.5 inches ( $3\sigma$ ) in the amplitude for the VRCS-induced motion. The measured peak-to-peak displacements were small—only 0.65 and 0.73 inches for the two tips. Moreover, all peak-to-peak displacements were determined to an accuracy of less than  $\pm 0.5$  inches ( $3\sigma$ ), except the airlock depressurization event (2 tips) and tip F for the start- and end-of-pivot on Flight Day 8.
- The magnitudes of the peak-to-peak deflections for the airlock depressurization event were 6.5 and 9.7 inches. These deflections were much larger than all the other solar array deflections. The next-largest deflection was 1.4 inches.
- All solar array motion exhibited the dominant frequency at 0.1 Hz as expected.

### **8.3 Conclusions on Imagery Acquisition**

- The pre-mission planning for imagery acquisition was successful. Essentially all data were acquired as planned. Moreover, the additional requirement for imagery of the solar array slew due to EVA airlock depressurization was accommodated in real time. Inadequate lighting required only a few changes in data acquisition plans, and these changes were also accommodated in real time. However, some lighting and background conditions occurred during the imagery acquisition that significantly affected the solar array motion measurements.

### **8.4 Conclusions on Robustness of Methodologies**

Specific deficiencies have been noted with regard to SM-2 data acquisition and analysis methodologies. These deficiencies are:

- An inadequate quantity and distribution of control points common to both images in each static twist solution not only affected the accuracy of the results, but also the ability to make proper assessments on the accuracy of the results.
- The phototheodolite technique, although fundamentally sound, is not as robust as the bundle adjustment technique, and did not have the advantages of incorporating weights and constraints and providing standard errors as part of the solution.
- The Orbiter video cameras were not adequate to meet the requirements for 3D position accuracy at the precision that was required for HST.
- The Monte Carlo error model used in the validation tests and in the real-time analyses underestimated the errors in the static twist analyses.
- The line-tracking and point-tracking methods both exhibited a loss of tracking under particularly adverse conditions of lighting and scene background. However, one of the two methods was always successful at tracking the array tip.
- The analyses did not include the necessary calibration of camera parameters and corrections for lens distortions.

### **8.5 Recommendations**

Should similar measurements during SM-3, for other Shuttle payloads, or for ISS be required, the following recommendations are made:

- Any new or additional Shuttle-borne equipment should consider higher-resolution video cameras for improved solar array motion results. For improved determination of the positions of features in object space, consideration should also be given to externally mounted high-resolution digital still cameras and to internal bracket-mounted film or digital still cameras.
- Given the current complement of Shuttle video cameras, CTVCs should be used for photogrammetric applications. In particular, the narrow FOV and low resolution of the MLA cameras on SM-2 prohibited post-mission calculations of Flight Day 8 coordinates for tips E and F, and resulted in larger uncertainties for tips C, D, G, and H.

- Cameras must be calibrated to allow geometric distortion corrections to be incorporated into the photogrammetric analyses.
- A near-real-time capability using the photogrammetric bundle adjustment for position determinations should continue to be developed. Additional evaluations and sensitivity analyses should be performed for the specific type of tasks to be encountered. Modifications may be required to improve or add features to the user interfaces.
- The number and distribution of control points should be improved for the specific camera and object configurations to support object-oriented camera calibrations, camera resections, scale determinations, bundle adjustments, motion analyses, and accuracy assessment of results.

## 9. REFERENCES

1. JSC-27943, Hubble Space Telescope SM-2 Multi-Layer Insulation (MLI) Damage Assessment, MLI Damage Photobook. NASA Johnson Space Center. August 7, 1997.
2. Micrometeoroid and Orbital Debris Impact Assessment of the Hubble Space Telescope, STS-82 SM-2. NASA Johnson Space Center. To be released.
3. JSC-48000, STS-82 Flight Plan, Final. NASA Johnson Space Center. January 8, 1997.
4. Photo/TV Checklist, STS-82 Flight Supplement, Final. NASA Johnson Space Center. January 17, 1997.
5. Slama, Chester C., Editor in Chief, Manual of Photogrammetry, Fourth Edition. American Society of Photogrammetry, Falls Church, VA. 22046. 1980.
6. Munji, R., M. Hussain, and D. Peckham, "UMENS Unconventional Mensuration Software," presented paper, ASPRS Annual Convention, Spring 1997.

## **Appendix A: Validation Test Case Results**



# **HST SM-2 Solar Array Static Twist Determination Analysis Validation Test Case Results**



Mike Gaunce

Clyde Sapp

Mark Holly

Image Science & Analysis Group

Earth Science Branch

October 10, 1996

## **Overview**

- Objective
- Validation Test Case Description
- OSVS Imagery Analysis
- Error Model
- OSVS Error Analysis Results
- Implications for SM-2
- Revised SM-2 Error Estimate
- Summary

## **Objective**

“Validation” of SM-2 solar array static twist analysis technique and error estimation using test case data.

### **SM-2 Solar Array Static Twist Analysis Requirements**

- 3-D position determination of each SA tip.
- Number: 5 analyses, 8 tips per analysis.
- Accuracy: +/- 1 inch.
- Turn-around time: 8 hours.

## Validation Test Case Approaches

	Pros	Cons
<b>Ground Test</b>		
GSFC simulator	<ul style="list-style-type: none"> <li>Full Scale Model of the HST provides the potential for high fidelity replication of SM-2 conditions.</li> </ul>	<p>Payload Bay simulator is not equipped with payload bay cameras. Errors associated with camera placement for ground tests may hinder validation.</p> <p>Does not simulate on-orbit effects.</p>
JSC Full Fuselage Trainer (FFT)	<ul style="list-style-type: none"> <li>Bistem / target can be set-up to simulate the geometry expected on SM-2</li> </ul>	<ul style="list-style-type: none"> <li>Forward bulkhead is not fixed to the cargo bay section. This compromises the ground truth locations relative to forward payload bay cameras. Estimated ground truth accuracy of ~ 1 to 1.5 inches.</li> <li>Bistem/target will need to be produced for precise orientation and location.</li> </ul>
JSC Manipulator Development Facility (MDF)	<ul style="list-style-type: none"> <li>Objects can be placed in the simulator with an accuracy of .25 inches (Performed for OSVS Tests).</li> <li>Bistem / target can be set-up to simulate the geometry expected on SM-2</li> </ul>	<ul style="list-style-type: none"> <li>Bistem/target will need to be produced for precise orientation and location.</li> <li>Does not simulate on-orbit effects.</li> </ul>
<b>Pre-Planned On- Orbit Testing</b>		
STS - 80 Orbiter Space Vision System Targets (OSVS)	<p>High precision of ground truth location accuracies (.03 inch) .</p> <p>Each image set has 6 targets suitable for analysis. Each of those targets provides a different test case.</p>	<p>STS - 80 is 2.5 months before from STS - 82. This will limit time available to respond to the lessons learned.</p> <p>The point selection method for the OSVS target is different than that for SA tip selection.</p>
<b>Existing On-Orbit Video</b>		

Method / Example	Pros	Cons
<b>Pre-Planned On- Orbit Testing</b>		
STS - 80 Orbiter Space Vision System Targets (OSVS)	<ul style="list-style-type: none"> <li>High precision of ground truth location accuracies (.03 inch) .</li> <li>Each image set has 6 targets suitable for analysis. Each of those targets provides a different test case.</li> </ul>	<ul style="list-style-type: none"> <li>STS - 80 is 2.5 months before from STS - 82. This will limit time available to respond to the lessons learned.</li> <li>The point selection method for the OSVS target is different than that for SA tip selection.</li> </ul>
<b>Existing On-Orbit Video</b>		
STS - 68 Space Radar Laboratory (SRL) payload	<ul style="list-style-type: none"> <li>Point selections for this payload utilize line intersection method. This is the same method planned for SM-2.</li> </ul>	<ul style="list-style-type: none"> <li>Ground truth location accuracies of the radar platform are uncertain.</li> </ul>
STS - 75 Tethered Satellite System	<ul style="list-style-type: none"> <li>Point selections for this payload utilize line intersection method. This is the same method planned for SM-2.</li> </ul>	<ul style="list-style-type: none"> <li>Ground truth location accuracies of the booms and support are uncertain.</li> </ul>
STS - 76 Orbiter Space Vision System Targets (OSVS)	<ul style="list-style-type: none"> <li>High precision of ground truth location accuracies (.03 inch).</li> <li>Each image set has 6 targets suitable for analysis. Each of those targets provides a different test case.</li> </ul>	<ul style="list-style-type: none"> <li>The point selection method for the OSVS target is different than that for SA tip selection.</li> </ul>

## Validation Test Case Approaches

Method / Examples	Pros	Cons
<b>Ground Test</b>		
GSFC simulator	<ul style="list-style-type: none"> <li>Full Scale Model of the HST provides the potential for high fidelity replication of SM -2 conditions.</li> </ul>	<ul style="list-style-type: none"> <li>Payload Bay simulator is not equipped with payload bay cameras. Errors associated with camera placement for ground tests may hinder validation.</li> <li>Does not simulate on-orbit effects.</li> </ul>
JSC Full Fuselage Trainer (FFT)	<ul style="list-style-type: none"> <li>Bistem / target can be set-up to simulate the geometry expected on SM-2</li> </ul>	<ul style="list-style-type: none"> <li>Forward bulkhead is not fixed to the cargo bay section. This compromises the ground truth locations relative to forward payload bay cameras. Estimated ground truth accuracy of ~ 1 to 1.5 inches.</li> <li>Bistem/target will need to be produced for precise orientation and location.</li> <li>Does not simulate on-orbit effects.</li> </ul>
JSC Manipulator Development Facility (MDF)	<ul style="list-style-type: none"> <li>Objects can be placed in the simulator with an accuracy of .25 inches (Performed for OSVS Tests).</li> <li>Bistem / target can be set-up to simulate the geometry expected on SM-2</li> </ul>	<ul style="list-style-type: none"> <li>Bistem/target will need to be produced for precise orientation and location.</li> <li>Does not simulate on-orbit effects.</li> </ul>

## Validation Test Case Approaches

Method / Example	Pros	Cons
<b>Pre-Planned On- Orbit Testing</b>		
STS - 80 Orbiter Space Vision System Targets (OSVS)	<ul style="list-style-type: none"> <li>High precision of ground truth location accuracies (.03 inch) .</li> <li>Each image set has 6 targets suitable for analysis. Each of those targets provides a different test case.</li> </ul>	<ul style="list-style-type: none"> <li>STS - 80 is 2.5 months before from STS - 82. This will limit time available to respond to the lessons learned.</li> <li>The point selection method for the OSVS target is different than that for SA tip selection.</li> </ul>
<b>Existing On-Orbit Video</b>		
STS - 68 Space Radar Laboratory (SRL) payload	<ul style="list-style-type: none"> <li>Point selections for this payload utilize line intersection method. This is the same method planned for SM-2.</li> </ul>	<ul style="list-style-type: none"> <li>Ground truth location accuracies of the radar platform are uncertain.</li> </ul>
STS - 75 Tethered Satellite System	<ul style="list-style-type: none"> <li>Point selections for this payload utilize line intersection method. This is the same method planned for SM-2.</li> </ul>	<ul style="list-style-type: none"> <li>Ground truth location accuracies of the booms and support are uncertain.</li> </ul>
STS - 76 Orbiter Space Vision System Targets (OSVS)	<ul style="list-style-type: none"> <li>High precision of ground truth location accuracies (.03 inch).</li> <li>Each image set has 6 targets suitable for analysis. Each of those targets provides a different test case.</li> </ul>	<ul style="list-style-type: none"> <li>The point selection method for the OSVS target is different than that for SA tip selection.</li> </ul>

## OSVS Test Case Description

- Orbiter Space Vision System (OSVS)
  - Uses array of targets to determine position based on 3D photogrammetric solution.
- OSVS targets flown on STS-76; located on the Orbiter Docking System.
- Targets were viewed from cameras A and D.
- Three sets of OSVS views from cameras A and D were analyzed.
  - Six targets per view.
  - 5-6 reference points per view.

## Applicability of Validation Test Case to SM-2

### Pros

- Representative video data (on-orbit, overlapping FOV, etc).
- High precision of ground truth location accuracy (0.03 in).
- Each image set has 6 targets suitable for analysis. Each of those targets provide a different test case.

### Cons

- The point selection method for the OSVS targets is different than that for SA tip selection.
- Different geometry (object distance, camera angular separation).
- Errors associated with HST rotation are not tested.
- OSVS targets are stationary.
- Acquisition procedure different for SM-2.

## **OSVS Validation Test Case Assumptions & Groundrules**

- Scaling & pointing information derived from payload bay imagery.
- Validation based on comparing measured values to ground truth locations plus estimated error.
- Error estimate will be calculated using the same technique as SM-2.
- Error associated with the line tracking and blob analysis are similar. Both blob analysis and line tracking algorithms use multiple pixels to determine a point of interest. The resulting pixel data is accurate to a fraction of a pixel.

## **OSVS Validation Test Case Analysis Procedure**

- Determine 2-D pixel locations for 5-6 observable reference points (hand rail edges).
- Perform blob analysis on images of the OSVS targets to determine the target's 2-D centroid position.
- Determine the angular field-of-view for each camera using reference points.
- Determine pointing parameters for each camera using reference points.
- Determine a vector for the Point of Interest (POI) for each camera.
- Determine the 3-D location of the POI by determining the intersection of the vectors.

## OSVS Validation Test Case Surveyed and Calculated Target Positions

Image Set 1	Surveyed			Calculated			Magnitude of Error	
	Target Number	X	Y	Z	X	Y		Z
1	704.19	14.69	447.28	704.64	14.57	447.54	0.53	
2	704.19	14.69	439.77	704.64	14.57	439.93	0.49	
3	699.95	2.68	447.66	700.07	2.56	447.87	0.27	
4	699.91	-2.61	442.34	700.00	-2.63	442.44	0.13	
5	704.61	-15.63	447.19	704.18	-15.60	447.27	0.44	
6	704.61	-15.61	439.68	704.45	-15.42	439.71	0.25	
							0.35	Average

Image Set 2	Surveyed			Calculated			Magnitude of Error	
	Target Number	X	Y	Z	X	Y		Z
1	704.19	14.69	447.28	704.59	14.78	447.84	0.69	
2	704.19	14.66	439.77	704.58	14.80	440.14	0.56	
3	699.95	2.68	447.66	699.80	2.61	448.19	0.56	
4	699.91	-2.61	442.34	699.77	-2.55	442.67	0.36	
5	704.61	-15.63	447.19	703.70	-15.56	447.60	1.00	
6	704.61	-15.61	439.68	704.22	-15.31	439.87	0.52	
							0.62	Average

Image Set 3	Surveyed			Calculated			Magnitude of Error	
	Target Number	X	Y	Z	X	Y		Z
1	704.19	14.69	447.28	704.16	14.23	447.20	1.07	
2	704.19	14.66	439.77	705.21	14.26	439.79	1.10	
3	699.95	2.68	447.66	700.93	2.55	447.51	1.00	
4	699.91	-2.61	442.34	700.91	-2.59	442.24	1.01	
5	704.61	-15.63	447.19	705.53	-15.33	446.94	1.00	
6	704.61	-15.61	439.68	705.56	-15.31	439.62	1.00	
							1.03	Average

Note: Orbiter PLB Coordinate System. All dimensions in inches.

## Error Model Description

- Monte Carlo error analysis methodology.
- Input variables modified by addition of randomly generated, normally distributed errors.
- Multiple iterations performed, with statistics collected on output position values.
- Output errors shown as three standard deviations of iteration results.

## Solar Array Static Twist Error Model Input Errors

Error Source	Contributors	Amount	Comments
Reference Points	Fabrication Specs	0.03 in	Interface Control Document ICD-3-0045-03
	Orbiter Distortion	0.1 in	Provided by CVS
	Attach Point Tolerances	0.177 in	Shuttle Orbiter/Cargo Standard Interface ICD-2-19001Section 3.3.1.2.1
OSVS Reference	Survey Accuracies	0.03 in	Provided by CVS
Image Point Selection	Operator Error	2 pixels	IS&AG estimate
	Blob Analysis Error	0.15 pixels	IS&AG estimate

## OSVS Validation Test Case Predicted and Calculated Errors

	Predicted Error			Calculated/Survey Error			Comparison			
	Target Number	X	Y	Z	X	Y	Z	X	Y	Z
Image Set 1	1	0.61	0.50	0.53	0.45	0.12	0.26	In	In	In
	2	0.61	0.50	0.52	0.45	0.09	0.16	In	In	In
	3	0.59	0.50	0.52	0.12	0.13	0.20	In	In	In
	4	0.61	0.50	0.51	0.09	0.02	0.10	In	In	In
	5	0.68	0.53	0.54	0.43	0.03	0.09	In	In	In
	6	0.67	0.53	0.52	0.16	0.18	0.04	In	In	In
Image Set 2	1	0.64	0.51	0.56	0.40	0.10	0.56	In	In	Out
	2	0.63	0.51	0.53	0.40	0.14	0.37	In	In	In
	3	0.61	0.51	0.56	0.15	0.08	0.53	In	In	In
	4	0.63	0.51	0.54	0.14	0.06	0.33	In	In	In
	5	0.68	0.54	0.56	0.91	0.07	0.41	Out	In	In
	6	0.67	0.53	0.54	0.39	0.30	0.19	In	In	In
Image Set 3	1	0.67	0.52	0.56	0.97	0.45	0.09	Out	In	In
	2	0.66	0.52	0.53	1.02	0.40	0.01	Out	In	In
	3	0.61	0.52	0.54	0.98	0.14	0.15	Out	In	In
	4	0.59	0.52	0.52	1.00	0.02	0.10	Out	In	In
	5	0.63	0.53	0.54	0.92	0.30	0.24	Out	In	In
	6	0.64	0.53	0.53	0.95	0.29	0.06	Out	In	In

## **Summary of OSVS Validation Test Case Results**

- Error between surveyed and calculated positions ranged from 0.13 to 1.10 inches, with a mean of 0.67 inches.
- Targets 3 & 4 were less skewed in the image, and therefore exhibited lower error.
- Image set 3 considered an “off-nominal” case. Lighting and focus were less than optimal (~50% less sharp, compared to image sets 1 and 2).
- Error model correctly accounts for geometric variations, but does not, in general, account for poor image quality.
- In general, error model agrees with calculated error. However, error model underpredicts estimated error in off-nominal conditions.

## **HST SM-2 Error Estimate**

- Same input error assumptions as validation test case.
- One analysis geometry analyzed (SA tips A&B, using PLB cameras B and D).
- Initial error analysis estimated to be 3.8 inches.
- Minor changes to acquisition and analysis procedures reduced error to 2.8 inches.
- Errors expected to be reduced further through procedure changes.

## Open Issues/Concerns

- On-orbit distortions still need to be modeled (RI-DNY analysis of STS-82 configuration in work). Current error model likely underestimates.
- Error model does not currently account for camera lens distortions. Data to be obtained from Canadians and incorporated into SM-2 analysis procedures.
- Acquisition and analysis procedures to be revised to reduce static twist analysis errors.

## Summary

- Validation test case valuable exercise for reviewing data acquisition and analysis techniques and upgrading error modeling.
- Predicted error for validation case mostly agrees with the measured error.
- Based on new model, estimated SM-2 analysis accuracy does not currently meet the requirement of 1 inch.
  - Acquisition and analysis procedures under review.
  - Accounting for additional input errors may be warranted.

## Backup Charts

### General Error Sources for 3-D Triangulation

Calculation Parameters	Error Source
Scale	<ul style="list-style-type: none"><li>• Reference point selection error.</li><li>• Number of reference points.</li><li>• Position uncertainty of scaling reference features.</li><li>• Magnitude of angle subtended by planned scaling points.</li></ul>
Camera Pointing (Azimuth & Elevation)	<ul style="list-style-type: none"><li>• Reference point selection error.</li><li>• Position uncertainty of pointing reference features.</li><li>• Number of reference points.</li></ul>
Point Selection	<ul style="list-style-type: none"><li>• Point of interest selection error.</li></ul>

## OSVS Test Case Video Shuttle Mission STS-76

Image Set	Camera View	Tape Number	Time(GMT) Day:Hour:Min:Sec
One	Camera A	612028	84:21:33:00
	Camera D	612028	84:21:45:45
Two	Camera A	612029	84:18:13:53
	Camera D	612028	84:21:33:40
Three	Camera A	612029	84:19:46:56
	Camera D	612029	84:19:50:47

## OSVS Target Locations

Target Number	X	Y	Z
1	704.19	14.69	447.28
2	704.19	14.66	439.77
3	699.95	2.68	447.66
4	699.91	-2.61	442.34
5	704.61	-15.63	447.19
6	704.60	-15.61	439.68

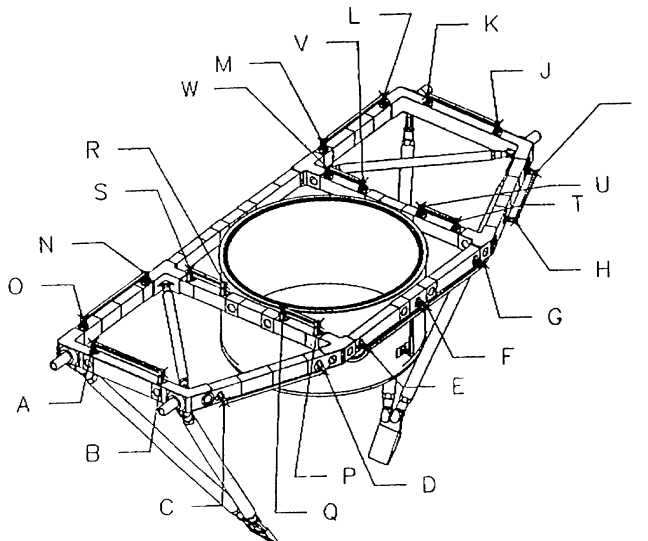
Note: Orbiter PLB Coordinate System. All dimensions in inches.

## OSVS Test Case ODS Support Truss Reference Point Locations

Standoff Post	Xo (in)	Yo (in)	Zo (in)
A	706.79	-86.36	420.48
B	734.90	-86.36	420.48
C	754.77	-80.02	413.61
D	769.28	-47.50	413.61
E	772.93	-29.71	413.61
F	772.93	0.00	413.61
G	772.93	29.71	413.61
H	766.36	54.06	413.61
I	754.77	80.02	413.61
J	734.91	86.36	420.48
K	706.79	86.36	420.43

Standoff Post	Xo (in)	Yo (in)	Zo (in)
L	695.99	77.91	420.23
M	695.99	45.79	420.23
N	695.99	-45.79	420.23
O	695.99	-77.91	420.23
P	757.31	-35.61	420.08
Q	743.19	-35.61	420.08
R	720.01	-35.61	420.08
S	705.89	-36.61	420.08
T	757.31	35.61	420.08
U	743.19	35.61	420.08
V	720.01	35.61	420.08
W	705.89	35.61	420.08

## Reference Points on Orbiter Docking System Truss





## **Appendix B: Solar Array Motion Feasibility Study and Proof of Concept**

# **STS-82 HST/SM-2 Solar Array Motion Assessment Feasibility Study**

## **JSC Image Science & Analysis Group**

During the Hubble Space Telescope's (HST's) second servicing mission, a reboost test will be performed whose purpose is to determine the HST solar array response to reaction control subsystem (RCS) firings. The purpose of the solar array motion assessment is to photogrammetrically determine the amplitude and frequency of the HST solar array motion during the reboost test. This 'quick look' study addresses the basic geometry and camera limitations involved in this analysis to determine the feasibility of performing the required analysis using payload bay (PLB) cameras.

### **GRAF Laboratory—Field of View Visualizations**

Using a CAD (computer-aided design) model of the HST obtained from Goddard Space Flight Center (GSFC), Lorraine Hancock of the Graphics Research and Analysis Facility (GRAF) laboratory created 16 images for visualizing the field-of-view (FOV) range for each of the Shuttle payload bay cameras. For each camera position, four views were generated: color television camera (CTVC)\_full-in, CTVC\_full-out, monochrome lens assembly (MLA)\_full-in, MLA\_full-out. The images were centered about the outer tip of the edge of the solar array closest to each camera. These images acted both as an aid in visualizing the situation as well as bounding the available FOVs from each camera position.

### **Data Collection**

Using the GRAF system, positional information was extracted from each corner of each solar array in the Orbiter coordinate system. These data points were extracted with the solar arrays in the nominal experiment position (approximately parallel to Orbiter XY plane). Payload bay camera positions were obtained from Orbiter drawings.

### **Assumptions**

For the purposes of this 'quick look' analysis, some basic assumptions were made to simplify the problem:

- The HST and solar arrays will be in the nominal position.
- The solar array motion will be primarily along the Orbiter  $Z_0$  axis.
- The overall magnitude of the solar array motion will be small compared to the spreader bar length.
- Downlink will be available during the reboost tests.

### **Basic Analysis Approach**

A basic analysis approach was determined. The basic plan is to acquire imagery of both tips of a solar array edge (i.e., a spreader bar). The camera FOV should be set to maximize the resolution while maintaining both tips in the FOV. The torsion component can then be separated from the other components through comparison of the motion between the two tips. The other three components will be differentiated in the frequency domain. System motion should be well separated from bistem bending in the frequency domain, and the array slippage should come through as broad band noise.

### **Calculations Performed**

An attached spreadsheet shows the results of calculations performed in support of this study along with a brief explanation of the meaning of each column in the spreadsheet. (It should be noted that GSFC has not yet confirmed the CAD verification calculations.) The primary calculations were:

- Distance from each camera to each solar array corner.
- Aspect angle of expected motion from each camera to each solar array corner.
- Required FOV size for each camera looking at each spreader bar.
- Smallest resolvable motion at each solar array tip from each camera.

## Findings

The pointing criteria in the original GRAF FOV visualizations were based on the assumption that the highest accuracy would come from a camera looking at the solar array edge to which it was closest. The calculations show that this assumption was not true, due mainly to the aspect angle and to the versatility of the camera focal lengths. Basically, the primary limitation to resolution was determined to be the viewing angle. Because of this, the highest resolution (on the order of 0.25 inches/pixel) will be obtained by looking at the solar array edge furthest away from the camera. However, the resolution is still sufficient to do the analysis even if forced to use the closest solar array edge.

Summary of findings:

- Both CTVC and MLA FOVs are sufficient to perform the task.
- The primary limitation to resolution is view angle.
- Minimum resolvable motion is more than sufficient to perform the task.
- The analysis system will be versatile enough to adapt to dynamic on-orbit situations.

## Issues to be Addressed During Analysis Technique Definition

This ‘quick look’ study was not an in-depth study of the problem. It looked strictly at the basic geometry and camera limitations to determine the overall feasibility of the task. There are several issues that will have to be addressed during the analysis technique definition phase of this project. Obviously, all of the assumptions mentioned above will have to be examined for validity. In addition, the following issues will have to be addressed:

- Lighting
- Feature extraction from background
- Magnitude of expected motion and ramifications on solar array edge visibility
- Turnaround time for near-real-time response
- Method for dynamic determination of camera/solar array tip combination to use for analysis (i.e., if the situation is other than nominal, how to quickly choose current best data collection)
- Expected accuracies of motion study (i.e., throughput accuracy)

For further information contact:

Mike Gaunce  
 NASA-JSC  
 (713) 483-5153  
 gaunce@snmail.jsc.nasa.gov

Clyde A. Sapp  
 Lockheed ESC  
 (713) 483-5141  
 sapp@snmail.jsc.nasa.gov

SM-2 Solar Array Motion Assessment Feasibility Study

Payload Bay Cameras		HST Solar Array Tips		CAD Verification		Camera to solar array Tips						
CamA_x	589	A_x	748.9				Distance (inches)	Angle Off Horizontal (deg)	Resolution Modifier	Camera Alpha (rads)	Resolvable Distance (inches)	FOV (deg)
CamA_y	-71.5	A_y	-122.8	<b>Spreader Bar Lengths</b>		CamA_A	237.0	44.9	334.6	0.0010	0.33	28.1
CamA_z	446	A_z	613.3	A_B	114.13	CamA_B	278.1	34.2	336.2	0.0008	0.28	23.9
				C_D	116.63	CamA_C	661.4	18.1	695.9	0.0004	0.25	10.1
CamB_x	1294	B_x	749.3	E_F	118.40	CamA_D	673.2	15.4	698.3	0.0003	0.24	10.0
CamB_y	-87	B_y	-236.4	G_H	115.62	CamA_E	309.3	35.2	378.6	0.0008	0.29	22.2
CamB_z	446	B_z	602.3			CamA_F	377.5	22.5	408.7	0.0006	0.26	18.1
				<b>Dual Bistem Lengths</b>		CamA_G	680.0	14.7	703.1	0.0003	0.24	9.8
CamC_x	1294	C_x	1215.5	A_C	468.18	CamA_H	725.7	15.6	753.3	0.0003	0.24	9.1
CamC_y	87	C_y	-122.8	B_D	467.95							
CamC_z	446	C_z	651.7	E_G	468.33	CamB_A	571.3	17.0	597.5	0.0004	0.24	11.5
				F_H	468.77	CamB_B	586.0	15.5	608.1	0.0004	0.24	11.2
CamD_x	589	D_x	1216.7			CamB_C	223.1	67.2	576.7	0.0011	0.62	30.7
CamD_y	71.5	D_y	-236.3			CamB_D	245.5	46.8	358.5	0.0010	0.35	27.7
CamD_z	446	D_z	624.9			CamB_E	611.5	17.0	639.3	0.0004	0.25	11.1
						CamB_F	650.1	12.9	666.8	0.0004	0.24	10.5
NPix	500	E_x	748.6			CamB_G	283.7	37.5	357.6	0.0008	0.30	23.7
		E_y	124.4			CamB_H	386.7	30.2	447.6	0.0006	0.27	17.3
		E_z	624.4									
						CamC_A	607.6	16.0	632.0	0.0004	0.24	10.8
		F_x	749.8			CamC_B	652.5	13.9	672.0	0.0004	0.24	10.0
		F_y	237.9			CamC_C	304.1	42.6	412.9	0.0008	0.32	22.2
		F_z	590.7			CamC_D	377.5	28.3	428.7	0.0006	0.27	17.8
						CamC_E	575.1	18.1	604.9	0.0004	0.25	11.8
		G_x	1216.9			CamC_F	583.0	14.4	601.8	0.0004	0.25	11.7
		G_y	124.4			CamC_G	192.8	63.6	433.7	0.0012	0.54	35.4
		G_z	618.7			CamC_H	258.4	48.9	393.0	0.0009	0.36	26.1
		H_x	1215.9			CamD_A	302.2	33.6	362.9	0.0008	0.28	21.9
		H_y	237.9			CamD_B	380.7	24.2	417.5	0.0006	0.25	17.3
		H_z	640.7			CamD_C	687.4	17.4	720.4	0.0003	0.25	9.7
						CamD_D	721.6	14.4	744.9	0.0003	0.24	9.3
						CamD_E	245.1	46.7	357.4	0.0010	0.35	28.2
						CamD_F	272.9	32.0	321.9	0.0009	0.28	25.3
						CamD_G	653.4	15.3	677.5	0.0004	0.24	10.2
						CamD_H	677.2	16.7	707.1	0.0003	0.24	9.8

## SM-2 Solar Array Motion Assessment Feasibility Study

- Note:** HST Solar Array Tips: Coordinates (Orbiter coordinate system) obtained from GRAF CAD of solar array tips in nominal position.
- Note:** Distance: Distance in inches from camera to solar array tip.
- Note:** Angle Off Horizontal: For this exercise, I am making the assumption that the solar array motion will occur along the  $Z_o$  axis.
- Note:** Resolution modifier is the distance divided by the cosine of the angle off horizontal. When this is multiplied by the sine of the minimum angle, resolution resolvable by the camera will result in the smallest resolvable motion of the solar array.
- Note:** Camera Alpha: Measurement in radians of smallest resolvable angle of camera set with FOV optimized to contain full length of spreader bar. This assumes that the camera FOV is equivalent to 500 resolvable pixels. This number is intentionally left small to account for “slop” in FOV setting.
- Note:** Resolvable Distance: (Inches) Smallest distance (i.e. one pixel) able to be measured in direction of motion. This takes into account distance, FOV size, and aspect angle.
- Note:** FOV (deg): Field of view required to contain entire length of spreader bar. This calculation performed primarily to compare to documented FOV limitations for CTVC and MLA cameras.

**Hubble Space Telescope**  
**Solar Array Motion**  
**Proof-of-Concept Analysis**  
October 19, 1995

**Introduction**

An altitude reboost of the Hubble Space Telescope (HST) is required during Servicing Mission 3 (SM-3), currently manifested for late 1999, to maintain full vehicle operational capability. The reboost will be performed using a select set of Shuttle primary reaction control subsystem (PRCS) thrusters with the HST in a berthed configuration with the solar arrays deployed. Analytic studies indicate negative structural margins for the solar arrays under most closed-loop reboost options. Other studies, however, indicate positive structural margins for all vehicle structures (with the solar arrays being the most critical structure) under reboost conditions using short-duration PRCS thruster firings in an open-loop scenario (i.e., no attitude error or rate correction firings). To correlate and reduce the uncertainty factors in the analytic models, a reboost confidence test is required for Servicing Mission 2 (SM-2) planned for February 1997. The test will involve a series of increasing-duration PRCS thruster firings using selected jets, which have been shown analytically to provide the highest solar array structural margins. The PRCS thruster firings will induce motion of the solar arrays and subsequent deflection of the solar array bistem tips. The magnitude of the bistem tip displacement can be directly mapped to the solar array structural load margin. Video analysis of the motion will be used in near-real-time to determine bistem tip displacements after each PRCS thruster firing. This data will in turn be used to assess the structural margin of the solar array and to determine whether to increase the duration of the subsequent thruster firings.

The Image Science and Analysis Group (IS&AG) has completed a proof-of-concept analysis of the motion of a solar array on the HST during SM-1 on [Space Transportation System, or Shuttle Flight] STS-61. This analysis was designed to assess the accuracy of similar measurements planned for SM-2. This document presents the results of this analysis and a discussion of the relationship between SM-1 and SM-2 results. The goal of the analysis has been to assess the accuracy achievable from the video analysis technique and identify technical or procedural issues required to improve the accuracy or speed of the SM-2 analysis. Future efforts will address the technical concerns of the requested data reduction turnaround time.

**Video Screening**

Approximately 14 hours of video from SM-1 were screened to find solar array motion. Several video sequences were identified which displayed some motion. The interval selected for the proof-of-concept analysis was chosen based on the magnitude of the visible motion and the relative quality of the imagery over the analysis interval. The view used had a background consisting primarily of the cloud cover on the Earth. The variation in this background during the analysis sequence suggested the use of an internal feature of the solar array which was parallel with the solar array tip. An interface between two different colors of solar array material was used instead. This interface provided a relatively low contrast, which increased the data collection error.

The proof-of-concept analysis used a 48-second interval of video from Orbit #32 starting at 338:11:42:33 UTC (coordinated universal time). The HST was berthed with the solar arrays oriented approximately perpendicular to the Orbiter PLB. The video was recorded in a split-screen mode during this interval. Figure 1 shows a representative frame from the analyzed sequence. The left half of the split screen was from Orbiter PLB camera B (port aft corner of PLB) viewing the top end of the +V2 solar array on the port side. The right half of the view was from camera C (starboard aft corner of PLB) of the highest end of the -V2 solar array on the starboard side. The view of the +V2 solar array was not used due to noticeable bending or twisting along the span of the array. The -V2 solar array edge was visible from camera C so this view was used for analysis.

### **Image Analysis Technique**

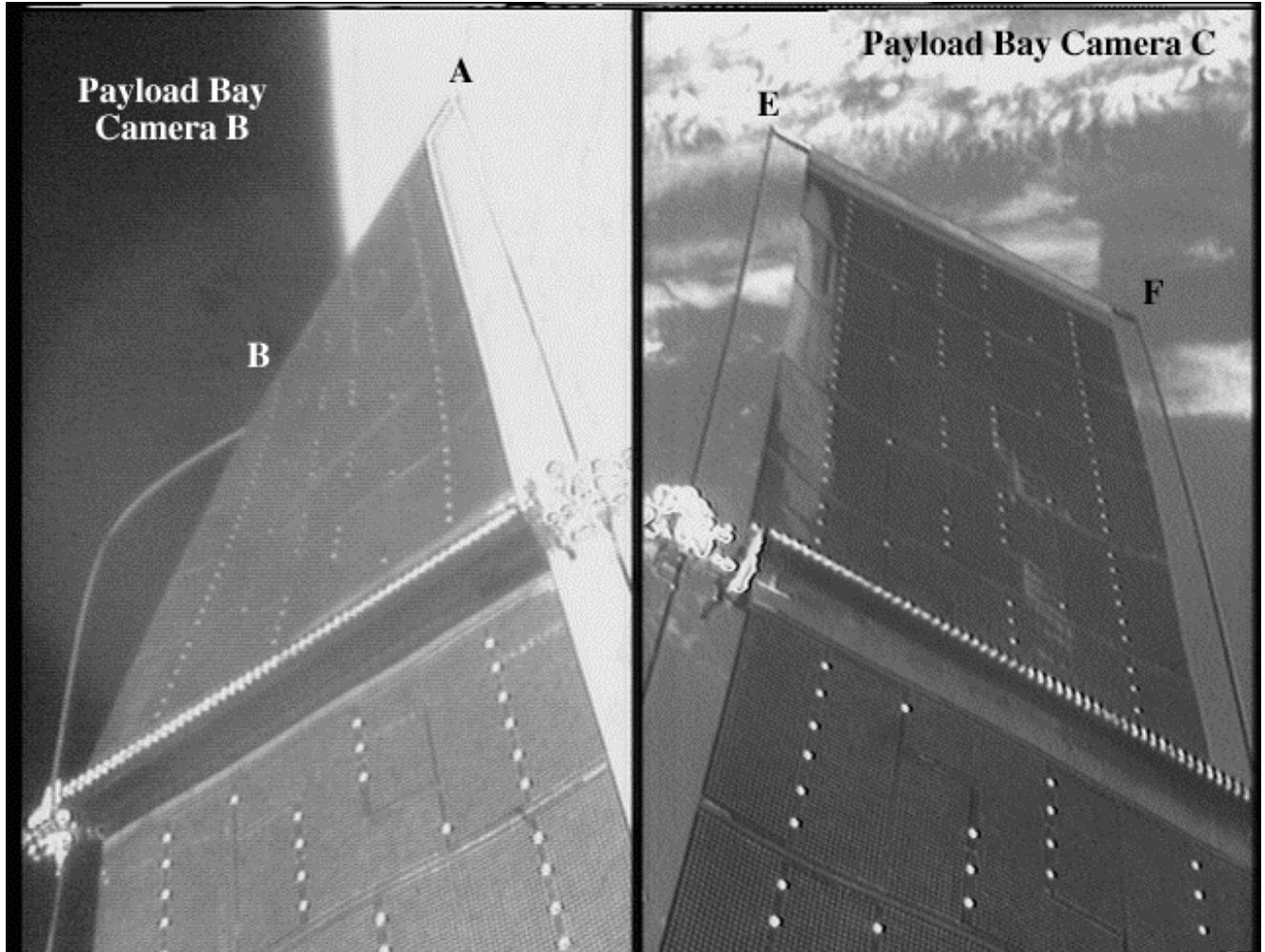
The digital images used for the analysis were digitized from video using an Abekas digital disk recorder. This digital recorder converts video signals into 720x486 arrays of 16-bit color which are accessible by computer. The resulting image has non-square pixels, so appropriate corrections had to be made to produce accurate scaling information. Only the intensity information was used for each image for processing speed improvements.

Image analysis techniques which had been used in previous IS&AG analysis tasks were tailored and integrated into a program to complete the analysis on a frame-by-frame basis. The program first applies a Gaussian edge detection algorithm to each image. The result is a monochrome image with intensity values based on the gradients of the values in the input image.

A sliding window technique was used to identify a solar array edge to be tracked. The motion of this edge on the image was used to calculate the real-world motion of the solar array. Monochrome intensity values inside the window were thresholded to produce a binarized image. The x and y image coordinates of the "on" pixels in the window were used in the calculation of a linear least-squares line fit. The slope and y-intercept of the line fit was the output of the image analysis algorithm.

GSFC supplied the Orbiter coordinates of the solar array end points for SM-1. These values were calculated under the assumption of a fully extended solar array along the Orbiter Z-axis (straight up) with no twist or bend. A rotational offset of the solar array by approximately 2.5 deg and some twisting of the solar array were expected. (The amount of twist was not available at the time of this analysis so these numbers were not corrected.) The possible impacts to the precision and accuracy will be addressed during the discussion of the error considerations.

The motion of the solar array edge in image coordinates was determined by using the slope and y-intercept from the output of the image analysis algorithm discussed previously. The x-coordinates for the endpoints of the line segment defining the solar array edge on the first analyzed image were used in the linear equation to determine a y-coordinate for each endpoint for each frame. Since the motion of the solar array edge was not entirely vertical on the image, a constant correcting factor was applied to the measured motion to correct the motion values.



*Figure 1: Frame of video from Servicing Mission 1 used in proof-of-concept analysis.*

## **Results**

Figure 2 presents the results of the proof-of-concept analysis for both the left and right corners of the solar array. The maximum deflection for both measurements is near the start of the analyzed interval with a magnitude of approximately 1 inch.

The measured motion was expected in general to resemble a damped sinusoid function. Figures 3 and 4 compare the measured motion to a fit of a damped sinusoid function for both the left and right corners of the top of the -V2 solar array.

Research has indicated that the interval of video used for the proof-of-concept analysis coincided with Orbiter RCS firings. Specifically, thruster information JSC's Structures and Mechanics Division provided indicates that thrusters L5D and R5D were active for 2 seconds before and 2 seconds into the analysis interval. Due to these thruster firings during the early portion of the analyzed interval, the first 3 seconds of the measured data were not used to calculate the line fit. This explains the poor fit during this period. The divergence of corner E from the measurements of corner F and the damped sinusoid line fit at the end of the analysis interval is not yet fully understood. The information from the Structures and Mechanics Division shows no other thruster firings in the analyzed time interval. Other

possibilities for causing this divergence include astronaut activity, reconfiguration of the solar array, thermal effects, or camera motion.

The frequency of the sinusoid component of the least-squares fit was determined to be 0.097 Hz for corner E and 0.098 Hz for corner F. A fast Fourier transform was also run on both sets of measured data. This frequency analysis showed a peak in both signals at a frequency of 0.087 Hz, with a frequency resolution of approximately 0.029 Hz. The frequencies determined from the damped sinusoid line fits agree with the dominant frequency of the frequency analysis to the available resolution. Another peak in the frequency analysis occurred at a frequency of around 0.3 Hz. This is near the expected frequency of the HST body motion, but the magnitude at this frequency was barely distinguishable from the higher frequency noise. If other modes of motion exist in the measured signal, it is less than approximately 0.09 inches. Efforts to identify a higher frequency using a multiple damped sinusoid function with two harmonics instead of one were not successful.

### **Errors**

This section discusses the errors expected from the SM-1 proof-of-concept analysis. These errors are calculated using data specific to the SM-1 mission. Included in this information are the solar array configurations (perpendicular to the PLB) and the camera used. The errors expected for SM-2 were also calculated. SM-2 will have a different solar array configuration (parallel to the PLB) which will change many of the camera parameters. An additional consideration is that SM-1 only offered a half-screen view. The SM-2 mission might provide full-screen views for analysis, which would lower the expected errors. These differences will cause differences in the expected errors. The following discussion tries to explain the factors that went in to the error assessment.

The error considerations in this analysis are of two types. The first is a random noise component in the data collection procedure with respect to the location of the solar array edge in the image. This analysis uses an edge-detection technique to define the edge of the solar array. The use of multiple pixels achieves a resolution of less than 1 pixel. The SM-1 proof-of-concept analysis used approximately 200 pixels. The associated data collection error was 0.08 inches. The same data collection error would hold for SM-2 in the half-screen mode if the same number of pixels were available. For the full-screen mode with twice the number of available pixels, the data collection error would drop to 0.03 inches. This value is constant for a specified viewing angle and camera resolution, and would not change if the magnitude of solar array motion changed.

***Table 1: Errors in Data Collection***

	Half-screen View	Full-screen View
Error	0.08	0.03

inches

The other type of error is the uncertainty in the calculation of scale (conversion from measured distances on the image to real world values). Because this error is an error in a conversion factor from pixels to inches, the absolute error in inches will increase if more motion is visible on the image. For the following calculations, the peak-to-peak motion for SM-1 was assumed to be 2 inches (derived from analysis). The peak-to-peak motion for SM-2 was assumed to be 6 inches (maximum expected from structural models). This results in a higher absolute error for the SM-2 analysis than the similar values for SM-1, even though the error in scale remains the same.

A simple scaling method was used to determine the scale for the SM-1 analysis. This involved the comparison of the size of the spreader bar on the image to its known length (113.5 inches). Some assumptions about the location and orientation of the spreader bar relative to the camera were necessary. The sources of scaling error and their currently assumed bounds for this analysis were derived from the expected accuracy of a triangulation determination of the solar array geometry. Table 2 presents the resulting error values for the simple scaling method.

**Table 2: Scaling Errors for Simple Scaling Method**

	SM-1 Half-screen	SM-2 Half-screen	SM-2 Full-screen	
Image coordinates	0.02	0.06	0.03	inches
Camera-solar array edge distance	0.03	0.06	0.06	inches
Scaling foreshortening	0.06	0.16	0.16	inches
Motion foreshortening	0.01	0.04	0.04	inches
<b>Total scaling error</b>	<b>0.12</b>	<b>0.32</b>	<b>0.29</b>	<b>inches</b>

(Calculations assume solar array edge motion of 2 inches for SM-1 and 6 inches for SM-2.)

Table 3 presents the error assessments for SM-2 based on the use of a more advanced scaling method. The use of this procedure greatly improves the accuracy of the analysis and is currently considered necessary to achieve the motion accuracy requested. The use of this more advanced method to determine scale instead of the simple scaling method used for the proof-of-concept analysis would eliminate entirely the impact of the scaling foreshortening error to the calculations. Methods of calculating the array configuration on orbit are being considered to improve the error in the solar array edge location.

**Table 3: Scaling Errors for More Advanced Scaling Method**

	SM-2 Half-screen	SM-2 Full-screen	
Image coordinates	0.02	0.01	inches
Camera-solar array edge distance	0.06	0.06	inches
Motion foreshortening	0.04	0.04	inches
<b>Total scaling error</b>	<b>0.12</b>	<b>0.11</b>	<b>inches</b>

(Calculations assume solar array edge motion of 6 inches for SM-2.)

Table 4 presents the total error assessment including random noise and scaling considerations. The scaling error considerations included assumptions about the accuracy with which the solar array geometry is known. If the solar array geometry is known to a greater accuracy than is assumed in these calculations, the error assessments would improve.

**Table 4: Total Error Assessment**

	SM-1 Half	SM-2 Half	SM-2 Full	SM-2 Half	SM-2 Full	
Scaling method	simple	simple	simple	advanced	advanced	
Data collection error	0.08	0.08	0.03	0.08	0.03	inches
Scaling error	0.12	0.32	0.29	0.12	0.11	inches
Total error	0.20	0.40	0.32	0.20	0.14	inches
Percentage of motion	9.7	6.7	5.3	3.3	2.3	percent

**Correlation of Proof-of-Concept to Servicing Mission 2 Analysis**

To correlate the results of this analysis to those expected on the 2nd servicing mission, the changes in geometry, equipment, and data acquisition procedure need to be considered.

The major changes in component configuration for this mission are that the HST body will be tilted in the PLB and the solar arrays will be approximately parallel with the PLB. This changes the distance from the camera to the solar array tips. The percentage of the FOV occupied by the solar array edge provided a good balance between maximizing the size of the spreader bar in the image and allowing for motion inside the available viewing window. A similar FOV was assumed for the SM-2 error calculations.

The change in the relative location of the solar array edge and the camera will change the sensitivity of the scaling calculations due to location error. The sensitivity will be lower for a camera view of the solar array edge which is farthest away from the camera. The viewing angle also effects this sensitivity. This indicates that the camera farthest from the solar array tip being measured should be used to reduce the sensitivity of the calculations to the location error.

The decision to use a full screen or a half screen will need to be based on a trade-off between the screen resolution and the number of views recorded. Using full-screen views provides an error improvement due to improved resolution. Using the half-screen views allows for the recording of more views. If a half-screen view is used instead of a full-screen view, the image resolution decreases by a factor of 2. The impact of this resolution decrease on the error assessment is a 0.06-inch increase in the solar array motion error.

**Conclusions and Recommendations**

The data used in the proof-of-concept analysis offered a view of the solar array edge with a background consisting primarily of the cloud cover on the Earth. The variation in this background during the analysis sequence suggested the use of an internal feature of the solar array which was parallel with the solar array tip. An interface between two different colors of solar array material was used instead. This interface provided a relatively low contrast, which increases the data collection error. For SM-2, IS&AG is requesting the use of darkened space as a background. This will provide a higher and more consistent contrast along the edge being tracked. Quantitatively assessing the resulting improvement is difficult considering the other factors to be modeled including lighting and camera configuration.

To improve the accuracy of the measurements of the solar array motion, we recommend that a different scaling procedure be used for the reboost test. This procedure would be executed before initiating the array motion firings and would require that the camera focal length not be changed during the duration of the test. The general nature of the calibration is to acquire a camera view of an object of known geometry and location relative to the camera. This view would more accurately determine the scaling of the view than the technique used in the proof-of-concept analysis. The features used in the scaling technique have not been defined. It is preferred that the features be distributed across the FOV as completely as possible. The placing of targets at pre-defined positions could assist with this calculation. This will be investigated further in the analysis technique development phase. An accuracy improvement of 0.15 inches for a 6-inch peak-to-peak deflection of the solar array is expected if the different scaling procedure is used.

An on-orbit solar array geometry calculation before each reboost test would improve the accuracy of the analysis results. If solar array geometry were available from another source to an equal or greater accuracy, this procedure would not be required. The solar array edge motion accuracy improvement produced will be dependent on the errors expected from the geometry calculation. If the expected errors in the solar array geometry are decreased by a factor of 2, an accuracy improvement of 0.11 inches is expected relative to the values presented in the preceding tables.

Acquiring RCS firing information greatly improved the post-measurement interpretation of the results of the proof-of-concept analysis. Accessing this information after the SM-1 mission proved difficult. Knowledge of the RCS activity would facilitate the near-real-time analysis and be helpful to interpret the overnight analysis. IS&AG requires near-real-time information on the thruster firing times to assist with the coordination of the near-real-time analysis. The post-mission analysis will require a log of more detailed thruster firing information to assist with the interpretation of the analysis results.

## **Appendix C: SM-1 Analysis**

# Hubble Space Telescope

## Solar Array Motion Analysis from Servicing Mission #1

### JSC Image Science & Analysis Group

#### April 1996

## I. Introduction

During the second Hubble Space Telescope (HST) servicing mission (SM-2) on STS-82, currently scheduled for February 1997, the HST will be captured and serviced. The Image Science and Analysis Group (IS&AG) of the Johnson Space Center Earth Science Branch (SN5) has been tasked with providing analysis of the deflections of the HST solar array (SA) bistems under different loading conditions. This analysis will be performed using video imagery as the primary data source.

In FY95, IS&AG completed a proof-of-concept (POC) analysis of SA motion on the HST from video acquired during the first servicing mission (SM-1) on STS-61. The goal of the analysis was to assess the accuracy achievable from the video analysis technique and to identify technical and procedural issues that could affect similar measurements planned for SM-2.

After completion of the POC analysis, IS&AG was requested to perform analysis on additional SM-1 video data as a means of refining the structural dynamics models of the HST SAs. This document presents the results of this analysis. The primary goal of the analysis was to provide accurate data from video analysis techniques, but it also served to identify technical and procedural issues that can affect the accuracy and speed of the planned SM-2 analysis.

## II. Approach

The SA motion analysis consisted of three basic parts:

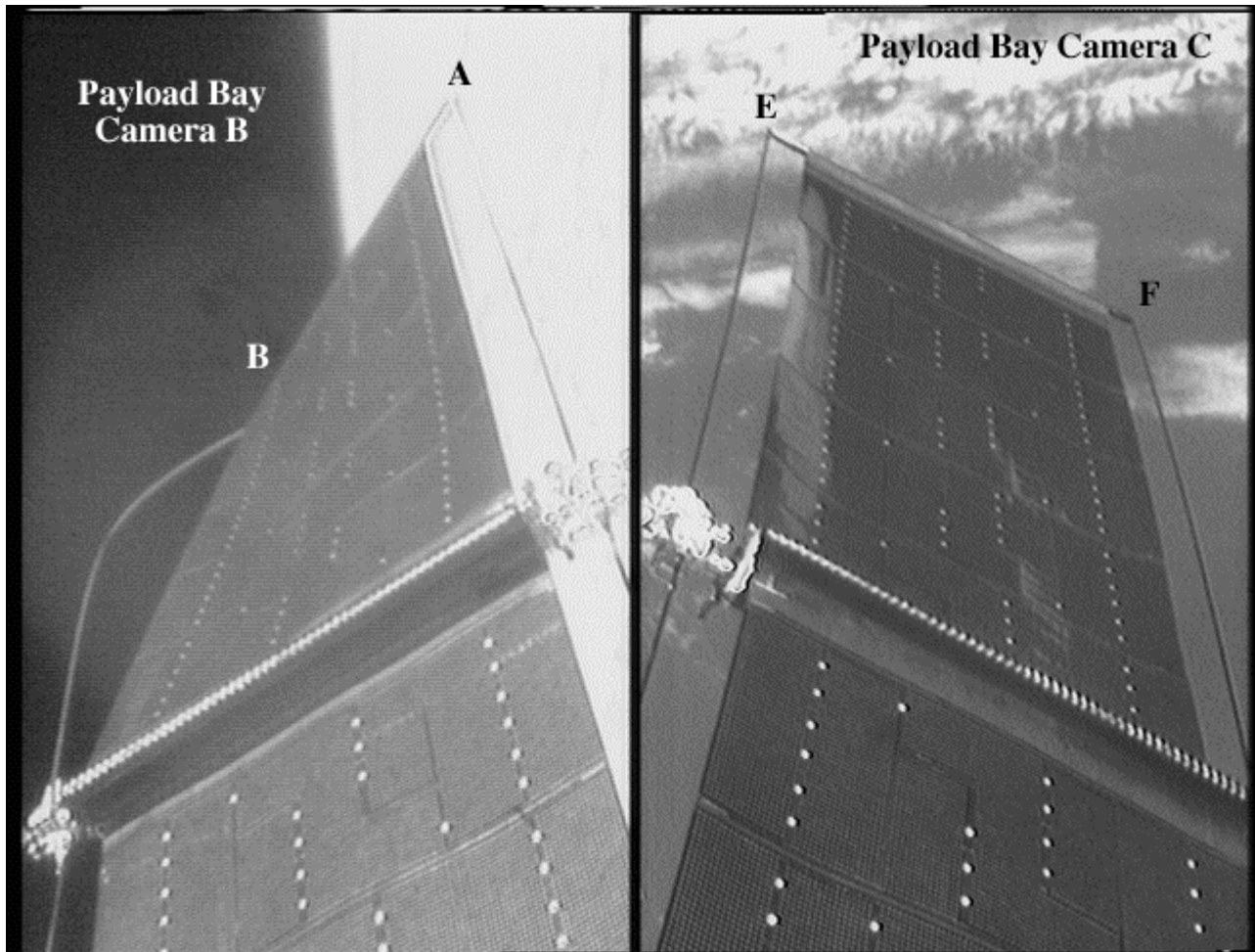
1. **Video screening** - determining what data to analyze.
2. **Data collection** - performing edge detection & tracking in the image coordinate system.
3. **Data analysis** - converting image positional information into real-world measurements (relative displacement in inches).

### A. Video Screening

The first step in performing the additional SM-1 analysis was to locate video segments from the SM-1 mission that would permit SA motion analysis. A video scene-list search revealed 78 possible video segments from STS-61. All video segments were assessed for the qualities of camera steadiness, SA tip coverage, and segment length. Of the videos viewed, 8 were considered sufficient for analysis. The best analysis candidate turned out to be the video segment which included the previously analyzed imagery for the POC study. After discussions of the available options with Mr. Greg Frazier (Goddard Space Flight Center), an agreement was reached to perform the analysis on the full length of that video segment.

The video used for the analysis was a 23-minute, 19-second interval of continuous video starting at 338:11:37:33.696 UTC (coordinated universal time). Throughout this segment, the HST was berthed with the SAs oriented approximately perpendicular to the Orbiter payload bay. The video was recorded in a split-screen mode during this interval. Figure 1 shows a representative frame from the analyzed sequence. The left half of the split screen was from Orbiter payload bay camera B (port aft corner of payload bay) viewing the top end of the +V2 SA on the port side. The right half of the view was from camera C (starboard aft corner of payload bay) of the upper end of the -V2 SA on the starboard side. The view of the +V2 SA was not used for analysis due to noticeable bending or twisting along the span of the array, which caused the spreader bar to be partially obscured. The spreader bar on the -V2 SA edge was visible from camera C, which permitted this view to be used for the analysis.

**Figure 1: Frame of video from Servicing Mission 1 used in motion analysis.**



## B. Data Collection

During the initial POC analysis, a prototype data collection software package was developed. This package made use of existing subroutines and functions, with some rapidly developed software to tie them all together. The software performed the tasks of edge tracking and data collection well, but had several primary limitations:

- Dependency on specialized image processing hardware which caused the majority of the video digital analysis system (VDAS) laboratory processing capabilities to be allocated to this operation. This severely limited resource availability to other users of the VDAS laboratory when the motion analysis software was running.
- A laborious user interface, which resulted in excessive labor hours and opportunities for human errors.
- Hardware limitations which forced the maximum length of a video sequence processed to be 1615 frames of video (53.8 seconds).

Due to the massive quantities of data involved in the analysis of 23 minutes of video (approximately 42,000 images or 28 gigabytes of digital data), it was imperative that these limitations be addressed before attempting to perform additional analyses. A revised software package was developed, based on the initial prototype, which attempted to resolve the shortcomings of the prototype software. The new software package, named ABMOTION, performed all of the necessary calculations independent of the specialized image analysis hardware. This enabled the analysis program to be run continually with minimal impact to other VDAS users. The user interface was drastically improved, not only in the ease of use, but in reduction of the amount of required human interaction. The analysis sequence length limitations imposed by our Abekas A66 digital disk recorder (maximum storage of 1615 frames) can be overcome only through the addition of extra hardware, so the software was written to enable communications between data sets. This permitted processing of multiple data sets with no loss of analysis information.

The analysis algorithm has remained fundamentally unchanged between the POC study and the current analysis. The algorithm consists of the following steps:

1. **Gaussian Filter** - smoothes the image slightly, reducing video noise.
2. **Canny Filter** - gradient edge detector, results in edge information output as intensities proportional to the gray scale gradient.
3. **Threshold binarization** - discriminates between “on” and “off” pixels based on a gray scale threshold value.
4. **Least Squares Linear Fit** - “On” pixels within the current search window are used to find the best fitting straight line.
5. **Preparation for next frame** - Center search window for next frame about fitted line and output results of current frame.

The analyst performed the data collection by following these steps:

1. Transfer a 1615 frame block of video from the Sony DVR-20 digital videotape recorder to Abekas A66.
2. Determine starting frame on A66.
3. Transcribe timing information to checksheet.
4. Start ABMOTION software.
5. When run is done, verify tracking results.
6. Prepare for next run.

The Abekas A66 digital disk recorder has a maximum storage capacity of 1615 video frames, which forces the video processing to be performed in discrete “loads” of 1615 frames or less. A total of 12 “loads” were processed through this portion of the analysis. To reduce the throughput time, only every fourth frame of the data was used in the analysis. The resultant data sample rate was 7.5 samples/second. The primary impact of this reduction in sampling rate is a loss of the ability to detect motions with frequencies higher than 3.75 Hz. Since the expected motions have an oscillation frequency on the order of 0.1 Hz, it was decided that the reduction in sample rate would have a minimal impact on the usefulness of the data.

The data transfer between the DVR-20 and the A66 is digital in nature, but the initiation of the transfer is manual. This caused the position of the beginning frame for each load on the A66 to be semi-arbitrary. The analyst selected the proper frame via the UTC time code, which had been inserted into each frame when the D2 tape was originally dubbed. This time code enabled correlation of one load to the next, as well as verifying data transfer rates. It was discovered during the first load that the transfer rate between the two devices was not always constant, so the time displayed on selected frames throughout each processed load was manually documented. These times were then entered into a spreadsheet, the frame rates were verified, and the resultant data was used later to tie the positional data back to real-world UTC.

For the first video load, the analyst manually selected the approximate location of the edges to be tracked, and the program found the exact location of the edges. For subsequent loads, the program used the edge positions from the last frame processed on the previous load. In general, once the analysis parameters have been defined for a given video sequence, they do not need to be modified again throughout the rest of the processing.

After the data collection portion of the analysis, it was discovered that a hardware problem existed in the link between the Sony DVR-20 and the Abekas A66. This problem resulted in a shifting of the image position at infrequent random intervals. The effect of this on the outputs of the edge-tracking software was to cause occasional spikes of bad data points. Due to the nature of the tracking algorithm, a single bad frame can affect the data results for several frames following. The bad data points, including the following affected frames, were removed by hand. The final number of output data points was 7654.

### **C. Data Analysis**

The length of the available video sequence was 23 minutes, 19 seconds, but due to manual camera parameter changes and lighting changes at the beginning and ending of the video segment, only 18 minutes, 5 seconds of data were completely analyzed. The final analysis segment covered the period from 338:11:39:51.20 to 338:11:57:56.40 UTC.

The motion of the SA edge in image coordinates was determined by using the slope and y-intercept from the output of the edge-tracking algorithm discussed previously. The x-coordinates for the endpoints of the line segment defining the SA edge on the first analyzed image were used in the linear equation to determine a y-coordinate for each endpoint for each frame. Since the motion of the SA edge was not entirely vertical on the image, a constant correcting factor based on the overall average slope was applied to the measured motion to correct the motion values. The displacements for each SA tip were normalized about the average position across the entire video sequence.

The displacements were multiplied by a scaling factor that was determined based on the camera field-of-view size and the viewing aspect angle. This scale factor is based to a large degree on the assumed position of the SA. GSFC supplied the Orbiter coordinates of the SA endpoints for SM-1. These values were calculated under the assumption of a fully extended SA along the Orbiter Z-axis (straight up) with no twist or bend.

### III. Results

A Microsoft Excel spreadsheet containing the results of the analysis was provided to GSFC on March 20, 1996. Table 1 displays the first few rows of data in the output. The largest displacements (from the overall average position measured during the entire sequence) were 1.4 inches for the left tip of the SA and 1.6 inches for the right tip of the SA.

**Table 1: Sample Output Data**

Time (hh:mm:ss.ss)	Left Displacement (Inches)	Right Displacement (Inches)
11:39:51.20	-0.51	0.57
11:39:51.34	-0.35	0.51
11:39:51.48	-0.30	0.59
11:39:51.61	-0.58	0.62
11:39:51.75	-0.48	0.70
11:39:51.89	-0.44	0.76
11:39:52.02	-0.04	0.63

Figure 2 displays the entire output data set in graphical format. Note that the time scale is severely compressed in this graph, causing the 0.1 Hz. cycles to appear as data spikes. The firing times of the various Vernier Reaction Control System (VRCS) jets are also plotted on this graph. (Note: The “displacement” coordinates of the VRCS firing times are arbitrary values assigned as an aid to visibility.) There appears to be a very clear (and expected) correlation between the VRCS firings and the periods of maximum dynamic motion. It is also very noticeable in this graph that the “rest” position (i.e., the position about which the oscillations occur) changes with time. There appears to be a gradual inversely correlated change in position of the two SA tips over the first 10 minutes of the analysis, followed by a very rapid reversal back to (approximately) the original positions, possibly to begin the cycle again. Note that the inverse correlation between the two tip positions means that it is the slope of the spreader bar that is changing, not its actual position. This implies a change in the amount of twisting in the SA over time.

Eight detailed graphs (Figures 3.1-3.8) of the array motion are also attached to this document. The entire output data set was divided into eight equal time segments, and each segment printed out individually. These graphs are included to enable the reader to see greater detail in areas of interest. These graphs also include the VRCS firing times. It appears that at no time during the analysis period did the oscillations of the SAs ever completely dampen, even during the longest break between firings (3 minutes, 10 seconds).

### IV. Lessons Learned and Outstanding Issues

The analysis discussed here represented a new challenge to IS&AG. In most previous analyses involving motion from video, the length of the video segment ranged from a few seconds to a minute. The massive amounts of data involved in this analysis, as well as the fact that the length of time analyzed was sufficient to result in significant changes in lighting conditions, forced IS&AG to confront several novel situations. The difficulties encountered during this processing are addressed below.

- Contrast Changes - The primary reason that the tracking algorithm would occasionally “lose” the edge being tracked was due to changes in the amount of contrast across the edge. These contrast changes were caused by changes in the lighting conditions over time and by having the rotating Earth as the background. The software will be modified to use an adaptive thresholding technique during the binarization portion of the edge detection. This should significantly reduce the sensitivity to these problems.

- Random Noise - Having a varying background (e.g. rotating Earth) frequently causes false edge information to be included in the line fit data. The result of this tends to be a larger-magnitude random noise component in the final output. Currently, the algorithm uses a least-squares algorithm to define the line which best defines the tracked edge. The least-squares approach is notorious for its sensitivity to outliers (erroneous data points) in the data. It may be beneficial to switch to a median fit approach, which is much less sensitive to outliers. During the POC analysis, a median fit was tested briefly, but was discarded in favor of the least-squares approach to reduce CPU requirements. The tests at that time did not account for changing contrast levels. Tests will be conducted in the near future with the median fit using edges with a varying background. If this results in noise reductions, then the ABMOTION software will be modified to make use of a median fit.
- Hardware Problems - The hardware problems (communication “glitches” between the DVR-20 and the A66) discovered during this analysis will be investigated and resolved as soon as possible. The analysis is still possible while the problem exists, but intermittent data points are lost, and there is the additional labor involved in the tedious task of removing the bad data by hand. The problem was not present during the POC analysis, so the problem is caused either by a change in the connection configuration or by a failed component. Either way, this problem will be resolved in the very near future.

Corrective actions for each of these items have been identified and will be implemented in support of SM-2. These implementations should result in a more robust analysis package as well as significantly improved output products for the planned SM-2 analysis.



## **Appendix D: Storyboards**

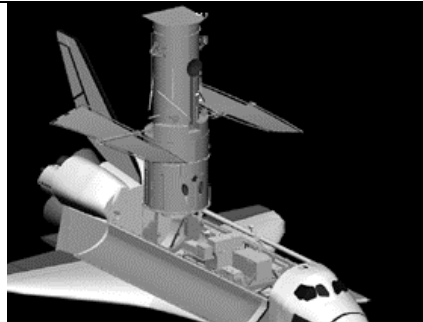
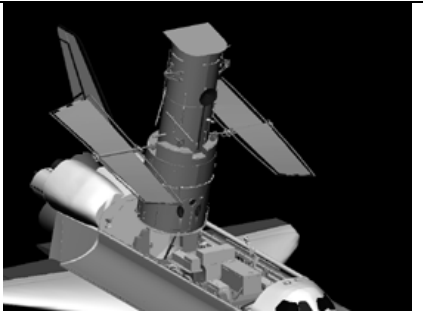
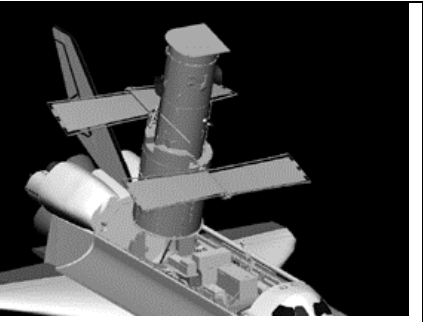
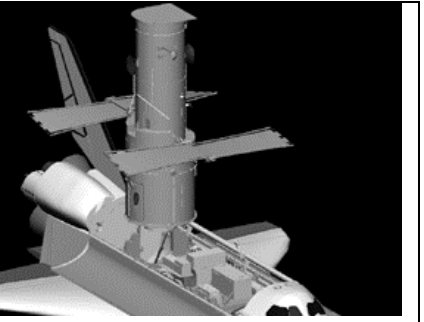
## Hubble Space Telescope (HST) Repositioning

Purpose: Estimate the deflections of solar array caused by the HST repositioning.

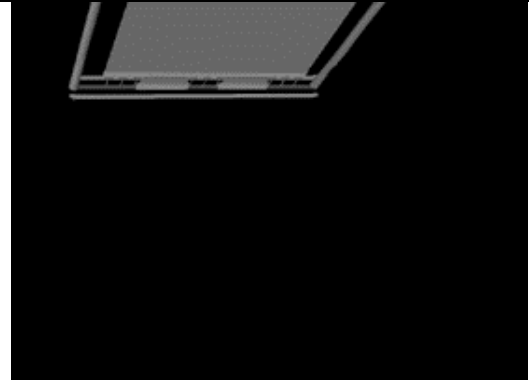
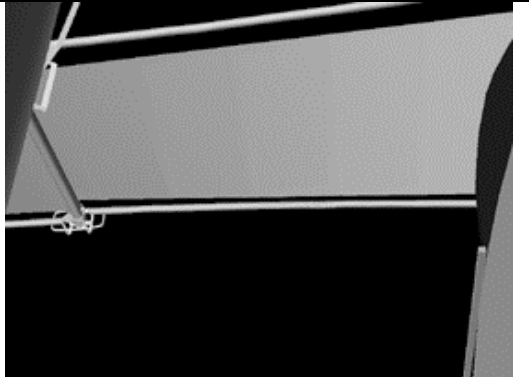
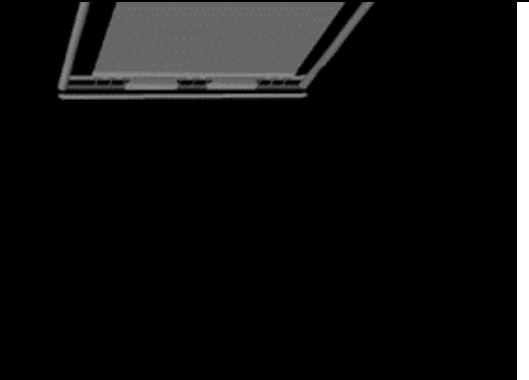
### Resources Required

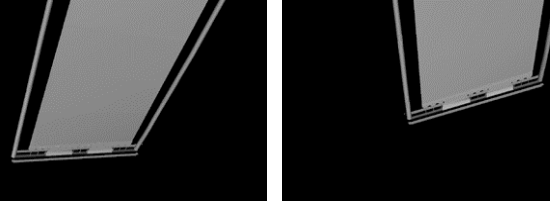
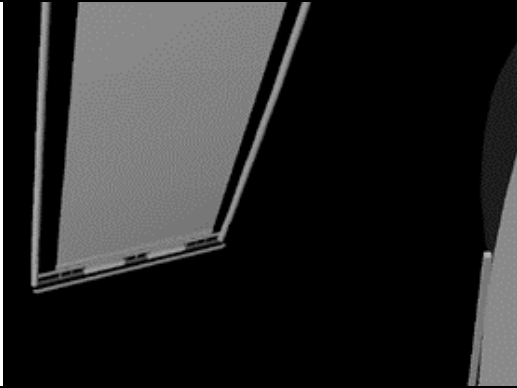
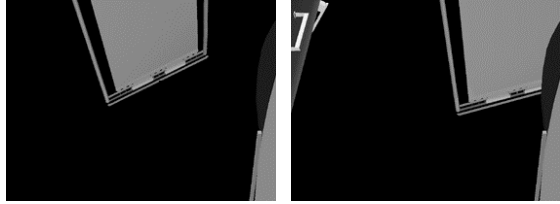
<b>Camera control:</b>	Crew.
<b>Cameras:</b>	Payload bay cameras B and C.
<b>Video downlink:</b>	Near-real-time playback and on-ground recording.
<b>Video data:</b>	Payload bay camera data: camera ID, field-of-view (FOV) status when available, exposure settings.  Synchronized timing for both onboard recordings and direct downlink video.
<b>Estimated time required:</b>	25-30 minutes.

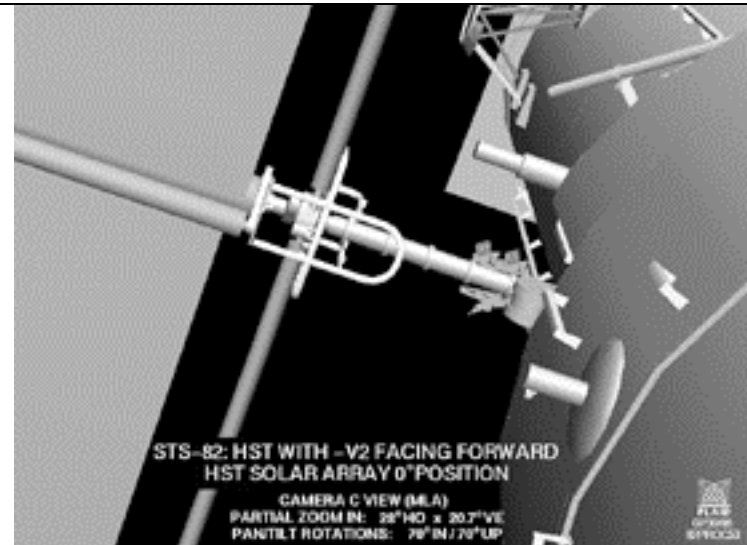
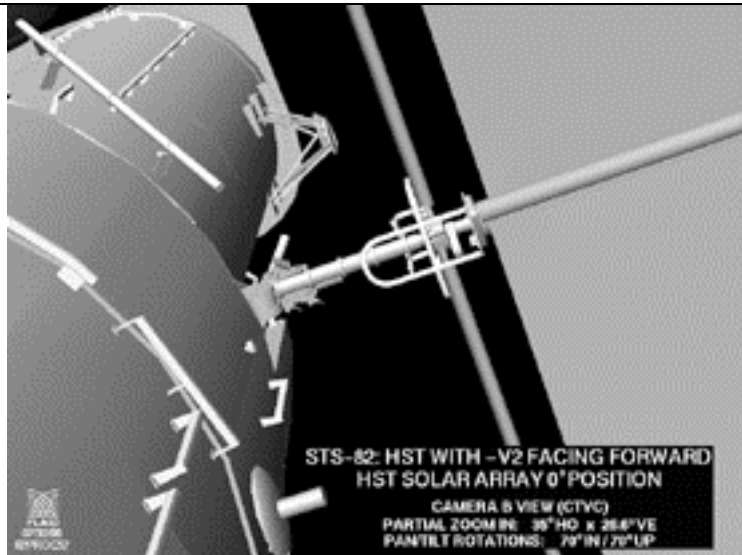
Overview of HST Repositioning before EVA Day 1

			
<ul style="list-style-type: none"> <li>• HST in the berth position</li> <li>• -V3 axis forward</li> </ul>	<ul style="list-style-type: none"> <li>• HST pivoted forward 15 deg</li> <li>• -V3 axis forward</li> </ul>	<ul style="list-style-type: none"> <li>• HST pivoted 15 deg</li> <li>• Rotated 90 deg.</li> <li>• +V2 axis forward</li> </ul>	<ul style="list-style-type: none"> <li>• HST pivot back to 0 deg</li> <li>• Rotated 90 deg</li> <li>• +V2 axis forward</li> </ul>
File name 82SAMAI2.TGA	File name 82SAMAI2.TGA	File name 82SAMAI5.TGA	File name 82SAMAI6.TGA

**Procedure**

		
<p><b>Step 1</b> <b>Set up camera C.</b></p> <p>Video recorders should be configured to allow switching between cameras B and C. Switch to camera C and start recording.</p> <p>Adjust the pan, tilt, and zoom of camera C to position solar array tip to the center upper third of the image.</p> <p><b>Camera C Settings:</b>  <b>HFOV 28 deg      VFOV 20.7 deg</b>  <b>Pan 19 deg out    Tilt 29 deg up</b></p>	<p><b>Step 2</b> <b>Set up camera B.</b></p> <p>Point camera B at the starboard portion of the aft bulkhead. Adjust the pan, tilt, and zoom so that the -V2 solar array makes up the upper half of the image.</p> <p><b>Camera B Settings:</b>  <b>HFOV 35 deg      VFOV 26.6 deg</b>  <b>Pan 82 deg in     Tilt 40 deg up</b></p>	<p><b>Step 3</b> <b>Capture start of HST pivot.</b></p> <p>At the start of the repositioning, view the camera C imagery. Maintain this camera's view until the solar array rotates out of the FOV.</p> <p><b>Camera C Settings:</b>  <b>HFOV 28 deg      VFOV 20.7 deg</b>  <b>Pan 19 deg out    Tilt 29 deg up</b></p>
<p>File name STS82SAMA20.TGA</p>	<p>File name STS82SAMA26.TGA</p>	<p>File name STS82SAMA20.TGA</p>

		
<p><b>Step 4</b></p> <p><b>Capture stop of pivot and start of rotation.</b></p> <p>The sequence observed from camera C should appear similar to those illustrated above.</p> <p><b>Camera C Settings:</b>  <b>HFOV</b> 28 deg      <b>VFOV</b> 20.7 deg  <b>Pan</b> 19 deg out      <b>Tilt</b> 29 deg up</p>	<p><b>Step 5</b></p> <p><b>Capture stop of rotation.</b></p> <p>Switch to the camera B view. Hold this camera's view until the HST finishes the repositioning sequence.</p> <p><b>Camera B Settings:</b>  <b>HFOV</b> 35 deg      <b>VFOV</b> 26.6 deg  <b>Pan</b> 82 deg in      <b>Tilt</b> 40 deg up</p>	<p><b>Step 6</b></p> <p><b>Capture start and stop of final pivot.</b></p> <p>The sequence observed from camera B should appear similar to those illustrated above.</p> <p><b>Camera B Settings:</b>  <b>HFOV</b> 35 deg      <b>VFOV</b> 26.6 deg  <b>Pan</b> 82 deg in      <b>Tilt</b> 40 deg up</p>
<p>File name STS82SAMA21.TGA</p>	<p>File name STS82SAMA23.TGA</p>	<p>File name STS82SAMA24.TGA</p>
<p>File name STS82SAMA22.TGA</p>		<p>File name STS82SAMA25.TGA</p>



**Step 7**

**Scale reference image—camera B.**

Leaving the zoom of camera B unchanged, point the camera at the scaling feature. Record for 3-5 seconds.

**Camera B Settings:**

**HFOV** 35 deg      **VFOV** 26.6 deg  
**Pan** 70 deg in      **Tilt** 70 deg up

File name 82PROC52.TGA

**Step 8**

**Scale reference image—camera C.**

Leaving the zoom of camera C unchanged, point the camera at the scaling feature. Record for 3-5 seconds.

**Camera C Settings:**

**HFOV** 28 deg      **VFOV** 20.7 deg  
**Pan** 70 deg in      **Tilt** 70 deg up

File name 82PROC53.TGA

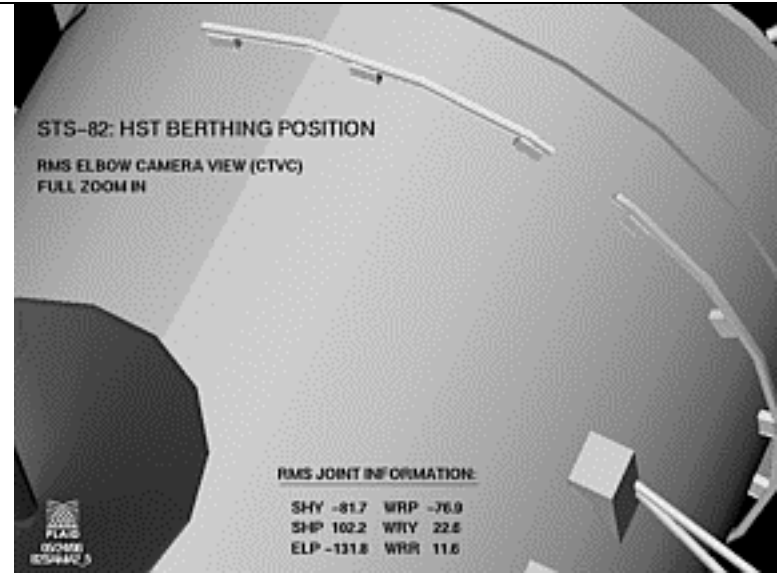
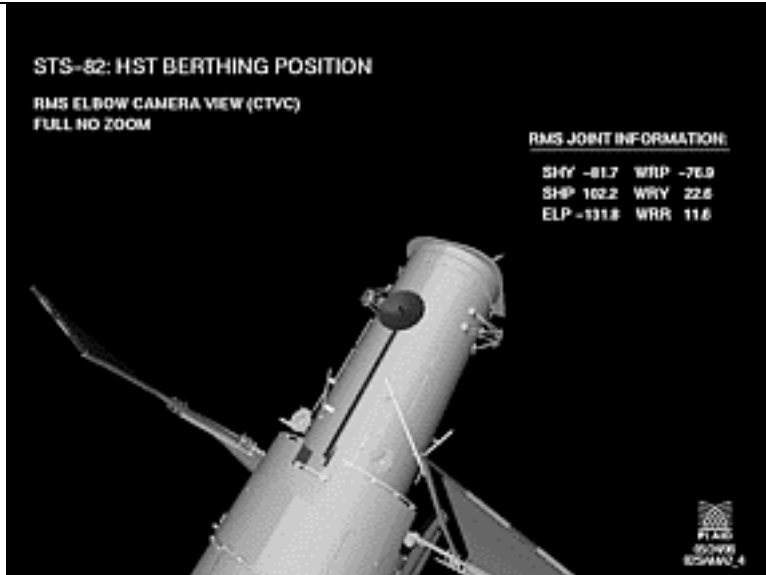
## HST Surface Survey

Purpose: Identify and map anomalous features on the surfaces of the HST.

### *Resources Required*

<b>Camera Control:</b>	Crew and Instrumentation and Communication Officer (INCO)
<b>Cameras:</b>	Payload bay cameras A, B, C, and D Remote manipulator subsystem (RMS) elbow camera RMS wrist camera (crew only) Hasselblad (crew only)
<b>Video Downlink:</b>	Crew operation: playback of cumulative video data by start of second EVA day INCO: real-time on-ground recording
<b>Survey Acquisition Priorities:</b>	1st aft shroud 2nd high gain antennae (HGA) 3rd solar arrays 4th light and forward shields

**Procedure: RMS Camera Systems**



**Step 1**

**Set up and overview.**

- Set up RMS cameras for recording and/or downlink. Start video recording or downlink.
- Zoom the FOV fully out to capture the entire HST vehicle.

File name 82SAMA2\_4.TGA

**Step 2**

**Map upper surfaces of the HST.**

- Zoom in to maximum.
- Map the visible light and forward shield sections, pausing for 3 seconds between camera repositionings.
- Provide an approximate 20% overlap between adjacent scenes.
- Move RMS within provided safety guidelines to maximize coverage.

File name 82SAMA2\_5.TGA

**Procedure: Payload Bay Cameras**

<p><b>Step 1</b></p> <p><b>Set up and overview.</b></p> <ul style="list-style-type: none"> <li>• Set up cameras for recording and/or downlink. Start video recording or downlink.</li> <li>• Zoom the FOV fully out to capture the entire HST vehicle.</li> </ul>	<p><b>Step 2</b></p> <ul style="list-style-type: none"> <li>• Fill the FOV with prioritized HST section (i.e., aft shroud).</li> <li>• Zoom in to maximum or prescribed zoom.</li> <li>• Map the visible areas of the section, pausing for 3 seconds between camera repositionings.</li> <li>• Provide an approximate 20% overlap between adjacent scenes.</li> <li>• Repeat for each payload bay camera.</li> </ul>	<p><b>Step 3</b></p> <ul style="list-style-type: none"> <li>• Repeat Step 2 for each prioritized HST section.</li> <li>• This procedure should be repeated for each payload bay camera and for each HST servicing position (i.e., -V3 forward).</li> </ul>
<p>File name 82HST_DZ0.TGA</p>	<p>File name 82HST_DZ2.TGA</p>	<p>File name 82HST_DZ1.TGA</p>

**Procedure : Photographic**

<p><b>Step1</b></p> <p><b>Set up and overview.</b></p> <ul style="list-style-type: none"> <li>• Prepare the Hasselblad camera for use as per the Photo/TV Checklist.</li> <li>• Use the Hasselblad Camera with the 40-mm lens to capture an overview of the HST.</li> </ul>	<p><b>Step 2</b></p> <p><b>Map at medium detail.</b></p> <ul style="list-style-type: none"> <li>• Use the Hasselblad with 100-mm lens to map large sections of the HST. Photographic exposures should be bracketed one stop above and below the normal exposure.</li> </ul>	<p><b>Step 3</b></p> <p><b>Map at high detail.</b></p> <ul style="list-style-type: none"> <li>• Use the Hasselblad with 250-mm lens to map entire HST surface. Photographic exposures should be bracketed one stop above and below the normal exposure.</li> </ul>
<p>File name 82PROC32.TGA</p>	<p>File name 82PROC35.TGA</p>	<p>File name 82PROC36.TGA</p>

## Solar Array Motion Video Acquisition

Purpose: Determine solar array deflection as a function of time. This event shall be captured for HST service door openings and closings as well as Vernier reaction control subsystem (VRCS) firings. The solar array motion analysis (SAMA) for HST service door access has a single acquisition requirement.

### *Resources Required*

<b>Camera Control:</b>	INCO (first choice).  Crew (second choice).
<b>Cameras:</b>	Payload bay camera A, B, C, or D.
<b>Video Downlink:</b>	Real-time on-ground recording (for INCO camera control).  Near-real-time playback and on-ground recording (for crew camera control).
<b>Video Data:</b>	Payload bay camera data: camera ID, FOV status when available, exposure settings.  Synchronized timing for both onboard recordings and direct downlink video.
<b>Estimated Time Required:</b>	At least 10 minutes per impulse (VRCS firing or service door access).
<b>Best Time for Acquisition:</b>	Start procedure five minutes before impulse.

***Camera and Solar Array Combinations***

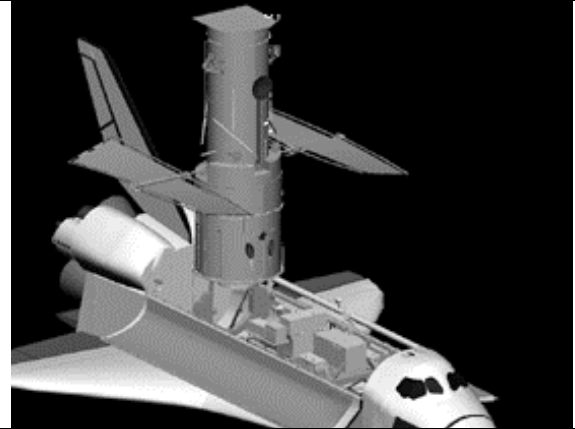
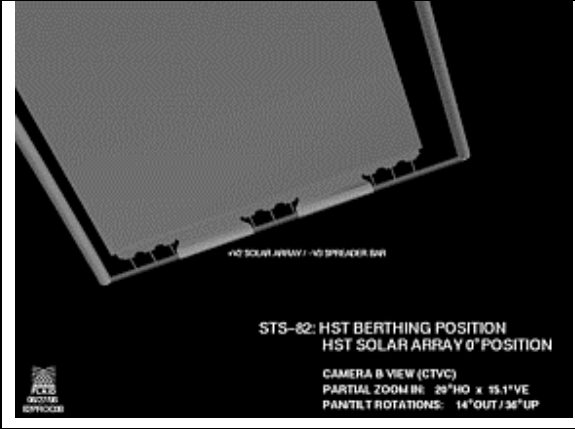
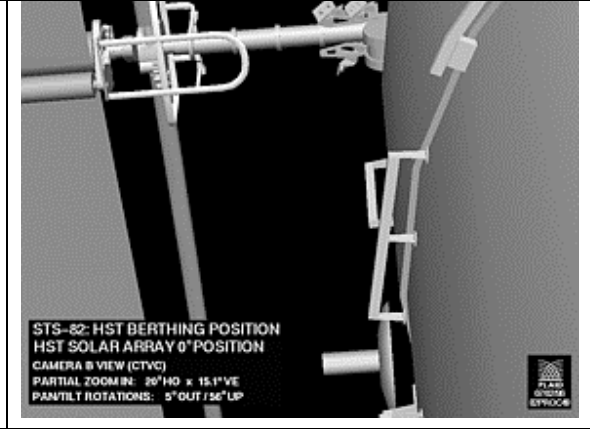
<b>Priority</b>	<b>Solar Array Tips [Spreader Bar Location]</b>	<b>Payload Bay Camera</b>	<b>Camera Type*</b>
1	A & B [+V2, -V3]	Camera B	CTVC
2	C & D [+V2, +V3]	Camera A	MLA
3	G & H [-V2, +V3]	Camera D	CTVC
4	E & F [-V2, -V3]	Camera C	MLA

\*CTVC: color television camera

MLA: monochrome lens assembly

**Procedure**

This storyboard illustrates the video acquisition required for any impulse-induced solar array motion. This includes nominal VRCS firings, extravehicular activities (EVAs), berthing and positioning subsystem post installations, portable foot restraint installations, and VRCS reboost activities. It is desired to capture the same spreader bar for all of these activities. Spreader bar A-B is highly desired as the feature of analysis and serves as the instruction case for this procedure. This storyboard assumes the HST has its -V3 axis facing forward. Alternative spreader bar scenarios can be found in the prioritized list preceding this section.

		
<p><b>Step 1</b></p> <p><b>Set up.</b></p> <p>Spreader bar A-B will be imaged by payload bay camera B. The Photo/TV setup for recording with this camera should be completed and recording should be started before continuing the procedure.</p>	<p><b>Step 2</b></p> <p><b>Frame spreader bar.</b></p> <p>Adjust the camera's pan, tilt, and zoom so the spreader bar makes up ~3/4 of the image width. Start recording at least 30 seconds before the impulse. Continue to record this view until the oscillation dampens (5 minutes).</p> <p><b>Camera B Settings:</b></p> <p><b>HFOV</b> 20 deg      <b>VFOV</b> 15.1 deg  <b>Pan</b> 14 deg out      <b>Tilt</b> 36 deg up</p>	<p><b>Step 3</b></p> <p><b>Scale reference image.</b></p> <p>Leaving the zoom of the camera B unchanged, point the camera at the +V2 bitem cassette and trunnion. Record for 3-5 seconds.</p> <p><b>Camera B Settings:</b></p> <p><b>HFOV</b> 20 deg      <b>VFOV</b> 15.1 deg  <b>Pan</b> 5 deg out      <b>Tilt</b> 56 deg up</p>
<p>File name STS82SAMAI7</p>	<p>File name 82PROC08.TGA</p>	<p>File name 82PROC49</p>

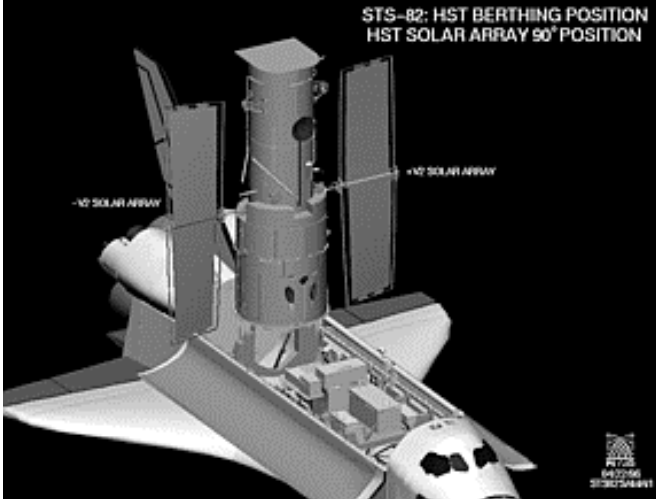
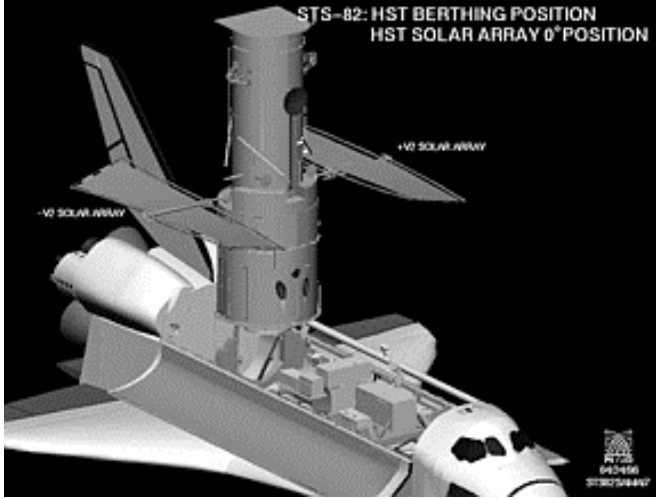
## Solar Array Slew Motion Analysis

Purpose: Determine the solar array oscillations associated with the array slew start and stop.

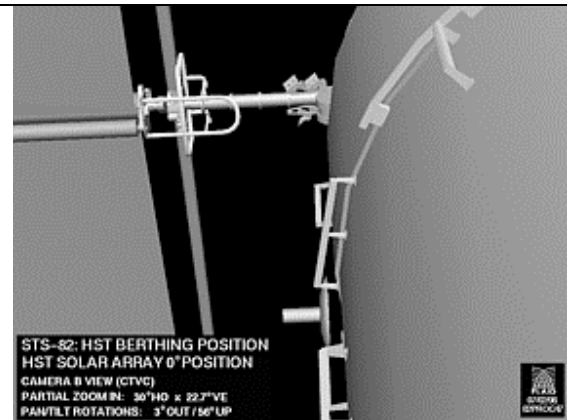
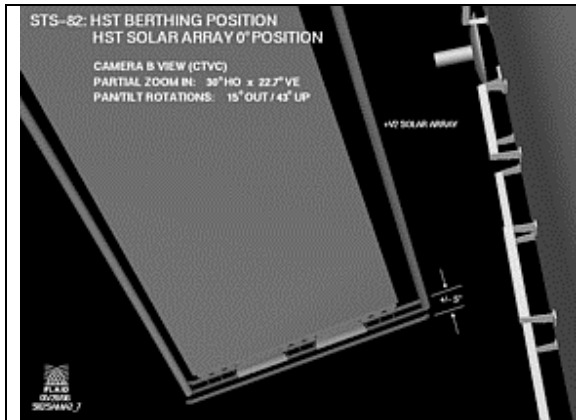
### Resources Required

<b>Camera Control:</b>	Crew.
<b>Cameras:</b>	Payload bay cameras B and C.
<b>Video Downlink:</b>	Near-real-time playback and on-ground recording.
<b>Video Data:</b>	Payload bay camera data: camera ID, FOV status when available, exposure settings. Synchronized timing for both onboard recordings and direct downlink video.
<b>Estimated Time Required:</b>	25-30 minutes.

### Overview of the Solar Array Slew Following Berthing

 <p>STS-82: HST BERTHING POSITION HST SOLAR ARRAY 90° POSITION</p> <p>-V3 SOLAR ARRAY</p> <p>+V3 SOLAR ARRAY</p> <p>040456 378025A447</p>	 <p>STS-82: HST BERTHING POSITION HST SOLAR ARRAY 0° POSITION</p> <p>-V3 SOLAR ARRAY</p> <p>+V3 SOLAR ARRAY</p> <p>040456 378025A447</p>
<ul style="list-style-type: none"> <li>• HST -V3 axis facing forward.</li> <li>• Solar Array in 90 deg position.</li> </ul>	<ul style="list-style-type: none"> <li>• HST -V3 axis facing forward.</li> <li>• Solar Array in 0 deg position.</li> </ul>
<p>File name STS82SAMAI1.TGA</p>	<p>File name STS82SAMAI7</p>

<p><b>STEP 1</b></p> <p><b>Set up camera C.</b></p> <ul style="list-style-type: none"> <li>Configured video recorders to allow switching between cameras B and C. Switch to camera C and start recording.</li> <li>Adjust the pan and tilt settings on camera C to view solar array spreader bar E-F. Adjust the camera's zoom so that the spreader bar makes up the center 3/4 of the image.</li> </ul> <p><b>Camera C Settings:</b>  <b>HFOV</b> 14 deg      <b>VFOV</b> 10.3 deg  <b>Pan</b> 34 deg out      <b>Tilt</b> 71 deg up</p>	<p><b>Step 2</b></p> <p><b>Set up camera B.</b></p> <ul style="list-style-type: none"> <li>Adjust the pan and tilt settings on camera B to view the +V2 trunnion on the top right section of the image.</li> <li>Adjust the zoom to view the three rails below the trunnion.</li> </ul> <p><b>Camera B Settings:</b>  <b>HFOV</b> 30 deg      <b>VFOV</b> 22.7 deg  <b>Pan</b> 15 deg out      <b>Tilt</b> 43 deg up</p>	<p><b>Step 3</b></p> <p><b>Capture start of slew.</b></p> <ul style="list-style-type: none"> <li>Switch to camera C view.</li> <li>Leaving all camera settings constant, record the start of solar array slew until spreader bar leaves the image.</li> </ul> <p><b>Camera C Settings:</b>  <b>HFOV</b> 14 deg      <b>VFOV</b> 10.3 deg  <b>Pan</b> 34 deg out      <b>Tilt</b> 71 deg up</p>
<p>File name STS82SAMA34.TGA</p>	<p>File name S82SAMA2_6.TGA</p>	<p>STS82SAMA34.TGA</p>



**Step 4**

**Capture end of slew.**

- Switch to camera B view directly after step 3.
- Leaving all camera settings constant, record the solar array entering the image.
- Continue recording the completion of the slew through dampening of the array tips (slew stop + 5 minutes).

**Camera B Settings:**

**HFOV** 30 deg      **VFOV** 22.7 deg  
**Pan** 15 deg out      **Tilt** 43 deg up

File name S82SAMA2\_7.TGA

**Step 5**

**Scale reference image B.**

- Leaving the zoom of camera B unchanged, point the camera at the +V2 bitem cassette and trunnion. Record for 3-5 seconds.

**Camera B Settings:**

**HFOV** 30 deg      **VFOV** 22.7 deg  
**Pan** 3 deg out      **Tilt** 56 deg up

File name 82PROC47.TGA

**Step 6**

**Scale reference image C.**

- Leaving the zoom of camera C unchanged, point the camera at the -V2 bitem cassette and trunnion. Record for 3-5 seconds.

**Camera C Settings:**

**HFOV** 14 deg      **VFOV** 10.3 deg  
**Pan** 9 deg out      **Tilt** 61 deg up

File name 82PROC54.TGA

## Solar Array Static Twist Baseline and Update

Purpose: Determine the three-dimensional location of the each tip of the HST solar arrays (eight total tips).

### *Resources Required*

<b>Camera Control:</b>	<ul style="list-style-type: none"> <li>• INCO (first choice)</li> <li>• Crew (Second choice)</li> </ul>
<b>Cameras:</b>	<ul style="list-style-type: none"> <li>• Payload bay camera A, B, C, and D</li> </ul>
<b>Video Downlink:</b>	<ul style="list-style-type: none"> <li>• Real-time on-ground recording (for INCO camera control)</li> <li>• Near real-time playback and on-ground recording (for crew camera control)</li> </ul>
<b>Video Data:</b>	<ul style="list-style-type: none"> <li>• Payload bay camera data: camera ID, FOV status when available, exposure settings</li> <li>• Synchronized timing for both onboard recordings and direct downlink video</li> </ul>
<b>Estimated Time Required:</b>	<ul style="list-style-type: none"> <li>• 30 minutes</li> </ul>
<b>Acquisition Requirements:</b>	<ul style="list-style-type: none"> <li>• Based on 8-hour analysis turnaround time, more than 12 hours before EVAs</li> <li>• Video data collection for this procedure is limited to following conditions:             <ol style="list-style-type: none"> <li>1. HST's + or -V3 axis is facing the forward bulkhead.</li> <li>2. Solar arrays are approximately parallel with the payload bay.</li> <li>3. HST is approximately perpendicular to the FSS.</li> </ol> </li> </ul>

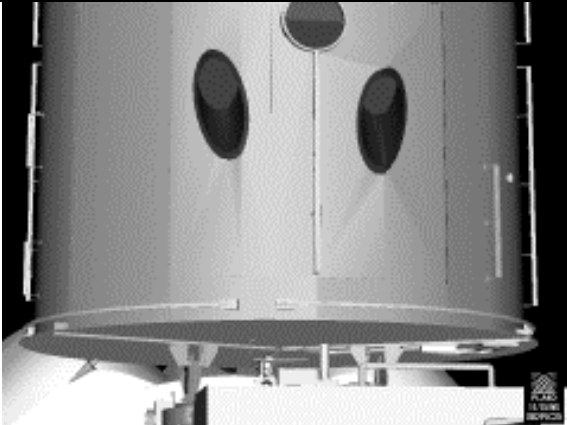
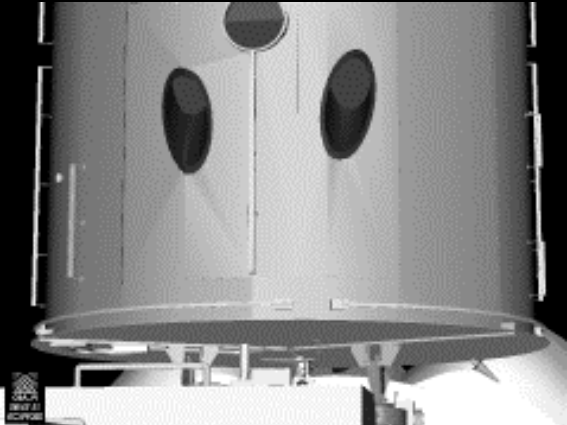
### *Required Camera Assignments for Respective Spreader Bars.*

Acquisition Order	Solar Array Tips [SA Spreader Bar Location]	Camera Combination: HST -V3 forward	Camera Combination: HST +V3 forward
1	A&B [+V2,-V3]	Camera B&D	Camera C&D
2	C&D [+V2,+V3]	Camera A&B	Camera A&C
3	G&H [-V2,+V3]	Camera C&D	Camera B&D
4	E&F [-V2,-V3]	Camera A&C	Camera A&B

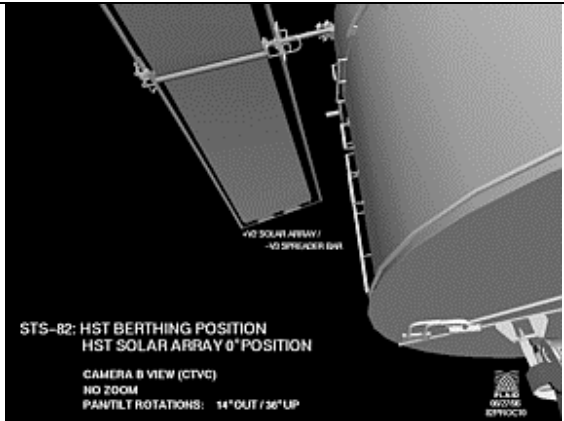
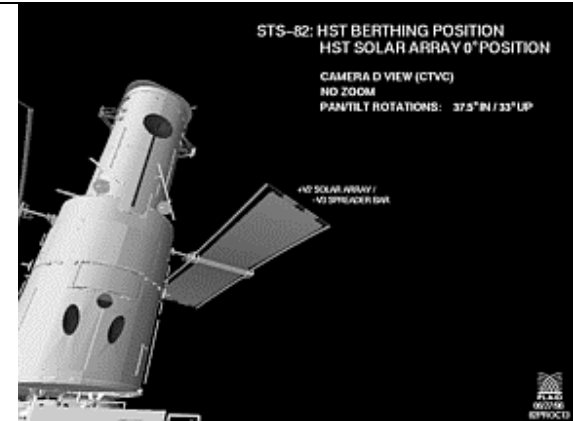
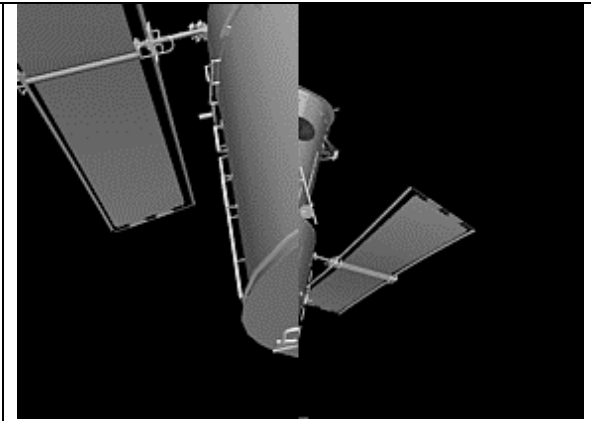
**Procedure**

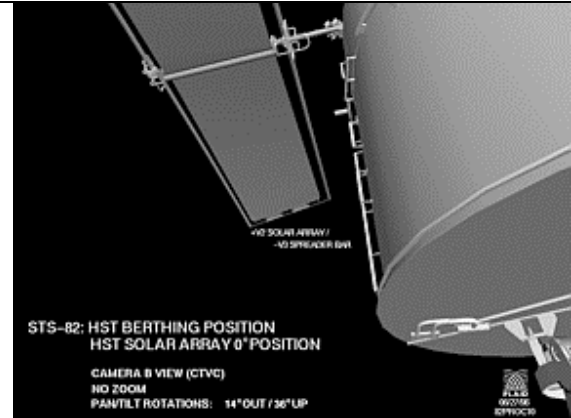
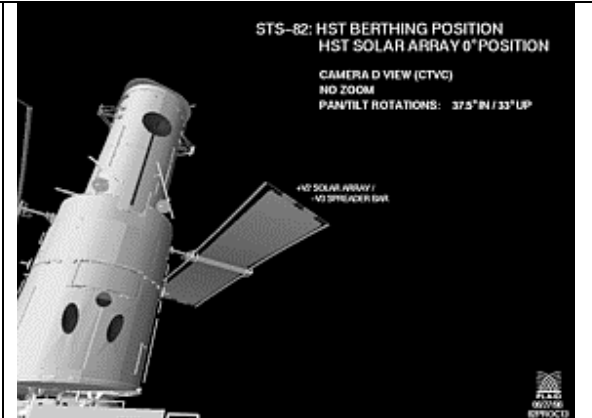
This storyboard shall cover one of four solar array spreader bar image acquisitions and the HST rotation offset imagery. The HST's -V3 axis is facing forward for these illustrations and instructions. The illustrated procedure should be iteratively performed for each spreader bar to complete the total daily data collection. In the case where the HST is in the +V3 forward position, refer to the camera assignment's table for appropriate changes to the procedure.

**ACQUISITION ROTATION FEATURES**

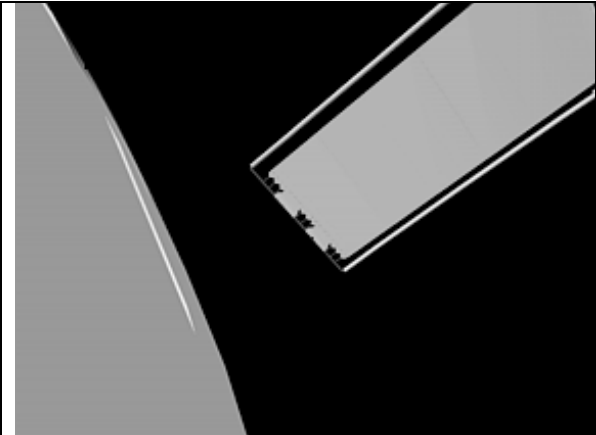
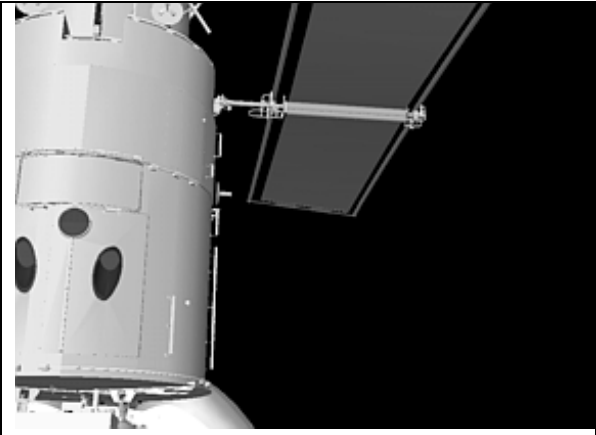
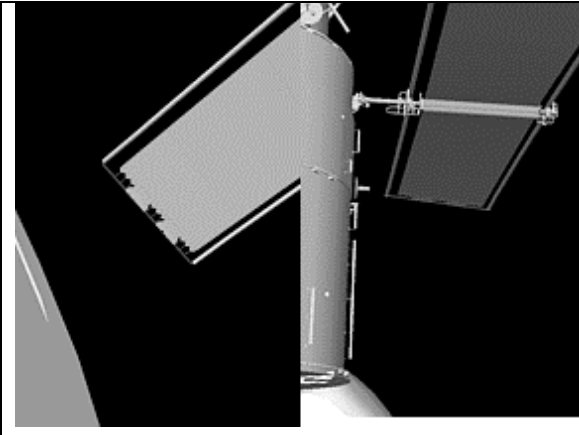
	
<p><b>Step 1</b> <b>Frame the aft shroud from camera D.</b></p> <p>Center the HST aft shroud in the horizontal FOV. Ensure that the bulkhead of the HST is in full view. Record this view for 30 seconds.</p> <p><b>Camera Settings:</b> <b>20 deg HFOV</b>      <b>15.1 deg VFOV</b> <b>Pan</b> 7.5 deg in      <b>Tilt</b> 10 deg up</p>	<p><b>Step 2</b> <b>Frame the aft shroud from camera A.</b></p> <p>Center the HST aft shroud in the horizontal FOV. Ensure that the bulkhead of the HST is in full view. Record this view for 30 seconds.</p> <p><b>Camera Settings:</b> <b>20 deg HFOV</b>      <b>14.8 deg VFOV</b> <b>Pan</b> 7.5 deg in      <b>Tilt</b> 10 deg up</p>
<p>File name s82pic25</p>	<p>File name 82proc25 flipped</p>

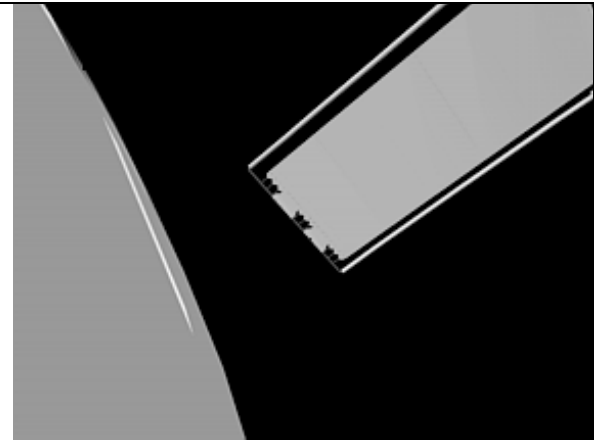
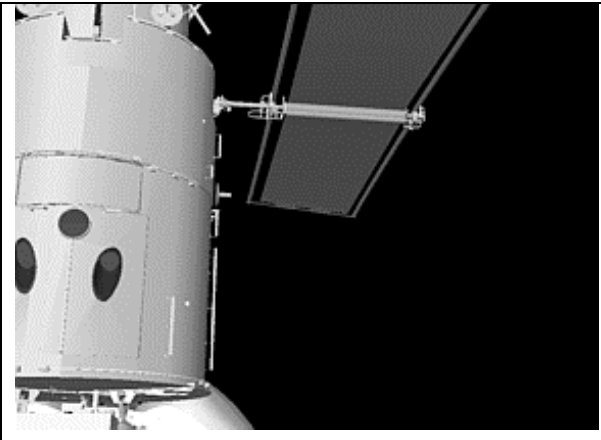
## ACQUISITION OF SOLAR TIPS A & B

 <p>ST5-82: HST BERTHING POSITION HST SOLAR ARRAY 0° POSITION</p> <p>CAMERA B VIEW (CTVC) NO ZOOM PANTILT ROTATIONS: 14° OUT / 36° UP</p>	 <p>ST5-82: HST BERTHING POSITION HST SOLAR ARRAY 0° POSITION</p> <p>CAMERA D VIEW (CTVC) NO ZOOM PANTILT ROTATIONS: 37.5° IN / 33° UP</p>	
<p><b>Step 1</b></p> <p><b>Frame spreader bar—camera B.</b></p> <p>Center solar array spreader bar A&amp;B in the center of the image and fully zoomed-out camera view.</p> <p><b>Camera Settings:</b> Fully zoomed-out HFOV and VFOV Pan 14 deg out    Tilt 36 deg up</p>	<p><b>Step 2</b></p> <p><b>Frame spreader bar—camera D.</b></p> <p>Center solar array spreader bar A&amp;B in the center of the image and fully zoomed-out camera view.</p> <p><b>Camera Settings:</b> Fully zoomed-out HFOV and VFOV Pan 37.5 deg in    Tilt 33 deg up</p>	<p><b>Step 3</b></p> <p><b>Multiplex views from camera B and D.</b></p> <p>Leaving the FOV and pointing settings of both cameras unchanged, record this view for 30 seconds.</p> <p><b>Camera Settings:</b> Unchanged from steps 1 and 2</p>
<p>File name 82PROC10.TGA</p>	<p>File name 82PROC13.TGA</p>	

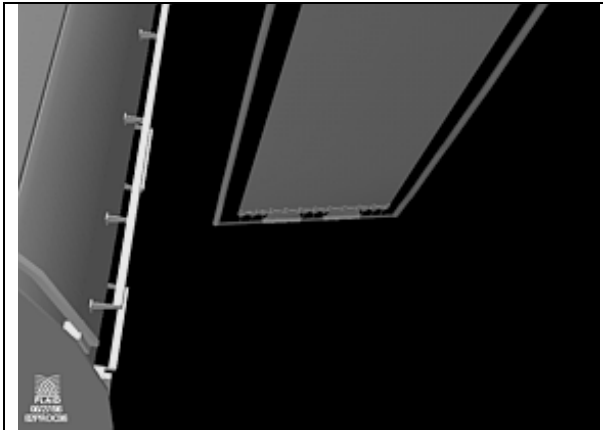
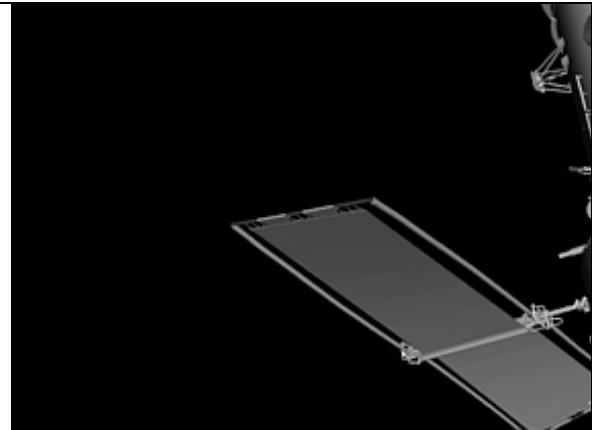
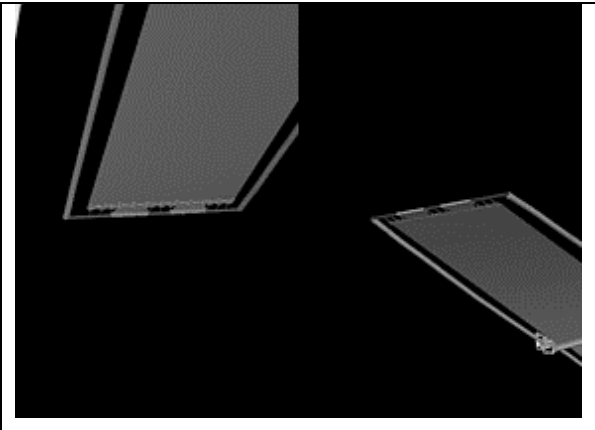
 <p>ST5-82: HST BERTHING POSITION HST SOLAR ARRAY 0° POSITION</p> <p>CAMERA B VIEW (CTVC) NO ZOOM PAN/TILT ROTATIONS: 14° OUT / 36° UP</p>	 <p>ST5-82: HST BERTHING POSITION HST SOLAR ARRAY 0° POSITION</p> <p>CAMERA D VIEW (CTVC) NO ZOOM PAN/TILT ROTATIONS: 37.5° IN / 33° UP</p>
<p><b>Step 4</b></p> <p><b>Scale reference image—camera B.</b></p> <p>Demux cameras B and D views. Leaving the FOV fully zoomed-out and the pointing settings of camera B unchanged, record the view for 10 seconds.</p> <p><b>Camera Settings:</b> <b>Unchanged from steps 3</b></p>	<p><b>Step 5</b></p> <p><b>Scale reference image—Camera D.</b></p> <p>Leaving the FOV fully zoomed-out and the pointing settings of camera D unchanged, record the view for 10 seconds.</p> <p><b>Camera Settings:</b> <b>Unchanged from steps 3</b></p>
<p>File name 82PROC10.TGA</p>	<p>File name 82PROC13.TGA</p>

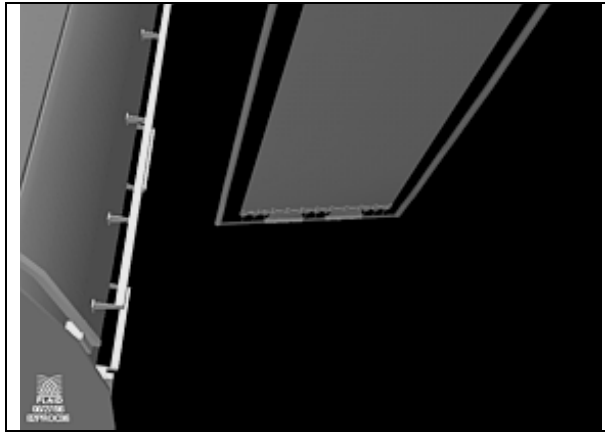
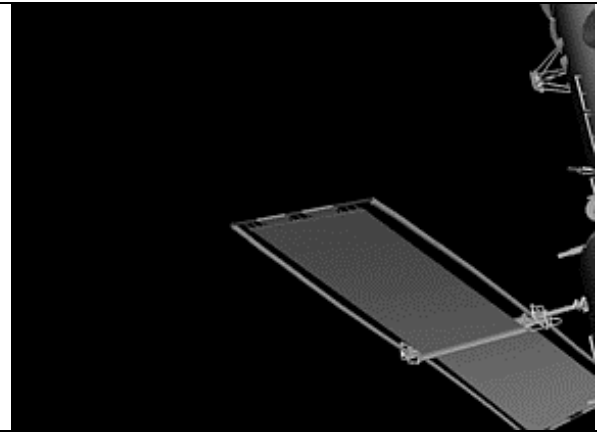
## ACQUISITION OF SOLAR TIPS C & D

		
<p><b>Step 1</b></p> <p><b>Frame spreader bar—camera B.</b></p> <p>Center solar array spreader bar C&amp;D in the center of the image and fully zoomed-out camera view.</p> <p><b>Camera Settings:</b>  <b>Fully zoomed-out HFOV and VFOV</b>  <b>Pan</b> 130 deg in    <b>Tilt</b> 64 deg up</p>	<p><b>Step 2</b></p> <p><b>Frame spreader bar—camera A.</b></p> <p>Center solar array spreader bar C&amp;D in the center of the image and fully zoomed-out camera view.</p> <p><b>Camera Settings:</b>  <b>Fully zoomed-out HFOV and VFOV</b>  <b>Pan</b> 8.5 deg out    <b>Tilt</b> 18 deg up</p>	<p><b>Step 3</b></p> <p><b>Multiplex views from cameras B and A.</b></p> <p>Leaving the FOV and pointing settings of both cameras unchanged, record this view for 30 seconds.</p> <p><b>Camera Settings:</b>  <b>Unchanged from steps 1 and 2</b></p>
<p>File name 82PROC20.TGA</p>	<p>File name 82PROC17.TGA</p>	

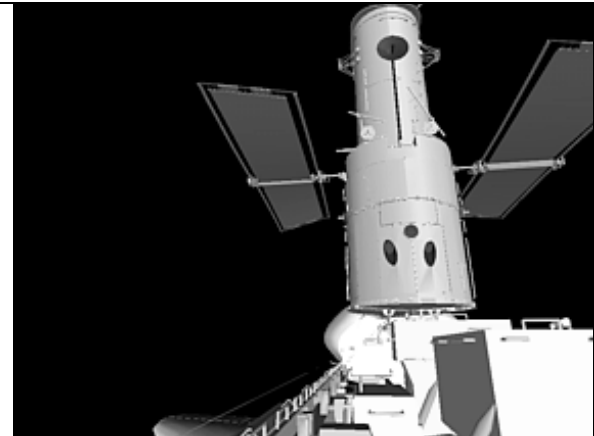
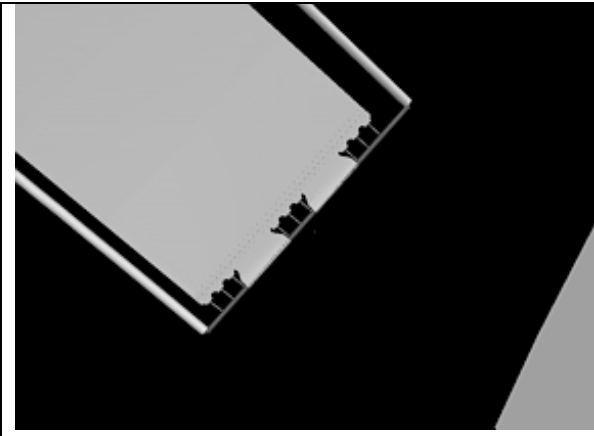
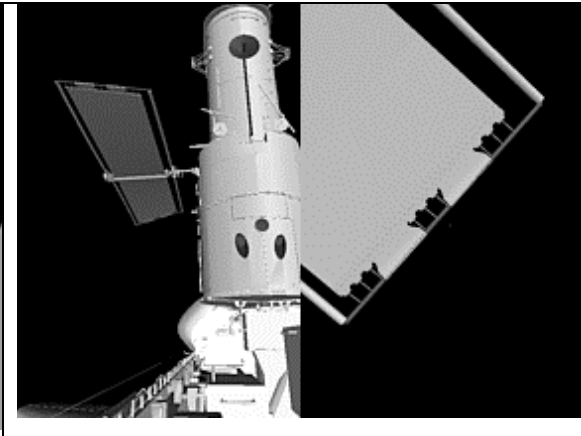
	
<p><b>Step 4</b></p> <p><b>Scale reference image—camera B.</b></p> <p>Demux cameras B and A views. Leaving the FOV fully zoomed-out and the pointing settings of camera B unchanged, record the view for 10 seconds.</p> <p><b>Camera Settings:</b>  <b>Unchanged from steps 3</b></p>	<p><b>Step 5</b></p> <p><b>Scale reference image—camera A.</b></p> <p>Leaving the FOV fully zoomed-out and the pointing settings of camera A unchanged, record the view for 10 seconds.</p> <p><b>Camera Settings:</b>  <b>Unchanged from steps 3</b></p>
<p>File name 82PROC20.TGA</p>	<p>File name 82PROC17.TGA</p>

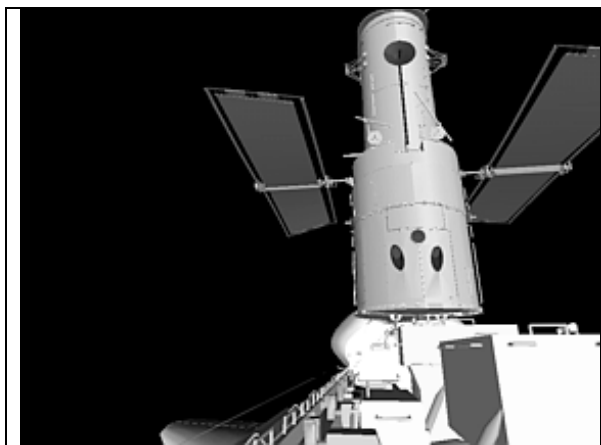
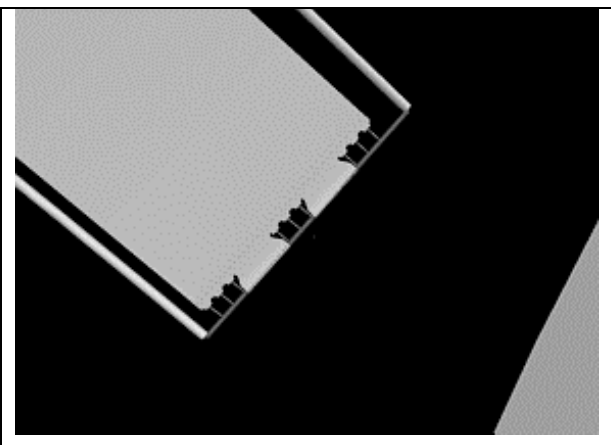
# ACQUISITION OF SOLAR TIPS E & F

		
<p><b>Step 1</b></p> <p><b>Frame spreader bar—camera C.</b></p> <p>Center solar array spreader bar E&amp;F in the center of the image and fully zoomed-out camera view.</p> <p><b>Camera Settings:</b>  <b>HFOV and VFOV fully zoomed out</b>  <b>Pan</b> 14.5 deg out    <b>Tilt</b> 35 deg up</p>	<p><b>Step 2</b></p> <p><b>Frame spreader bar—camera A.</b></p> <p>Center solar array spreader bar E&amp;F in the center of the image and fully zoomed-out camera view.</p> <p><b>Camera Settings:</b>  <b>HFOV and VFOV fully zoomed out</b>  <b>Pan</b> 37.5 deg in    <b>Tilt</b> 33 deg up</p>	<p><b>Step 3</b></p> <p><b>Multiplex views from cameras C and A.</b></p> <p>Leaving the FOV and pointing settings of both cameras unchanged, record this view for 30 seconds.</p> <p><b>Camera Settings:</b>  <b>Unchanged from steps 1 and 2</b></p>
<p>File name 82PROC06.TGA</p>	<p>File name 82PROC03.TGA</p>	

	
<p><b>Step 4</b></p> <p><b>Scale reference image—camera C.</b></p> <p>Demux cameras C and A views. Leaving the FOV fully zoomed-out and the pointing settings of camera C unchanged, record the view for 10 seconds.</p> <p><b>Camera Settings:</b>  <b>Unchanged from steps 3</b></p>	<p><b>Step 5</b></p> <p><b>Scale reference image—camera A.</b></p> <p>Leaving the FOV fully zoomed-out and the pointing settings of camera A unchanged, record the view for 10 seconds.</p> <p><b>Camera Settings:</b>  <b>Unchanged from steps 3</b></p>
<p>File name 82PROC06.TGA</p>	<p>File name 82PROC03.TGA</p>

## ACQUISITION OF SOLAR TIPS G & H

		
<p><b>Step 1</b></p> <p><b>Frame spreader bar—camera D.</b></p> <p>Center solar array spreader bar G&amp;H in the center of the image and fully zoomed-out camera view.</p> <p><b>Camera Settings:</b>  <b>HFOV and VFOV fully zoomed out</b>  <b>Pan</b> 8 deg out      <b>Tilt</b> 19 deg up</p>	<p><b>Step 2</b></p> <p><b>Frame spreader bar—camera C.</b></p> <p>Center SA spreader bar G&amp;H in the center of the image and fully zoomed-out camera view.</p> <p><b>Camera Settings:</b>  <b>HFOV and VFOV fully zoomed out</b>  <b>Pan</b> 133 deg out      <b>Tilt</b> 64 deg up</p>	<p><b>Step 3</b></p> <p><b>Multiplex views from cameras D and C.</b></p> <p>Leaving the FOV and pointing settings of both cameras unchanged, record this view for 30 seconds.</p> <p><b>Camera Settings:</b>  <b>Unchanged from steps 1 and 2</b></p>
<p>File name 82PROC24.TGA</p>	<p>File name 82PROC26.TGA</p>	

	
<p><b>Step 4</b></p> <p><b>Scale reference image—camera D.</b></p> <p>Demux cameras C and D views. Leaving the FOV fully zoomed-out and the pointing settings of camera D unchanged, record the view for 10 seconds.</p> <p><b>Camera Settings:</b>  <b>Unchanged from steps 3</b></p>	<p><b>Step 5</b></p> <p><b>Scale reference image—camera C.</b></p> <p>Leaving the FOV fully zoomed-out and the pointing settings of camera C unchanged, record the view for 10 seconds.</p> <p><b>Camera Settings:</b>  <b>Unchanged from steps 3</b></p>
<p>File name 82PROC24.TGA</p>	<p>File name 82PROC26.TGA</p>



## **Appendix E: Lighting Study**

# Hubble Space Telescope (HST) Lighting Analysis Summary Report

## Introduction

The Graphics Research and Analysis Facility conducted an analysis of the expected lighting conditions during the static twist analyses (STAs), selected solar array motion analyses (SAMAs), and selected HST surveys. (Lorraine Hancock of Johnson Space Center's Crew Station Branch was the principal analyst.) The lighting analysis will be used for imagery data acquisition planning and as an aide to real-time imagery acquisition.

## STA Views

A daylight pass during crew sleep period number 5 was chosen as representative of the lighting conditions for all the required STAs. (STAs will occur during crew sleep periods 3, 4, 5, 6, and 7.) Based on the range of solar beta angles for each crew sleep period, it was believed that views during crew sleep period #5 would be representative of all lighting conditions for all STA opportunities. The lighting analysis was applied to the actual STA data acquisition views for each array tip plus the rotation view.

Results indicated that, for each camera view, there will be periods of good lighting and periods of unacceptable lighting in which the sun will shine directly into the camera or unacceptable specular reflection off the HST will shine into the camera. In general, the lighting was poor (i.e. excessive reflection or direct sun shining into cameras) at sunrise and near sunset with periods of 20 to 50 minutes of good lighting in between. Since the lighting conditions will vary it was suggested that the camera aperture control be set on manual and adjusted real time by Mission Control's instrumentation and communication officer.

See appendix A for a detailed assessment of the lighting for each view.

## SAMA Views

### *Vernier Reaction Control Subsystem (VRCS) SAMA*

A lighting analysis was performed for acquiring imagery for the VRCS SAMA, which occurs during crew sleep period #3 (MET 02:08:55 to 0:09:30). Overall the lighting conditions were considered acceptable for use in measuring the solar array motion. The lighting was very similar to the camera B view for the STA.

See Appendix B for a detailed assessment of the VRCS SAMA views.

### *Potential SAMA for solar array slew to 0 deg at MET 02:02:25 to 02:03:25*

Due to a solar inertial orbit and a fairly tight field of view, all views had fairly constant lighting. The views were acceptable for use in measuring the solar array motion.

See Appendix B for a detailed assessment of the SAMA slew views.

## **HST Survey Views**

### ***+V2 Survey after 1st extravehicular activity (EVA) day at MET 03:01:10 to 03:01:55***

Views were obtained for an entire daylight pass from cameras A and D. Both sets of camera views had poor lighting at sunrise. The view from camera A continued to have poor lighting until about 15 minutes after sunrise, while the view from camera D had good lighting at sunrise + 10 minutes. Lighting for both camera views was generally good from about 15 minutes after sunrise until sunrise + 55 minutes. (Note that the view from camera D at sunrise + 5 minutes exhibited specular reflection.) Both camera views had unacceptable lighting conditions at sunset.

See Appendix B for a detailed assessment of the +V2 survey views.

### ***-V3 Survey just after berthing at MET 02:00:45 to 02:01:50***

Views were obtained from an entire daylight pass from cameras A and D. The lighting remains fairly constant for both views and is sufficient for conducting the survey. However, the position of the Earth relative to the Orbiter does change, causing a good deal of earthshine reflection to move across the HST. There is no direct sunlight shining into either of the camera A or D lenses.

See Appendix B for a detailed assessment of the +V3 survey just after berthing.

## **Night Lighting Analysis**

A night lighting analysis was performed for the STA views and the flight support structure (FSS) pivot to 85 deg. The night lighting analyses followed the constraints in the STS-82 flight rules for using the payload bay lights. For this lighting assessment, the mid payload bay lights were turned off (According to the flight rules, these lights are to remain off at all times.) and the port forward payload bay light was also turned off since its use will be restricted during the mission. The aft payload bay lights and the starboard forward payload bay light were turned on since there are no constraints on their use. The night lighting using payload bay lights was generally considered unacceptable for measuring the positions of the solar array tips. The primary reason for the night views being unacceptable was low contrast and the presence of excessive noise (especially for color television cameras, or CTVCs) for views of the array tips. Although the entire STA data acquisition cannot be performed at night, the lighting should be adequate for collecting the following data at night using payload bay lights:

- STA rotation from camera D or A
- Setting each cameras pan/tilt to the 0 deg position
- Initial camera positioning; the cameras could be positioned at night to view the first set of array tips

## Appendix A STA Lighting Analysis

### ***Setup assumptions:***

All views emulate an ALC setting of AVERAGE, with a gamma of NORMAL. All views demonstrate the available lighting for an Orbiter attitude of -ZLV -XVV, and are representative of all of the daylight passes of each of the crew sleep periods 3 through 7.

The following is a specific lighting assessment for each view from Lorraine Hancock:

### ***Camera D rotation reference:***

Lighting is very uniform for the middle part of the day (from about 20 minutes after sunrise to 20 minutes before sunset). Times near sunrise and sunset do not provide good lighting due to specular reflection of the sunlight off of the HST and its various carriers in the payload bay.

### ***Camera B view of tips A/B:***

Sunrise to about 10 minutes after sunrise provides good lighting and good imagery of the spreader bar. Times before the middle part of the day provide quickly moving shadows across the solar array. Also, after terminator rise, the Earth provides the background to the spreader bar you're looking at. Mid afternoon lighting is fairly uniform, however there is a bit of specular reflection off of the bisters that may interfere with your viewing of the spreader bar. Very late in the day (10 minutes before sunset through sunset), the sun will shine directly into the camera lens.

### ***Camera D view of tips A/B:***

There is direct sunlight shining into the camera lens at sunrise and for about 5 minutes after that. Specular reflection of the sun on the bisters causes camera lens scattering for roughly 20 minutes, but then there is good uniform lighting throughout the middle part of the day. At sunset minus 15 minutes through sunset itself, there is a large amount of specular reflection of the sun off of the HST and its various carriers in the payload bay, which will interfere with camera viewing. Again, as with most of the scenes analyzed in this memo, the Earth provides the background against which you will be viewing the spreader bar.

### ***Camera B view of tips C/D:***

Much of the lighting for this scene is quite uniform, with some specular reflection of the sun off of the bistem. The Earth provides all of the background while the Orbiter is travelling between terminator rise and terminator set.

***Camera A view of tips C/D:***

For the first 20 minutes or so of the day, there will be so much direct sunlight into the camera lens or specular reflection of the sun off of the HST body or solar array bisters that it is unreasonable to think that the camera would even be on, because the monochrome lens assembly (MLA) camera is so sensitive to sunlight. The middle part of the day provides nice uniform lighting, with a black backdrop for the spreader bar you wish to view. The last 20 minutes of the day provide very harsh lighting conditions for this MLA camera view because of specular reflection of the sun off of the HST or its carriers in the payload bay; again, it would be most likely that the camera would be turned off to avoid burning out the lens.

***Camera C view of tips E/F:***

Very uniform lighting throughout the whole daylight pass for this MLA camera view without direct sunlight or harsh specular reflections. The Earth provides the backdrop for the spreader bar you are viewing for travel between terminators.

***Camera A view of tips E/F:***

Some specular reflection off of the solar array bisters may interfere with the camera viewing of the spreader bar very early and late in the day. Otherwise, there is uniform lighting for much of the middle part of the day, with the Earth providing the background to the spreader bar.

***Camera D view of tips G/H:***

Very early in the day—the first 20 minutes or so—there is either direct sunlight into the camera or a lot of specular reflection off of the HST body and its various carriers that will prevent good camera viewing. Up until about 20 minutes before sunset, there will be fairly good lighting, but not necessarily on the spreader bar you are viewing. That, plus the fact that that spreader bar is against a black background, may make it a challenge to obtain good imagery of it. The last 20 minutes of the daylight pass allow for too much specular reflection of the sun off of the HST and its various carriers to get any useful camera viewing at that time.

***Camera C view of tips G/H:***

Very uniform lighting throughout the whole daylight pass for this MLA camera view without direct sunlight or harsh specular reflections. The Earth provides the backdrop for the spreader bar you are viewing for travel between terminators.

## **Appendix B VRCS and Solar Array Slew SAMA and HST Surveys Lighting Analysis**

The following is a specific lighting assessment for each view from Lorraine Hancock:

### **VRCS FIRING TEST DURING CREW SLEEP #3:**

-----  
*Orbit 37 partial day pass: 02/09:15:53 - 02/09:50/55*  
*Orbiter attitude is -ZLV -XVV*

Eight scenes make up the views, starting at about 3½ minutes after terminator rise, and ending at about 14½ minutes after Orbiter noon. Both sets of views were created to emulate an ALC setting of AVERAGE and a gamma setting of NORMAL.

#### ***Camera B view of solar array edge A/B for VRCS firing test:***

The very first scene is against a black background because the terminator is not yet visible with the camera tilt used in this particular view. Subsequent scenes show quickly moving shadows across the solar array, with the Earth providing the complete background. The last 15 minutes or so do provide fairly uniform lighting of the solar array and its spreader bar, with just a bit of specular reflection off of the bistems.

#### ***Camera B scale reference for VRCS firing test:***

Just about the first five minutes of this period provide good uniform lighting of the viewing area. This is followed by a 5-minute period of quite a bit of specular reflection, and then by a 20-minute period of good uniform lighting again. The last 5-10 minutes show quite a bit of specular lighting, which may again hinder your camera viewing. The Earth provides the background for the whole period of this particular camera view.

### **SOLAR ARRAY SLEW TO 0 DEG:**

-----  
*Orbit 33 day pass: 02/02:39:53 - 02/03:41:09*  
*Orbiter attitude is a biased -XSI*

Starting at Orbiter sunrise and ending with Orbiter sunset, 11 scenes make up the sequence of views, with each scene about 6 minutes apart. With the exception of the view from camera B (which is noted immediately below), all views were created to emulate an ALC setting of AVERAGE and a gamma setting of NORMAL.

***Camera B view of solar array edge A/B for solar array slew to 0 deg.:***

This is the one set of views that was made to emulate an ALC setting of NORMAL and a gamma setting of NORMAL. This was done because it was determined that the ALC setting of AVERAGE caused too much scattering of the light in the camera lens from the HST handrails. As expected from the inertial attitude, the lighting remains fairly constant throughout the day. Near sunrise and sunset the image can be viewed with a black background. At the other times throughout the middle portion of the day, the Earth provides the background.

***Camera B scale reference view for solar array slew to 0 deg.:***

Again, due to the inertial attitude, the lighting is very uniform throughout the day and the viewing looks good with the ALC setting of AVERAGE. About 20-30 minutes of the middle of the day will provide the Earth as the background.

***Camera C scale reference view for solar array slew to 0 deg.:***

See comments for camera B scale reference view.

***Camera B view of solar array edge A/B for solar array slew to 0 deg.:***

See comments for camera B scale reference view.

***Camera C view of solar array edge E/F for solar array slew to 0 deg.:***

The image remains virtually the same throughout the day, with a constant black background. Viewing of this activity with camera C should be excellent.

**+V2 HST SURVEY AFTER 1st EVA DAY:**

-----  
*Orbit 47 day pass: 03/01:10:54 - 03/02:12:16*  
*Orbiter attitude is -ZLV -XVV*

The sequence contains 13 views each from camera A and camera D, starting at Orbiter sunrise and ending with Orbiter sunset, with each scene about 5 minutes apart. Both sets of views were created to emulate an ALC setting of AVERAGE and a gamma setting of NORMAL.

***Camera A view of HST survey after 1st EVA day:***

Direct sunlight into the camera at sunrise provides unacceptable viewing from this MLA camera at that time. From just after sunrise to about 24 minutes after sunrise, there is a lot of specular reflection of the sun off of the solar array bisters, causing unstable MLA operations at that time. About 25 minutes around the middle part of the day provide uniform lighting. Sunset minus 15 minutes up until sunset again finds a lot of specular reflection of the sun off of the solar array bisters, causing unstable MLA operations. At sunset, there is a lot of specular reflection of the sun off of the HST body, which will be unacceptable for MLA operations.

***Camera D view of HST survey after 1st EVA day:***

Depending on the amount of the camera pan angle, you may get direct sunlight into the camera lens at sunrise. We are using a pan of 9 deg inboard, which is allowing for the HST body to block the camera's view of the sun. Until about 10 minutes after sunrise, there will be specular reflection of the sun off of the solar array bisters that may interfere with your camera viewing due to the scattering of the light in the lens. For the better part of the middle of the day, there is good uniform lighting, with the Earth providing the background for the area that you are looking at. Starting at about 10 minutes before sunset, the camera view of HST body becomes quite saturated. At sunset and just before, specular reflection of the sun off of the HST body and its various carriers in the payload bay will interfere with camera viewing.

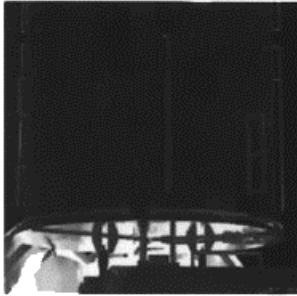
**-V3 HST SURVEY JUST AFTER BERTHING:**

-----  
*Orbit 32 day pass: 02/01:03:23 - 02/02:04:38*  
*Orbiter attitude is a biased -XSI*

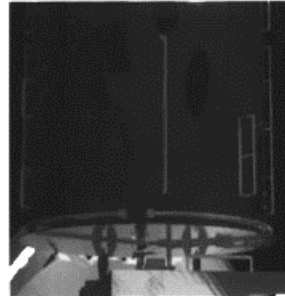
***Camera A view of HST survey just after berthing; camera D view of HST survey just after berthing:***

Starting at Orbiter sunrise and ending with Orbiter sunset, 11 scenes make up these views, with each scene about 6 minutes apart. Both sets of views were created to emulate an ALC setting of AVERAGE and a gamma setting of NORMAL. Because this is an inertial attitude, the lighting remains fairly constant over time. However, what does change is the position of the Earth relative to the Orbiter, and thus to your camera views. The change in the position of the Earth causes much earthshine reflection that moves across the HST body surface. There is no direct sunlight into either of the camera A or D lenses during this daylight pass.

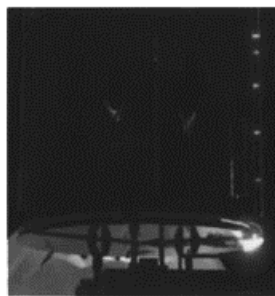
## Lighting for Rotation Reference View From Camera D



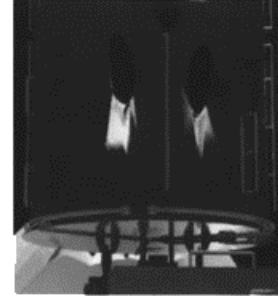
Sunrise



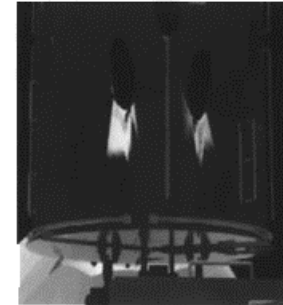
Sunrise + 5 Min.



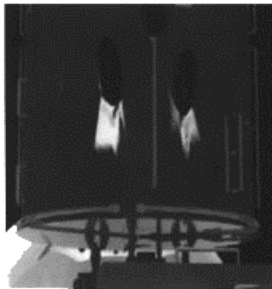
Sunrise + 10 Min.



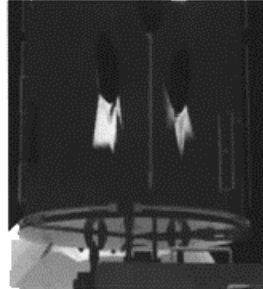
Sunrise + 15 Min.



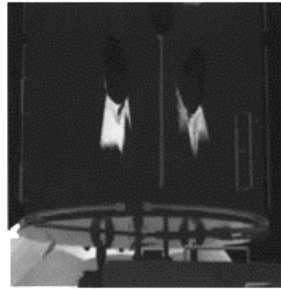
Sunrise + 20 Min.



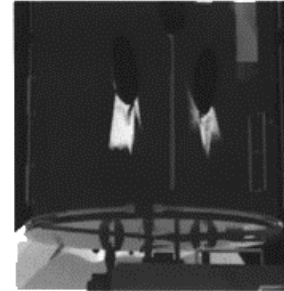
Sunrise + 25 Min.



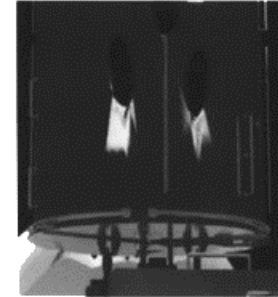
Sunrise + 30 Min.



sunrise + 35 Min.



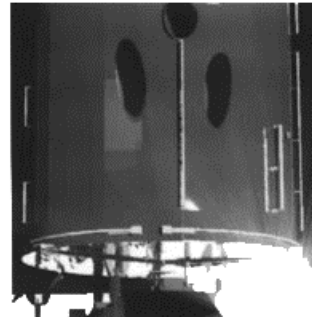
Sunrise + 40 Min.



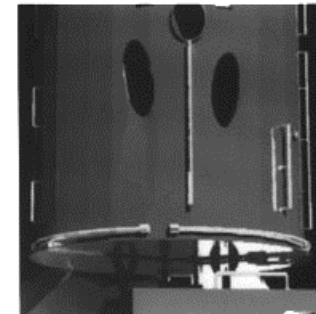
Sunrise + 45 Min.



Sunrise + 50 Min.



Sunrise + 55 Min.



Sunset

### Lighting for Tips A/B View From Camera B



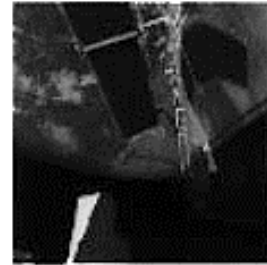
Sunrise



Sunrise + 5 minutes



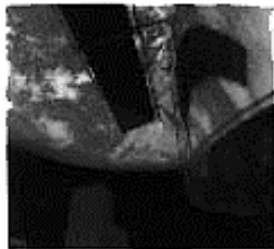
Sunrise + 10 minutes



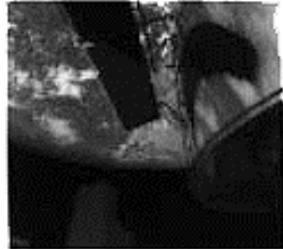
Sunrise + 15 minutes



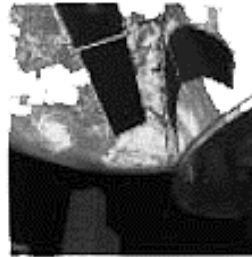
Sunrise + 20 minutes



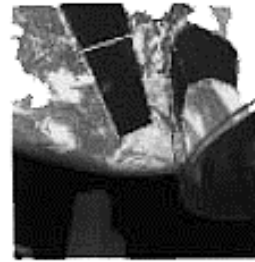
Sunrise + 25 minutes



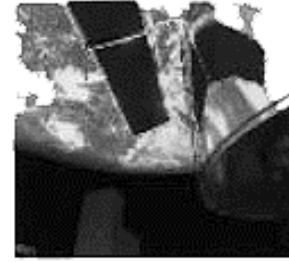
Sunrise + 30 minutes



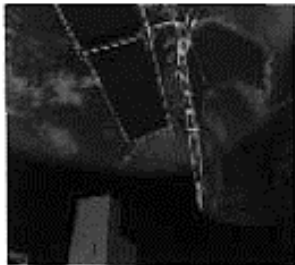
Sunrise + 35 minutes



Sunrise + 40 minutes



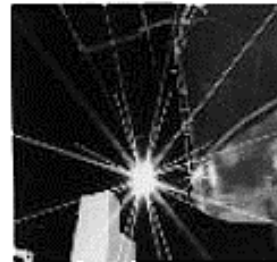
Sunrise + 45 minutes



Sunrise + 50 minutes



Sunrise + 55 minutes



Sunset

## Lighting for Tips A/B View From Camera D



Sunrise



Sunrise + 5 minutes



Sunrise + 10 minutes



Sunrise + 15 minutes



Sunrise + 20 minutes



Sunrise + 25 minutes



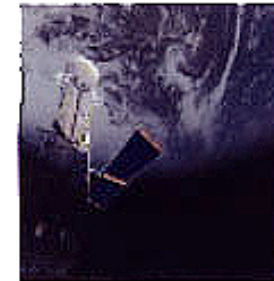
Sunrise + 30 minutes



Sunrise + 35 minutes



Sunrise + 40 minutes



Sunrise + 45 minutes



Sunrise + 50 minutes

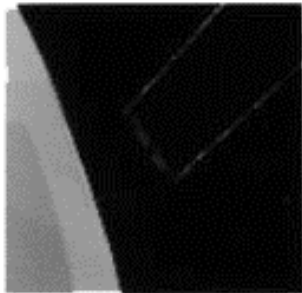


Sunrise + 55 minutes

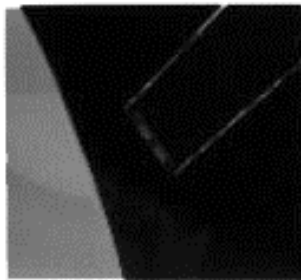


Sunset

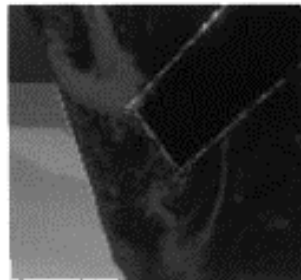
### Lighting for Tips C/D View From Camera B



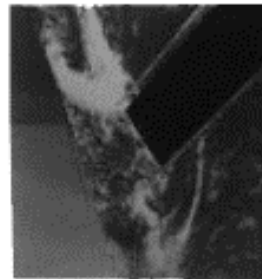
Sunrise



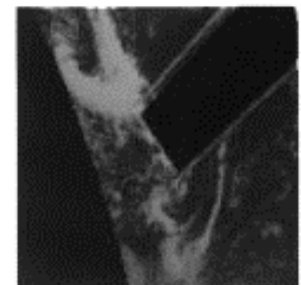
Sunrise + 5 minutes



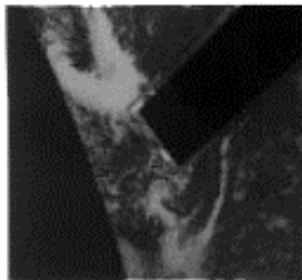
Sunrise + 10 minutes



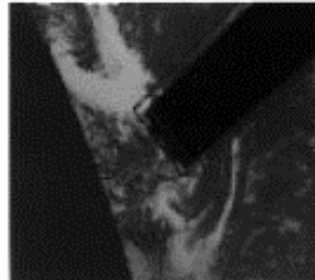
Sunrise + 15 minutes



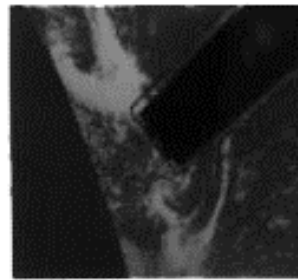
Sunrise + 20 minutes



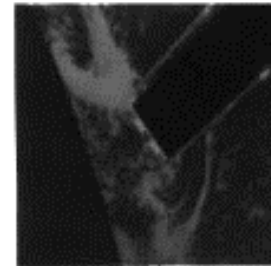
Sunrise + 25 minutes



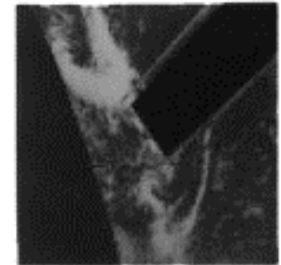
Sunrise + 30 minutes



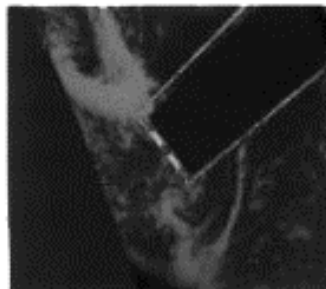
Sunrise + 35 minutes



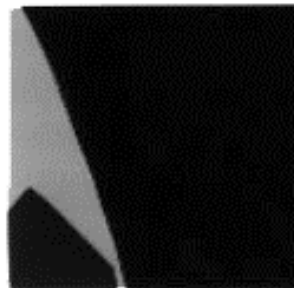
Sunrise + 40 minutes



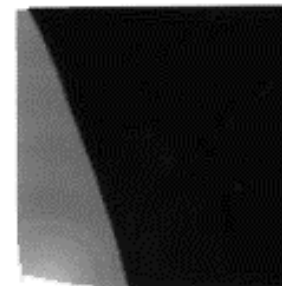
Sunrise + 45 minutes



Sunrise + 50 minutes



Sunrise + 55 minutes



Sunset

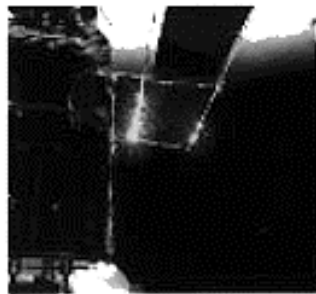
### Lighting for Tips C/D View From Camera A



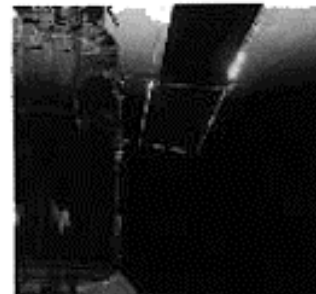
Sunrise



Sunrise + 5 minutes



Sunrise + 10 minutes



Sunrise + 15 minutes



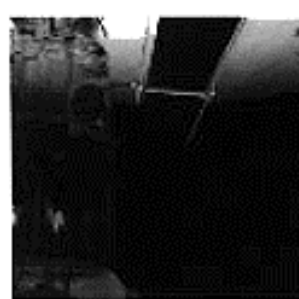
Sunrise + 20 minutes



Sunrise + 25 minutes



Sunrise + 30 minutes



Sunrise + 35 minutes



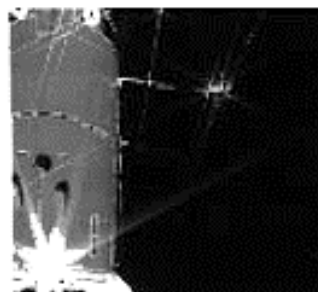
Sunrise + 40 minutes



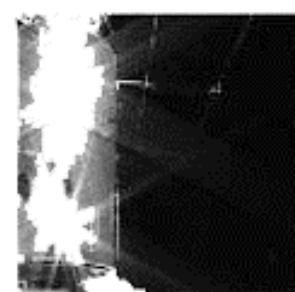
Sunrise + 45 minutes



Sunrise + 50 minutes

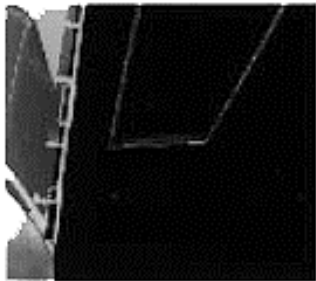


Sunrise + 55 minutes

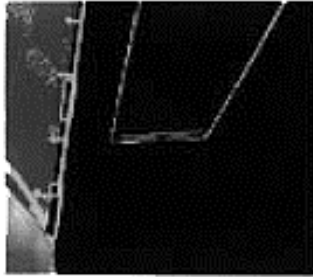


Sunset

### Lighting for Tips E/F View From Camera C



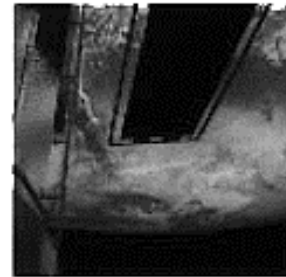
Sunrise



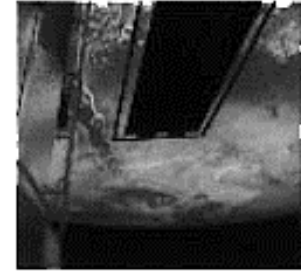
Sunrise + 5 minutes



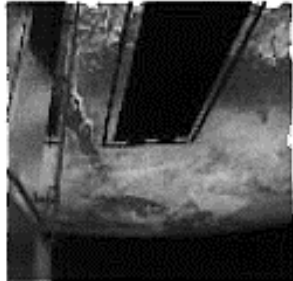
Sunrise + 10 minutes



Sunrise + 15 minutes



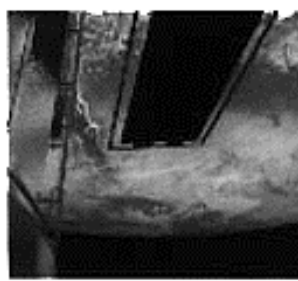
Sunrise + 20 minutes



Sunrise + 25 minutes



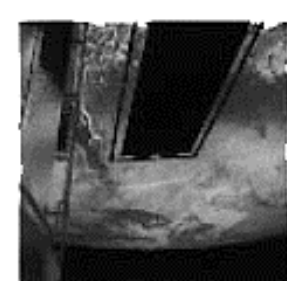
Sunrise + 30 minutes



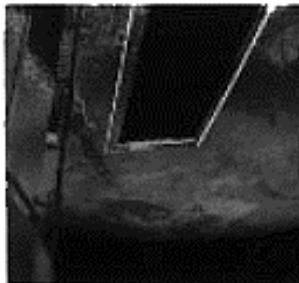
Sunrise + 35 minutes



Sunrise + 40 minutes



Sunrise + 45 minutes



Sunrise + 50 minutes

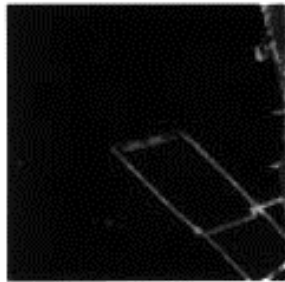


Sunrise + 55 minutes

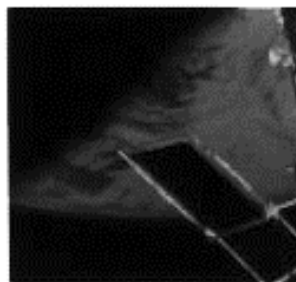


Sunset

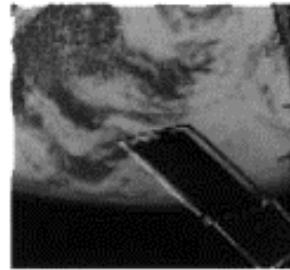
### Lighting for Tips E/F View From Camera A



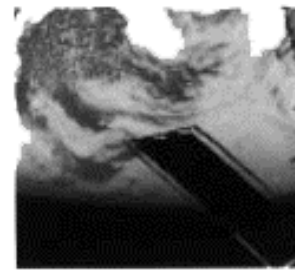
Sunrise



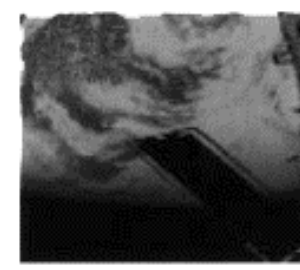
Sunrise + 5 minutes



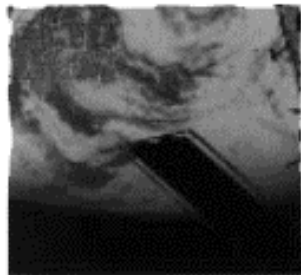
Sunrise + 10 minutes



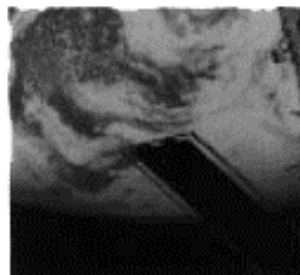
Sunrise + 15 minutes



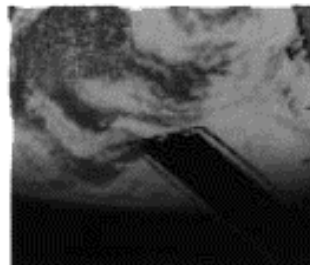
Sunrise + 20 minutes



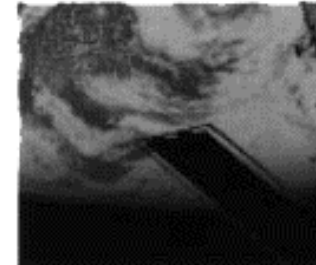
Sunrise + 25 minutes



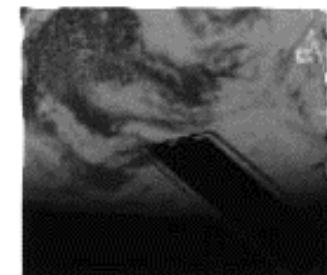
Sunrise + 30 minutes



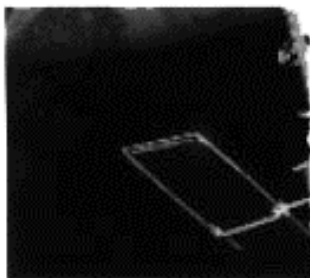
Sunrise + 35 minutes



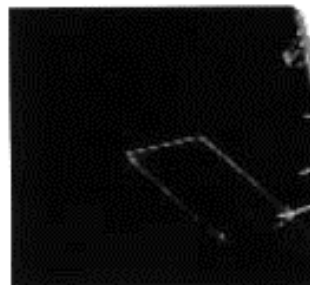
Sunrise + 40 minutes



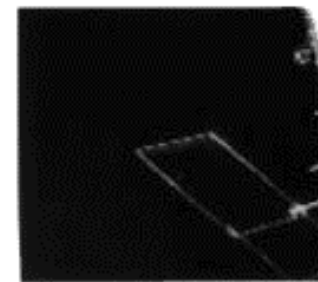
Sunrise + 45 minutes



Sunrise + 50 minutes

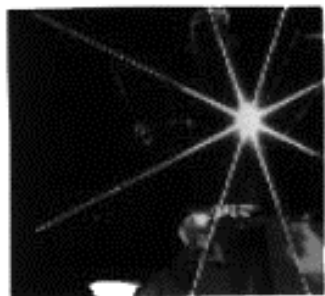


Sunrise + 55 minutes

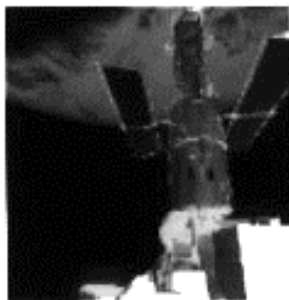


Sunset

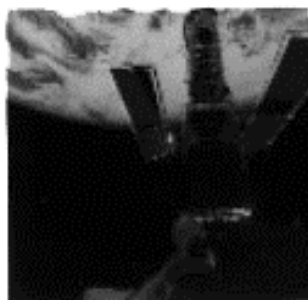
### Lighting for Tips G/H View From Camera D



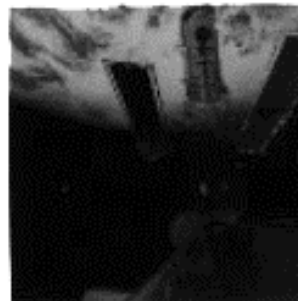
Sunrise



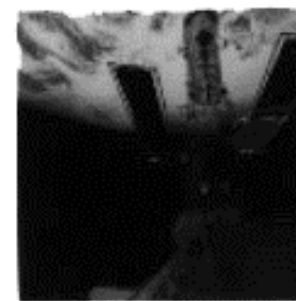
Sunrise + 5 minutes



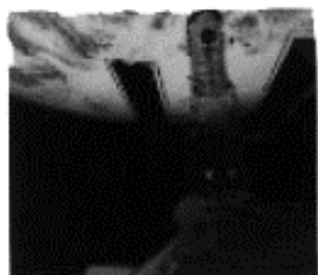
Sunrise + 10 minutes



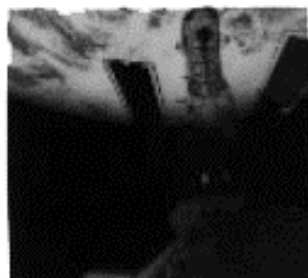
Sunrise + 15 minutes



Sunrise + 20 minutes



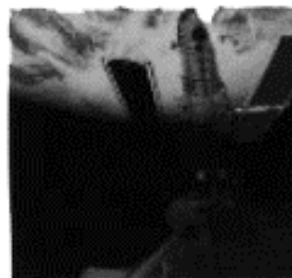
Sunrise + 25 minutes



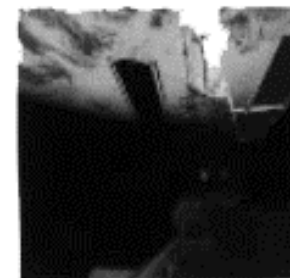
Sunrise + 30 minutes



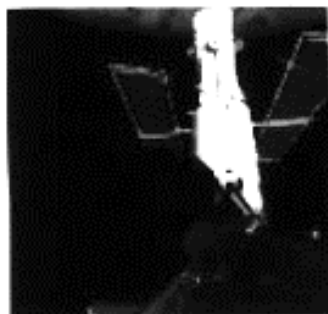
Sunrise + 35 minutes



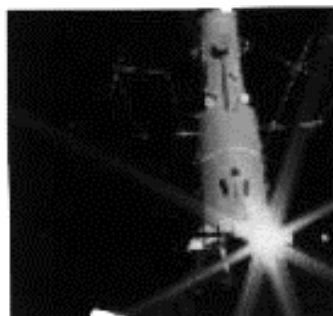
Sunrise + 40 minutes



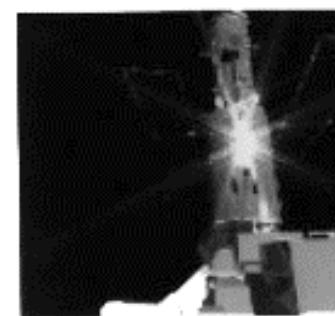
Sunrise + 45 minutes



Sunrise + 50 minutes

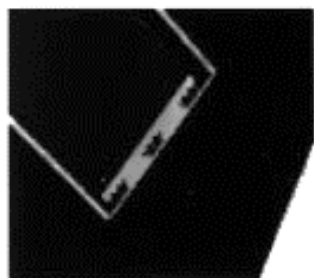


Sunrise + 55 minutes

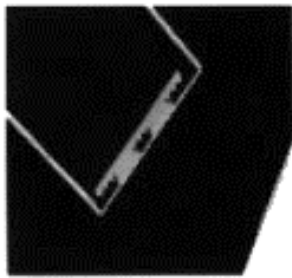


Sunset

### Lighting for Tips G/H View From Camera C



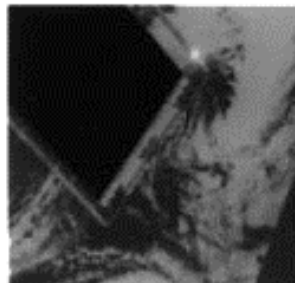
Sunrise



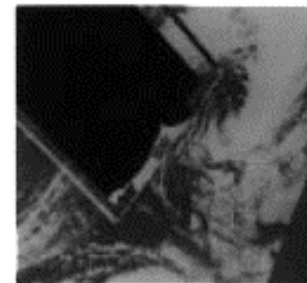
Sunrise + 5 minutes



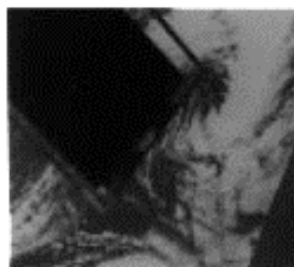
Sunrise + 10 minutes



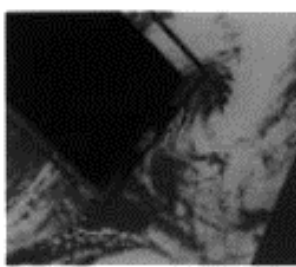
Sunrise + 15 minutes



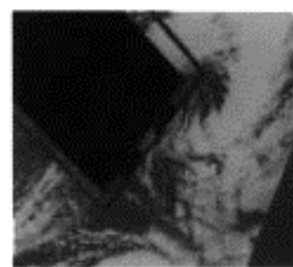
Sunrise + 20 minutes



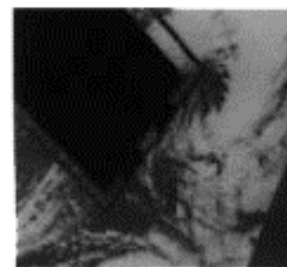
Sunrise + 25 minutes



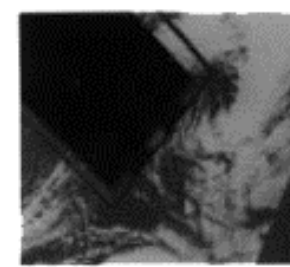
Sunrise + 30 minutes



Sunrise + 35 minutes



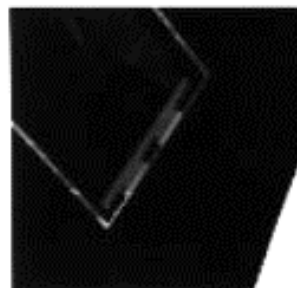
Sunrise + 40 minutes



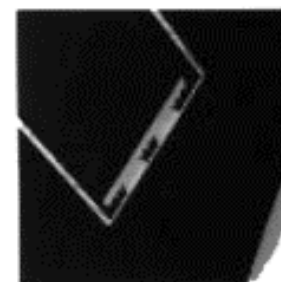
Sunrise + 45 minutes



Sunrise + 50 minutes



Sunrise + 55 minutes

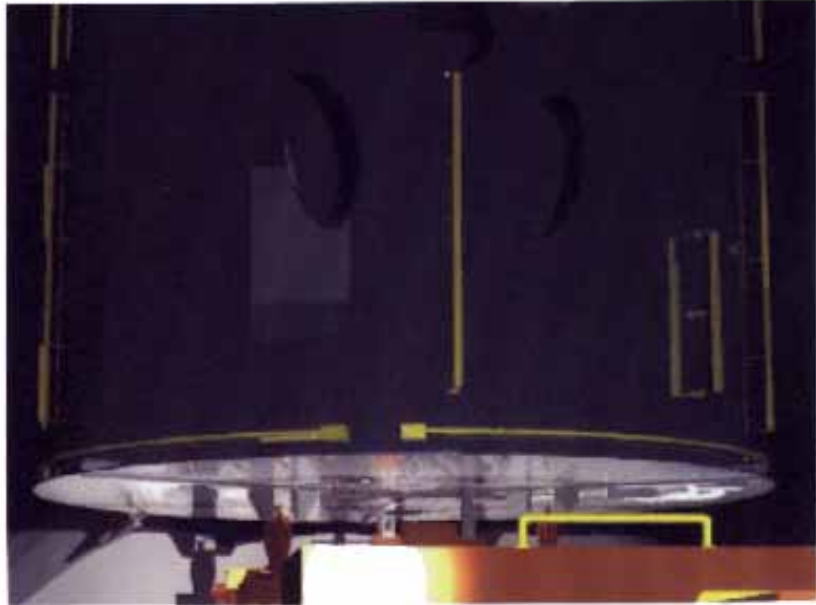


Sunset

## Static Twist Analysis Night Lighting Study

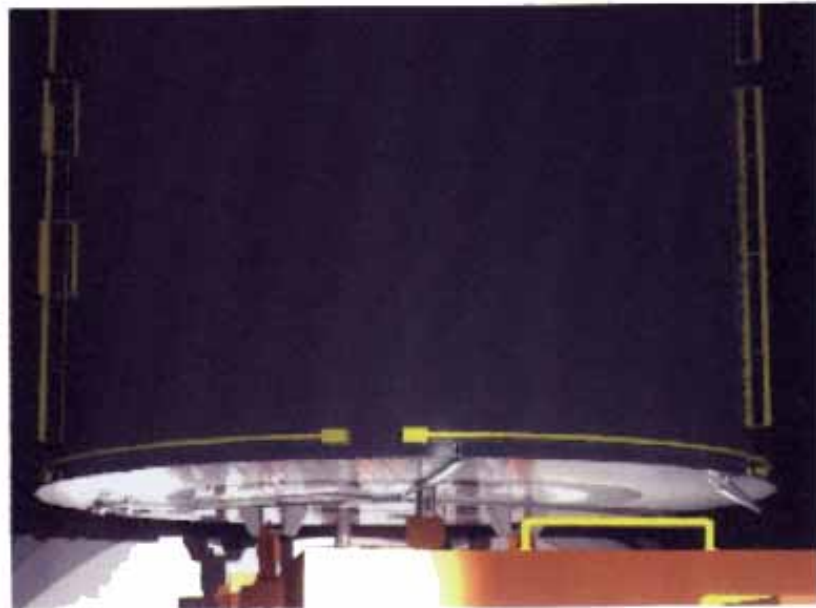
Rotation Reference  
(-V3 Configuration)  
for Camera D (CTVC)

*Low light levels will introduce noise into the camera image, though some areas of the scene may provide just barely acceptable viewing.*



Rotation Reference  
(+V3 Configuration)  
for Camera D (CTVC)

*Low light levels will introduce noise into the camera image, though some areas of the scene may provide just barely acceptable viewing.*



## Static Twist Analysis Night Lighting Study

**Camera B (CTVC) View  
of Solar Array Edge A/B**

*Low light levels will introduce noise into the camera image, thus interfering with the camera view of the solar array edge.*



**Camera D (CTVC) View  
of Solar Array Edge A/B**

*Low light levels will introduce noise into the camera image, thus interfering with the camera view of the solar array edge.*



## Static Twist Analysis Night Lighting Study

Camera B (CTVC) View  
of Solar Array Edge C/D

*Low light levels will introduce noise into the camera image, thus interfering with the camera view of the solar array edge.*



Camera A (MLA) View  
of Solar Array Edge C/D

*MLA capabilities of viewing in low light levels allow for the viewing of the solar array edge at night.*



## Static Twist Analysis Night Lighting Study

**Camera D (CTVC) View  
of Solar Array Edge G/H**

*Low light levels will introduce noise into the camera image, thus interfering with the camera view of the solar array edge.*



**Camera C (MLA) View  
of Solar Array Edge G/H**

*MLA capabilities of viewing in low light levels allow for the viewing of the solar array edge at night, though specular reflection of the lights off of the bismems will cause some scattering of the light in the lens.*



## Static Twist Analysis Night Lighting Study

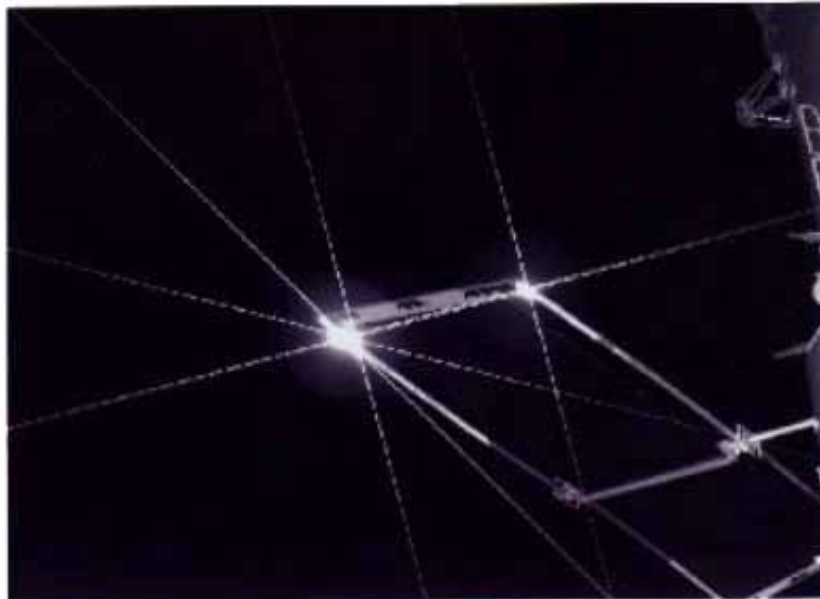
Camera C (MLA) View  
of Solar Array Edge E/F

*MLA capabilities of viewing  
in low light levels allow for  
the viewing of the solar  
array edge at night.*



Camera A (MLA) View  
of Solar Array Edge E/F

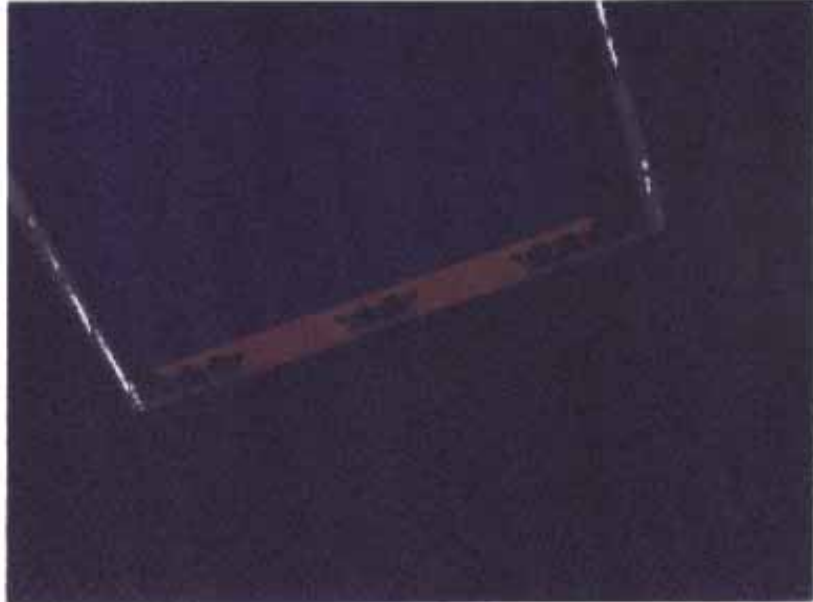
*MLA capabilities of viewing  
in low light levels allow for  
the viewing of the solar  
array edge at night, though  
specular reflection of the  
lights off of the bistrans will  
cause some scattering of  
the light in the lens.*



## FSS Pivot to 85 deg Night Lighting Study

Camera B (CTVC) View  
of Solar Array Edge A/B

*Low light levels will introduce noise into the camera image, though some areas of the scene may provide just barely acceptable viewing.*



Scale Reference View for  
Camera B (CTVC)

*Low light levels will introduce noise into the camera image, though some areas of the scene may provide just barely acceptable viewing.*





## **Appendix F: Daily Mission Reports**

**Hubble Space Telescope (HST) Servicing Mission 2 (SM-2) Solar Array  
Photogrammetric Analysis  
Image Science & Analysis Group  
Flight Day 3 (FD3) Analysis Status Report**

**Static Twist Analysis**

Video data were obtained of all 8 solar array tips over a 3-hour time frame, from UTC (coordinated universal time) 044:16:15 to 044:18:55. All camera views were obtained with the expected setups. However, harsh and variable lighting required multiple camera gain settings. This increased the selection time of analysis frames and delayed completion of the overall analysis. However, we do not believe it had an appreciable effect on the calculated error. We have determined that some of the alternate camera views obtained provided beneficial analysis data sets. Based on this, we plan to use the following camera pairs for spreader bar acquisition on FD4:

<b>Camera Pair</b>	<b>SA Spreader Bar</b>
D and B	Port forward tip
A and B	Port Aft tip
D and B	Starboard Aft Tip
D and C	Starboard Forward Tip

This updated acquisition procedure does not require multiplexed views on the aft tips or widening of the deadbands.

One to four frames were analyzed for each tip. Estimates were made of the array tips in HST coordinates with an associate root mean square error for each tip (see attached sheet). In addition, HST rotation was measured to be -1.4 deg, and camera pan/tilt positions were confirmed. The analysis took approximately 10 hours to complete.

**Solar Array Motion Assessment**

A one-minute sequence of video of the A-B solar array tip, taken from payload bay (PLB) camera B, was analyzed from UTC 044:20:28:39.48 to 044:20:29:39.48. The video data were of very good quality, with lighting and camera positioning as expected.

The analysis sample rate was 3 frames per second, for a total of 180 frames analyzed. The tip-to-tip measured deflection was 0.8 inches, with a frequency of approximately 0.1 Hz (see attached sheet). There was slight motion noted for approximately 3 minutes after the analysis interval. The analysis took approximately 6 hours to complete.

## **HST SM-2 Solar Array Photogrammetric Analysis Image Science & Analysis Group FD4 Analysis Status Report**

### **Static Twist Analysis**

Video data were obtained of all 8 solar array tips in a single day pass from UTC 045:17:00 to 045:17:30. All camera views were obtained with the expected setups. Lighting conditions were improved over FD3. There was obstruction of the solar array A tip from PLB camera D by the extravehicular activity (EVA) device mounted on the end of the remote manipulator subsystem (RMS). This meant the precise location of the tip from camera view D had to be estimated from the position of the bistem and spreader bar. However, we believe this did not have a serious effect on the analysis results.

The revised acquisition procedures and views, based on FD3 results, worked well, and will be used for the remaining static twist acquisitions. We do not expect to require widening of the deadbands on subsequent flight days.

Four frames were analyzed for each tip. Estimates were made of the array tips in HST coordinates with an associated root mean square error for each tip (see attached sheet). The results were compared with the FD3 results, which show a reduction in the uncertainty in each analysis case. (A negative value in the spreadsheet indicates a reduction from the previous day's analysis.) In addition, HST rotation was measured to be  $-1.3 \pm 0.5$  deg, and camera pan/tilt positions were confirmed. The analysis took approximately 8 hours to complete.

### **Video Survey**

Video of the HST was obtained during a ground-controlled survey of the PLB video cameras. The survey was conducted over six day passes from UTC 045:18:00 to 045:23:15. Good imagery was obtained from all four PLB cameras, and additional video from the RMS elbow camera was obtained. Several locations of minor multilayer insulation (MLI) damage and possible micrometeoroid/orbital debris strikes were identified. The video survey objectives for the -V3 position have been achieved. Additional video for the +V3 position will be obtained on FD6.

### **Solar Array Motion Assessment**

No solar array motion assessment was required for FD4. Video data will be acquired during the vernier reaction control subsystem (VRCS) reboost tonight, and will analyzed as required.

## **HST SM-2 Solar Array Photogrammetric Analysis Image Science & Analysis Group FD5 Analysis Status Report**

### **Static Twist Analysis**

Video data were obtained of all 8 solar array tips in two day passes from UTC 046:16:25 to 046:17:40. All camera views were obtained with the expected setups, and lighting conditions were acceptable. There was a slight obstruction of the solar array A tip from PLB camera D by the EVA manipulator foot restraint mounted on the end of the RMS. This meant the precise location of the tip from camera view D had to be estimated from the position of the bistem and spreader bar. However, we believe this did not have a serious effect on the analysis results.

Between 3 and 6 frames were analyzed for each tip. Estimates were made of the array tips in HST coordinates with an associated root mean square error for each tip (see attached sheet). The results were compared with the FD4 results, which show a reduction in the uncertainty for tips A-B and E-F. However, the uncertainty increased for the H tip, since the precise location of the tip from camera view B had to be estimated from the position of the bistem and spreader bar. There also were difficulties encountered in the analysis of the C-D tip, which is believed to be a result of the high camera tilt angle (approximately 90 deg) during acquisition. After attempting four separate analyses, none of which would converge, we notified HST Mechanical Systems of the problem, and they agreed to accept analysis of 3 of 4 tips.

The HST rotation was measured to be 0.1 +/- 0.3 deg. Camera pan/tilt positions were confirmed and are attached. The analysis took approximately 9 hours to complete.

### **Video Survey**

Video of the HST was obtained during a ground-controlled survey of the PLB video cameras. The survey was conducted over three day passes from UTC 046:18:50 to 046:22:50. Good imagery was obtained from all four PLB cameras. Additional video from the RMS elbow camera was also obtained. A significant portion of the survey was dedicated to obtaining detailed video of MLI damage on bays 5, 7, 8, and 10, and on the -V3 light shield. The video survey objectives for the -V3 position have been completed. Video of the +V3 side will be obtained on FD6.

### **Solar Array Motion Assessment**

No solar array motion assessment was required for FD5.

## **HST SM-2 Solar Array Photogrammetric Analysis Image Science & Analysis Group FD6 Analysis Status Report**

### **Static Twist Analysis**

Video data of the HST in the +V3 position were obtained of all 8 solar array tips in three day passes from UTC 047:15:50 to 047:17:40. All camera views were obtained with the expected setups, and lighting conditions were acceptable.

Between x and y frames were analyzed for each tip. Estimates were made of the array tips in HST coordinates with an associated root mean square error for each tip (see attached sheet). The results were compared with the FD5 results, which show .....

The HST rotation was measured to be  $x \pm y$  degrees. Camera pan/tilt positions were confirmed and are attached. The analysis took approximately 8 hours to complete.

### **Video Survey**

Video of the HST in the +V3 position was obtained during a ground-controlled survey of the PLB video cameras. The survey was conducted over four day passes from UTC 047:17:40 to 047:23:00. All four PLB cameras provided good imagery, including detailed imagery of the sun-facing side of the HST, with particular emphasis on MLI damage. This completes the scheduled ground-based survey of the HST, though additional survey may be required after the FD7 EVA.

### **Solar Array Motion Assessment**

No solar array motion assessment was required for FD6.

## **HST SM-2 Solar Array Photogrammetric Analysis Image Science & Analysis Group FD7 Analysis Status Report**

### **Static Twist Analysis**

Video data of the HST in the +V3 position were obtained of all 8 solar array tips in four day passes from UTC 048:15:50 to 048:18:05. All camera views were obtained with the expected setups, and lighting conditions were acceptable, though somewhat degraded from the previous days.

Between 3 and 4 frames were analyzed for each tip. Estimates were made of the array tips in HST coordinates with an associated root mean square error for each tip (see attached sheet). The results were compared with the FD6 results. For tips A-B, harsh lighting conditions limited the number of useable analysis frames and increased the resulting analysis uncertainty. Increases in uncertainty for the C-D tip may have been due to limited selection of reference points from the camera C view.

The HST rotation was measured to be  $179.6 \pm 0.1$  deg. Camera pan/tilt positions were confirmed and are attached. The analysis took approximately 6 hours to complete.

The sixth and final STA will be conducted on FD8.

### **Video Survey**

A short ground-controlled video survey was conducted on FD7, focusing on views of bays 1, 2, and 3, and views of the handrail along bay J. Required views were coordinated with SMM.

### **Solar Array Motion Assessment**

No solar array motion assessment was required for FD7.

## **HST SM-2 Solar Array Photogrammetric Analysis Image Science & Analysis Group FD8 Analysis Status Report**

### **Static Twist Analysis**

Video data of the HST in the -V3 position were obtained of all 8 solar array tips in four day passes from UTC 049:15:50 to 049:18:05. All camera views were obtained with the expected setups, and lighting conditions were acceptable.

Four frames were analyzed for each tip. Estimates were made of the array tips in HST coordinates with an associated root mean square error for each tip (see attached sheet). The results were compared with the FD5 results, which indicated similar tip twist values, with comparable or lower uncertainty. For the G-H tip, there is potential for additional error which may not be reflected in the uncertainty. This was determined by comparing +V3 to -V3 results.

The HST rotation was measured to be -0.8 deg. Camera pan/tilt positions were confirmed and are attached. The analysis took approximately 6 hours to complete.

### **Video Survey**

A short ground-controlled video survey was conducted on FD8, focusing on views of MLI repair from EVA #5, and detailed views of the high-gain antenna. Required views were coordinated with SMM.

### **Solar Array Motion Assessment**

An unexpected solar array slew of approximately 5 deg on the -V2 array was observed at approximately 049:03:12:44.052 UTC. HST Mechanical Systems subsequently requested a solar array motion assessment, to be completed within 8 hours, to determine the displacement of the solar array tips.

A video sequence of approximately one minute (UTC 049:03:12:32 to 049:03:13:32) taken from camera B of the -V2 forward solar array tip (G-H) was analyzed. Because of the low contrast of the spreader bar in the image, the automated edge detection and line-tracking analysis procedure could not be used. Therefore, all data points were taken by hand. Two analyses were performed by separate analysts to minimize selection point bias. The analysis sample rate was 3 frames per second, for a total of 161 frames analyzed.

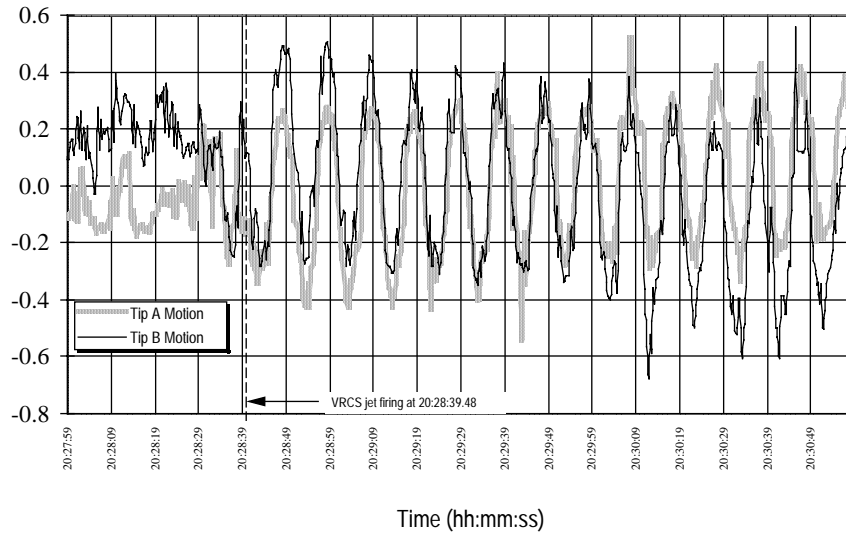
The results indicated a total slew at the tip of approximately 22 inches. After the initial slew, the array was seen to oscillate at a frequency of approximately 0.1 Hz (see attached sheet). The initial peak-to-peak displacement was measured to be approximately 7 inches, with the last measured peak-to-peak displacement being approximately 5 inches. The analysis was completed in approximately 5 hours.



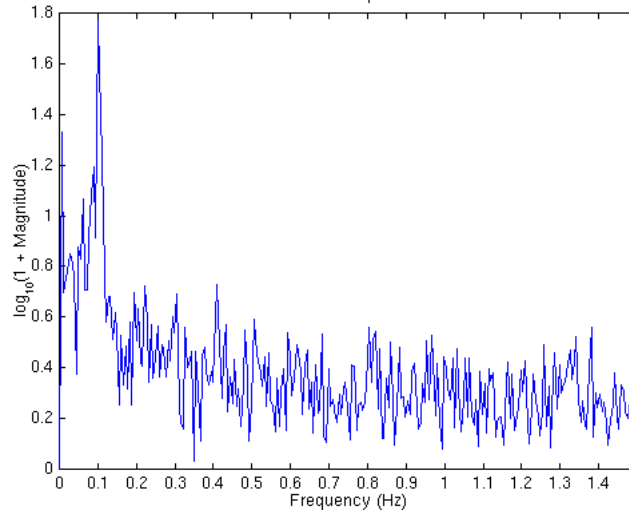
## **Appendix G: Solar Array Motion Analysis Results**

## Plots for VRCS-Induced Array Motion on Flight Day 3

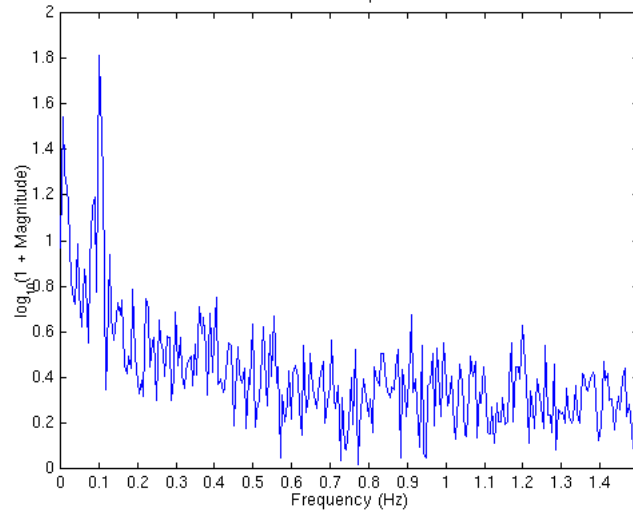
### *Plot of Non-Smoothed Tip Displacement Oscillatory Motion*



### *Frequency Plot for Tip A*

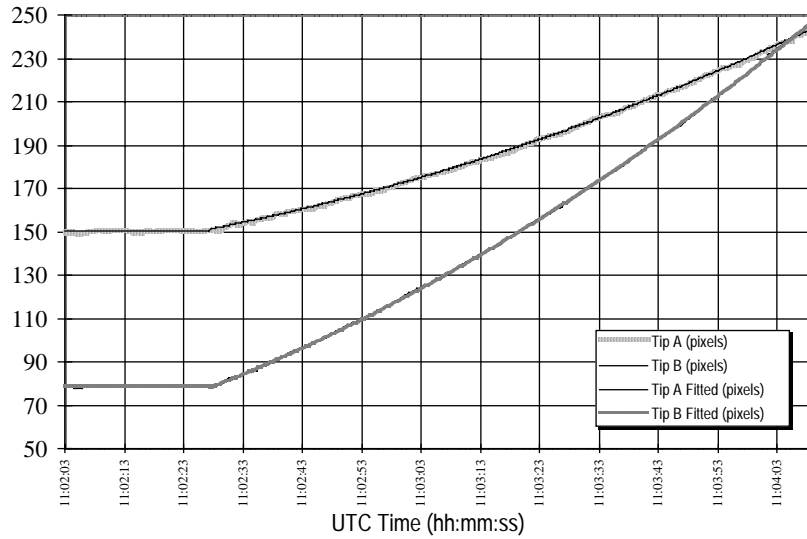


***Frequency Plot for Tip B***

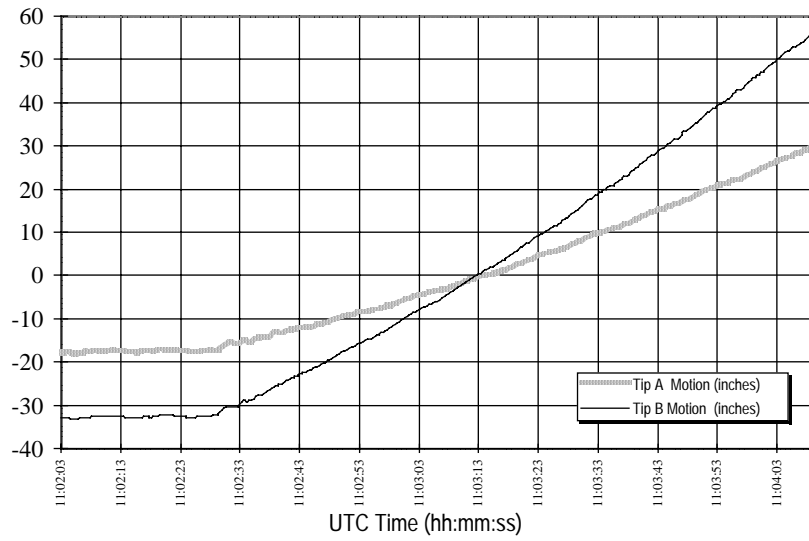


**Plots for Array Motion during Start of Rotation on Flight Day 5**

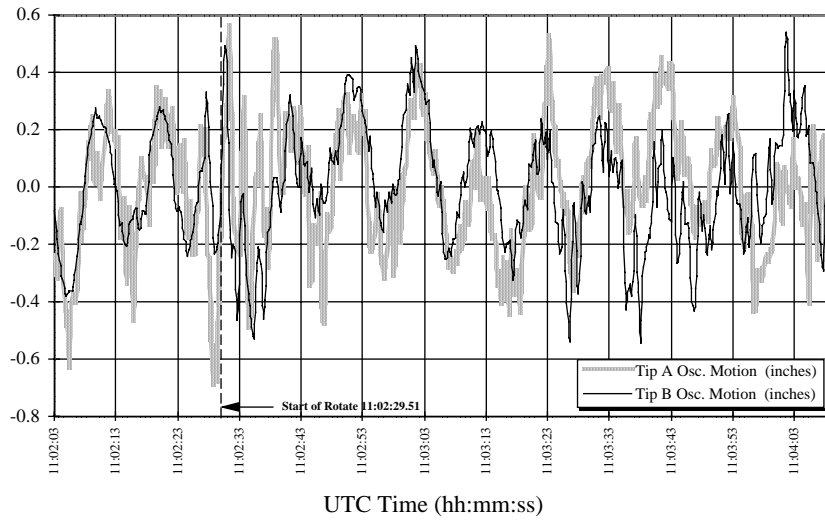
***Raw Data Plot of Absolute pixel position prior to Rotation Correction***



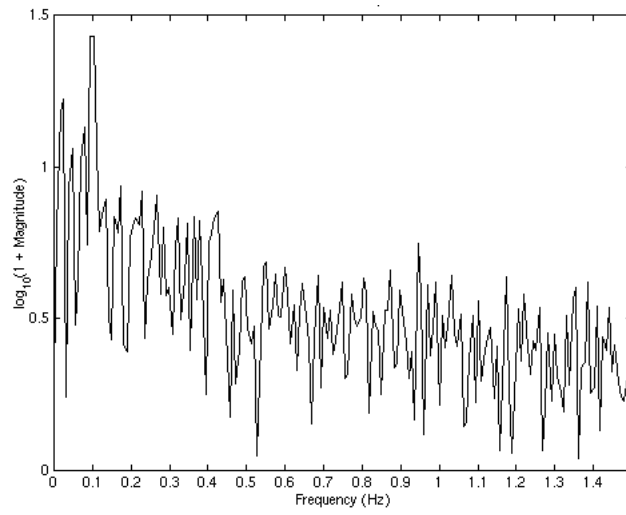
***Motion Tip Displacement Plot in Inches Prior to Rotation Correction***



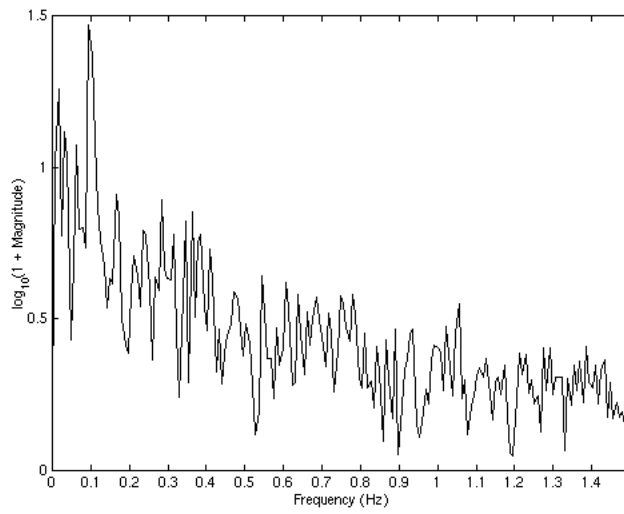
***Plot of Non-Smoothed Tip Displacement Oscillatory Motion***



***Frequency Plot for Tip A***

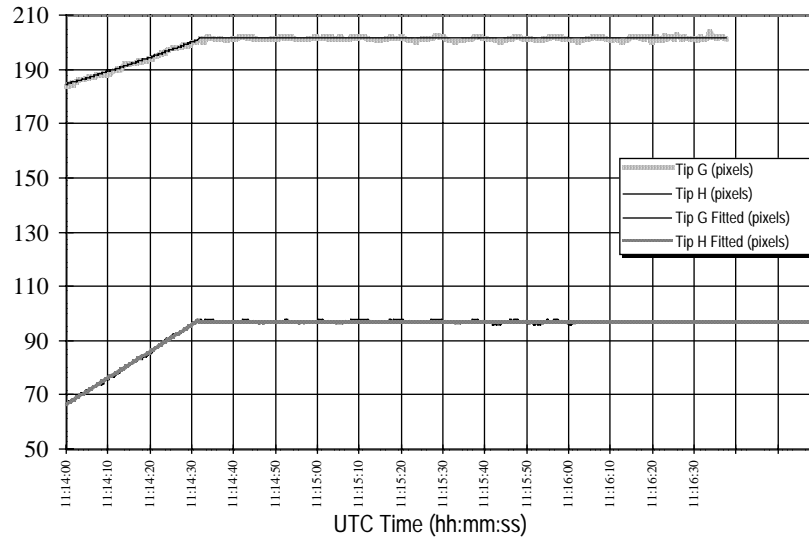


***Frequency Plot for Tip B***

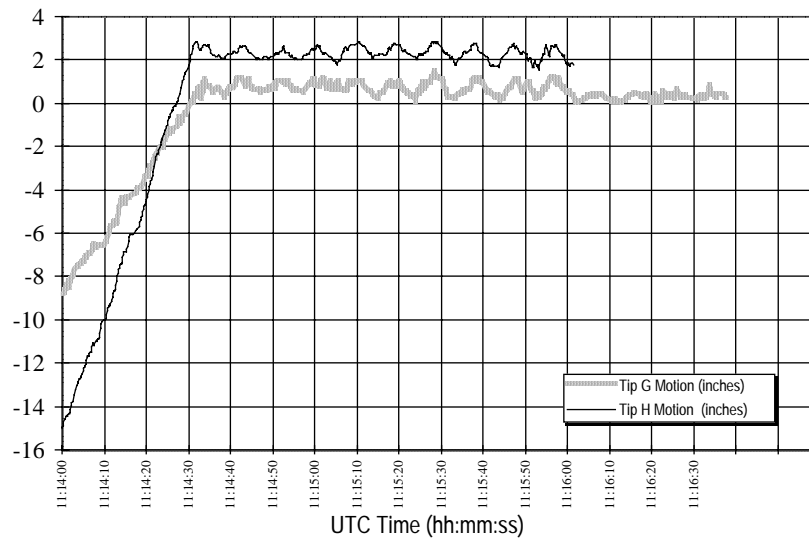


## Plots for Array Motion during End of Rotation on Flight Day 5

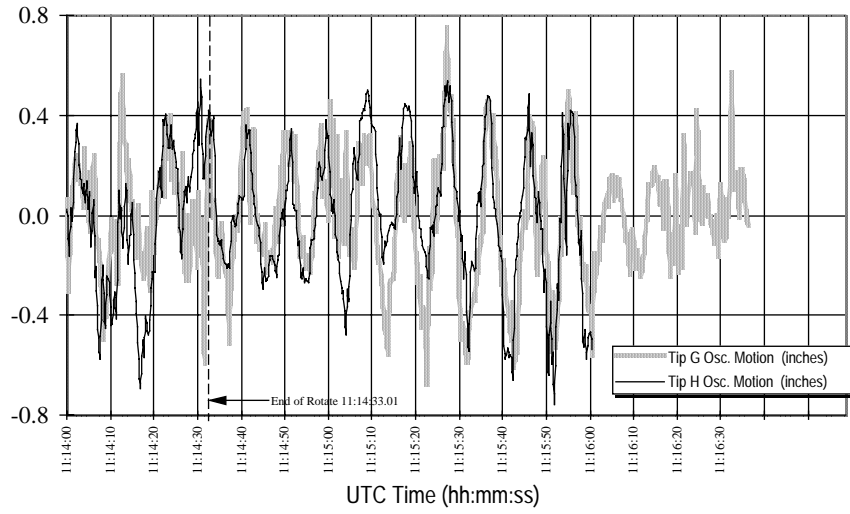
*Raw Data Plot of Absolute Pixel Position Prior to Rotation Correction*



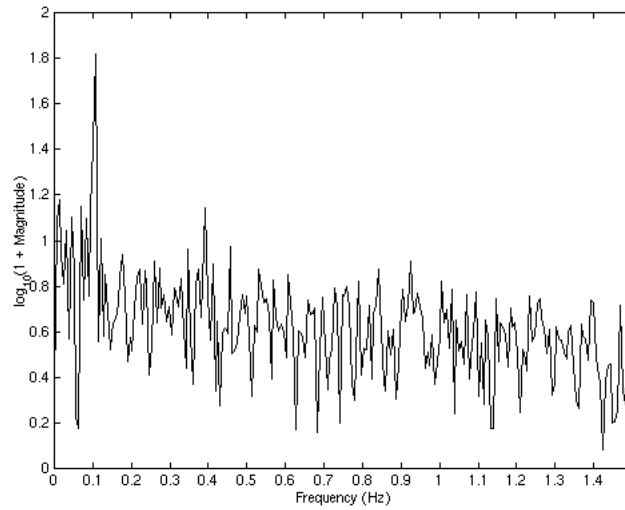
*Motion Tip Displacement Plot in Inches Prior to Rotation Correction*



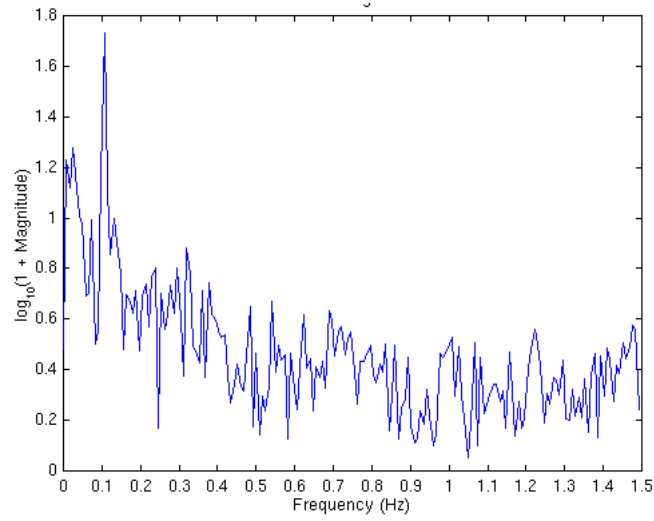
**Plot of Non-Smoothed Tip Displacement Oscillatory Motion**



**Frequency Plot for Tip G**

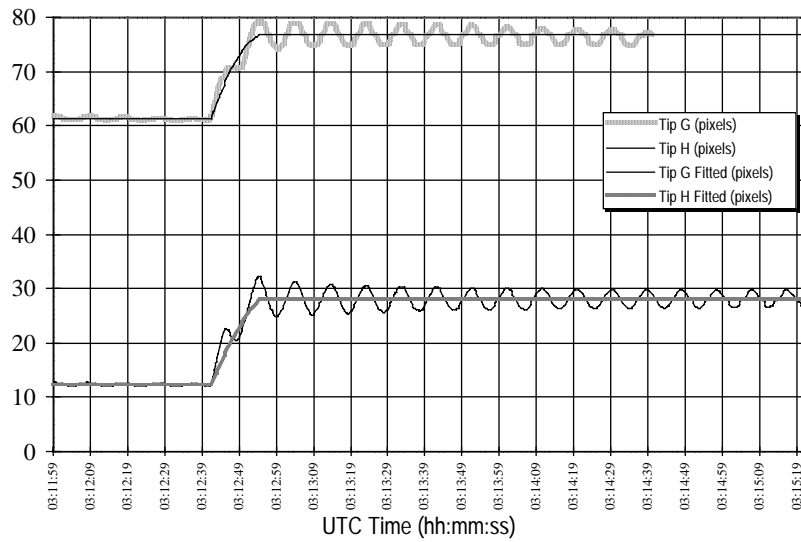


***Frequency Plot for Tip H***

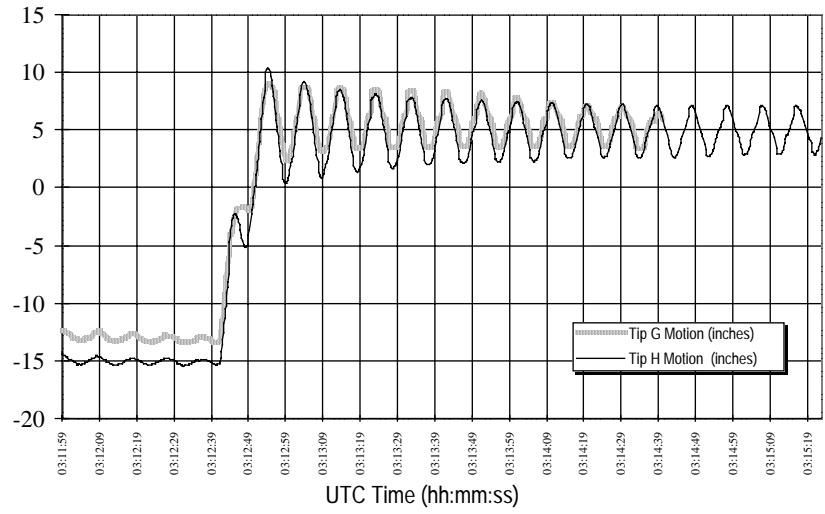


**Plots for Air Lock Depressurization induced Motion on Flight Day 8**

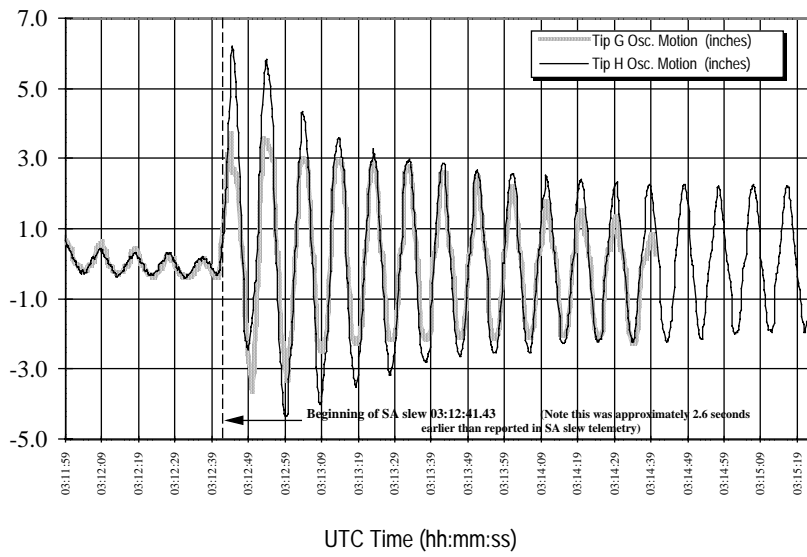
***Raw Data Plot of Absolute pixel position prior to Slew Correction***



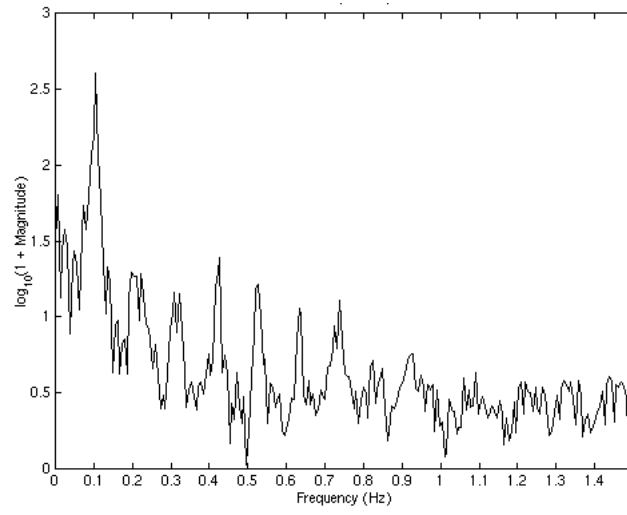
***Motion Tip Displacement Plot in Inches Prior to Slew Correction***



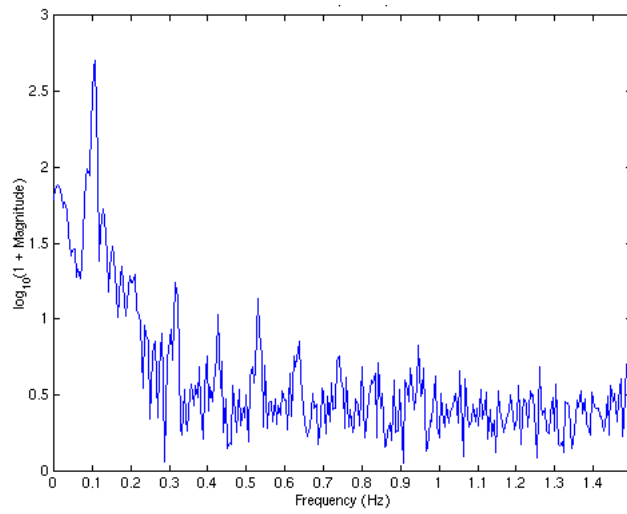
***Plot of Non-Smoothed Tip Displacement Oscillatory Motion***



***Frequency Plot for Tip G***

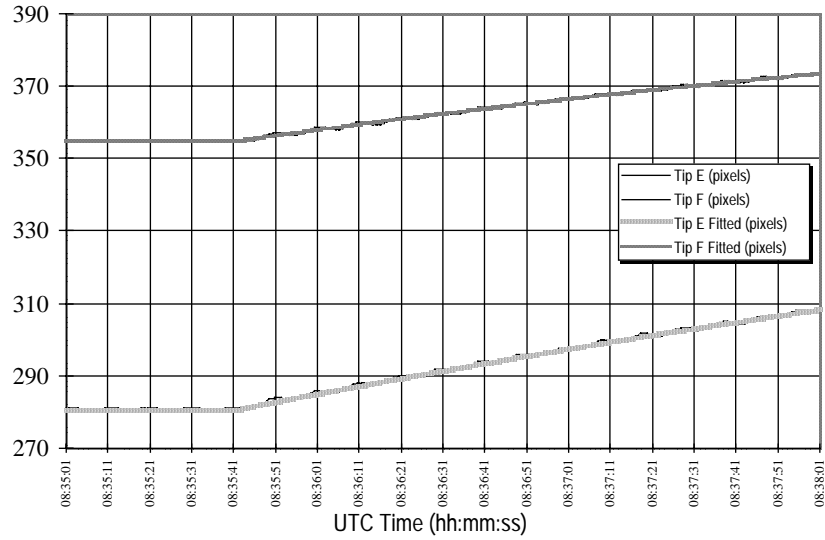


***Frequency Plot for Tip H***

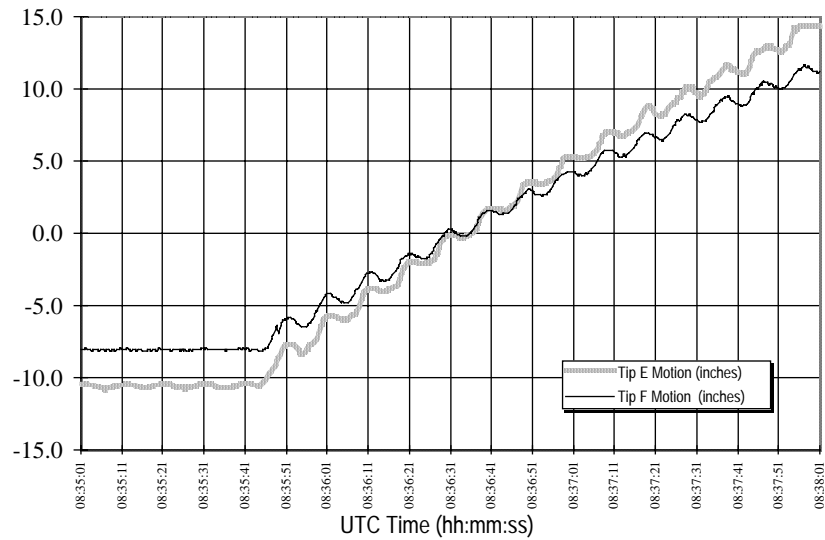


## Plots for Array Motion During Start of Pivot on Flight Day 8

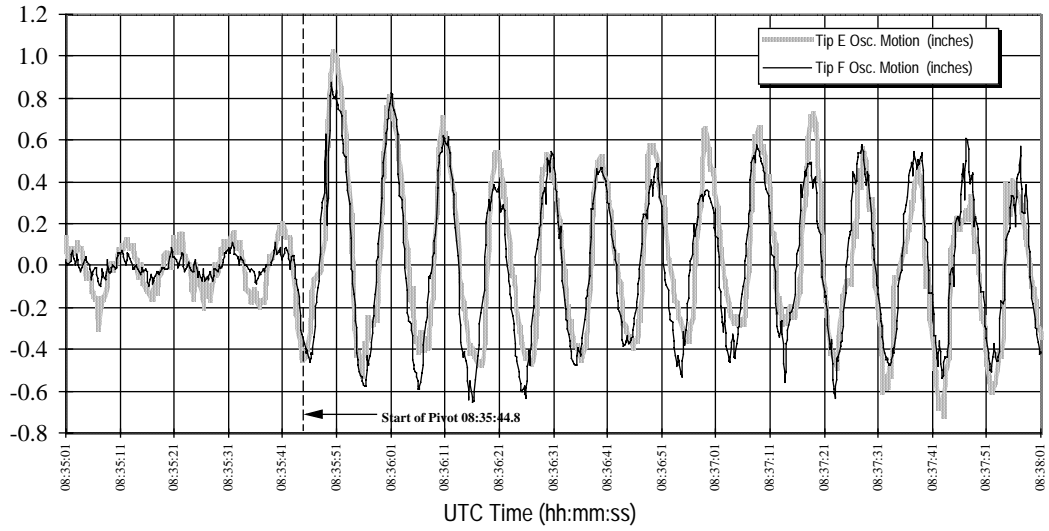
### *Raw Data Plot of Absolute Pixel Position Prior to Pivot Correction*



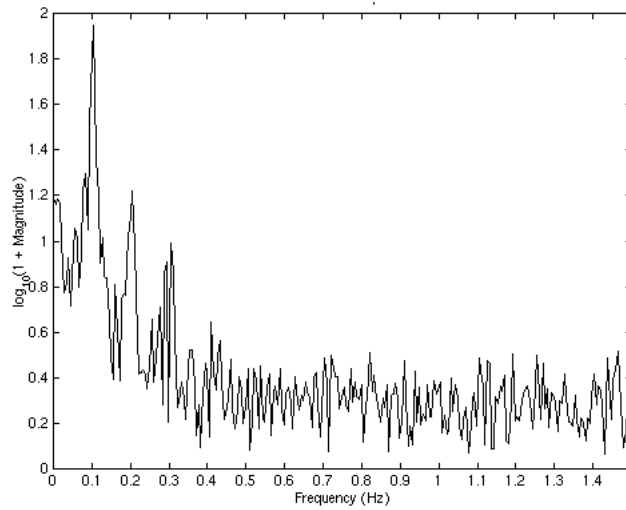
### *Motion Tip Displacement Plot in Inches Prior to Pivot Correction*



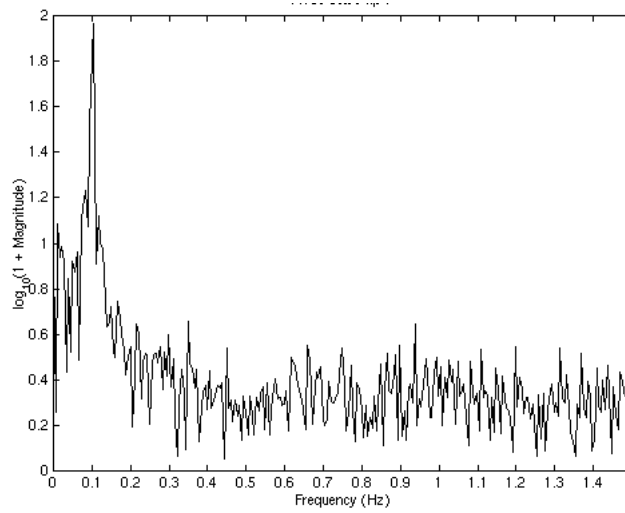
**Plot of Non-Smoothed Tip Displacement Oscillatory Motion**



**Frequency Plot for Tip E**

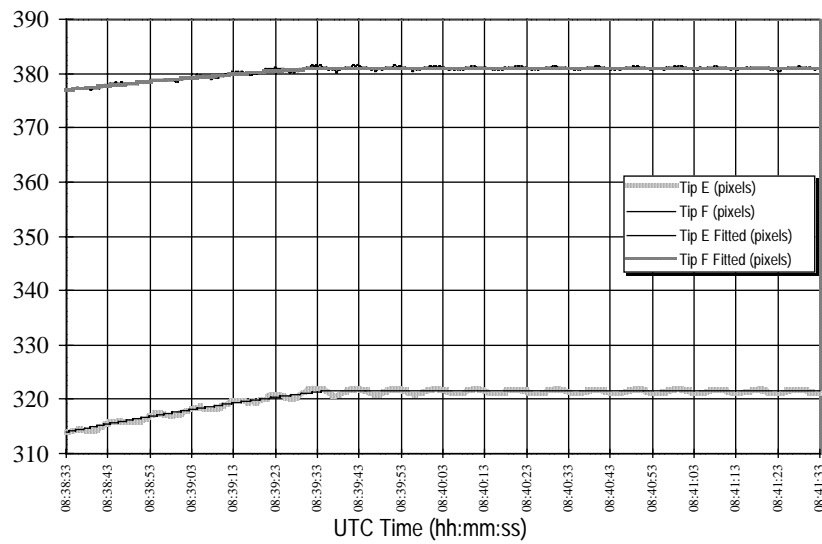


**Frequency Plot for Tip F**

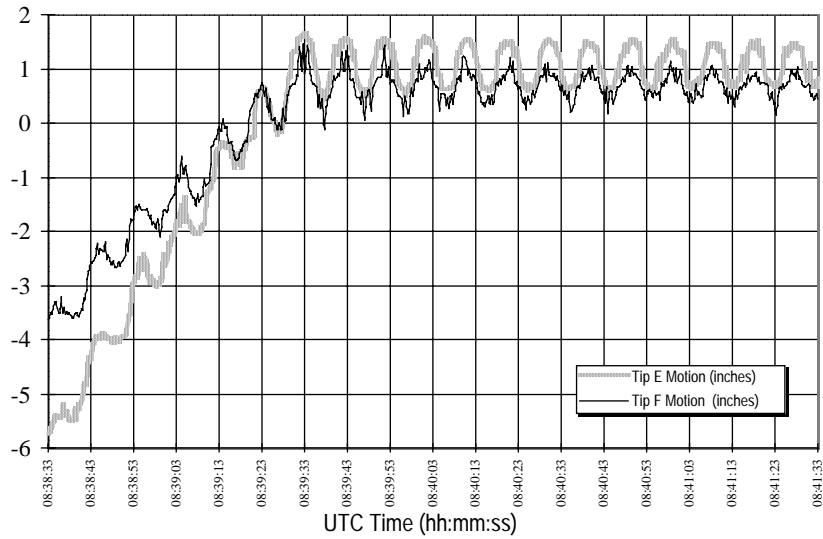


**Plots for Array Motion During End of Pivot on Flight Day 8**

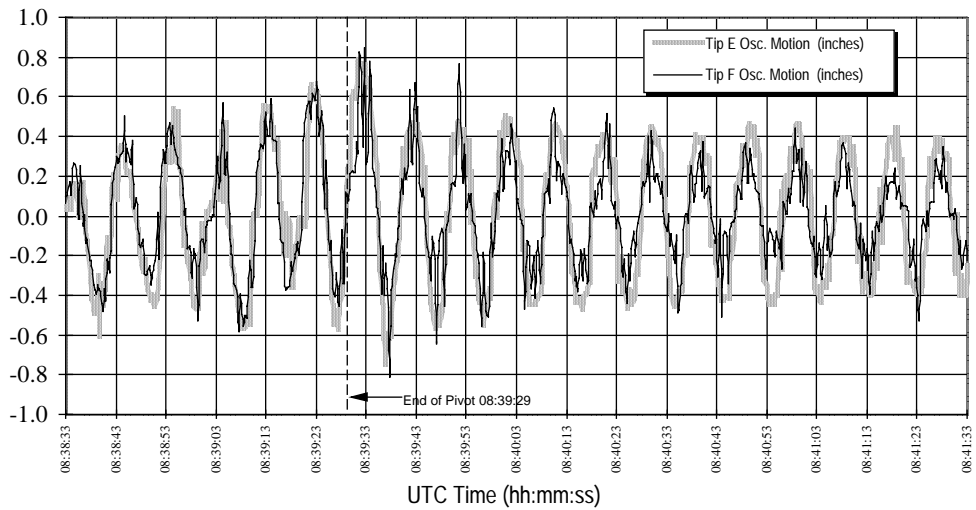
**Raw Data Plot of Absolute Pixel Position Prior to Pivot Correction**



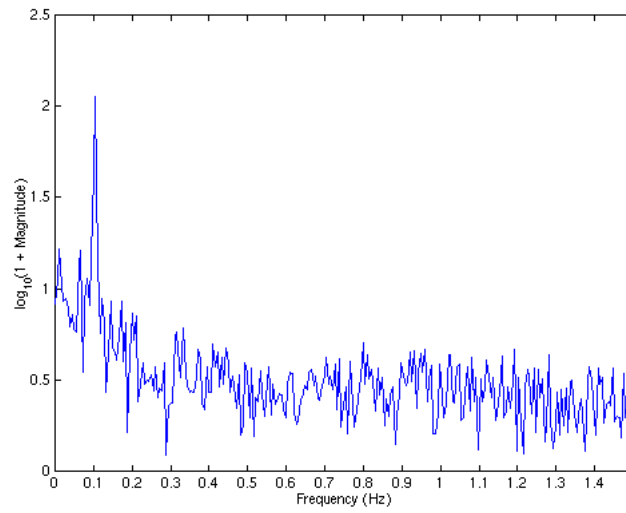
***Motion Tip Displacement Plot in Inches Prior to Pivot Correction***



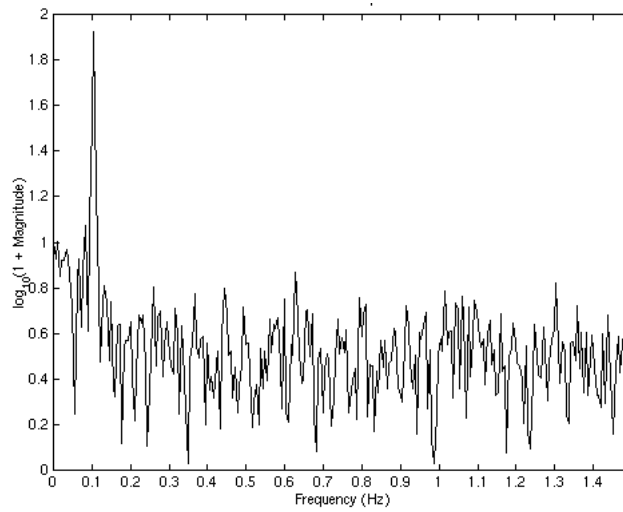
***Plot of Non-Smoothed Tip Displacement Oscillatory Motion***



***Frequency Plot for Tip E***

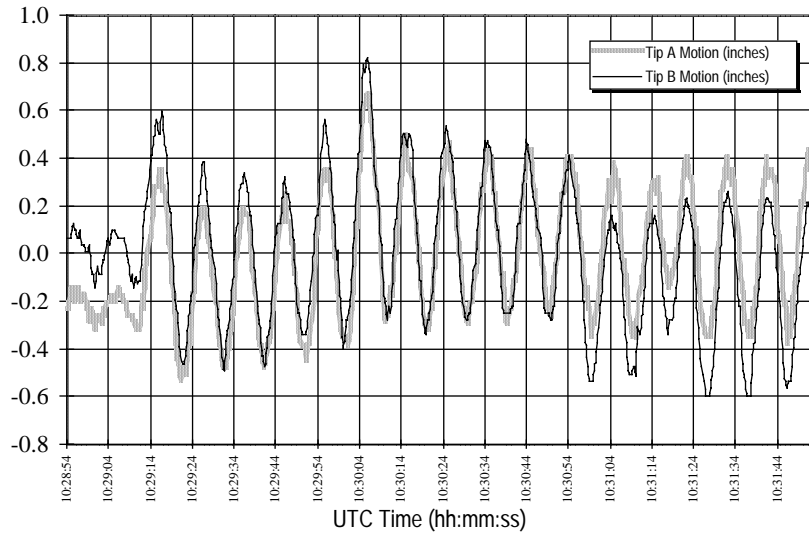


***Frequency Plot for Tip F***

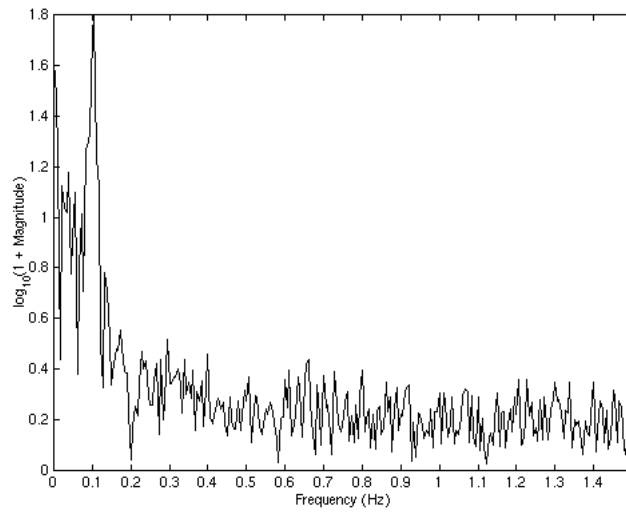


## Plots for Array Motion During Reboost on Flight Day 8

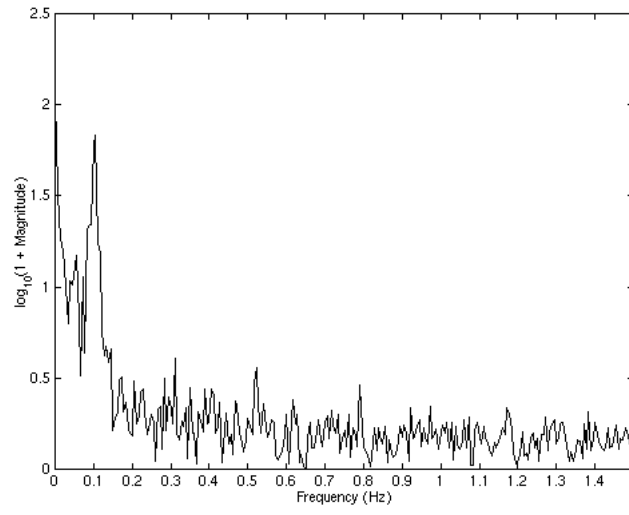
### *Plot of Non-smoothed Tip Displacement Oscillatory Motion*



### *Frequency Plot for Tip A*



***Frequency Plot for Tip B***



REPORT DOCUMENTATION PAGE			Form Approved OMB No. 0704-0188	
Public reporting burden for this collection of information is estimated to average 1 hour per response, including the time for reviewing instructions, searching existing data sources, gathering and maintaining the data needed, and completing and reviewing the collection of information. Send comments regarding this burden estimate or any other aspect of this collection of information, including suggestions for reducing this burden, to Washington Headquarters Services, Directorate for Information Operations and Reports, 1215 Jefferson Davis Highway, Suite 1204, Arlington, VA 22202-4302, and to the Office of Management and Budget, Paperwork Reduction Project (0704-0188), Washington, DC 20503.				
1. AGENCY USE ONLY (Leave Blank)	2. REPORT DATE April 1998	3. REPORT TYPE AND DATES COVERED NASA Technical Paper		
4. TITLE AND SUBTITLE Photogrammetric Assessment of the Hubble Space Telescope Solar Arrays During the Second Servicing Mission			5. FUNDING NUMBERS	
6. AUTHOR(S) C. A. Sapp*, M. W. Snyder**, J. L. Dragg*, M. T. Gaunce, J. E. Decker***				
7. PERFORMING ORGANIZATION NAME(S) AND ADDRESS(ES) Lyndon B. Johnson Space Center Houston, Texas 77058			8. PERFORMING ORGANIZATION REPORT NUMBERS S-839	
9. SPONSORING/MONITORING AGENCY NAME(S) AND ADDRESS(ES) National Aeronautics and Space Administration Washington, D.C. 20546-0001			10. SPONSORING/MONITORING AGENCY REPORT NUMBER TP-207193	
11. SUPPLEMENTARY NOTES *Lockheed Martin; **Hernandez Engineering; ***Goddard Space Flight Center				
12a. DISTRIBUTION/AVAILABILITY STATEMENT Unclassified/unlimited Available from the NASA Center for AeroSpace Information (CASI) 800 Elkridge Landing Rd Linthicum Heights, MD 21090-2934 (301) 621-0390 Subject Category: 20			12b. DISTRIBUTION CODE	
13. ABSTRACT (Maximum 200 words) This report documents the photogrammetric assessment of the Hubble Space Telescope (HST) solar arrays conducted by the NASA Johnson Space Center Image Science and Analysis Group during Second Servicing Mission 2 (SM-2) on STS-82 in February 1997. Two types of solar array analyses were conducted during the mission using Space Shuttle payload bay video: (1) measurement of solar array motion due to induced loads, and (2) measurement of the solar array static or geometric twist caused by the cumulative array loading. The report describes pre-mission planning and analysis technique development activities conducted to acquire and analyze solar array imagery data during SM-2. This includes analysis of array motion obtained during SM-1 as a proof-of-concept of the SM-2 measurement techniques. The report documents the results of real-time analysis conducted during the mission and subsequent analysis conducted post-flight. This report also provides a summary of lessons learned on solar array imagery analysis from SM-2 and recommendations for future on-orbit measurements applicable to HST SM-3 and to the International Space Station. This work was performed under the direction of the Goddard Space Flight Center HST Flight Systems and Servicing Project.				
14. SUBJECT TERMS Hubble Space Telescope, solar arrays, photogrammetry, solar dynamic power systems			15. NUMBER OF PAGES 195	16. PRICE CODE
17. SECURITY CLASSIFICATION OF REPORT Unclassified	18. SECURITY CLASSIFICATION OF THIS PAGE Unclassified	19. SECURITY CLASSIFICATION OF ABSTRACT Unclassified	20. LIMITATION OF ABSTRACT unlimited	



---

---